

TECHNICAL UNIVERSITY OF CRETE
SCHOOL OF MINERAL RESOURCES ENGINEERING

Laboratory of PVT and Core Analysis



Tryfonas Kiaitsis

Diploma Thesis

“Computer modeling of gravitational oil fields: The case of
an offshore Greek reservoir”

Advisory Committee

Asst. Prof. Andreas Yiotis (supervisor)

Dr. Dimitris Marinakis

Prof. Nikos Pasadakis

June 2022

Abstract

Reservoir fluids are considered to be in a state of equilibrium before the start of production. In some cases the gravitational forces are considerable with respect to the equilibrium compositions with depth. Thick reservoirs with volatile oil and significant vertical permeability are especially prone to component segregation with depth, even if no phase change is observed. Such compositional variations can lead to considerable errors in the estimation of the quantity of oil initially in place, as well as to non-optimum exploitation methods.

After thorough research of the existing literature, simulation software in the MATLAB® computing environment was developed for the estimation of equilibrium compositions with depth in gravitational oilfields. The software used a cubic EOS coupled with an isothermal GCE algorithm to simulate the case of a Greek oilfield reservoir located in the Mediterranean Sea. An EOS fluid characterization was developed by tuning the EOS to match measured data from conventional PVT experiments. The simulation results were compared with the ones derived from commercial PVT software. The comparison indicated that the developed software can accurately predict variations in pressure and fluid composition along the depth of the reservoir.

Περίληψη

Τα πετρελαϊκά ρευστά πριν την έναρξη της παραγωγικής εκμετάλλευσης του ταμιευτήρα θεωρούνται πως βρίσκονται σε κατάσταση ισορροπίας μεταξύ της βαρύτητας και της διάχυσης των συστατικών στο χώρο. Σε ταμιευτήρες με μη αμελητέα διαπερατότητα ως προς την κατακόρυφο, συχνά παρατηρούνται διαφοροποιήσεις της σύστασης τους λόγω βαρύτητας, παρόλο που τα ρευστά παραμένουν μονοφασικά. Τέτοιου είδους διαφοροποιήσεις της σύστασης μπορούν να επιφέρουν σημαντικά λάθη στην εκτίμηση των διαθέσιμων αποθεμάτων του κοιτάσματος καθώς και λάθη στην επιλογή των καταλλήλων μεθόδων εκμετάλλευσης.

Μετά από πλήρη βιβλιογραφική ανασκόπηση επί του θέματος, αναπτύχθηκε ένα υπολογιστικό πρότυπο σε περιβάλλον MATLAB® για την πρόβλεψη των μεταβολών στη σύσταση και πίεση διαφόρων ταμιευτήρων με το βάθος. Το πρότυπο βασίζεται σε μια κυβική καταστατική εξίσωση σε συνδυασμό με έναν αλγόριθμο για την περιγραφή της θερμοδυναμικής και βαρυτικής ισορροπίας, με σκοπό την προσομοίωση ενός υπεράκτιου πετρελαϊκού κοιτάσματος στην περιοχή της Μεσογείου. Το υπολογιστικό πρότυπο αναπτύχθηκε “ρυθμίζοντας” την κυβική καταστατική εξίσωση επάνω σε πειραματικά δεδομένα από συμβατικά εργαστηριακά πειράματα. Πραγματοποιήθηκε σύγκριση μεταξύ των αποτελεσμάτων του αναπτυχθέντος λογισμικού και εκείνων που προέκυψαν με χρήση εμπορικού λογισμικού. Η σύγκριση απέδειξε ότι το αναπτυχθέν λογισμικό δύναται να προβλέψει με ακρίβεια τις πιέσεις αλλά και τις συστάσεις του ρευστού καθ’ όλο το πάχος του ταμιευτήρα.

Acknowledgements

First and foremost, I would like to thank Honorary Professor Nikos Varotsis for initially trusting me with the subject of the current diploma thesis, as well as Dr. Dimitris Marinakis for his valuable help and guidance through the thesis' laboratory and computational part.

I would also like to thank Assistant Professor Andreas Yiotis for supervising this thesis and Professor Nikos Pasadakis for his participation in the advisory committee.

Lastly, I would like to thank my family for their moral support throughout my student years.

Ευχαριστίες

Αρχικά, θα ήθελα να ευχαριστήσω τον Ομότιμο Καθηγητή Νικόλαο Βαρότση για την εμπιστοσύνη που μου έδειξε στην ανάθεση της παρούσας διπλωματικής εργασίας, αλλά και τον Δόκτωρα Δημήτριο Μαρινάκη για την πολύτιμη βοήθεια και καθοδήγησή του στο εργαστηριακό και υπολογιστικό της σκέλος.

Θα ήθελα επίσης να ευχαριστήσω τον Επίκουρο Καθηγητή Ανδρέα Γιώτη για την επίβλεψη της εργασίας καθώς και τον Καθηγητή Νικόλαο Πασαδάκη για την συμμετοχή του στην εξεταστική επιτροπή.

Τέλος, θα ήθελα να ευχαριστήσω την οικογένειά μου για την ηθική τους στήριξη καθ'όλα τα φοιτητικά μου χρόνια.

Contents

Abstract	iii
Περίληψη	iv
Acknowledgements/Ευχαριστίες	v
Contents	vi
List of Figures	x
List of Tables	xv
1 Introduction	1
1.1 Oil and Gas Composition	1
1.1.1 Chemical Composition	1
1.1.2 Reservoir Fluid Composition	2
1.2 Oil and Gas Origins	2
1.2.1 Source Rocks	3
1.2.2 Migration	4
1.2.3 Reservoir Rocks	4
1.2.4 Traps	5
1.2.5 Cap Rocks	5

1.3	Petrophysical Properties	6
1.3.1	Porosity	6
1.3.2	Permeability	6
1.3.3	Saturation	6
1.4	Oil and Gas Units and Measurements	7
1.4.1	Pressure	7
1.4.2	Volume	7
1.4.3	Temperature	8
1.4.4	Standard Conditions	8
1.5	Reservoir Engineering	8
2	Reservoir Fluid Volumetric and Phase Behavior	10
2.1	Reservoir Fluid Phase Diagrams	10
2.1.1	The Gibbs Phase Rule	10
2.1.2	Pure Substances	11
2.1.3	Binary and Multi-Component Systems	14
2.2	Reservoir Fluid Classification	16
2.2.1	Black Oil	17
2.2.2	Volatile Oil	18
2.2.3	Gas Condensate	20
2.2.4	Wet Gas	21
2.2.5	Dry Gas	21
2.2.6	Ternary Diagram	23
2.3	Reservoir Fluid Properties and Units	24
2.3.1	Molecular Quantities	24
2.3.2	Mixing Rules	25
2.3.3	Critical and Reduced Properties	26
2.3.4	Volumetric Properties	27
2.3.5	PVT Properties	32
2.3.6	K-Values	35

3	Cubic Equations of State and EOS Calculations	36
3.1	Cubic Equations of State	36
3.1.1	The van der Waals Equation	37
3.1.2	The Redlich-Kwong Equation	38
3.1.3	The Soave-Redlich-Kwong Equation	39
3.1.4	The Peng-Robinson Equation	40
3.1.5	Volume Translation	41
3.1.6	EOS Quantities	43
3.2	Equation of State Calculations	44
3.2.1	Two-Phase Flash Calculation	44
3.2.2	Stability Analysis	49
3.2.3	Saturation Pressure Calculation	53
3.3	Equation of State Fluid Characterization	56
4	Compositional Grading	57
4.1	Overview	57
4.2	Review of Literature	58
4.3	Isothermal Gravity/Chemical Equilibrium	66
4.3.1	Isothermal GCE Algorithm	68
4.3.2	Gas/Oil Contact Location	70
4.4	Non-Isothermal Gravity/Chemical Equilibrium	71
5	Laboratory and Simulation Procedures	73
5.1	Sampling Data	73
5.2	Laboratory Procedures	74
5.2.1	Constant Composition Expansion	75
5.2.2	Differential Liberation	76
5.2.3	Separator Test	78
5.3	Simulation Procedures using Commercial Software	80
5.3.1	Constant Composition Expansion Calculation	81

5.3.2	Differential Liberation Calculation	83
5.3.3	Separator Test Calculation	86
5.3.4	Saturation Pressure Calculation	87
5.3.5	Two-Phase Envelope Calculation	87
5.3.6	Two-Phase Flash Calculation	91
5.3.7	Compositional Gradient Calculation	92
5.4	Simulation Procedures using MATLAB®	99
5.4.1	Stability Analysis	99
5.4.2	Saturation Pressure Calculation	100
5.4.3	Two-Phase Flash Calculation	101
5.4.4	Compositional Gradient Calculation	102
6	Conclusions and Recommendations	108
6.1	Conclusions	108
6.1.1	Software Comparison	108
6.1.2	EOS Comparison	109
6.1.3	EOS Tuning	111
6.1.4	Volume Shift	111
6.1.5	Offshore Greek Reservoir Fluid Classification	112
6.2	Recommendations for Future Work	112
	References	113
A	Supplementary Tables and Figures	121
B	MATLAB® Open Source Code	251

List of Figures

1.1 Methane, the simplest hydrocarbon compound	1
1.2 Five elements of a conventional petroleum accumulation	3
1.3 Four types of hydrocarbon traps	5
2.1 p-V diagram for Ethane	12
2.2 p-T diagram for a single component system	13
2.3 p-V-T diagram for a pure compound	14
2.4 Phase diagrams for pure components vs. mixtures	15
2.5 Phase envelope of a multi-component system	16
2.6 Phase envelope of an ordinary black oil	17
2.7 Phase envelope of a low shrinkage oil	18
2.8 Phase envelope of a volatile crude oil	19
2.9 Phase envelope of a near-critical crude oil	19
2.10 Phase envelope of a retrograde gas condensate	20
2.11 Phase envelope of a near-critical gas condensate	22
2.12 Phase envelope of a wet gas	22
2.13 Phase envelope of a dry gas	23
2.14 Ternary diagram for several reservoir fluids	23
2.15 Reservoir fluid densities vs. pressure	28
2.16 Z-factor vs. reduced pressure and temperature	31
3.1 The Rachford-Rice function $h(\beta)$ for a five component system	45
3.2 Reduced Gibbs energy curve for a binary system	50
5.1 Component composition plot	74
5.2 CCE for a volatile/black oil vs. a gas condensate	75
5.3 DL experiment for a typical oil sample	77
5.4 Multi-stage separator test for a typical oil sample	79
5.5 ROV plots using commercial software	82
5.6 Oil FVF plots using commercial software	84
5.7 Solution GOR plots using commercial software	85

5.8 Two-phase envelope of the offshore Greek reservoir fluid (SRK-EOS)	90
5.9 Two-phase envelope of the offshore Greek reservoir fluid (PR-EOS)	90
5.10 Pressure plots with volume shift using commercial software	94
5.11 Density plots with volume shift using commercial software	95
5.12 H ₂ S composition plots with volume shift using commercial software	96
5.13 CH ₄ composition plots with volume shift using commercial software	97
5.14 C ₁₃₊ composition plots with volume shift using commercial software	98
5.15 Pressure plots with volume shift using MATLAB®	104
5.16 H ₂ S composition plots with volume shift using MATLAB®	105
5.17 CH ₄ composition plots with volume shift using MATLAB®	106
5.18 C ₁₃₊ composition plots with volume shift using MATLAB®	107
6.1 Software comparison of the calculated dew-point pressures for the SRK and PR EOS models with and without volume shift	110
A.1 Component property plot for the SRK and PR EOS fluid characterizations	122
A.2 Liquid volume & oil compressibility plots using commercial software	129
A.3 Oil and gas viscosity plots using commercial software	130
A.4 Oil and gas Z-factor plots using commercial software	131
A.5 Oil and gas density plots using commercial software	132
A.6 IFT and Y function plots using commercial software	133
A.7 Oil SG plots using commercial software	135
A.8 Oil viscosity plots using commercial software	136
A.9 Gas viscosity plots using commercial software	137
A.10 Oil and gas volume plots using commercial software	142
A.11 Oil and gas SG plots using commercial software	143
A.12 Oil and gas FVF plots using commercial PVT software	144
A.13 ROV and solution GOR plots using commercial software	145
A.14 Oil and gas viscosity plots using commercial software	146
A.15 Gas Z-factor and IFT plots using commercial software	147
A.16 Two-phase envelope of the offshore Greek reservoir fluid (un-tuned SRK-EOS)	151

A.17 Two-phase envelope of the offshore Greek reservoir fluid (un-tuned PR-EOS)	151
A.18 CO ₂ composition plots with volume shift using commercial software	159
A.19 N ₂ composition plots with volume shift using commercial software	160
A.20 C ₂ H ₆ composition plots with volume shift using commercial software	161
A.21 C ₃ H ₈ composition plots with volume shift using commercial software	162
A.22 IC ₄ composition plots with volume shift using commercial software	163
A.23 NC ₄ composition plots with volume shift using commercial software	164
A.24 IC ₅ composition plots with volume shift using commercial software	165
A.25 NC ₅ composition plots with volume shift using commercial software	166
A.26 FC ₆ composition plots with volume shift using commercial software	167
A.27 FC ₇ composition plots with volume shift using commercial software	168
A.28 FC ₈ composition plots with volume shift using commercial software	169
A.29 FC ₉ composition plots with volume shift using commercial software	170
A.30 FC ₁₀ composition plots with volume shift using commercial software	171
A.31 FC ₁₁ composition plots with volume shift using commercial software	172
A.32 FC ₁₂ composition plots with volume shift using commercial software	173
A.33 Pressure plots without volume shift using commercial software	181
A.34 Density plots without volume shift using commercial software	182
A.35 H ₂ S composition plots without volume shift using commercial software	183
A.36 CO ₂ composition plots without volume shift using commercial software	184
A.37 N ₂ composition plots without volume shift using commercial software	185
A.38 CH ₄ composition plots without volume shift using commercial software	186
A.39 C ₂ H ₆ composition plots without volume shift using commercial software	187
A.40 C ₃ H ₈ composition plots without volume shift using commercial software	188
A.41 IC ₄ composition plots without volume shift using commercial software	189

A.42 NC ₄ composition plots without volume shift using commercial software	190
A.43 IC ₅ composition plots without volume shift using commercial software	191
A.44 NC ₅ composition plots without volume shift using commercial software	192
A.45 FC ₆ composition plots without volume shift using commercial software	193
A.46 FC ₇ composition plots without volume shift using commercial software	194
A.47 FC ₈ composition plots without volume shift using commercial software	195
A.48 FC ₉ composition plots without volume shift using commercial software	196
A.49 FC ₁₀ composition plots without volume shift using commercial software	197
A.50 FC ₁₁ composition plots without volume shift using commercial software	198
A.51 FC ₁₂ composition plots without volume shift using commercial software	199
A.52 C ₁₃₊ composition plots without volume shift using commercial software	200
A.53 CO ₂ composition plots with volume shift using MATLAB®	210
A.54 N ₂ composition plots with volume shift using MATLAB®	211
A.55 C ₂ H ₆ composition plots with volume shift using MATLAB®	212
A.56 C ₃ H ₈ composition plots with volume shift using MATLAB®	213
A.57 IC ₄ composition plots with volume shift using MATLAB®	214
A.58 NC ₄ composition plots with volume shift using MATLAB®	215
A.59 IC ₅ composition plots with volume shift using MATLAB®	216
A.60 NC ₅ composition plots with volume shift using MATLAB®	217
A.61 FC ₆ composition plots with volume shift using MATLAB®	218
A.62 FC ₇ composition plots with volume shift using MATLAB®	219
A.63 FC ₈ composition plots with volume shift using MATLAB®	220

A.64 FC ₉ composition plots with volume shift using MATLAB®	221
A.65 FC ₁₀ composition plots with volume shift using MATLAB®	222
A.66 FC ₁₁ composition plots with volume shift using MATLAB®	223
A.67 FC ₁₂ composition plots with volume shift using MATLAB®	224
A.68 Pressure plots without volume shift using MATLAB®	232
A.69 H ₂ S composition plots without volume shift using MATLAB®	233
A.70 CO ₂ composition plots without volume shift using MATLAB®	234
A.71 N ₂ composition plots without volume shift using MATLAB®	235
A.72 CH ₄ composition plots without volume shift using MATLAB®	236
A.73 C ₂ H ₆ composition plots without volume shift using MATLAB®	237
A.74 C ₃ H ₈ composition plots without volume shift using MATLAB®	238
A.75 IC ₄ composition plots without volume shift using MATLAB®	239
A.76 NC ₄ composition plots without volume shift using MATLAB®	240
A.77 IC ₅ composition plots without volume shift using MATLAB®	241
A.78 NC ₅ composition plots without volume shift using MATLAB®	242
A.79 FC ₆ composition plots without volume shift using MATLAB®	243
A.80 FC ₇ composition plots without volume shift using MATLAB®	244
A.81 FC ₈ composition plots without volume shift using MATLAB®	245
A.82 FC ₉ composition plots without volume shift using MATLAB®	246
A.83 FC ₁₀ composition plots without volume shift using MATLAB®	247
A.84 FC ₁₁ composition plots without volume shift using MATLAB®	248
A.85 FC ₁₂ composition plots without volume shift using MATLAB®	249
A.86 C ₁₃₊ composition plots without volume shift using MATLAB®	250

List of Tables

5.1 Reservoir fluid feed composition	73
5.2 Experimental CCE data at 134.6°F	76
5.3 Experimental DL data at 134.6°F	77
5.4 Single-stage separator test for the offshore Greek reservoir fluid	79
5.5 Experimental single-stage separator data	79
5.6 Modified vs. initially correlated properties of the C ₁₃ + fraction	80
5.7 CCE experimental vs. calculated ROV's using commercial software	81
5.8 DL experimental vs. calculated FVF's and GOR's using commercial software	83
5.9 Experimental vs. calculated single-stage separator data using commercial software	86
5.10 Separator test calculation results for the SRK-EOS using commercial software	86
5.11 Separator test calculation results for the PR-EOS using commercial software	87
5.12 Saturation pressure calculation results for the SRK-EOS using commercial software	88
5.13 Saturation pressure calculation properties for the SRK-EOS using commercial software	88
5.14 Saturation pressure calculation results for the PR-EOS using commercial software	89
5.15 Saturation pressure calculation properties for the PR-EOS using commercial software	89
5.16 Two-phase flash calculation results using commercial software	91
5.17 Two-phase flash calculation properties using commercial software	91
5.18 Constant volume shift parameters for the SRK and PR EOS fluid characterizations	92

5.19 Reservoir pressure, saturation pressure and reservoir fluid density gradient results for the tuned SRK and PR EOS models with volume shift using commercial software	93
5.20 H ₂ S, CH ₄ , C ₁₃ + compositional gradient results for the tuned SRK and PR EOS models with volume shift using commercial software	93
5.21 Stability analysis results using MATLAB®	99
5.22 Saturation pressure calculation results for the SRK-EOS using MATLAB®	100
5.23 Saturation pressure calculation results for the PR-EOS using MATLAB®	101
5.24 Calculated vapor phase molar fractions using MATLAB®	101
5.25 Two-phase flash calculation results using MATLAB®	102
5.26 Reservoir and saturation pressure gradient results for the tuned SRK and PR EOS models with volume shift using MATLAB®	103
5.27 H ₂ S, CH ₄ , C ₁₃ + compositional gradient results for the tuned SRK and PR EOS models with volume shift using MATLAB®	103
A.1 Component properties for the SRK and PR EOS fluid characterizations	121
A.2 Binary interaction coefficients for the SRK-EOS fluid characterization	123
A.3 Binary interaction coefficients for the PR-EOS fluid characterization	124
A.4 CCE calculated results for the SRK-EOS using commercial software	125
A.5 CCE calculated results for the PR-EOS using commercial software	126
A.6 CCE calculated results for an un-tuned SRK-EOS using commercial software	127
A.7 CCE calculated results an un-tuned the PR-EOS using commercial software	128
A.8 DL experimental vs. calculated oil SG's using commercial software	134
A.9 DL experimental vs. calculated oil and gas viscosities using commercial software	134
A.10 DL calculated results for the SRK-EOS using commercial software	138
A.11 DL calculated results for the PR-EOS using commercial software	139
A.12 DL calculated results for an un-tuned SRK-EOS using commercial software	140

A.13 DL calculated results for an un-tuned PR-EOS using commercial software	141
A.14 Separator test calculation results for an un-tuned SRK-EOS using commercial software	148
A.15 Separator test calculation results for an un-tuned PR-EOS using commercial software	148
A.16 Experimental vs. calculated single-stage separator data using commercial software (un-tuned EOS models)	148
A.17 Saturation pressure calculation results for an un-tuned SRK-EOS using commercial software	149
A.18 Saturation pressure calculation properties for an un-tuned SRK-EOS using commercial software	149
A.19 Saturation pressure calculation results for an un-tuned PR-EOS using commercial software	150
A.20 Saturation pressure calculation properties for an un-tuned PR-EOS using commercial software	150
A.21 Un-tuned EOS two-phase flash calculation results using commercial software	152
A.22 Un-tuned EOS two-phase flash calculation properties using commercial software	152
A.23 CO ₂ , N ₂ , C ₂ H ₆ compositional gradient results for the tuned SRK and PR EOS models with volume shift using commercial software	153
A.24 C ₃ H ₈ , IC ₄ , NC ₄ compositional gradient results for the tuned SRK and PR EOS models with volume shift using commercial software	153
A.25 IC ₅ , NC ₅ , FC ₆ compositional gradient results for the tuned SRK and PR EOS models with volume shift using commercial software	154
A.26 FC ₇ , FC ₈ , FC ₉ compositional gradient results for the tuned SRK and PR EOS models with volume shift using commercial software	154
A.27 FC ₁₀ , FC ₁₁ , FC ₁₂ compositional gradient results for the tuned SRK and PR EOS models with volume shift using commercial software	155

A.28 Reservoir pressure, saturation pressure and reservoir fluid density gradient results for the un-tuned SRK and PR EOS models with volume shift using commercial software	155
A.29 H ₂ S, CO ₂ , N ₂ compositional gradient results for the un-tuned SRK and PR EOS models with volume shift using commercial software	156
A.30 CH ₄ , C ₂ H ₆ , C ₃ H ₈ compositional gradient results for the un-tuned SRK and PR EOS models with volume shift using commercial software	156
A.31 IC ₄ , NC ₄ , IC ₅ compositional gradient results for the un-tuned SRK and PR EOS models with volume shift using commercial software	157
A.32 NC ₅ , FC ₆ , FC ₇ compositional gradient results for the un-tuned SRK and PR EOS models with volume shift using commercial software	157
A.33 FC ₈ , FC ₉ , FC ₁₀ compositional gradient results for the un-tuned SRK and PR EOS models with volume shift using commercial software	158
A.34 FC ₁₁ , FC ₁₂ , C ₁₃ + compositional gradient results for the un-tuned SRK and PR EOS models with volume shift using commercial software	158
A.35 Reservoir pressure, saturation pressure and reservoir fluid density gradient results for the tuned SRK and PR EOS models without volume shift using commercial software	174
A.36 H ₂ S, CO ₂ , N ₂ compositional gradient results for the tuned SRK and PR EOS models without volume shift using commercial software	174
A.37 CH ₄ , C ₂ H ₆ , C ₃ H ₈ compositional gradient results for the tuned SRK and PR EOS models without volume shift using commercial software	175
A.38 IC ₄ , NC ₄ , IC ₅ compositional gradient results for the tuned SRK and PR EOS models without volume shift using commercial software	175
A.39 NC ₅ , FC ₆ , FC ₇ compositional gradient results for the tuned SRK and PR EOS models without volume shift using commercial software	176
A.40 FC ₈ , FC ₉ , FC ₁₀ compositional gradient results for the tuned SRK and PR EOS models without volume shift using commercial software	176
A.41 FC ₁₁ , FC ₁₂ , C ₁₃ + compositional gradient results for the tuned SRK and PR EOS models without volume shift using commercial software	177

A.42 Reservoir pressure, saturation pressure and reservoir fluid density gradient results for the un-tuned SRK and PR EOS models without volume shift using commercial software	177
A.43 H ₂ S, CO ₂ , N ₂ compositional gradient results for the un-tuned SRK and PR EOS models without volume shift using commercial software	178
A.44 CH ₄ , C ₂ H ₆ , C ₃ H ₈ compositional gradient results for the un-tuned SRK and PR EOS models without volume shift using commercial software	178
A.45 IC ₄ , NC ₄ , IC ₅ compositional gradient results for the un-tuned SRK and PR EOS models without volume shift using commercial software	179
A.46 NC ₅ , FC ₆ , FC ₇ compositional gradient results for the un-tuned SRK and PR EOS models without volume shift using commercial software	179
A.47 FC ₈ , FC ₉ , FC ₁₀ compositional gradient results for the un-tuned SRK and PR EOS models without volume shift using commercial software	180
A.48 FC ₁₁ , FC ₁₂ , C ₁₃ + compositional gradient results for the un-tuned SRK and PR EOS models without volume shift using commercial software	180
A.49 Saturation pressure calculation results for an un-tuned SRK-EOS using MATLAB®	201
A.50 Saturation pressure calculation results for an un-tuned PR-EOS using MATLAB®	202
A.51 Un-tuned EOS two-phase flash calculation results using MATLAB®	203
A.52 CO ₂ , N ₂ , C ₂ H ₆ compositional gradient results for the tuned SRK and PR EOS models with volume shift using MATLAB®	204
A.53 C ₃ H ₈ , IC ₄ , NC ₄ compositional gradient results for the tuned SRK and PR EOS models with volume shift using MATLAB®	204
A.54 IC ₅ , NC ₅ , FC ₆ compositional gradient results for the tuned SRK and PR EOS models with volume shift using MATLAB®	205
A.55 FC ₇ , FC ₈ , FC ₉ compositional gradient results for the tuned SRK and PR EOS models with volume shift using MATLAB®	205
A.56 FC ₁₀ , FC ₁₁ , FC ₁₂ compositional gradient results for the tuned SRK and PR EOS models with volume shift using MATLAB®	206
A.57 Reservoir and saturation pressure gradient results for the un-tuned SRK and PR EOS models with volume shift using MATLAB®	206

A.58 H ₂ S, CO ₂ , N ₂ compositional gradient results for the un-tuned SRK and PR EOS models with volume shift using MATLAB®	207
A.59 CH ₄ , C ₂ H ₆ , C ₃ H ₈ compositional gradient results for the un-tuned SRK and PR EOS models with volume shift using MATLAB®	207
A.60 IC ₄ , NC ₄ , IC ₅ compositional gradient results for the un-tuned SRK and PR EOS models with volume shift using MATLAB®	208
A.61 NC ₅ , FC ₆ , FC ₇ compositional gradient results for the un-tuned SRK and PR EOS models with volume shift using MATLAB®	208
A.62 FC ₈ , FC ₉ , FC ₁₀ compositional gradient results for the un-tuned SRK and PR EOS models with volume shift using MATLAB®	209
A.63 FC ₁₁ , FC ₁₂ , C ₁₃ + compositional gradient results for the un-tuned SRK and PR EOS models with volume shift using MATLAB®	209
A.64 Reservoir and saturation pressure gradient results for the tuned SRK and PR EOS models without volume shift using MATLAB®	225
A.65 H ₂ S, CO ₂ , N ₂ compositional gradient results for the tuned SRK and PR EOS models without volume shift using MATLAB®	225
A.66 CH ₄ , C ₂ H ₆ , C ₃ H ₈ compositional gradient results for the tuned SRK and PR EOS models without volume shift using MATLAB®	226
A.67 IC ₄ , NC ₄ , IC ₅ compositional gradient results for the tuned SRK and PR EOS models without volume shift using MATLAB®	226
A.68 NC ₅ , FC ₆ , FC ₇ compositional gradient results for the tuned SRK and PR EOS models without volume shift using MATLAB®	227
A.69 FC ₈ , FC ₉ , FC ₁₀ compositional gradient results for the tuned SRK and PR EOS models without volume shift using MATLAB®	227
A.70 FC ₁₁ , FC ₁₂ , C ₁₃ + compositional gradient results for the tuned SRK and PR EOS models without volume shift using MATLAB®	228
A.71 Reservoir and saturation pressure gradient results for the un-tuned SRK and PR EOS models without volume shift using MATLAB®	228
A.72 H ₂ S, CO ₂ , N ₂ compositional gradient results for the un-tuned SRK and PR EOS models without volume shift using MATLAB®	229
A.73 CH ₄ , C ₂ H ₆ , C ₃ H ₈ compositional gradient results for the un-tuned SRK and PR EOS models without volume shift using MATLAB®	229

A.74 IC ₄ , NC ₄ , IC ₅ compositional gradient results for the un-tuned SRK and PR EOS models without volume shift using MATLAB®	230
A.75 NC ₅ , FC ₆ , FC ₇ compositional gradient results for the un-tuned SRK and PR EOS models without volume shift using MATLAB®	230
A.76 FC ₈ , FC ₉ , FC ₁₀ compositional gradient results for the un-tuned SRK and PR EOS models without volume shift using MATLAB®	231
A.77 FC ₁₁ , FC ₁₂ , C ₁₃₊ compositional gradient results for the un-tuned SRK and PR EOS models without volume shift using MATLAB®	231

Chapter 1

Introduction

1.1 Oil and Gas Composition

1.1.1 Chemical Composition

The branch of Chemistry associated with the study of organic compounds and their physical and chemical properties is called Organic Chemistry. All organic compounds are comprised of at least one Carbon (C) atom bonded with elements such as Hydrogen (H), Oxygen (O), Nitrogen (N), Sulfur (S), etc. Compounds comprised in their entirety of Carbon and Hydrogen are called hydrocarbons and constitute the main components of oil and natural gas. Every Carbon atom is able to form four single bonds, two double bonds, or one triple bond combined with a single one [1]. The simplest and most common hydrocarbon found in nature is Methane (CH_4), consisting of one Carbon and four Hydrogen atoms (Figure 1.1).

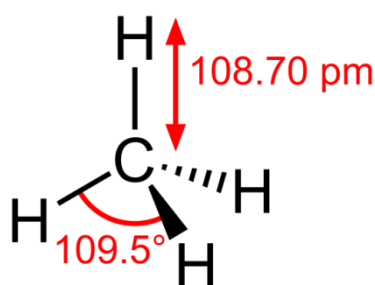


Figure 1.1: Methane, the simplest hydrocarbon compound (Source: [Wikimedia Commons](#))

Methane belongs to the functional group known as the Alkanes or Paraffins (Methane, Ethane, Propane, Butane, Octane, etc.), a group consisting only of single bonds (saturated hydrocarbons). Other hydrocarbon functional groups are the Alkenes or Olefins (Ethylene, Propylene, etc.) with at least one double bond, the Alkynes (Acetylene, etc.) with at least one triple bond (unsaturated

hydrocarbons) and the Naphthenes and Aromatics (Benzene, etc.), with multiple bonds and cyclic structures.

Hydrocarbons with up to four Carbon atoms are considered “light” and are usually found in nature in gaseous form, being easier to break down, while those with five or more Carbon atoms are considered the “heavy” ones, found in liquid or solid state and harder to break down [1]. In Reservoir Engineering (see Sec. 1.5), the heaviest components are often lumped into a “plus” fraction – usually the heptanes-plus fraction, denoted as C_{7+} .

1.1.2 Reservoir Fluid Composition

Reservoir fluids are natural mixtures of crude oil and natural gas found in elevated pressures and temperatures. They usually contain hundreds of thousands of hydrocarbon compounds and often come along with heterocomponents (non-hydrocarbon compounds) such as Hydrogen Sulfide (H_2S), Carbon Dioxide (CO_2), Nitrogen (N_2), etc., with water presence being certain at nearly all times. Natural gas mainly contains light Alkanes (Methane, etc.), Nitrogen, Carbon Dioxide and Hydrogen Sulfide. Crude oil mainly contains intermediate and heavier types of hydrocarbons, Nitrogen, Oxygen, Sulfur and trace metals. Reservoir oils also contain amounts of dissolved gas, as well as tars and asphalts (bitumen, pitch, waxes and resins). The latter constitute complex colloidal solid/semi-solid mixtures of Carbides, Carbenes, Asphaltenes and Maltenes [2].

1.2 Oil and Gas Origins

Oil and gas deposits are located in underground and undersea reservoirs, trapped under natural sealants –impervious rocks that do not allow water or other liquids to flow through them [1]. There are five essential elements for the formation of a typical hydrocarbon system (Figure 1.2):

- Source rocks –rocks at great depths where hydrocarbons were formed
- Migration –the process at which hydrocarbons move toward reservoir rocks
- Reservoir rocks –porous and permeable “sponge like” rocks where hydrocarbons reside
- Traps –geological structures encasing the hydrocarbons
- Cap rocks –impermeable sealants that prevent hydrocarbons from escaping

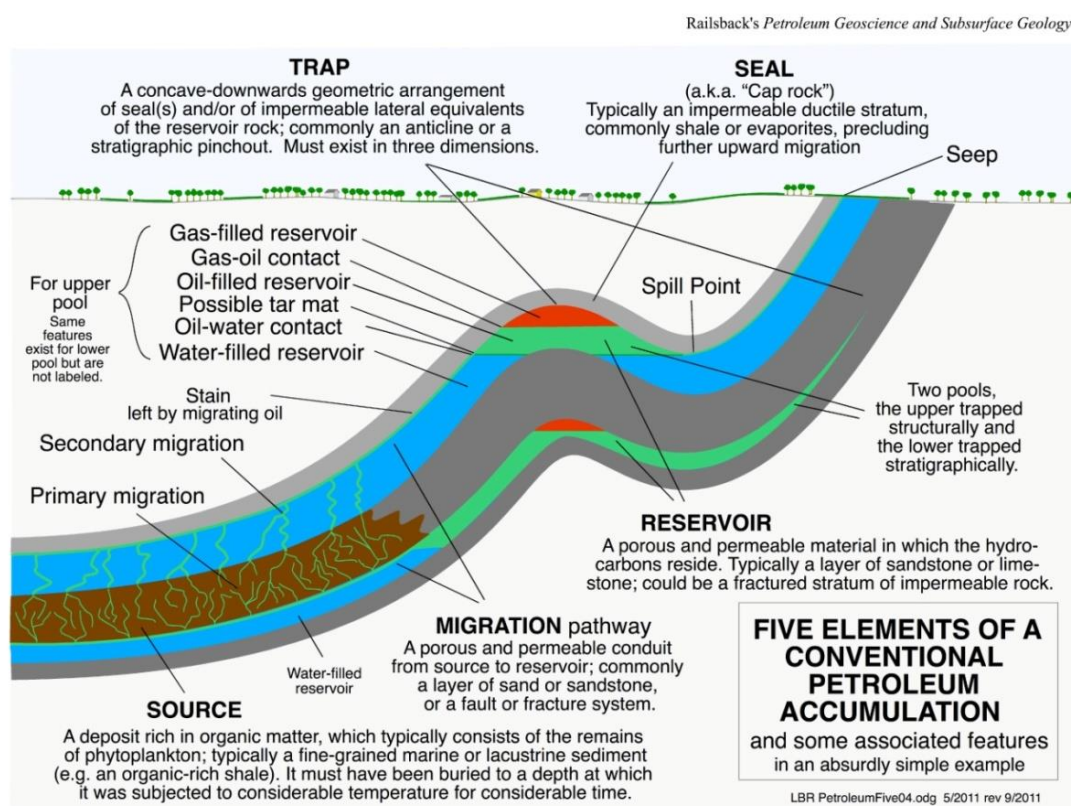


Figure 1.2: Five elements of a conventional petroleum accumulation (Source: Railsback [3])

1.2.1 Source Rocks

Oil and gas are formed inside the source rocks, which are non-permeable rocks rich in organic matter that will eventually be transformed into hydrocarbon compounds [1]. This organic matter is known as Kerogen, the type of which will affect the type of hydrocarbons that will form.

1.2.2 Migration

Hydrocarbons –like any other fluid– tend to move from high pressure fields to lower pressure ones through cracks, pores or bedding planes until they reach the surface through oil seeps and gas chimneys or become entrapped inside the reservoirs. This is the process of migration and is made up of two stages: primary and secondary migration. Primary migration is caused by micro-fracturing and consists of the release of oil and its movement through the narrow pores of mature source rocks. The subsequent oil movement through the wider pores into either reservoir rocks or the surface is called secondary migration and its primary cause is buoyancy caused by different fluid densities due to capillary pressure [1].

1.2.3 Reservoir Rocks

A plain rock must have the following characteristics in order to be considered a reservoir rock [1]:

- Petrophysical properties (porosity, permeability, etc.)
- Natural hydrocarbon accumulation
- Natural sealant (cap rock or aquifer barrier)
- Natural pre-production pressure conditions

The most usual types of reservoir rocks are sedimentary rocks (sandstones, carbonates), as they are the most porous and also inhabit depths where conditions are suitable for oil and gas preservation. Distribution of oil and gas inside the reservoir occurs in three layers: natural gas –being the lightest– is on the top layer, crude oil –which is heavier– stays in the middle one, whereas the bottom layer is occupied by water –being the heaviest fluid of three.

1.2.4 Traps

Traps are defined as geological structures created as a result of underground deformations in the earth's crust that obstruct the upward movement of hydrocarbons and force them to accumulate inside reservoir rocks. Hydrocarbon traps can either be structural (faults, anticlines, domes) or stratigraphic traps (Figure 1.3).

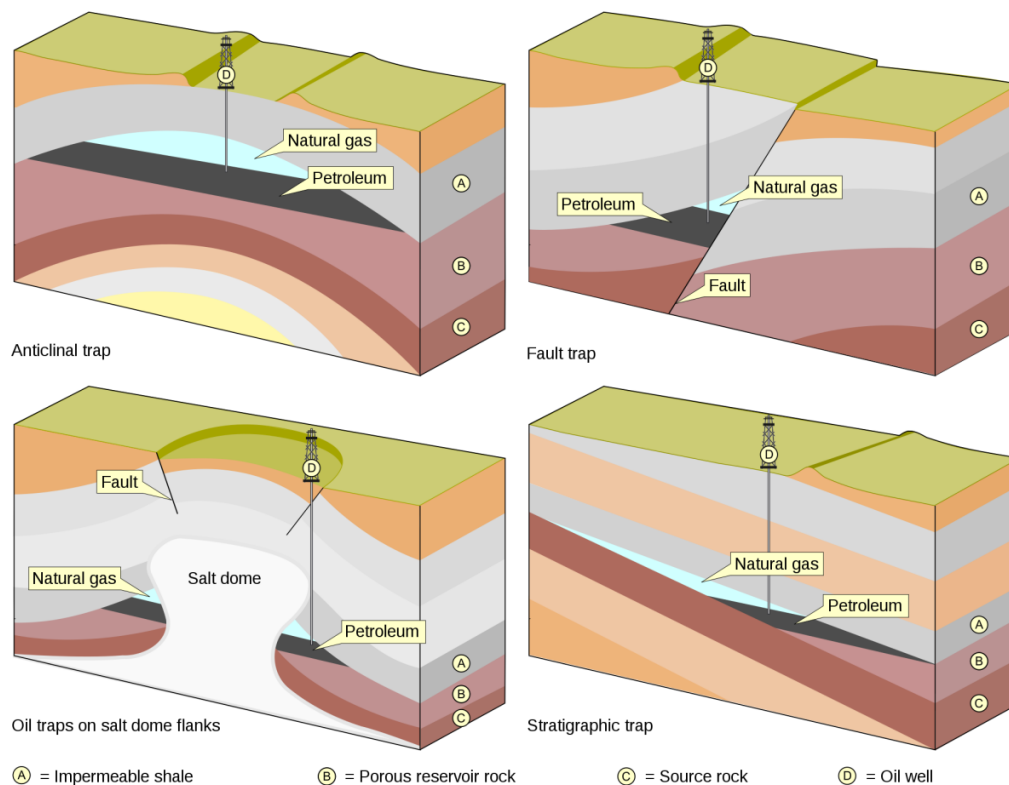


Figure 1.3: Four types of hydrocarbon traps (Source: [Wikimedia Commons](#))

1.2.5 Cap Rocks

Cap rocks are impermeable layers in the upper reservoir that halt the movement of hydrocarbons and prevent further migration or escape to the surface. This is a result of natural sealants having a capillary pressure greater than or equal to the buoyancy pressure of the moving oil and gas. If buoyancy pressure exceeds capillary pressure, natural seepage occurs until buoyancy pressure drops causing the rock to re-seal [1].

1.3 Petrophysical Properties

The basic petrophysical properties concerning a petroleum engineer when studying a typical formation are:

- Porosity
- Permeability
- Saturation

1.3.1 Porosity

All types of rocks have openings of various shapes and sizes throughout them called pores. The total volume occupied by those pores is called porosity and rocks that contain a large percentage of that volume are considered highly porous. However, effective porosity is the one contributing to oil production, representing the amount of pores that are interconnected and/or connected to other formations [1]. It is a key property regarding the storage of oil and gas inside the reservoir rock.

1.3.2 Permeability

The ability of a porous medium to make a fluid flow through itself is called permeability. Permeability depends on the characteristics of the porous medium and varies through both the vertical and horizontal dimensions. The most common unit of permeability in Petroleum Engineering is the Darcy (D) or the milliDarcy (mD).

1.3.3 Saturation

It is believed that in most reservoirs, pore spaces were filled with water prior to migration. Moving in, hydrocarbons replaced a large amount of water

before reaching a state of equilibrium with the remaining water inside the pore spaces (connate water). Fluid saturation is a key factor in reserves estimation and is expressed as the volume of oil, gas or water divided by the overall pore volume.

1.4 Oil and Gas Units and Measurements

1.4.1 Pressure

Pressure, denoted as p , is the shear force applied to a surface per unit area. Absolute pressure is the pressure zero-referenced to a complete vacuum measured in an absolute scale and is equal to gauge pressure plus atmospheric pressure. Gauge pressure is the pressure zero-referenced to ambient air pressure and is equal to absolute pressure minus atmospheric pressure. Typical pressure units of measurement include the following: Pa (N/m^2), psi (lbf/in^2), bar, atm. The most common field unit for pressure is the psi, expressed either as an absolute (psia), or as a gauge (psig) pressure. Whatever the unit, it should always be denoted if the measured pressure is absolute or gauge pressure.

1.4.2 Volume

Volume, denoted as V , is the quantity of three-dimensional space encased by a closed surface, or generally understood as the space occupied by a certain substance or mixture. The most common units of measurement for volume are: litres (L), cubic meters (m^3), cubic feet (ft^3), gallons (gal) and barrels (bbl). Standard oilfield units for oil and gas respectively are: barrels (bbl) –reservoir barrels (RB) when referring to reservoir conditions, or stock tank barrels (STB) when referring to stock tank conditions; and cubic feet (ft^3) –standard cubic feet (scf) when referring to standard conditions (14.7 psi and 60°F).

1.4.3 Temperature

Temperature, denoted as T , is the manifestation of thermal energy and the physical property that expresses hot and cold. There are four basic temperature scales: Celsius ($^{\circ}\text{C}$), Fahrenheit ($^{\circ}\text{F}$), Kelvin (K) and Rankine ($^{\circ}\text{R}$), with the last two being absolute scales. A change in temperature in the Celsius scale is the same as in Kelvin, whereas a change in Fahrenheit is the same as in the Rankine scale. The most common temperature scales used in Petroleum Engineering are the Fahrenheit and Rankine scales.

1.4.4 Standard Conditions

Pressure and temperature present considerable variations from place to place around the globe. Hence, it is crucial that standard reference conditions for pressure and temperature be defined when it comes to measuring and documenting physical and chemical processes. Standard Temperature and Pressure (STP) was established by IUPAC (International Union of Pure and Applied Chemistry) for this cause. STP is defined as air at temperature of 32°F (0°C) and pressure of 100 kPa (1 bar). Petroleum Engineering applications broadly use the Imperial system where STP is defined as air at temperature of 60°F (15.6°C) and pressure of 14.7 psia (1 atm).

1.5 Reservoir Engineering

Reservoir Engineering is the field of Petroleum Engineering that applies scientific principles to the flow of fluids through porous media during field development and reservoir production in order to acquire the highest economic recovery. Its main goals are the assessment of the available oil and gas reserves (e.g. hydrocarbons initially in place), the study of reservoir behavior (e.g. reservoir drainage, evolution of reservoir pressure, etc.) and the optimization of field development [1].

Reservoir engineering implements various techniques such as core analysis, well logging, fluid sampling, etc. in order to confirm the presence of oil and gas and also acquire the desirable reservoir data (PVT data, reservoir thickness, pay zone, etc.). The sampled reservoir fluids are analyzed for their composition, viscosity, saturation pressure (bubble-point or dew-point pressure), formation volume factor (FVF), etc. PVT (Pressure-Volume-Temperature) analysis performed on reservoir fluids aims to determine their chemical and physical characteristics and predict their behavior at different conditions of pressure and temperature [1]. Throughout production, reservoir temperature is assumed to be constant while reservoir pressure is gradually decreased, with the remaining hydrocarbons inside the reservoir changing in composition, volumetric properties and phase behavior.

Reservoir Simulation

Reservoir Simulation is the branch of Reservoir Engineering that involves the construction and/or utilization of numerical models in order to predict reservoir fluid behavior inside porous media and therefore decide the optimal field development plan before the start of production. Equation of State (EOS) compositional simulation (see Chap. 3) –a subject that largely concerns the current thesis– became possible with the introduction of the first supercomputers in the early 1980's [4] [5]. Several reservoir simulation softwares that incorporate EOS compositional simulation exist, including both commercial and open-source (OSS) softwares.

Chapter 2

Reservoir Fluid Volumetric and Phase Behavior

2.1 Reservoir Fluid Phase Diagrams

Reservoir fluids display a variety of different behaviors over a wide range of pressures and temperatures. When combined with the petrophysical properties of reservoir rocks, they result in various reservoir types that exhibit multi-phase behavior. In order to study the phase behavior of these fluids, x-y diagrams are utilized. Each dimension represents a thermodynamic variable (e.g. Pressure, Volume, Temperature), with Pressure-Volume (p-V) and Pressure-Temperature (p-T) diagrams most widely used. Pressure-Temperature (p-T) diagrams are mainly used for the classification of reservoir fluid systems (phase envelope construction).

2.1.1 The Gibbs Phase Rule

According to the Gibbs phase rule [6], the number of degrees of freedom (i.e. the number of independent intensive variables) of a given system with pressure p and temperature T is:

$$F = C - P + 2 \quad (2.1)$$

where C is the number of components and P the number of phases (gas, liquid, solid). By specifying F , one is able to determine the system's thermodynamic state of equilibrium. In order for equilibrium to be attained, pressure, temperature and the chemical potentials of components are assumed to be uniform in all of the system's phases (i.e. zero mass transfer).

For a two-phase single-component system ($F=1$), only pressure or temperature needs to be found in order to define the system's thermodynamic state. In the same way, for a two-phase two-component system ($F=2$), both pressure and temperature need to be determined for the same cause. As a result, one is able to assume that for a two-phase n -component system, except for pressure and temperature, $n-2$ variables must be defined in order to find the system's thermodynamic state of equilibrium. For a system with more than two phases, the amount of variables that need to be specified is $n-P$ [2].

The previous rule neglects the effect of gravity and other types of energy fields upon the system. If one takes into consideration the gravitational effect (e.g. when studying compositional grading), the rule becomes [7]:

$$F = C - P + 3 \quad (2.2)$$

2.1.2 Pure Substances

p-V diagram

Figure 2.1 is a p-V diagram of Ethane at three different temperatures (60°F, 90°F and 110°F), with the area encased by the envelope being the two-phase region ($F=1$), where the fluid has the properties of both a liquid and a gas. The area on the left is the liquid region ($F=2$) –where the fluid behaves like a liquid– whereas the area on the right is the vapor region ($F=2$) –where the fluid behaves like a gas.

Starting from the liquid region with a fixed temperature of 60°F, successive increases in volume result in the drop of pressure following the 60°F isothermal curve until the bubble-point (point A) is reached. At this point, the first bubble of gas is released from the liquid, making the system a saturated liquid in equilibrium with an infinitesimal amount of saturated gas. Until this point, any slight increase in volume results in a large decrease in pressure due to liquids having a small compressibility factor (see Sec. 2.3.4). However, the

discontinuity in the system's volumetric behavior at the bubble-point results in a significant increase in compressibility [8].

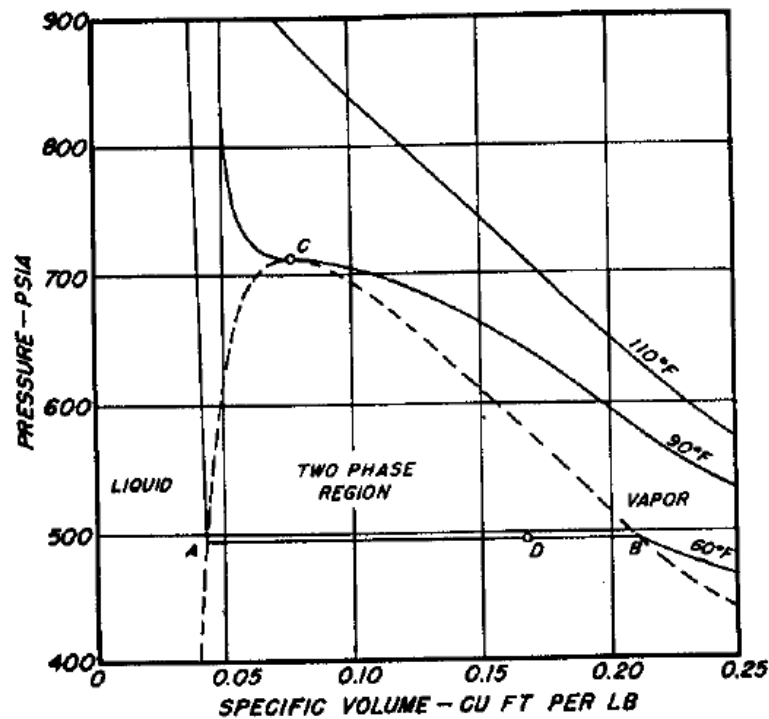


Figure 2.1: p-V diagram for Ethane (Source: Standing [9])

From this point on, any further increase in volume does not affect pressure ($F=1$), yet the amount of saturated gas being released from the liquid to the vapor phase is proportionally ever-increasing until the dew-point (point B) is reached. At this point, the last droplet of liquid is left inside the gas, making the system a saturated gas in equilibrium with an infinitesimal amount of saturated liquid. Any further increase in volume slightly reduces pressure due to the high compressibility of gases. One can repeat the previous experiment with another fixed temperature, which will result in an isothermal curve either above ($T_2 > T_1$) or below ($T_2 < T_1$) the previous temperature.

In the case of single-component systems, bubble-point pressure always equals dew-point pressure. The bubble-point curve (curve AC) –where the fluid is a saturated liquid– and the dew-point curve (curve CB) –where the fluid is a saturated gas– converge and meet at the critical point (point C). At this point,

both phases coexist in a critical mixture (i.e. their intensive properties are equal) and are indistinguishable.

p-T diagram

Figure 2.2 is a p-T diagram for a single component system in the region of vapor/liquid behavior near the critical point (point C: p_c =critical pressure, T_c =critical temperature –see Sec. 2.3.2).

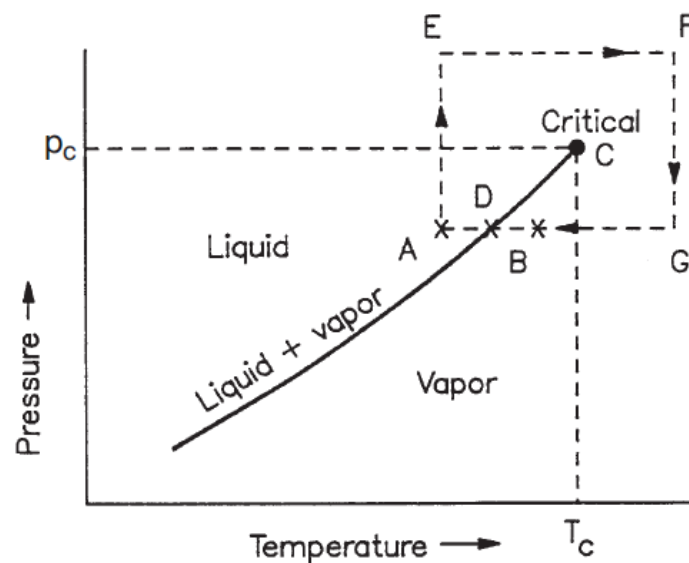


Figure 2.2: p-T diagram for a single component system (Source: Whitson & Brule [2])

Along the vapor pressure curve (liquid+vapor curve), the liquid and vapor phase of the fluid coexist in equilibrium until the end of the curve at the critical point. Above and to the left of the curve, the fluid has the properties of a liquid; while below and to the right of it the fluid has those of a gas.

p-V-T diagram

Figure 2.3 shows a p-V-T three-dimensional diagram for a pure compound, where temperature has been added as the third dimension to the p-V diagram.

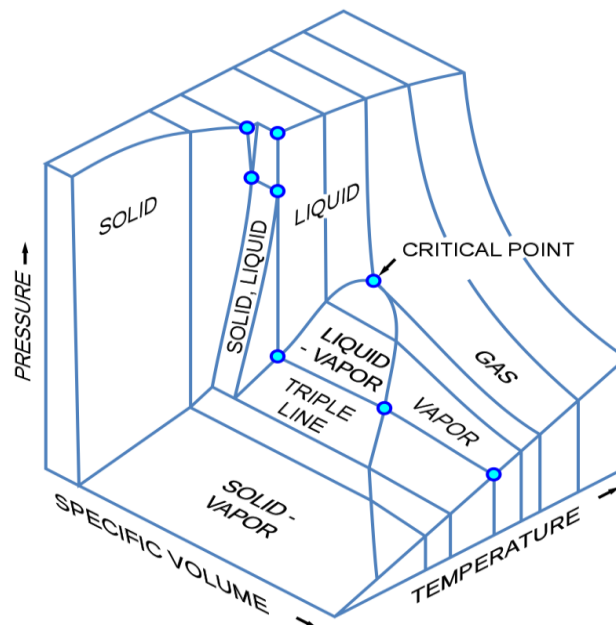


Figure 2.3: p-V-T diagram for a pure compound (Source: [Wikimedia Commons](#))

2.1.3 Binary and Multi-Component Systems

In the case of a binary or multi-component system, bubble-point pressure no longer equals dew-point pressure. This is illustrated in the p-V diagrams of Figure 2.4, which compares p-V and p-T diagrams between single components and mixtures. In the p-T diagram for mixtures, the vapor pressure curve no longer exists and a phase envelope has now taken its place, formed by the bubble-point curve (the curve that separates the liquid from the two-phase region) and the dew-point curve (the curve that separates the vapor from the two-phase region) intersecting at the critical point (point C: p_c , T_c). The area encased by the envelope represents the two-phase region. Above and to the left of the envelope the fluid behaves like a liquid and below and to the right of it behaves like a gas, similarly to the vapor pressure curve in the single component case.

Moreover, for binary and multi-component systems, the two-phase region can exist in pressures and temperatures greater than the critical pressure and temperature (beyond the critical point). This region is known as the

supercritical region, where distinct liquid and vapor phases do not exist and the fluid is supposed to be neither a liquid nor a gas, but a supercritical mixture. As a result, the highest pressure and temperature at which the two phases can coexist must be defined. They are defined as cricondenbar and cricondentherm respectively.

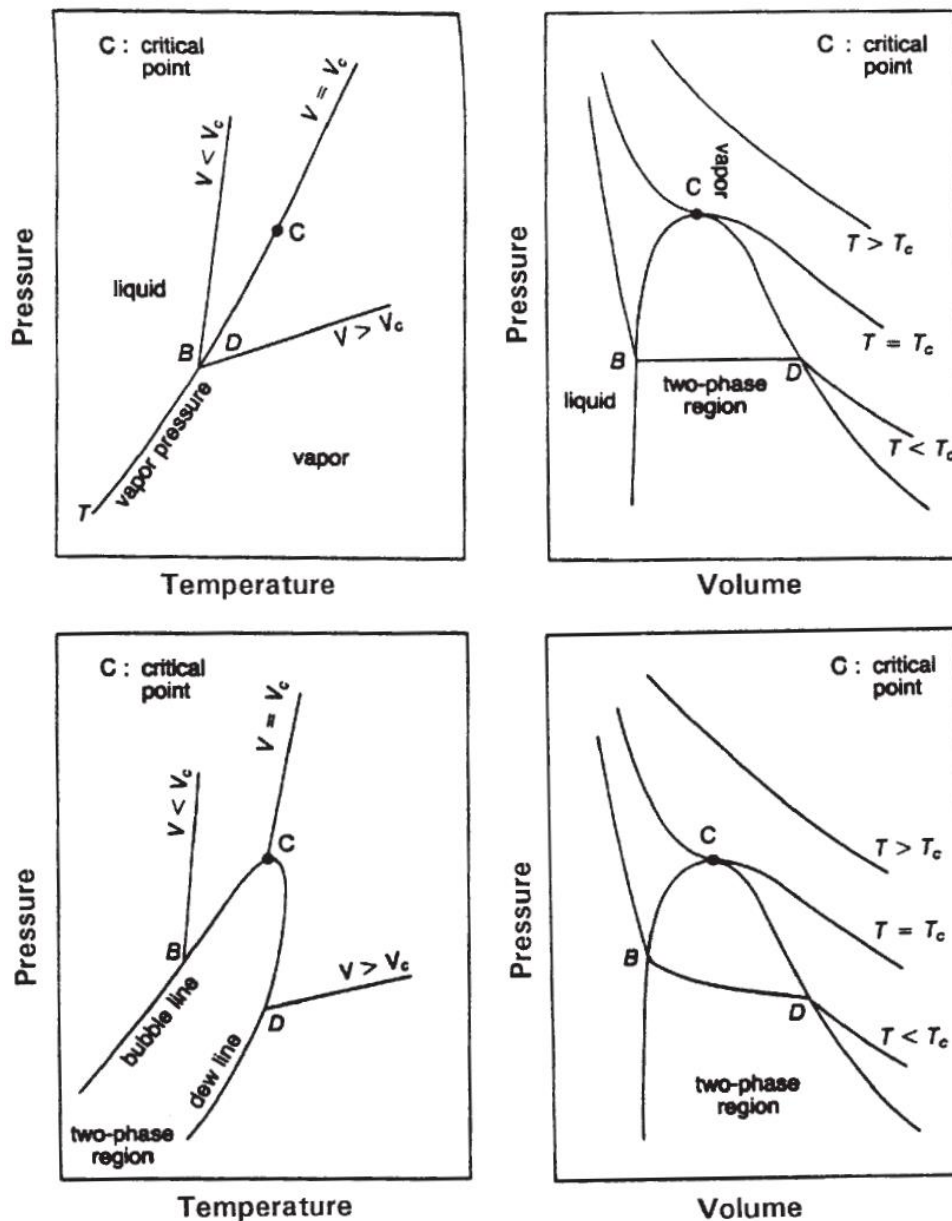


Figure 2.4: Phase diagrams for pure components vs. mixtures (Source: Whitson & Brule [2])

The shape of the phase envelope and the location of the critical point are both dependent on the composition of the mixture. Also, the critical pressures of most mixtures are higher than the critical pressures of their individual

components [2]. A typical p-T diagram of a multi-component system is shown in Figure 2.5. The percentage curves inside the envelope are called quality lines. They represent equal volumes of liquid within the mixture and all converge at the critical point.

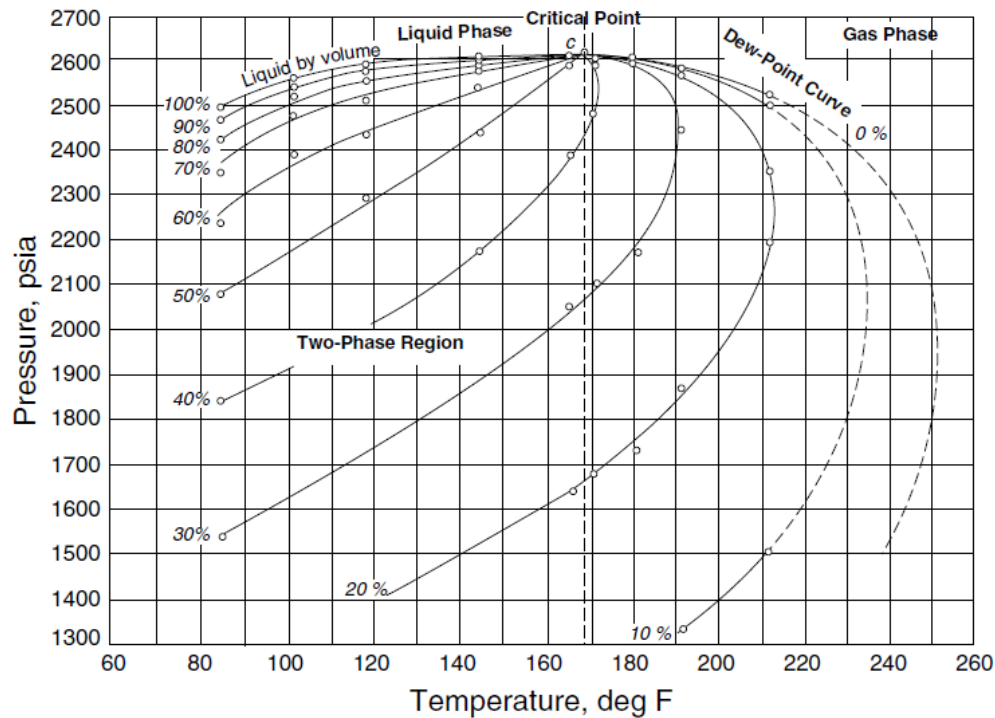


Figure 2.5: Phase envelope of a multi-component system (Source: Ahmed [10])

2.2 Reservoir Fluid Classification

Reservoir fluids can be classified regarding their chemical complexity into the following general categories:

- Black Oil
- Volatile Oil
- Gas Condensate
- Wet Gas
- Dry Gas

This classification is made on the basis of the location of: (1) the initial reservoir conditions and (2) the surface conditions (first stage separator), all with respect to the p-T diagram of the fluid.

2.2.1 Black Oil

Ordinary black oil

A crude oil is classified as an ordinary black oil when the reservoir temperature is smaller than the critical temperature of the mixture and the quality lines of the phase envelope are equally spaced [10]. A typical ordinary black oil p-T diagram is shown in Figure 2.6.

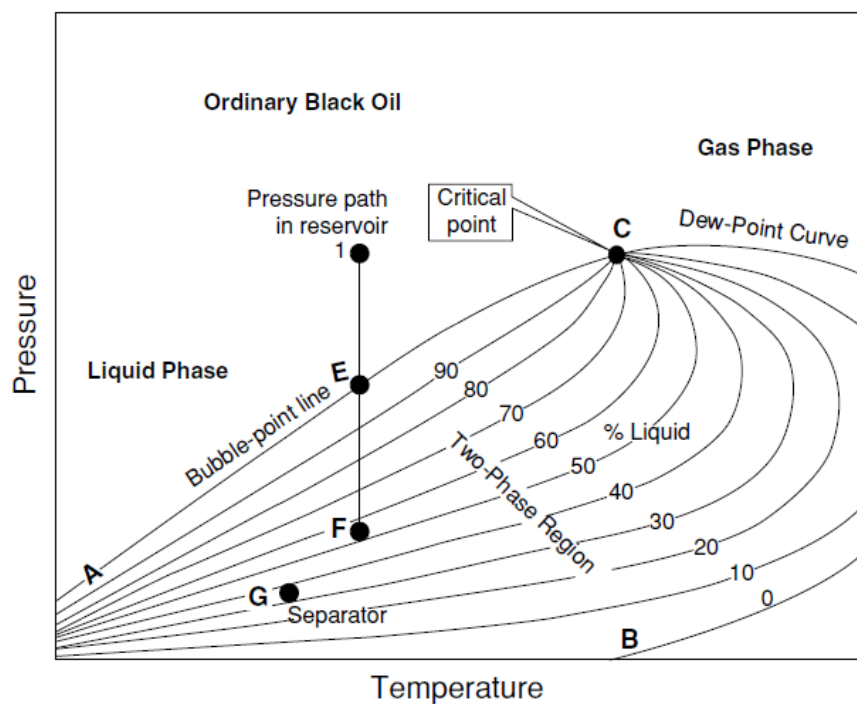


Figure 2.6: Phase envelope of an ordinary black oil (Source: Ahmed [10])

Low-shrinkage crude oil

A crude oil is classified as a low-shrinkage oil when the reservoir temperature is smaller than the critical temperature but the quality lines are

closely spaced near the dew-point curve [10]. A typical low-shrinkage oil p-T diagram is shown in Figure 2.7.

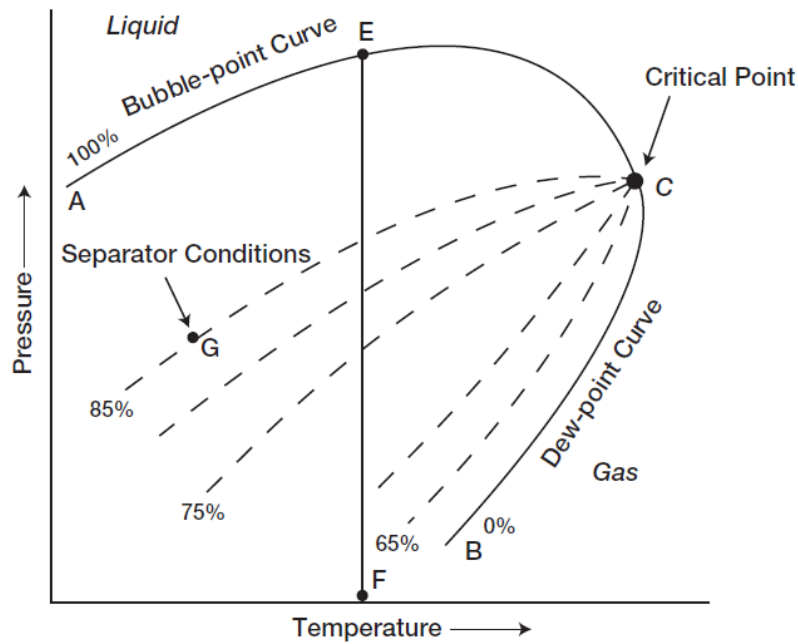


Figure 2.7: Phase envelope of a low-shrinkage crude oil (Source: Ahmed [10])

2.2.2 Volatile Oil

Volatile crude oil

A crude oil is classified as a volatile oil (high-shrinkage oil) when the reservoir temperature is smaller than the critical temperature but the quality lines are closely spaced near the bubble-point curve and more widely spaced at lower pressures. This results in a high shrinkage of liquid during production [10]. A typical volatile oil p-T diagram is shown in Figure 2.8.

Near-critical crude oil

A crude oil is classified as a near-critical oil when the reservoir temperature is smaller than but really close to the critical temperature while the quality lines are closely spaced near the bubble-point curve and more widely spaced at

lower pressures. A high shrinkage of liquid is also present in this case [10]. A typical near-critical oil p-T diagram is shown in Figure 2.9.

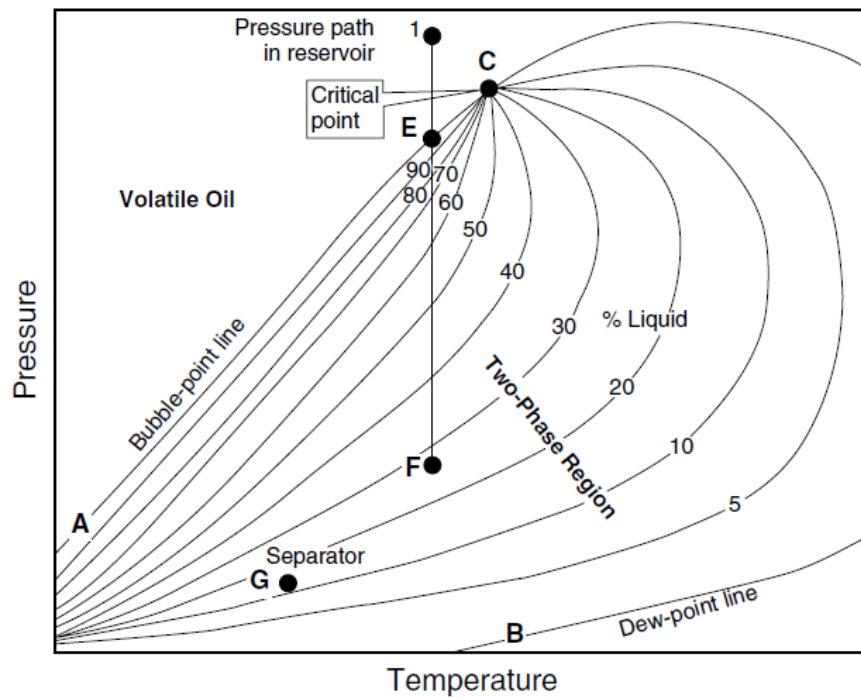


Figure 2.8: Phase envelope of a volatile crude oil (Source: Ahmed [10])

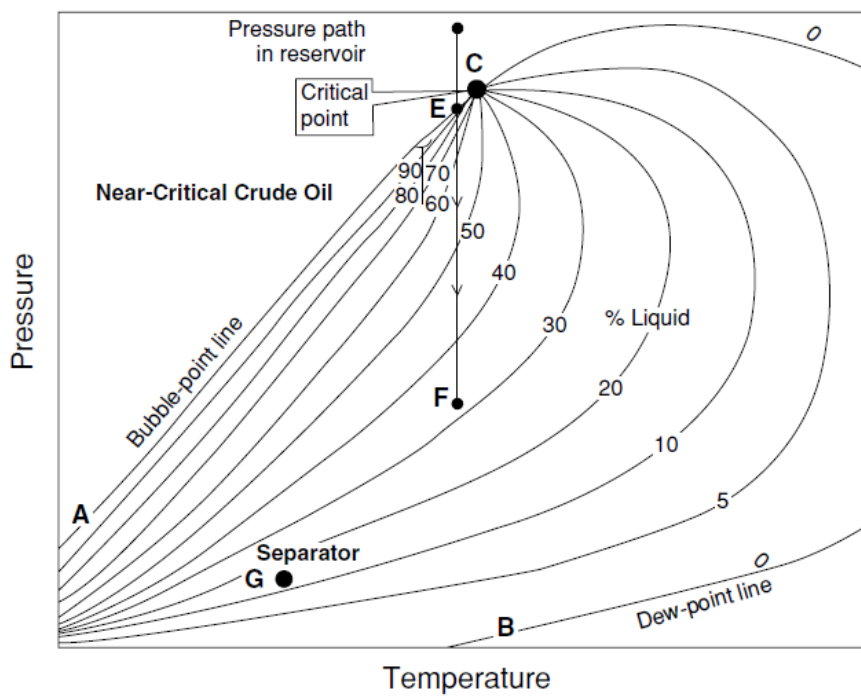


Figure 2.9: Phase envelope of a near-critical crude oil (Source: Ahmed [10])

2.2.3 Gas Condensate

Retrograde gas condensate

A natural gas is classified as a retrograde gas condensate when the reservoir temperature is greater than the critical temperature and smaller than the cricondentherm [10]. This is a special occasion of natural gas that when produced condenses instead of expanding. The previous process is known as retrograde condensation [11] and is illustrated in Figure 2.10.

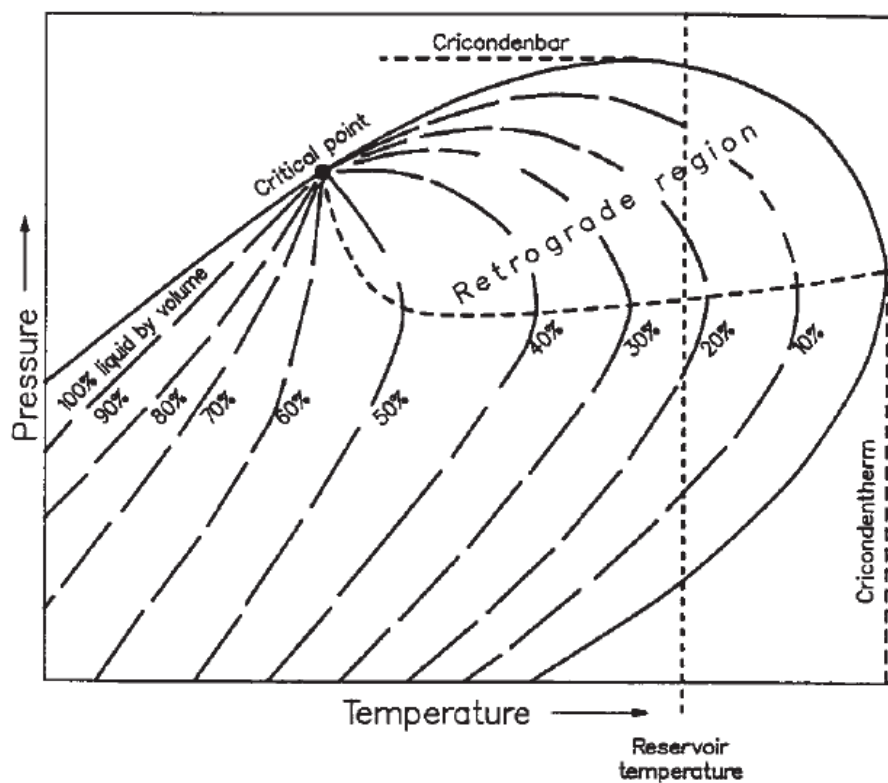


Figure 2.10: Phase envelope of a retrograde gas condensate (Source: Whitson & Brule [2])

Starting from an initial pressure point in the vapor region, as pressure drops isothermally, the upper dew-point is reached. At this point, the attraction between the heavy molecules is greater than the attraction between the light and the heavy ones. This causes the heavy molecules to move to the liquid zone apart from the light ones. As pressure drop continues, a point is reached where maximum liquid dropout occurs. The dashed curve represents the lower limit of the retrograde behavior region. Further drop of pressure results in the

normal vaporization process, where liquid molecules start moving to the vapor phase until the lower dew-point is reached. Retrograde condensation only exists in binary and multi-component mixtures.

Near-critical gas condensate

A natural gas is classified as a near-critical gas condensate when the reservoir temperature is greater than but really close to the critical temperature and smaller than the cricondenthem. When the fluid is produced, it results in a swift formation of liquid just below the dew-point curve due to the quality lines being closely spaced near the critical point [10]. A typical near-critical gas condensate p-T diagram is shown in Figure 2.11.

2.2.4 Wet Gas

A natural gas is classified as a wet gas when the reservoir temperature is greater than the cricondenthem but the surface conditions are inside the two-phase region [2]. This is a result of the heavy molecules having a low kinetic energy causing them to attract and form into liquid when both pressure and temperature drop during production [10]. A typical wet gas p-T diagram is shown in Figure 2.12.

2.2.5 Dry Gas

A natural gas is classified as a dry gas when the reservoir temperature is greater than the cricondenthem and the surface conditions are outside the two-phase region [2]. A typical dry gas p-T diagram is shown in Figure 2.13.

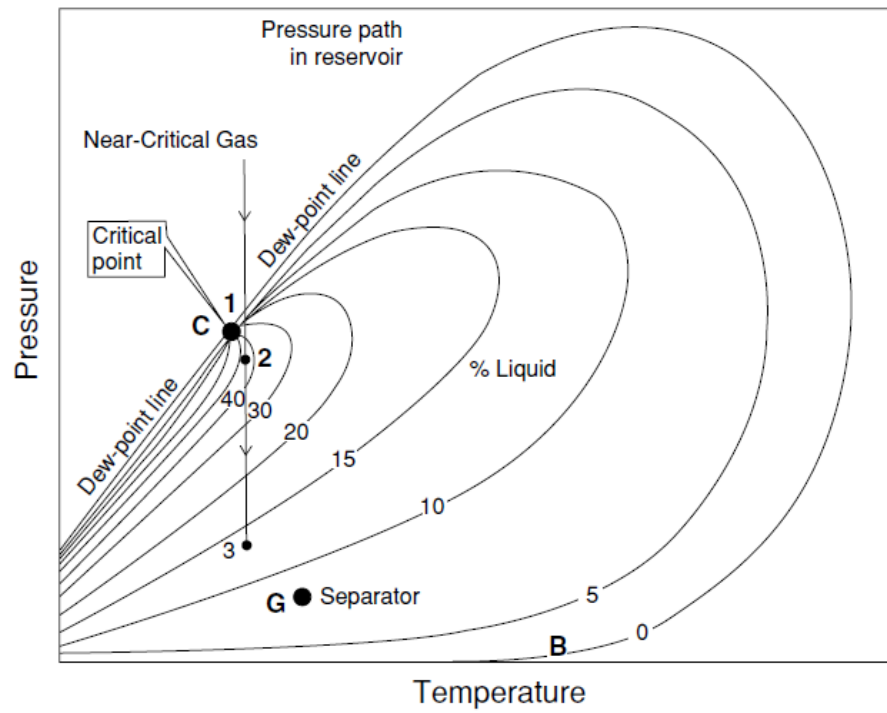


Figure 2.11: Phase envelope of a near-critical gas condensate (Source: Ahmed [10])

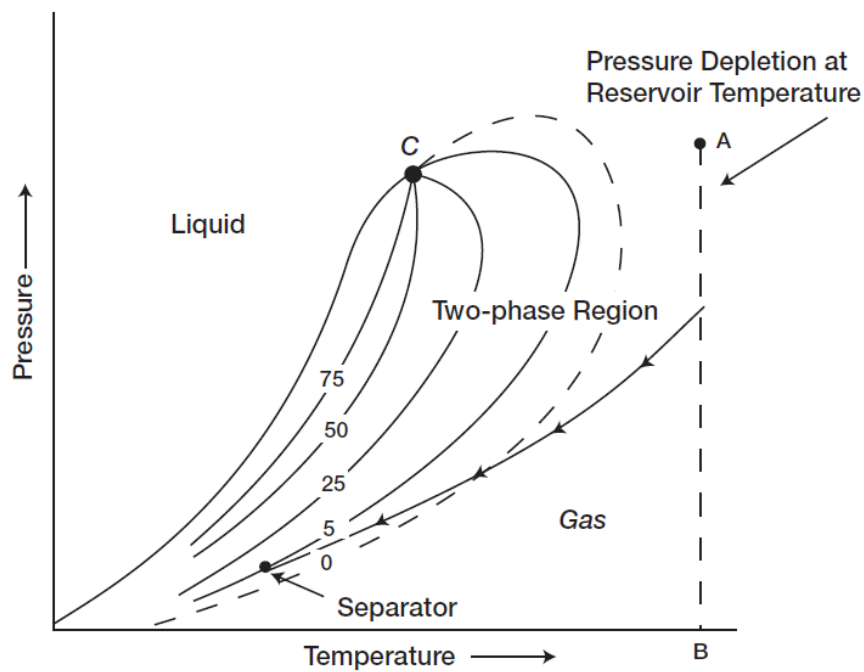


Figure 2.12: Phase envelope of a wet gas (Source: Ahmed [10])

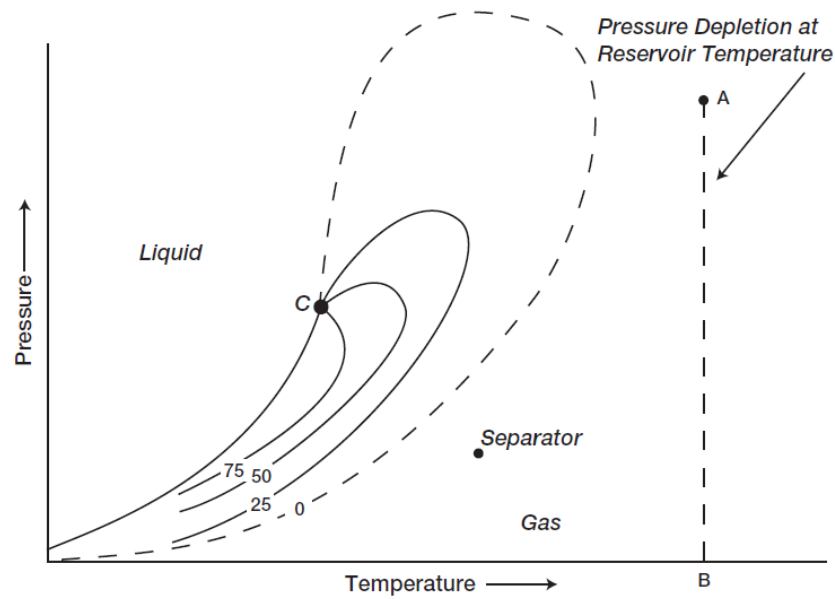


Figure 2.13: Phase envelope of a dry gas (Source: Ahmed [10])

2.2.6 Ternary Diagram

Figure 2.14 shows a ternary diagram used to qualitatively classify reservoir fluids depending on their chemical composition.

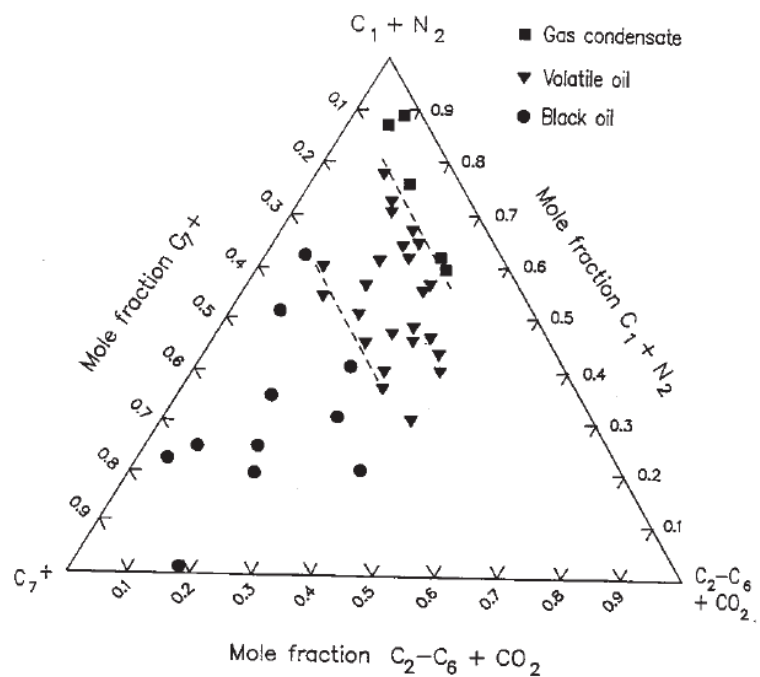


Figure 2.14: Ternary diagram for several reservoir fluids (Source: Whitson & Brule [2])

2.3 Reservoir Fluid Properties and Units

In order for one to accurately describe the volumetric and phase behavior of a reservoir fluid, several fundamental properties, molecular quantities, and mixing rules must first be defined.

2.3.1 Molecular Quantities

Mole

Mole, denoted as n , is a unit of measurement in Chemistry used for expressing amounts of chemical substance. It is defined as the amount of substance that contains as many elementary entities as there are atoms in twelve grams (12g) of Carbon-12 (^{12}C), an isotope of Carbon with a relative atomic mass of 12 (Avogadro constant). It is denoted as mol (=gmol), with its most common field unit being the kmol (=1000 mol or gmol).

Molar Mass/Molecular Weight

Mass, denoted as m , is the fundamental quantity for the measure of the amount of substance. Molar mass or molecular weight, denoted as M or MW , is defined as the mass per mole of a given compound:

$$M = \frac{m}{n} \quad (2.3)$$

Molecular weight (MW) is a dimensionless quantity as long as mass and mole units are consistent with one another (e.g. kg/kmol, g/gmol, lbm/lbm mol). Molar mass (M) is usually expressed in kg/mol.

Mole Fraction

The component mole fraction in a mixture comprised of N components is:

$$z_i = \frac{n_i}{\sum_{j=1}^N n_j} = \frac{m_i/M_i}{\sum_{j=1}^N m_j/M_i} \quad (2.4)$$

where n is the number of moles of component i ($i=1,\dots,N$), m its mass and M its molar mass. The sum of component mole fractions equals unity (i.e. $\sum z_i=1$). Component mole fraction z_i normally represents the component feed composition of a given mixture, with oil and gas compositions denoted as x_i and y_i respectively. Mole fraction is also expressed as mole percent (mol %).

2.3.2 Mixing Rules

Amagat's law

According to Amagat's law [12], the total volume of a gas mixture equals the sum of each individual component's volume provided that they are at the same pressure and temperature conditions.

Similarly, for oil mixtures at standard conditions and assuming ideal-solution mixing, the total volume of the mixture is an approximation of the sum of the volumes of all constituents [2].

Kay's rule

Kay's mixing rule [13] is widely used for averaging a given property of a mixture in order to simplify computations (see Sec. 2.3.3). For example, Kay's rule for molecular weight gives:

$$\bar{M} = \sum_{i=1}^n z_i M_i \quad (2.5)$$

2.3.3 Critical and Reduced Properties

Critical and pseudocritical properties

Critical pressure of a pure component, denoted as p_c , is the pressure above which no vapor/liquid mixture can coexist, regardless of temperature. Likewise, critical temperature of a pure component, denoted as T_c , is the temperature above which no vapor/liquid mixture can coexist, regardless of pressure [2].

In the case of more complicated mixtures, molar average critical properties are computed using mixing rules instead of “true” critical properties [9]. They are known as pseudocritical properties and are calculated by Kay’s rule [13]:

$$p_{pc} = \sum_{i=1}^n x_i p_{ci} \quad (2.6.a)$$

$$T_{pc} = \sum_{i=1}^n x_i T_{ci} \quad (2.6.b)$$

where x_i is liquid phase composition (y_i for vapor phase composition).

Reduced and pseudoreduced properties

In most Equation of State (EOS) calculations (see Chap. 3), pressure and temperature are not directly used for the description of the system’s behavior. Hence, the more generalized reduced properties are introduced, where each property is reduced to a common datum (i.e. its critical value) [9]. They are dimensionless and are defined as follows:

$$p_r = \frac{p}{p_c} \quad (2.7.a)$$

$$T_r = \frac{T}{T_c} \quad (2.7.b)$$

When calculating reduced properties, absolute units must be used at all times. In most applications, reduced pressure ranges from 0.03 to 40 for oils

and 0.02 to 30 for gases; whereas reduced temperature varies from 0.4 to 1.1 for oils and from below 1 to 2.5 for gases [2].

Pseudoreduced properties are calculated similarly to the reduced ones:

$$p_{pr} = \frac{p}{p_{pc}} \quad (2.8.a)$$

$$T_{pr} = \frac{T}{T_{pc}} \quad (2.8.b)$$

Critical volume

Critical volume is defined as the volume of a fixed mass of a fluid in its critical state (i.e. critical pressure and critical temperature) [14]. Critical specific volume is defined as the volume per mass unit in said state.

2.3.4 Volumetric Properties

Molar Volume

Molar volume, denoted as v or V_m , is the ratio of volume per mole, namely:

$$v = \frac{V}{n} \quad (2.9)$$

Molar volume is widely used in EOS calculations and is normally expressed in L/mol. Critical molar volume (v_c) is also widely used in Reservoir Engineering applications.

Density

Density or volumetric mass density, denoted as ρ , is defined as the ratio of mass per unit volume of a substance, namely:

$$\rho = \frac{m}{V} \quad (2.10)$$

Typical units of density are: kg/m³, g/cm³ and lbm/ft³. Typical oil densities range from 30 lbm/ft³ for light volatile oils to 60 lbm/ft³ for heavy crudes with little to no solution gas [2]. Figure 2.15 shows the densities of various types of reservoir fluids as functions of pressure. The visible “knees” in some density curves indicate a phase change (single-phase to two-phase condition) in their respective reservoir fluids.

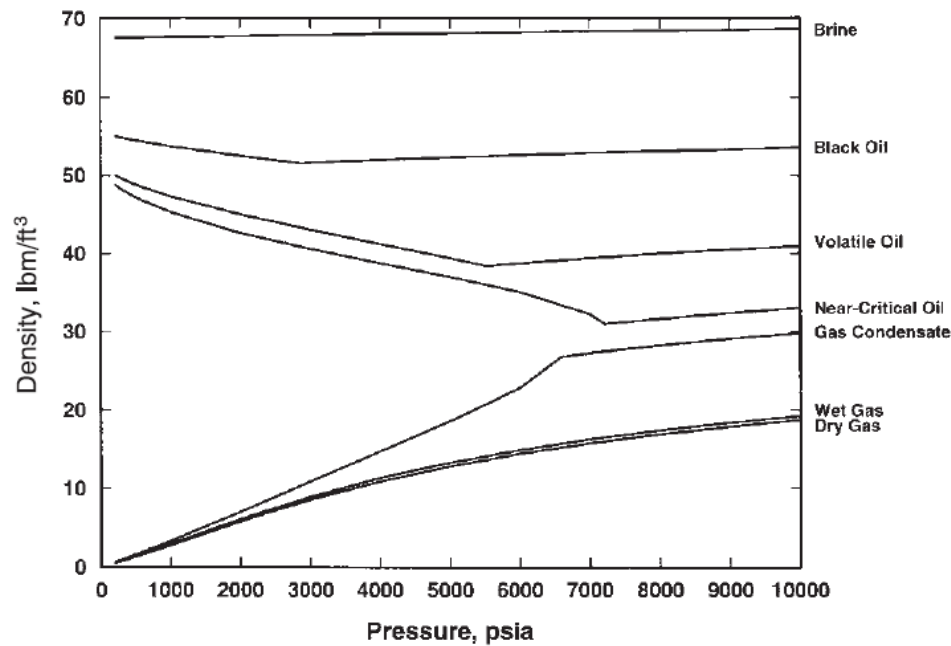


Figure 2.15: Reservoir fluid densities vs. pressure (Source: Whitson & Brule [2])

Relative Density/Specific Gravity

Relative density or specific gravity, denoted as γ or SG, is the dimensionless property defined as the ratio of the density of a given substance to the density of a reference material:

$$\gamma = \frac{\rho(p_{sc}, T_{sc})}{\rho_{ref}(p_{sc}, T_{sc})} \quad (2.11)$$

As for both materials, they must be compared at the same specified pressure and temperature conditions and their densities have to be measured at standard conditions [2]. The reference material for liquids is water, with air being used as the reference material for gases. Specific gravities of oil and gas are defined as follows:

$$\gamma_o = \frac{\rho_{o|sc}}{\rho_{w|sc}} \quad (2.12.a)$$

$$\gamma_g = \frac{\rho_{g|sc}}{\rho_{air|sc}} \quad (2.12.b)$$

It is evident that the specific gravities of air and water equal unity (i.e. $\gamma_{air}=1$, $\gamma_w=1$).

API Gravity

Another measure of oil gravity is API (American Petroleum Institute) gravity. It designates how “heavy” or “light” a particular crude oil is compared to water and is defined as follows:

$$^{\circ}API = \frac{141.5}{\gamma_o} - 131.5 \Leftrightarrow \gamma_o = \frac{141.5}{^{\circ}API + 131.5} \quad (2.13)$$

It is referred as a scale of degrees ($^{\circ}API$) despite being a dimensionless quantity. Lighter than water oils have an API gravity greater than 10° and float on it, while heavier ones have an API gravity less than 10° and sink. Thus, API gravity is inversely proportional to specific gravity. Most crude oils have API gravities between $10^{\circ}API$ (heavy asphaltic crudes) and $70^{\circ}API$ (lighter crudes) [10].

Compressibility

Compressibility or isothermal compressibility, denoted as c , is the measure of the relative change of volume of a fluid in response to changing pressure, namely:

$$c = -\frac{1}{V} \left(\frac{\partial V}{\partial p} \right)_T = -\frac{1}{v} \left(\frac{\partial v}{\partial p} \right)_T \quad (2.14)$$

Typical compressibility units are the psi^{-1} and kPa^{-1} . Reservoir oil compressibilities vary from $3 \cdot 10^{-6} \text{ psi}^{-1}$ for heavy crudes to $50 \cdot 10^{-6} \text{ psi}^{-1}$ for light oils. Even though pressure hardly affects oil compressibility, the effect can become great when it comes to volatile oils [2].

Z-factor

An ideal gas is a supposed aerial mixture with negligible in size molecules that have no intermolecular forces. The behavior of a real gas approaches that of an ideal gas at low pressures and high temperatures, due to the volume of the mixture being much larger than the volume of the molecules that constitute it. Most gases at low pressures follow the ideal gas law:

$$pV = nRT \quad (2.15)$$

where R is the universal gas constant usually given as $R=8.3143 \text{ kPa} \cdot \text{m}^3/\text{K} \cdot \text{kmol}$. At moderate or high pressures and low temperatures, intermolecular forces become significant and therefore greatly influence the volumetric behavior of the gas, rendering the ideal-gas law invalid.

Compressibility factor or Z-factor represents the deviation of a real gas from ideal gas behavior. It is a dimensionless quantity and is defined as:

$$Z = \frac{v_{real}(p, T)}{v_{ideal}(p, T)} \quad (2.16)$$

Most natural gases have a Z-factor between 0.7 and 1.2 (Figure 2.16).

Incorporating Eq. (2.16) into the ideal gas law results in the standard expression for gas volumetric behavior:

$$pV = nZRT \quad (2.17)$$

or in terms of molar volume v :

$$pv = ZRT \quad (2.18)$$

As a result, Z-factor can be defined as:

$$Z = \frac{pV}{nRT} = \frac{pv}{RT} \quad (2.19)$$

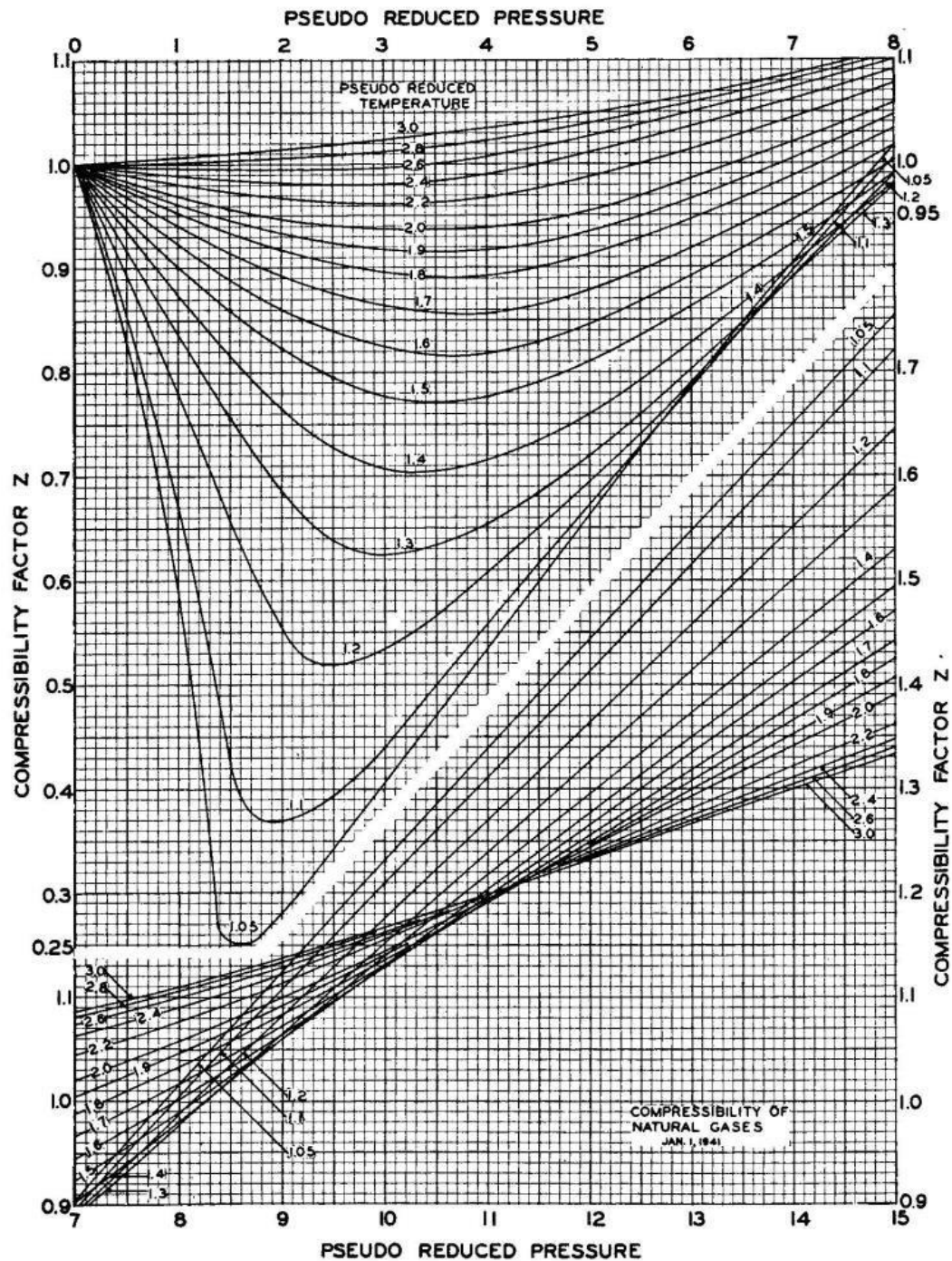


Figure 2.16: Z-factor vs. reduced pressure and temperature (Source: Standing & Katz [15])

The generalized compressibility factor chart (Figure 2.16) was developed by Standing and Katz [15] in 1942 and constitutes an industry standard to this day for the prediction of natural gas volumetric behavior.

2.3.5 PVT Properties

Formation Volume Factor

Formation volume factor or FVF, denoted as B , is the volume of a mixture at elevated conditions (e.g. reservoir conditions) divided by the volume of a product at surface conditions (i.e. standard conditions). The product at surface conditions may be equal to or only part of the first mixture. Formation volume factor is defined as:

$$B = \frac{V_{mix}(p, T)}{V_{prod}(p_{sc}, T_{sc})} \quad (2.20)$$

Several FVF's exist such as oil FVF (B_o), gas FVF (B_g) and total FVF (B_t). Oil FVF is defined as:

$$B_o = \frac{V_o}{V_{o|sc}} \quad (2.21)$$

where V_o is oil volume at elevated pressure and temperature and $V_{o|sc}$ is stock tank oil volume at standard conditions. Its units are bbl/STB and its value varies from 1 bbl/STB for oils containing little solution gas to nearly 2.5 bbl/STB for volatile oils [2].

Gas FVF is defined as:

$$B_g = \frac{V_g}{V_{g|sc}} \quad (2.22)$$

where V_g is gas volume at elevated pressure and temperature and $V_{g|sc}$ is surface gas volume at standard conditions. Its units are ft³/scf. Sometimes, the

reciprocal gas FVF ($b_g=1/B_g$) is used due to B_g being inversely proportional to pressure.

Lastly, total FVF is defined as the volume of a two-phase –or sometimes a single-phase– mixture at elevated conditions divided by the stock tank oil volume produced when the mixture is brought to surface conditions:

$$B_t = \frac{V_t}{V_{o|sc}} = \frac{V_o + V_g}{V_{o|sc}} \quad (2.23)$$

If $V_g=0$, B_t equals B_o ; and for gas condensate reservoirs where $V_o=0$, B_t is used for the calculation of oil initially in place [2].

Gas/Oil Ratio

Gas/oil ratio or GOR is defined as the volume of gas divided by the volume of oil –usually stock tank oil– when both fluids are at standard conditions:

$$GOR = \frac{V_{g|sc}}{V_{o|sc}} \quad (2.24)$$

This happens when a reservoir mixture is brought to surface conditions and both oil and gas are produced. GOR's units are scf/STB.

Solution gas/oil ratio, denoted as R_s , is a special occasion of GOR defined as the volume of gas at standard conditions liberated from a produced single-phase reservoir oil divided by the remaining volume of stock tank oil. Volatile oils usually display large R_s 's [2].

Viscosity

Fluid viscosity, denoted as η or μ , is a measure of its resistance to flow and shear stress, or the informal concept of the fluid's "thickness". The less viscous a fluid is, the faster it flows (e.g. water); whereas more viscous fluids like oil have a slower flowing rate. Viscosity is inversely proportional to temperature,

meaning that with increasing temperature, oil –like any other fluid– becomes less viscous and flows faster.

There are two types of viscosities used in Chemical Engineering: dynamic viscosity and kinematic viscosity, with dynamic viscosity being used in most Petroleum Engineering applications. The most common unit of viscosity in Petroleum Engineering is the poise (P) or centipoise (cP).

Reservoir oil viscosities range from 0.1 cP for near-critical oils to greater than 100 cP for heavy crudes. Factors that influence oil viscosity include temperature, stock-tank oil density and solution gas. Oil viscosity decreases with: increasing temperature, decreasing stock-tank oil density and increasing amount of dissolved gas. Natural gas viscosities often vary between 0.01 to 0.03 cP at standard and reservoir conditions to nearly 0.1 cP for near-critical gas condensates [2].

Interfacial Tension

Interfacial tension or IFT, denoted as σ , represents the interfacial forces which act between the oil, gas and water phases that coexist inside the pore volume of a reservoir rock. IFT's units are dyn/cm (=mN/m) and its value ranges from 50 dyn/cm for crude oil/gas systems to lower than 0.1 dyn/cm for high-pressure gas/oil mixtures [2].

Capillary pressure, denoted as P_c , is normally regarded as proportional to interfacial tension as stated by the Young-Laplace equation:

$$P_c = \frac{2\sigma}{\bar{r}} \quad (2.25)$$

with \bar{r} being the pore mean radius.

2.3.6 K-values

A K-value or equilibrium coefficient of a component is the dimensionless quantity defined as the ratio between its gas and oil compositions existing in thermodynamic equilibrium, namely:

$$K_i = \frac{y_i}{x_i} \quad (2.26)$$

K-values are functions of overall composition, pressure and temperature and are computed using empirical correlations and EOS calculations.

Chapter 3

Cubic Equations of State and EOS Calculations

3.1 Cubic Equations of State

Cubic Equations of State (EOS's) are simple equations about pressure, volume and temperature (PVT) that are used to describe the volumetric and phase behavior of pure components and mixtures with great accuracy, provided that one knows the critical properties and acentric factor of each component inside the system under examination [2]. This behavior is calculated via the solution of a simple cubic equation in terms of Z-factor, namely:

$$Z^3 + A_2 Z^2 + A_1 Z + A_0 = 0 \quad (3.1)$$

where $A_0, A_1, A_2 = \text{const.}$ are functions of pressure, temperature and phase composition.

If the condition of chemical equilibrium is satisfied, one can calculate the phase equilibria with the aid of an EOS. For two-phased systems, the chemical potentials of the liquid phase components must equal the ones of the vapor phase components, i.e. $\mu_i(x) = \mu_i(y)$. Chemical potential is normally expressed in terms of fugacity, denoted as f , as follows:

$$\mu_i = RT \ln f_i + \lambda_i(T) \quad (3.2)$$

where R is the universal gas constant and $\lambda_i(T)$ the temperature dependent ideal gas contribution to chemical energy, dropping out of the equation in most problems [16]. Hence, $\mu_i(x) = \mu_i(y)$ is satisfied when the component fugacities of the liquid phase equal those of the vapor phase, i.e. $f_{Li} = f_{vi}$. Fugacity is calculated via the following expression:

$$\ln \phi_i = \ln \frac{f_i}{x_i p} = \frac{1}{RT} \int_V^\infty \left(\frac{\partial p}{\partial n_i} - \frac{RT}{V} \right) dV - \ln Z \quad (3.3)$$

where ϕ_i is the fugacity coefficient and x_i the liquid phase composition (y_i in the case of vapor phase composition).

Various cubic EOS's have been developed since the van der Waals EOS [17] such as the Redlich-Kwong (RK) EOS in 1949 [18] and the Peng-Robinson (PR) EOS in 1976 [19], with the Redlich-Kwong equation being the most popular basis for the development of new EOS's. They still maintain the repulsive term $RT/(v-b)$ of the original equation, while modifying the denominator of the attractive term. Most petroleum engineers use the PR EOS or a modified RK EOS for their computations, with Soave's modification [20] (SRK EOS) being the simplest and most widely accepted one.

3.1.1 The van der Waals Equation

The first cubic EOS was introduced by van der Waals in 1873 [17], who proposed a simple and accurate relation between pressure p , temperature T and molar volume v :

$$p = \frac{RT}{v-b} - \frac{a}{v^2} \quad (3.4)$$

where a is the attraction parameter, b the repulsion parameter and R the universal gas constant. The previous equation is a major improvement to the ideal gas law ($p=RT/v$), giving a more accurate prediction of liquid behavior, as the molar volume has the limiting value of b (also known as co-volume):

$$\lim_{p \rightarrow \infty} v(p) = b \quad (3.5)$$

The first term of the van der Waals equation is an approximation to the ideal gas behavior (i.e. $p \approx RT/v$), while the second term represents non-ideal gas behavior, reducing the pressure of the system. The EOS constants of the van der Waals equation are:

$$a = \frac{27 R^2 T_c^2}{64 p_c} \quad (3.6.a)$$

$$b = \frac{1 R T_c}{8 p_c} \quad (3.6.b)$$

Written in terms of Z-factor, the van der Waals equation is:

$$Z^3 - (B + 1)Z^2 + AZ - AB = 0 \quad (3.7)$$

with $A = a \frac{p}{(RT)^2}$ and $B = b \frac{p}{RT}$. The critical compressibility factor is $Z_c = 3/8 = 0.375$.

3.1.2 The Redlich-Kwong Equation

As stated above, in 1949, Redlich and Kwong [18] proposed the RK EOS:

$$p = \frac{RT}{v - b} - \frac{a}{v(v + b)} \quad (3.8)$$

which is also expressed in terms of Z-factor:

$$Z^3 - Z^2 + (A - B - B^2)Z - AB = 0 \quad (3.9)$$

The dimensionless parameters A, B are the same as the van der Waals equation and the critical compressibility factor is $Z_c = 1/3$. The EOS constants are:

$$a = 0.42748 \frac{R^2 T_c^2}{p_c} \alpha \quad (3.10.a)$$

where $\alpha = \sqrt{T_r}$ is a dimensionless factor that equals one at $T = T_c$.

$$b = 0.08664 \frac{R T_c}{p_c} \quad (3.10.b)$$

Cubic equations are normally solved using analytical methods, where three roots are usually present: the largest root is chosen for liquids and the smallest root is chosen for gases, whereas the middle root is always dropped as a non-physical root [2].

For pure components, fugacity is calculated through the following expression:

$$\ln \frac{f}{p} = \ln \phi = Z - 1 - \ln(Z - B) - \frac{A}{B} \ln \left(1 + \frac{B}{Z} \right) \quad (3.11)$$

For a vapor-liquid mixture, multicomponent fugacity is given by:

$$\begin{aligned} \ln \frac{f_i}{x_i p} = \ln \phi_i = & \frac{b_i}{b} (Z - 1) - \ln(Z - B) + \\ & + \frac{A}{B} \left(\frac{b_i}{b} - \frac{2}{a} \sum_{j=1}^N x_j a_{ij} \right) \ln \left(1 + \frac{B}{Z} \right) \end{aligned} \quad (3.12)$$

Mixing Rules

The mixing rules a , b used in Eq. (3.12) are computed using a quadratic mixing rule and a linear mixing rule respectively:

$$a = \sum_{i=1}^N \sum_{j=1}^N x_i x_j a_{ij} \quad (3.13.a)$$

$$a_{ij} = (1 - k_{ij}) \sqrt{a_i a_j} \quad (3.13.b)$$

where k_{ij} 's are the binary interaction coefficients (see Sec. 3.1.6)

$$b = \sum_{i=1}^N x_i b_i \quad (3.14)$$

and a_i , b_i the component EOS constants.

3.1.3 The Soave-Redlich-Kwong Equation

Since the RK EOS, various attempts have been made for the improvement of the original equation and the results it yields. In 1971, Soave [20] applied a modification to the term of α as follows:

$$\alpha = [1 + m(1 - \sqrt{T_r})]^2 \quad (3.15.a)$$

$$m = 0.480 + 1.574\omega - 0.176\omega^2 \quad (3.15.b)$$

where ω is component acentric factor (see Sec. 3.1.6).

The SRK EOS is the most broadly used of the RK EOS's. However, for petroleum mixtures, it overestimates liquid volumes while underestimating liquid densities [2]. In 1982, Peneloux et al. [21] presented a volume translation method that modified the SRK EOS in order to improve its volumetric capabilities by adding a third constant to the equation (see Sec. 3.1.5).

3.1.4 The Peng-Robinson Equation

In 1976, Peng and Robinson [19] developed a new two-constant EOS:

$$p = \frac{RT}{v - b} - \frac{a}{v(v + b) + b(v - b)} \quad (3.16)$$

In terms of Z-factor:

$$Z^3 - (1 - B)Z^2 + (A - 3B^2 - 2B)Z - (AB - B^2 - B^3) = 0 \quad (3.17)$$

The dimensionless parameters A, B are the same as the van der Waals equation. The critical compressibility factor is $Z_c=0.3074$, a large improvement to the value of the RK EOS and closer to heavier hydrocarbon experimental values. The EOS constants are:

$$a = 0.45724 \frac{R^2 T_c^2}{p_c} \alpha \quad (3.18.a)$$

$$b = 0.07780 \frac{RT_c}{p_c} \quad (3.18.b)$$

with

$$\alpha = [1 + m(1 - \sqrt{T_r})]^2 \quad (3.19.a)$$

$$m = 0.37464 + 1.54226\omega - 0.26992\omega^2 \quad (3.19.b)$$

Fugacity for pure components is expressed by:

$$\ln \frac{f}{p} = \ln \phi = Z - 1 - \ln(Z - B) - \frac{A}{2\sqrt{2}B} \ln \left[\frac{Z + (1 + \sqrt{2})B}{Z - (1 - \sqrt{2})B} \right] \quad (3.20)$$

For mixtures:

$$\begin{aligned} \ln \frac{f_i}{x_i p} = \ln \phi_i = & \frac{b_i}{b} (Z - 1) - \ln(Z - B) + \\ & + \frac{A}{2\sqrt{2}B} \left(\frac{b_i}{b} - \frac{2}{a} \sum_{j=1}^N x_j a_{ij} \right) \ln \left[\frac{Z + (1 + \sqrt{2})B}{Z - (1 - \sqrt{2})B} \right] \end{aligned} \quad (3.21)$$

The mixing rules used are the same as the RK-EOS (Eqs. (3.13)–(3.14)).

According to Peng and Robinson, their EOS yields better results in terms of liquid density than the SRK-EOS. However, it is known that the PR-EOS underpredicts the saturation pressures of reservoir fluids in comparison with the SRK-EOS [2].

3.1.5 Volume Translation

The concept of volume translation in cubic EOS's was first introduced in 1979 by Martin [22]. In 1982, Peneloux et al. [21] used the volume translation method in order to prove that the shift in volume does not influence the efficiency of the SRK EOS.

Volume translation improves the poor liquid volumetric predictions of two-constant EOS's by subtracting a correction term from the molar volume calculated by the EOS, namely:

$$v' = v - c \quad (3.22)$$

where v' is the linearly translated molar volume, v the EOS-calculated molar volume and c the volume correction term.

Peneloux et al. introduced the correction term as a mole fraction average proving that multi-component Vapor/Liquid Equilibrium (VLE) is unaltered. The volume correction term is computed using the following correlation:

$$c = 0.40768 \frac{RT_c}{P_c} (0.29441 - Z_{RA}) \quad (3.23)$$

where Z_{RA} is Rackett's compressibility factor [23]. The corrected liquid and vapor phase molar volumes are expressed as follows:

$$v'_L = v_L - \sum_{i=1}^N x_i c_i \quad (3.24.a)$$

$$v'_v = v_v - \sum_{i=1}^N y_i c_i \quad (3.24.b)$$

where v_L and v_v are the EOS-calculated liquid and vapor phase molar volumes respectively and c_i the component-dependent volume correction term. They suggested that c_i be separately determined for every component by matching their saturated liquid densities at reduced temperature $T_r=0.7$.

Applying the volume shift to the EOS for mixtures leads to the following modified fugacity expressions:

$$f_{Li}^* = f_{Li} \exp(-c_i \frac{p}{RT}) \quad (3.25.a)$$

$$f_{vi}^* = f_{vi} \exp(-c_i \frac{p}{RT}) \quad (3.25.b)$$

where f_{Li} and f_{vi} are the liquid and vapor phase component fugacities respectively. Consequently, modified and original fugacity ratios remain unchanged:

$$\frac{f_{Li}^*}{f_{vi}^*} = \frac{f_{Li}}{f_{vi}} \quad (3.26)$$

Jhaveri and Youngren [24] suggested that c_i be written as a ratio for heptanes plus fractions. As a result, they introduced a dimensionless shift parameter defined as follows:

$$s_i = \frac{c_i}{b_i} \quad (3.27)$$

where b_i is component co-volume.

Applications such as gradient calculations (see Chap. 4) which directly use fugacity must incorporate the volume translation constant in their expressions. Volume translation can be applied to and works equally well with any two-constant cubic EOS, making the equation as accurate as any three-constant EOS [2].

3.1.6 EOS Quantities

Acentric factor

According to Pitzer et al. [25] acentric factor is the dimensionless quantity defined as follows:

$$\omega = -\log p_r^* - 1 \quad (3.28)$$

where p_r^* is the reduced vapor pressure at reduced temperature $T_r=0.7$. Acentric factor represents the steepness of the vapor-pressure curve from $T_r=0.7$ to $T_r=1$, with $\omega=0$ for $p_r^*=0.1$ and $\omega=1$ for $p_r^*=0.01$.

Binary interaction coefficients

Binary interaction coefficients, denoted as k_{ij} , represent the molecular interactions between the molecules of different components inside a mixture. According to Li et al. [26], binary interaction coefficients between hydrocarbon components are computed as follows:

$$k_{ij} = 1 - \left(\frac{2v_{ci}^{\frac{1}{6}}v_{cj}^{\frac{1}{6}}}{v_{ci}^{\frac{1}{3}} + v_{cj}^{\frac{1}{3}}} \right)^{\theta} \quad (3.29)$$

where v_{ci} is the critical molar volume of component i and θ the power used for the calculation of these coefficients. It is obvious that $k_{ii}=0$ and $k_{ij}=k_{ji}$.

3.2 Equation of State Calculations

3.2.1 Two-Phase Flash Calculation

The isothermal two-phase flash calculation is incorporated in most EOS calculations and implements the calculation of the liquid and vapor phase compositions of a given mixture, provided one knows pressure, temperature and feed composition. One does not a priori know whether the mixture is single-phase or two or more phases exist at the given pressure and temperature conditions.

The two-phase flash problem is normally solved numerically by satisfying the equal fugacity (i.e. $f_{Li}=f_{vi}$) and component/phase material balance (i.e. $nz_i=n_vy_i+v_Lx_i$) constraints using a successive substitution (SS) or Newton-Raphson method [27]. The measure of convergence used is:

$$\sum_{i=1}^N \left(\frac{f_{Li}}{f_{vi}} - 1 \right)^2 < \varepsilon \quad (3.30)$$

where ε is the convergence tolerance.

Two-Phase Split

Introducing the vapor phase molar fraction $\beta=n_v/(n_L+n_v)$ to the material balance constraint results in the following expression:

$$z_i = \beta y_i + (1 - \beta)x_i \quad (3.31)$$

The molar compositions of each phase along with the overall feed composition must sum to one, namely:

$$\sum_{i=1}^N y_i = \sum_{i=1}^N x_i = \sum_{i=1}^N z_i = 1 \quad (3.32)$$

Leading to the following constraint:

$$\sum_{i=1}^N (y_i - x_i) = 0 \quad (3.33)$$

With the use of Eq. (3.31) and the K-value definition ($K_i = y_i/x_i$), Eq. (3.33) can be rewritten as follows:

$$h(\beta) = \sum_{i=1}^N \frac{z_i(K_i - 1)}{1 + \beta(K_i - 1)} = 0 \quad (3.34)$$

This way, the number of unknown variables now is $N+1$ (K_i 's and β) instead of $2N+1$ (y_i 's, x_i 's and β). The previous equation is broadly known as the Rachford-Rice function [28] (Figure 3.1).

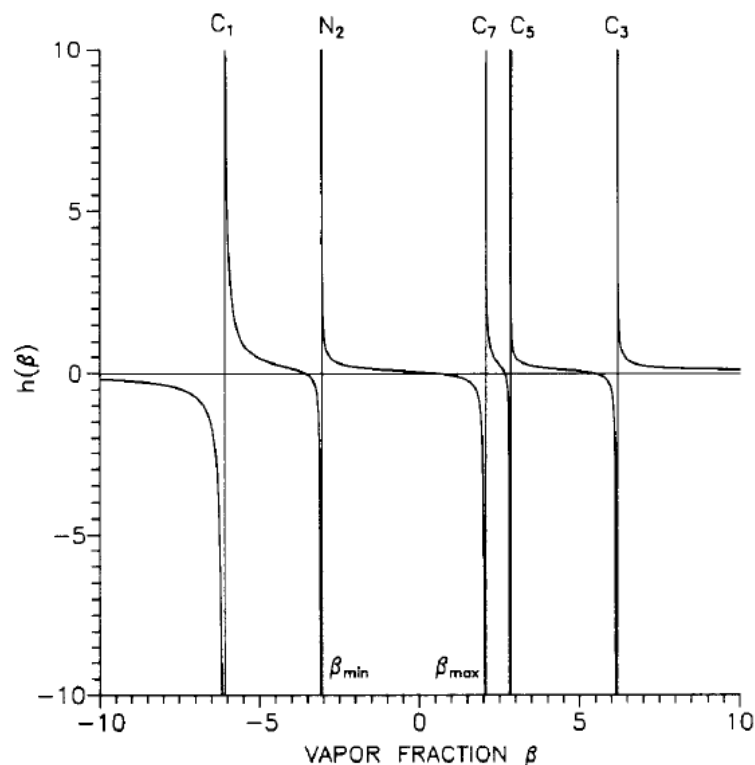


Figure 3.1: The Rachford-Rice function $h(\beta)$ for a five component system (Source: Whitson & Michelsen [29])

According to Whitson and Michelsen [29], the only solution with a physical meaning lies between the β_{\min} and β_{\max} boundary (i.e. $\beta_{\min} < \beta < \beta_{\max}$), with:

$$\beta_{\min} = \frac{1}{1 - K_{\max}} < 0 \quad (3.35.a)$$

$$\beta_{\max} = \frac{1}{1 - K_{\min}} > 1 \quad (3.35.b)$$

when $K_{\min} < 1$ and $K_{\max} > 1$.

The Rachford-Rice function is solved using the Newton-Raphson method:

$$\beta^{(n+1)} = \beta^{(n)} - \frac{h(\beta^{(n)})}{h'(\beta^{(n)})} \quad (3.36.a)$$

where

$$h'(\beta) = \frac{dh}{d\beta} = - \sum_{i=1}^N \frac{z_i(K_i - 1)^2}{[\beta(K_i - 1) + 1]^2} \quad (3.36.b)$$

with n indicating the number of iterations. The first guess for β is arbitrary.

Equilibrium phase compositions are found via the material balance expressions:

$$x_i = \frac{z_i}{1 + \beta(K_i - 1)} \quad (3.37.a)$$

$$y_i = \frac{z_i K_i}{1 + \beta(K_i - 1)} = x_i K_i \quad (3.37.b)$$

The best method of solution consists of a successful phase stability test (see Sec. 3.2.2) followed by the two-phase flash, although it comes at a higher cost than a plain two-phase flash calculation. Furthermore, successive substitution constitutes the safest solution method, yet it is extremely slow near the critical points and phase boundaries where a great many of thousands of iterations are needed to reach the convergence threshold [2].

Two-Phase Flash Algorithm

An isothermal two-phase flash successive-substitution solution method was originally developed by Michelsen [30]. The following algorithm constitutes an adaptation of that method by Whitson and Brule [2]:

1. Estimate K-values using the well-known Wilson method [31]:

$$K_i = \frac{\exp[5.37(1 + \omega_i)(1 - T_{ri}^{-1})]}{p_{ri}} \quad (3.38)$$

where ω_i is component acentric factor and T_{ri} , p_{ri} are component reduced properties.

At high pressures, the Wilson equation can lead to inaccurate K-value estimates causing the flash calculation to incorrectly converge to a trivial solution.

2. Compute K_{\min} and K_{\max} .
3. Solve the Rachford-Rice equation (Eq. (3.34)) for β , bounded by the constraints of β_{\min} and β_{\max} (Eq. (3.35)).
4. Compute liquid and vapor phase compositions x_i and y_i from the material balance expressions (Eq. (3.37)).
5. Compute liquid and vapor phase Z-factors Z_L and Z_v using an EOS:

$$Z_L = f(x, p, T) \quad (3.39.a)$$

$$Z_v = f(y, p, T) \quad (3.39.b)$$

6. Compute liquid and vapor phase fugacities f_{Li} and f_{vi} using an EOS:

$$f_{Li} = f(x, Z_L, p, T) \quad (3.40.a)$$

$$f_{vi} = f(y, Z_v, p, T) \quad (3.40.b)$$

7. Compute liquid and vapor phase reduced Gibbs energy functions g^* (see Sec 3.2.2):

$$g_L^* = \sum_{i=1}^N x_i \ln f_{Li} \quad (3.41.a)$$

$$g_v^* = \sum_{i=1}^N y_i \ln f_{vi} \quad (3.41.b)$$

If multiple Z-factor roots exist for each phase, choose the roots with the lowest reduced Gibbs energy. Then calculate the reduced mixture Gibbs energy using the material balance expression:

$$g_{mix}^* = \beta g_v^* + (1 - \beta) g_L^* \quad (3.42)$$

8. Check the fugacity constraint (Eq. (3.30)) for convergence tolerance (recommended tolerance $\epsilon=1 \times 10^{-13}$).
9. (i) If convergence is achieved, stop.
(ii) If convergence is not achieved, update the K-values with successive substitution:

$$K_i^{(n+1)} = K_i^{(n)} \frac{f_{Li}^{(n)}}{f_{vi}^{(n)}} \quad (3.43)$$

where n is the number of iterations. With new K-values, repeat steps 2 through 9 until convergence is reached.

10. Check for convergence at a trivial solution under the criterion:

$$\sum_{i=1}^N (\ln K_i)^2 < 10^{-4} \quad (3.44)$$

There are three types of converged solutions to be acquired:

- (a) A solution within $0 \leq \beta \leq 1$, where $\beta=0$ indicates a bubble-point condition, $\beta=1$ a dew-point condition and $0 < \beta < 1$ a two-phase condition.
- (b) A solution with $\beta < 0$ or $\beta > 1$ that is physically unacceptable, representing a thermodynamically stable mixture that will remain single-phase and not split into two or more phases. This flash calculation is known as “the negative flash” [29] due to the vapor phase mole fraction being negative.
- (c) A trivial solution with $x_i=y_i=z_i$ and $K_i=1$.

3.2.2 Stability Analysis

Stability analysis [32] examines whether a mixture will maintain its thermodynamic stability or split into multiple phases. According to the Gibbs tangent plane criterion [33], a mixture will split into two or more phases if its Gibbs energy is reduced enough (unstable condition) or remain single-phase throughout the process if its Gibbs energy remains high enough (stable condition).

The Gibbs energy for n moles of a mixture with feed composition z , considered as a single homogeneous phase is given by:

$$G_z = \sum_{i=1}^N (n_i \mu_i)_z = n \sum_{i=1}^N z_i \mu_{zi} \quad (3.45)$$

The overall mixture Gibbs energy of a two-phase system is given by:

$$G_{mix} = \sum_{i=1}^N (n_i \mu_i)_v + (n_i \mu_i)_L = \sum_{i=1}^N (n_{vi} + n_{Li}) \mu_i \quad (3.46)$$

Using Eq. (3.31), the previous equation can be written as follows:

$$G_{mix} = n \sum_{i=1}^N [\beta y_i + (1 - \beta) x_i] \mu_i \quad (3.47)$$

If $G_{mix} < G_z$, the mixture will split into two phases with compositions x and y .

The reduced Gibbs energy function (i.e. $g^* = G/RT$) for the same mixture with composition z (similarly to Eq. (3.41)) is given by:

$$g_z^* = \sum_{i=1}^N z_i \ln f_i(z) \quad (3.48)$$

and is plotted vs. a component mole fraction of a binary mixture in Figure 3.2.

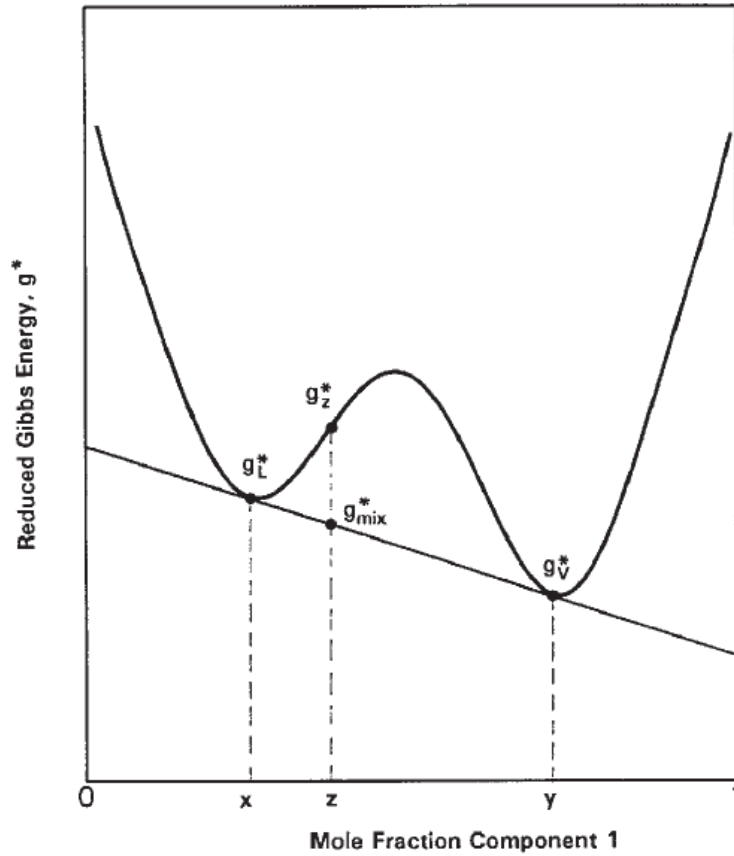


Figure 3.2: Reduced Gibbs energy curve for a binary system (Source: Whitson & Brule [2])

The points g_L^* and g_v^* where the tangent osculates the curve represent equilibrium conditions where $f_{Li}=f_{vi}$. If the mixture composition z lies between compositions x and y (i.e. $x < z < y$), the solution is physically acceptable, therefore the mixture is unstable and will split into two equilibrium phases with compositions of x and y . If $z < x$ or $z > y$, the material balance constraint is broken, therefore the mixture is stable. If $z = y$ or $z = x$, the mixture is stable with solutions representing a dew-point or bubble-point condition respectively.

Algorithm

Two stability tests need to be run separately: one that assumes the second phase to be vapor; and another one that assumes the second phase to be liquid. A successive-substitution method similar to the two-phase flash one, which determines if a mixture will split into two or more phases or remain

thermodynamically stable as single-phase was also developed by Michelsen [32]. The adaptation of the above method by Whitson and Brule [2] is outlined as follows:

1. Compute mixture fugacities f_{zi} . If multiple Z-factor roots exist, choose the one with the lowest reduced Gibbs energy g^* .
2. Estimate initial K-values using Eq. (3.38).
3. Begin iteration sequence. Compute second phase mole numbers:

$$(Y_i)_v = z_i(K_i)_v \quad (3.49.a)$$

or
$$(Y_i)_L = z_i/(K_i)_L \quad (3.49.b)$$

4. Sum the mole numbers:

$$S_v = \sum_{i=1}^N (Y_i)_v \quad (3.50.a)$$

or
$$S_L = \sum_{i=1}^N (Y_i)_L \quad (3.50.b)$$

5. Compute second phase mole fractions:

$$(y_i)_v = \frac{(Y_i)_v}{S_v} = \frac{(Y_i)_v}{\sum_{i=1}^N (Y_i)_v} \quad (3.51.a)$$

or
$$(y_i)_L = \frac{(Y_i)_L}{S_L} = \frac{(Y_i)_L}{\sum_{i=1}^N (Y_i)_L} \quad (3.51.b)$$

6. Compute second phase fugacities $(f_{yi})_v$ or $(f_{yi})_L$. If multiple Z-factor roots exist, choose the one with the lowest reduced Gibbs energy g^* .
7. Compute fugacity-ratio corrections:

$$(R_i)_v = \frac{f_{zi}}{(f_{yi})_v} \frac{1}{S_v} \quad (3.52.a)$$

or
$$(R_i)_L = \frac{(f_{yi})_L}{f_{zi}} S_L \quad (3.52.b)$$

8. Check for convergence (e.g. $\epsilon=1 \times 10^{-13}$) under the condition:

$$\sum_{i=1}^N (R_i - 1)^2 < \varepsilon \quad (3.53)$$

9. If convergence is not achieved, update K-values using the fugacity-ratio corrections:

$$K_i^{(n+1)} = K_i^{(n)} R_i^{(n)} \quad (3.54)$$

Repeat steps 3 through 9 until convergence is reached.

In 1975, Crowe and Nishio [34] proposed the General Dominant Eigenvalue Method (GDEM), an algorithm which uses the Newton-Raphson method for accelerating the iterative computation of steady state simulations of chemical processes. Michelsen suggested the acceleration of step 9 using four SS iterations ($n=4$) with $\lambda=1$, namely:

$$K_i^{(n+1)} = K_i^{(n)} [R_i^{(n)}]^\lambda \quad (3.55)$$

before a GDEM promotion with λ given as follows:

$$\lambda = \left| \frac{b_{11}}{b_{11} - b_{01}} \right| \quad (3.56)$$

where

$$b_{01} = \sum_{i=1}^N \ln R_i^{(n)} \ln R_i^{(n-1)} \quad (3.57.a)$$

$$b_{11} = \sum_{i=1}^N \ln R_i^{(n-1)} \ln R_i^{(n-1)} \quad (3.57.b)$$

with n suggesting the number of iterations.

10. Check for convergence at a trivial solution using Eq. (3.44).

If both tests indicate $S \leq 1$ (after Eq. (3.50)), or if both tests converge to a trivial solution, or if one test indicates $S \leq 1$ and the other converges to a trivial solution, then the mixture is stable. If at least one test yields $S > 1$, then the mixture is unstable, in which particular case the K-values from the test can be used for the initialization of a two-phase flash calculation.

3.2.3 Saturation Pressure Calculation

Saturation pressure calculation [35] constitutes the calculation of pressure or pressures at which a mixture with composition z and temperature T is in thermodynamic equilibrium with an infinitesimal incipient phase. In terms of two-phase flash, saturation pressure equals the pressure where: $\beta=0$ (bubble-point pressure) or $\beta=1$ (dew-point pressure).

Saturation pressure is valid under two conditions: the equal fugacity constraint between the dominant and the incipient phase (i.e. $f_{zi}=f_{yi}$); and the condition under which the molar composition of the incipient phase y_i must sum to one (after Eq. (3.32)). In terms of K -values, similarly to Eq. (3.49), the previous condition can be writtern as follows (for the bubble-point and dew-point calculation respectively):

$$1 - \sum_{i=1}^N z_i K_i = 0 \quad (3.58.a)$$

$$1 - \sum_{i=1}^N z_i / K_i = 0 \quad (3.58.b)$$

In terms of phase stability, the saturation pressure condition must sum the incipient phase mole numbers to one (after Eq. (3.50)):

$$\sum_{i=1}^N Y_i = 1 \quad (3.59)$$

Michelsen [35] proposed the following saturation point function in order to calculate the saturation pressure:

$$Q(y, p_{sat}) = 1 - \sum_{i=1}^N z_i \frac{\varphi_i(z)}{\varphi_i(y)} = 1 - \sum_{i=1}^N y_i \frac{f_{zi}}{f_{yi}} = 1 - \sum_{i=1}^N Y_i = 0 \quad (3.60)$$

where the incipient-phase composition y_i is computed using Eq. (3.51).

Algorithm

A saturation pressure calculation algorithm which incorporates an SS method with GDEM acceleration for composition and a Newton-Raphson method for pressure was originally developed by Michelsen [35]. The algorithm can be modified for the search of both upper and lower saturation points, plus a saturation temperature calculation for designated pressure. Whitson and Brule's [2] adaptation of the algorithm is outlined as follows:

1. Guess the saturation point type: bubble-point or dew-point. If the guess is false, the resulting K-values might be upside-down (i.e. $K_i=1/K_i$).
2. Guess a pressure p^* .
3. Conduct a phase stability analysis at p^* .
4. (i) If the mixture is stable, pressure p^* is the upper bound of the saturation pressure estimates. Return to step 1 and guess a lower pressure than p^* .
(ii) If the mixture is unstable, pressure p^* is the lower bound of the saturation pressure estimates.
5. With the unstable solution in hand, use the stability test K-values in order to compute the incipient-phase mole numbers Y_i after Eq. (3.49). In case of two unstable solutions, use the K-values with the biggest sum of mole numbers (Eq. (3.50)).
6. Begin iteration sequence. Compute incipient-phase composition y_i after Eq. (3.51).
7. Compute dominant and incipient phase Z-factors Z_z , Z_y and component fugacities f_{zi} , f_{yi} at pressure p^* using an EOS. If multiple Z-factor roots exist, choose the one with the lowest reduced Gibbs energy (Eq. (3.41)).
8. Compute fugacity-ratio corrections R_i after Eq. (3.52).
9. Update incipient-phase mole numbers using the fugacity-ratio corrections as follows:

$$Y_i^{(n+1)} = Y_i^{(n)} [R_i^{(n)}]^\lambda \quad (3.61)$$

using four SS iterations ($n=4$) with $\lambda=1$ before a GDEM promotion with λ given by Eq. (3.56).

10. Compute a new saturation pressure estimate using the Newton-Raphson method:

$$p_{sat}^{(n+1)} = p_{sat}^{(n)} - \frac{Q^{(n)}}{\left(\frac{\partial Q}{\partial p}\right)^{(n)}} \quad (3.62.a)$$

where

$$\frac{\partial Q}{\partial p} = \sum_{i=1}^N Y_i R_i \left(\frac{\partial f_{yi}}{\partial p} \frac{1}{f_{yi}} - \frac{\partial f_{zi}}{\partial p} \frac{1}{f_{zi}} \right) \quad (3.62.b)$$

If searching for an upper saturation point, p_{sat} must be higher than p^* . If $p_{sat} < p^*$, return to step 1 and guess a higher p^* than the previous one.

11. Check for convergence under the criteria:

$$\left| 1 - \sum_{i=1}^N Y_i \right| < 10^{-13} \quad (3.63.a)$$

$$\left[\sum_{i=1}^N \frac{\ln(R_i)}{\ln \frac{Y_i}{Z_i}} \right]^2 < 10^{-8} \quad (3.63.b)$$

12. Check for convergence at a trivial solution under the condition:

$$\sum_{i=1}^N \left(\ln \frac{Y_i}{Z_i} \right)^2 < 10^{-4} \quad (3.64)$$

13. (a) If convergence is not reached, return to step 6.
 (b) If convergence is reached, confirm the type of saturation pressure by comparing the composition of the heaviest component (component N) between the dominant (z) and the incipient phase (y). If $y_N < z_N$, a bubble-point pressure is present with $K_i = y_i/z_i$; else if $y_N > z_N$, a dew-point pressure is present with $K_i = z_i/y_i$.

3.3 Equation of State Fluid Characterization

It is widely known that the majority of EOS fluid characterizations are not truly predictive [36]. This is usually caused by inadequate data regarding the “heavy” fraction (e.g. properties, binary interaction coefficients, etc.). In order to develop a sufficient EOS fluid characterization, one must first “tune” the EOS used to match calculated with experimental PVT data as long as the latter are considered representative.

EOS tuning is done by modifying the properties (e.g. p_c , T_c , ω , MW, volume shift s_i , k_{ij} ’s, etc.) of the “heavy” fraction and/or the pseudo-components using various regression methods. Some regression techniques such as Coats and Smart’s [36] or Agarwal et al.’s [37] use non-linear regression to automatically modify EOS parameters. Most common regression parameters are the critical properties of the “heavy” fraction and the binary interaction coefficients between the “heavy” fraction and non-hydrocarbon components.

Regression methods are not able to correct any insufficiencies that might emerge from the EOS characterization, as the accuracy of the results is entirely dependent on the quality of the experimental data provided [37]. Consistency checks at every step of the procedure should always be performed to make sure that regression parameters are within reasonable limits. Calculated data using a tuned EOS should not differ significantly from experimental data, else results are deemed unreliable. EOS characterizations that use volume translation have much better initial predictions than those that do not, resulting in fewer modifications to reach the same “fit” quality between experimental and calculated data [2].

Chapter 4

Compositional Grading

4.1 Overview

In reservoirs with large thickness or a high dip angle, it is observed that gravity forces tend to generate and stabilize compositional variations along the hydrocarbon column over the geological time, leading to the decrease of lighter hydrocarbon mole fractions (e.g. Methane) and the increase of heavier ones from top to bottom. Reservoir fluid density also increases while GOR decreases with depth. Volatile and near-critical oils are the ones displaying the strongest compositional grading, whereas black oils are the least affected by grading effects.

Compositional grading is defined as the continual change of composition as a function of depth [2]. In general, the factors that create variations in reservoir fluid composition and PVT properties can be grouped in the following categories [38] [39]:

- i. Thermodynamic factors such as: reservoir pressure, temperature and fluid composition; and gravitational (elevation) and capillary forces (interfacial curvature of the local porous medium).
- ii. Thermochemical factors such as: molecular diffusion and geothermal/geological temperature gradients that lead to steady state thermal diffusion –segregating the lightest components toward higher temperatures and the heaviest toward lower ones; and thermal convection –creating a practically constant composition with depth.
- iii. Petrochemical factors such as precipitation of Asphaltenes leading to the formation of tar mats at the bottom of reservoirs.

- iv. Biochemical factors such as biodegradation causing variations in hydrogen sulfide content or API gravity.
- v. Rock factors such as faults and heterogeneity, porosity, wettability etc.
- vi. Mechanism factors of hydrocarbon accumulation during genesis, migration, entrapment, etc.

Most of the previous factors are outlined in the following section.

4.2 Review of Literature

In 1907, Gibbs [6] was the first one to formulate the equation used for calculating the compositional variation due to gravity inside an isothermal system (i.e. $dT/dh=0$):

$$d\mu_i + M_i g dh = 0 \Leftrightarrow \mu_i(p_0, z_0, T) = \mu_i(p, z, T) + M_i g (h - h_0) \quad (4.1)$$

where μ_i is the chemical potential of component i ($i=1,2,\dots,N$), M_i its molar mass, g the acceleration of gravity, z_0 a single-phase mixture composition at reference pressure p_0 and reference depth h_0 , and z a single-phase mixture composition at pressure p and depth h (positive below reference depth).

In 1930, Muskat [40] studied the distribution of non-reacting fluids inside a gravitational field. He presented an explicit solution to Eq. (4.1) for several cases assuming ideal mixing leading to the false result that gravity has negligible effect on compositional grading in hydrocarbon reservoirs due to the oversimplified formula he used. He also discussed the importance of compositional gradients.

In 1939, assuming ideal solution, Sage and Lacey [7] analyzed the influence of gravity on the spatial distribution of components in a given reservoir fluid system under thermodynamic equilibrium (i.e. each component's sum of chemical and gravity potential is constant throughout the column). They also presented examples proving considerable compositional variations with depth

and came to the crucial conclusion that near-critical systems will show significant variations with depth.

In 1941, Leverett [41] presented the general formulation for capillary-gravity equilibrium in porous media. His equations did not take into consideration any conditions for thermodynamic equilibrium or compositional variation in the capillary transition zone and his theory was only valid for immiscible oil-water systems. For deep reservoirs where considerable variations have been observed near the gas-oil transition zone, a more strict approach is needed for the prediction of PVT-VLE behavior under the influence of both gravitational and capillary forces.

Until 1980, no publications are found in petroleum literature on the subject of compositional gradient analysis. However, a handful of papers mentioning reservoirs with compositional gradients were published during that time [42] [43] [44] [45] [46] [47].

In 1980, Schulte [48] was the first one to solve Eq. (4.1) using a cubic EOS, indicating that gravity segregation has an important role in the establishment of compositional variation. Comparing the EOS calculated gradients, he highlighted the importance of aromatic content, binary interaction coefficients, overall pressure and the presence of a Gas-Oil Contact (GOC) on compositional gradients.

In 1980 and 1983, compositional gradients worthy of attention in the Brent field of the North Sea were studied [49] [50]. The Brent field consists of the Brent and Statfjord reservoirs. For the Brent reservoir, a typical (saturated) GOC was observed, where an increase in dew-point pressure of the gas column with depth and a concurrent decrease in bubble-point pressure of the oil column are present; while both pressures equal reservoir pressure at the GOC. For the Statfjord reservoir, no saturated GOC has been observed; and fluid analyses indicated that separate bubble-point and dew-point trends do not exist. It was concluded that the Statfjord reservoir probably consists of a

hypercritical mixture that behaves vapor-like (dew-point fluid) at the top and liquid-like (bubble-point fluid) at the bottom.

In 1983, Holt et al. [51] addressed the effect of gravity and temperature gradients on Methane distribution in binary systems using irreversible thermodynamics. Their results indicated that 10% of the observed value of segregation was due to gravitational and thermal effects, predicting a much smaller gravitational effect on composition than Schulte [48]. They also noted that the effect of temperature is considerable in near-critical oil systems.

In 1985, Montel and Gouel [52] presented a method incorporating numerical simulation for the prediction of compositional grading with depth, which took into consideration the effect of gravity alone. Assuming stationary state and knowing pressure, temperature and overall composition at a given depth, their developed algorithm –an iterative calculation based on the fugacity of each component vs. depth– was able to calculate compositional grading, GOC location and change of physical state in relation with depth from a single sampling test. Although they did not include this in their work, they suggested that incorporating thermal diffusion might help make calculated compositional gradients more reliable. They, as well as Schulte [48], did not take into account the capillary force, which does not pose a problem in case of a single-phase fluid system. In case of a two-phase fluid system however, their method would lead to inconsistencies.

Also in 1985, Creek and Schrader [53] studied the compositional grading of the East Painter Reservoir Field of the Wyoming Overthrust Belt. They provided data compared to measured and calculated gradients with the aid of an isothermal Gravity/Chemical Equilibrium (GCE) model and also reported compositional gradients of various degrees to exist from field to field along the Overthrust Belt.

In January 1988, Riemens et al. [54] presented the Birba field, a field in South Oman with a significant compositional gradient. Thermodynamic modeling that was made suggested that compositional variations along the

hydrocarbon column have been induced by gravity resulting in a notably undersaturated oil underneath a gas cap.

Also in January 1988, Hirschberg [55] studied the effect of Asphaltenes on compositional grading inside a fluid column concluding that light oils ($\gamma_o \leq 0.85$ g/cm³ [$\geq 35^\circ$ API]) tend to exhibit greater compositional grading when in near-critical conditions; whereas for moderately heavy oils ($0.85 \leq \gamma_o \leq 0.93$ g/cm³ [$20^\circ \leq \text{API} \leq 35^\circ$]), segregation of Asphaltenes is a key factor in the establishment of compositional grading resulting possibly in the formation of tar-mats.

In August 1988, Metcalfe et al. [56] observed compositional gradients in the Anschutz Ranch East Field, Overthrust Belt along the Wyoming/Utah border. They used an EOS to study the PVT behavior of the sampled fluids and correlated compositional variations using measured data instead of a GCE model.

In 1989, Lee [38] presented a theory and a general thermodynamic formulation describing the influence of gravity and capillarity on reservoir fluid properties and phase behavior of a gas condensate system. His developed theory, assuming thermodynamic equilibrium, used the Leverett J-function [41] to calculate the reservoir rock pore curvature as a function of saturation, permeability and porosity for a certain depth inside the reservoir. On the other hand, his general formulation was used to describe component chemical potential in relation to pressure, temperature, composition, gravity and capillarity. The developed model was then used to study the effect of both capillarity and gravity on PVT-VLE fluid behavior. Compositional and fluid phase variations located in the capillary transition zone and further were able to be interpreted and predicted concluding that fluid distribution in the zone is dictated by capillary equilibrium alone.

In 1990, Jacqmin [57] discussed the interaction of natural convection and diffusional gravity segregation in hydrocarbon reservoirs. His results showed that the effects of these two forces combined may result in significant compositional variations in both horizontal and vertical directions.

In 1991, Wheaton [58] presented an isothermal GCE model with the addition of the effect of capillary pressure applicable to both oil and gas condensate reservoirs, suggesting that neglecting compositional gradients can lead to serious inconsistencies in determining the amounts of oil and gas initially in place.

In 1994, Whitson and Belery [59] studied compositional gradients in petroleum reservoirs caused by gravity and thermal effects. They provided examples of calculated compositional gradients for four North Sea reservoir fluid systems (black oil, slightly volatile oil, volatile oil and near critical oil) using the SRK [20] and PR [19] EOS's. They presented a solution algorithm for the isothermal GCE problem based on Michelsen's saturation pressure calculation algorithm [35]; and another algorithm for locating a potential GOC. The effect of thermal diffusion on compositional gradients was found to enhance, reduce, or completely eliminate them. Studying Methane gradients, they found that this effect is dictated by the thermal diffusion ratio k_T , namely:

$$\frac{dz_i}{dh} = -k_{T_i} \frac{d \ln T}{dh} \quad (4.2)$$

According to Eq. (4.2), if k_T is negative, Methane will migrate to zones of higher temperature (downwards), contrary to what is normally expected. Whitson and Belery concluded that including a passive thermal gradient (i.e. a hypothetical situation with a thermal gradient in a system without thermal diffusion) term in GCE calculations would have little to no effect. Moreover, they made the observation that for highly undersaturated systems, compositional grading is greatly reduced; hence, the degree of undersaturation is inversely proportional to gradient size. Finally, they highlighted the importance of developing an EOS fluid characterization when studying compositional grading.

In 1998, Temeng et al. [60] studied the variations of composition and PVT properties with depth in the Ghawar Khuff carbonate reservoirs, Saudi Arabia. They observed a hydrocarbon content decrease with a simultaneous acidic gas content increase with depth. These variations are contrary to what is

encountered in a typical oilfield and what would be expected from GCE principles. It was proposed that the leading process for compositional grading was the post-migration generation of hydrogen sulfide by the thermo-chemical reduction of anhydrite using hydrocarbons as one group of reactants, namely:



According to the previous theory, H_2S content increases with depth at the expense of Methane and heavier hydrocarbons ignoring the effect of GCE. Temeng et al. expected convective and gravitational forces to work together in the future and establish stable compositional gradients by moving the lighter components upwards and heavier ones to the bottom of the reservoirs.

In 1998, Biswas and Carey [61] presented a method for calculating the compositional variation in large hydrocarbon reservoirs with thermal gradients. Assuming stationary state, their developed EOS model coupled with the least-squares finite-element method (LSFEM) was used to simulate the phase behavior of a multi-component reservoir fluid inside a porous medium. Results were in good agreement with finite-different solutions of the same problem.

In 1999, Padua [62] studied a large deep water field in Brazil with significant compositional variation and a temperature gradient in the opposite direction of the Earth's thermal gradient. He developed a model in order to study the effects of gravity and temperature on reservoir fluid composition and PVT properties. Results indicated an increase in oil segregation with decreasing temperature.

In 2001, Høier and Whitson [39] quantified the compositional and PVT variation with depth due to gravitational, chemical and thermal forces. They quantitatively compared all of the available gradient models at the time –with or without thermal diffusion– using the reservoir fluids provided by Whitson and Belery [59]; and concluded that thermal diffusion tends to counter the force of gravity, producing compositional gradients much smaller than the isothermal GCE models. They discussed fluid initialization in reservoir models, giving guidelines for: (1) defining initial fluid distribution by using measured

field data; and (2) extrapolating vertical compositional gradients to depths where samples are unavailable. Finally, they presented two field case studies: one with a continuous transition from a rich condensate to a volatile oil described by the isothermal GCE model; and another one with a practically constant composition with depth caused by convection or thermal diffusion.

In 2003, Pedersen and Lindeloff [63] presented a method based on irreversible thermodynamics for the calculation of compositional grading with depth in two high-pressure gas condensate reservoirs with a vertical temperature gradient under stationary conditions (no heat flux). Under such conditions, and if one assumes no gravity effect, compositional variations with temperature are determined by the absolute specific enthalpy (H_i/M_i) of each component in relation to mixture absolute specific enthalpy (H/M). Hence, a component with $H_i/M_i > H/M$ will have the tendency to migrate toward warmer zones (e.g. bottom of a reservoir with a positive thermal gradient) or else (i.e. $H_i/M_i < H/M$), it will migrate to a colder zone (e.g. top of the reservoir). Higher molecular weight components tend to have higher specific enthalpies than lower ones inside a typical reservoir. Namely, H_i/M_i is assumed to increase with increasing MW for components up to C_{7+} , whereas it is assumed to stay more or less constant for higher carbon number components. They concluded that a positive vertical temperature gradient (e.g. even a temperature gradient of the order of 0.01°C/m) will enhance compositional variation with depth in relation to gravity segregation alone.

In 2004, Barrufet and Jaramillo [64] studied near-critical fluids (gas condensates and volatile oils) from the Cusiana Field in Colombia. The main purpose of their study was to evaluate the effects of an isothermal compositional gradient due to gravity upon the determination of in-situ hydrocarbon content, concluding that ignoring such a gradient can lead to either underestimating or overestimating oil reserves.

In 2006, Pedersen and Hjerstad [65] studied a fluid column of an upper gas and a lower volatile oil zone with a GOC in-between. A vertical

compositional variation much higher than what should be expected just by gravity was found to exist. This variation was the result of a temperature gradient of $0.026^{\circ}\text{C}/\text{m}$, which was described using irreversible thermodynamics. Finally, they highlighted the importance of taking into consideration both the effects of a gravitational and a thermal gradient in simulation models instead of only a gravitational one.

In 2007, Kord and Zobeidi [66] studied the effect of compositional grading on fluid characterization in a giant Iranian oil field. They used several isothermal and non-isothermal GCE models in order to estimate the fluid composition in a “blank” interval where no sample could be taken. Experimental data were best matched using the isothermal GCE model.

In 2008, James and Patience [67] presented a case study where compositional grading was used to improve reservoir characterization. The main reservoir of the study was initially believed to be compartmentalized, but thanks to compositional grading data, the reservoir was found to be much better connected. A viscous zone rich in Asphaltenes (tar mat) that would otherwise be neglected was also predicted near the Oil-Water Contact (OWC).

In 2015, Pedersen and Hjermsstad [68] analyzed the compositional gradients of five different North Sea reservoirs where compositional variations higher than what could be explained by gravity alone were reported. The highest compositional gradient was found to exist in the reservoir with the highest Asphaltene content, due to the notably higher absolute specific ideal gas enthalpy of the condensed aromatic compounds than that of the paraffinic and naphthenic ones. Calculated compositional data suggest that positive vertical temperature gradients are caused by larger ideal gas specific enthalpies of the “heavy” fraction due to higher content of aromatics in reservoir fluids.

In 2021, Vinhal et al. [69] performed compositional gradient analyses on five heavy oil reservoir systems, observing higher variations than what would be expected by gravity and thermal effects. Their developed EOS model accounted for the effect of fluid viscosity and aromatics content on compositional grading,

indicating that higher viscosity and/or aromatics content will result in more pronounced compositional gradients. Their EOS model managed to attain a good match between experimental and calculated gradient data; and was also applicable to three other reservoir systems not part of the study.

4.3 Isothermal Gravity/Chemical Equilibrium

A multi-component system that is in true thermodynamic equilibrium inside a gravity field: (1) is isothermal ($dT/dh=0$) and (2) for each of the system's components the sum of chemical and gravity potential is constant. For a given hydrocarbon column, adding to the traditional VLE condition an additional term due to gravity leads to the following equation:

$$d\mu_i + M_i g dh = 0 \Leftrightarrow \mu_i(p_0, z_0, T) = \mu_i(p, z, T) + M_i g(h - h_0) \quad (4.1)$$

meaning that equilibria between heights h_0 and h can be directly related. The chemical potentials are functions of composition z , pressure p and temperature T . If ideal gas behavior for every component is assumed, there is a simple solution to the above non-linear equation; but since the case for a system of such kind is far more complex than that of an ideal gas one, explicit analytical solutions can no longer be given.

Eq. (4.1) is the condition for GCE representing a set of N equations. Along with the condition that the sum of feed composition z equals one (i.e. $\sum z_i(h)=1$), one can solve the set of $N+1$ equations for composition z and pressure p at a given depth –below (negative) and above (positive) reference depth. Fluid properties such as bubble point and dew point pressures can also be determined with the aid of a phase behavior software package. By testing whether or not the solution is stable, one can specify whether a phase transition exists (e.g. GOC) and where it is located inside the hydrocarbon column.

The expression for chemical potential in terms of fugacity is the following:

$$\mu_i = RT \ln f_i + \lambda_i(T) \quad (4.3)$$

where R is the universal gas constant and $\lambda_i(T)$ the temperature dependent ideal gas contribution to chemical energy that drops out of the equation in most problems [16].

This way, one can express Eq. (4.1) in terms of fugacity:

$$\ln f_i(p_0, z_0, T) = \ln f_i(p, z, T) + \frac{1}{RT} M_i g(h - h_0) \quad (4.4)$$

The fugacity of each component is related to its fugacity coefficient via:

$$f_i = \varphi_i z_i p \quad (4.5)$$

Therefore, Eq. (4.4) for a multi-component system can be written as follows:

$$\ln(\varphi_i^{h_0} z_i^{h_0} p^{h_0}) = \ln(\varphi_i^h z_i^h p^h) + \frac{1}{RT} M_i g(h - h_0) \quad (4.6)$$

Fugacity can also be written as a function of height for convenience purposes:

$$f_i(h) = f_i(h_0) \exp\left[-\frac{M_i g(h - h_0)}{RT}\right] \quad (4.7)$$

In order to correct volumetric deficiencies of cubic EOS's the method of volume translation by Peneloux et al. [21] is utilized. Peneloux et al. applied the volume shift correction term c_i , modifying the fugacity expression as follows:

$$f_i^* = f_i \exp\left(-c_i \frac{p}{RT}\right) \quad (4.8)$$

Except for gradient calculations, this correction must also be applied to the pressure derivative of fugacity computed when using the isothermal GCE algorithm. However, for most phase VLE calculations (e.g. two-phase flash, stability analysis, saturation pressure), $\exp[-c_i(p/RT)]$ cancels leaving the calculated compositions unaffected [59].

Combining Eq. (4.1) with the equation for mechanical equilibrium (i.e. $dp/dh = -\rho g$) leads to the following expression:

$$p(h) = p(h_0) + \int_{h_0}^h \rho(h) g dh \quad (4.9)$$

which can be applied even when a GOC is located between heights h and h_0 (i.e. when the $\rho(h)$ function is not a continuous one).

4.3.1 Isothermal GCE Algorithm

An isothermal GCE algorithm was proposed by Whitson and Belery [59] based on Michelsen's method [35] for calculating saturation pressure or temperature, namely the modified equation:

$$Q(p, z) = 1 - \sum_{i=1}^N z_i \frac{\tilde{f}_i(p_0, z_0)}{f_i(p, z)} = 1 - \sum_{i=1}^N Y_i \quad (4.10)$$

where

$$\tilde{f}_i(p_0, z_0) = f_i(p_0, z_0) \exp\left[-\frac{M_i g (h - h_0)}{RT}\right] \quad (4.11.a)$$

and

$$Y_i = z_i \frac{\tilde{f}_i(p_0, z_0)}{f_i(p, z)} \quad (4.11.b)$$

The scope of work is the following:

1. Compute reference feed and gravity-corrected fugacities from Eq. (4.11.a). This only needs to be made once. The initial estimates of pressure and composition are reference depth values (p_0, z_0).
2. Compute fugacities of the composition estimate z at pressure estimate p using an EOS. Calculate mole numbers from Eq. (4.11.b) and fugacity ratio corrections using:

$$r_i = \frac{\tilde{f}_i(p_0, z_0)}{f_i(p, z)} \left(\sum_{j=1}^N Y_j \right)^{-1} \quad (4.12)$$

3. Update mole numbers as follows:

$$Y_i^{(n+1)} = Y_i^{(n)} [r_i^{(n)}]^\lambda \quad (4.13)$$

using four SS iterations (n=4) with $\lambda=1$ before a GDEM [34] promotion with λ given by:

$$\lambda = \left| \frac{b_{11}}{b_{11} - b_{01}} \right| \quad (4.14)$$

where

$$b_{01} = \sum_{i=1}^N \ln r_i^{(n)} \ln r_i^{(n-1)} \quad (4.15.a)$$

$$b_{11} = \sum_{i=1}^N \ln r_i^{(n-1)} \ln r_i^{(n-1)} \quad (4.15.b)$$

4. Update the composition estimate using:

$$z_i^{(n+1)} = Y_i^{(n+1)} \left(\sum_{j=1}^N Y_j^{(n+1)} \right)^{-1} \quad (4.16)$$

5. Update the pressure estimate using the Newton-Raphson method:

$$p^{(n+1)} = p^{(n)} - \frac{Q^{(n)}}{(\partial Q / \partial p)^{(n)}} \quad (4.17.a)$$

where

$$\frac{\partial Q}{\partial p} = \sum_{i=1}^N Y_i R_i \frac{(\partial f_i / \partial p)}{f_i(p, z)} \quad (4.17.b)$$

6. Check for convergence tolerance using the following criteria:

$$\left| 1 - \sum_{i=1}^N Y_i \right| < 10^{-13} \quad (4.18.a)$$

$$\left(\sum_{i=1}^N \frac{\ln(R_i)}{\ln(Y_i/z_i)} \right)^2 < 10^{-18} \quad (4.18.b)$$

7. Iterate until convergence is attained.

After finding the pressure p and composition z that satisfy Eq. (4.1), a phase stability test must be run in order to check if the solution is valid. Only a thermodynamically stable single phase solution is valid. An unstable one splits the calculated pressure and composition into two or more phases. In that case, the gradient calculation is reinitialized using the stability test composition y , with the new starting pressure being p_o or, ideally, the converged pressure that led to the unstable gradient solution. These types of solutions are found to exist near saturated GOC's [59].

4.3.2 Gas/Oil Contact Location

In order to locate either a saturated GOC or an under-saturated one, Whitson and Belery [59] proposed the following algorithm:

1. Compute the pressure and composition at the top and the bottom of the reservoir (p_T , z_T and p_B , z_B respectively) along with saturation pressures p_{sT} and p_{sB} . No GOC exists if saturation types are the same. Else, begin search for GOC depth (h_{GOC}).
2. Use interval halving according to saturation type. For iteration n , a dew-point solution at depth $h^{(n)}$ replaces the top depth for the next iteration (i.e. $h_T^{(n+1)}=h^{(n)}$); whereas a bubble-point solution at the same depth replaces the bottom depth (i.e. $h_B^{(n+1)}=h^{(n)}$). The depth estimate is:

$$h^{(n)} = 0.5[h_B^{(n)} + h_T^{(n)}] \quad (4.19)$$

3. Check for convergence tolerance δh using:

$$n = 15 \ln \frac{h_T - h_B}{\delta h} \quad (4.20)$$

For example, in order to achieve a tolerance of 0.33 ft, only 13 iterations are needed for a reservoir thickness of 1.640 ft.

4.4 Non-Isothermal Gravity/Chemical Equilibrium

In most reservoirs, an increase of temperature with depth does exist. In typical reservoirs, it was found to increase by about $0.02^\circ\text{C}/\text{m}$ from top to bottom [65]. A temperature gradient causes a heat flow between different temperature zones. In a non-isothermal system, heat flow from warmer to colder zones results in component molecular flux. Hence, isothermal equilibrium is not feasible causing an entropy flux inside the reservoir.

At stationary state, compositional variation with depth is determined by component fugacities, molecular weights and heat content (i.e. absolute enthalpy per mass unit). According to Pedersen and Lindeloff [63], for a non-isothermal reservoir, Eq. (4.6) can be modified as follows:

$$\begin{aligned} RT\ln(\varphi_i^h z_i^h p^h) - RT\ln(\varphi_i^{h_0} z_i^{h_0} P_i^{h_0}) \\ = M_i g(h - h_0) - M_i \left(\frac{H}{M} - \frac{\tilde{H}_i}{M_i} \right) \frac{\Delta T}{T} \end{aligned} \quad (4.21)$$

where \tilde{H}_i is the component partial molar enthalpy, H the molar enthalpy of the mixture, M the average molecular weight and ΔT the temperature difference between depths h and h_0 . The non-isothermal GCE problem is solved using the isothermal GCE equations coupled with Eq. (4.21).

The overall molar enthalpy of a mixture of N components is:

$$H = \sum_{i=1}^N z_i \tilde{H}_i = \sum_{i=1}^N z_i H_i^{ig} + \sum_{i=1}^N z_i \tilde{H}_i^{res} \quad (4.22)$$

According to Pedersen and Hjermsstad [65], the partial molar enthalpy of a mixture component at temperature T is given by:

$$\tilde{H}_i(T) = H_i^{ig}(273.15\text{K}) + \left(H_i^{ig}(T) - H_i^{ig}(273.15\text{K}) \right) + \tilde{H}_i^{res} \quad (4.23)$$

where H_i^{ig} is the ideal gas enthalpy of component i and \tilde{H}_i^{res} its partial molar residual enthalpy that is obtained through:

$$\tilde{H}_i^{res} = -RT^2 \frac{\partial \ln \phi_i}{\partial T} \quad (4.24)$$

The ideal gas enthalpy (at 273.15K) in their work was calculated using the following correlations:

$$\frac{H_i^{ig}(273.15K)}{R} = -1342 + 8.367M_i \quad (4.25.a)$$

and

$$H_i^{ig}(T) - H_i^{ig}(273.15K) = \int_{273.15K}^T C_{p_i}^{id} \quad (4.25.b)$$

where $C_{p_i}^{id} = C_{1,i} + C_{2,i}T + C_{3,i}T^2 + C_{4,i}T^3$ is the ideal heat capacity, and C_1 through C_4 are the component heat capacities.

Chapter 5

Laboratory and Simulation Procedures

5.1 Sampling Data

A single-phase reservoir fluid was sampled from an offshore Greek reservoir located in the Mediterranean Sea. The reservoir spans from 7800 ft to 8700 ft in depth below sea level and is considered isothermal with $T_{\text{res}}=134.6^{\circ}\text{F}$. The fluid was sampled at 8134 ft (reference depth). The sampled fluid is comprised of 18 components and its feed composition is given in Table 5.1. The fluid's component composition plot is shown in Figure 5.1 for components H_2S through C_{13+} (Component ID: 1 through 18).

Table 5.1: Reservoir fluid feed composition

Component	Feed Composition (mole percent)
Hydrogen Sulfide (H_2S)	11.245
Carbon Dioxide (CO_2)	7.010
Nitrogen (N_2)	1.172
Methane (CH_4)	38.698
Ethane (C_2H_6)	1.522
Propane (C_3H_8)	0.687
iso-Butane (IC_4)	0.248
n-Butane (NC_4)	0.479
iso-Pentane (IC_5)	0.340
n-Pentane (NC_5)	0.319
Hexanes (FC_6)	1.056
Heptanes (FC_7)	0.900
Octanes (FC_8)	2.010
Nonanes (FC_9)	2.585
Decanes (FC_{10})	2.088
Undecanes (FC_{11})	1.768
Dodecanes (FC_{12})	2.058
Tridecanes plus (C_{13+})	25.815
Total	100.000

For the Tridecanes plus fraction (C_{13+}), also known as the “heavy” fraction, its molecular weight and specific gravity were measured using experimental procedures as $MW_{C_{13+}}=313$ and $SG_{C_{13+}}=0.855$ respectively.

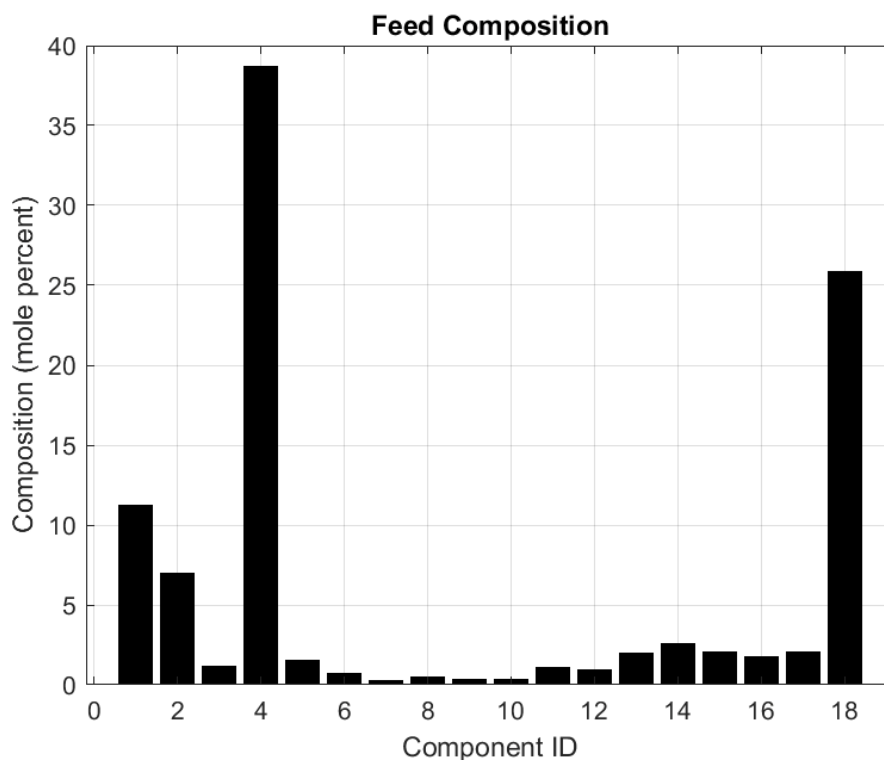


Figure 5.1: Component composition plot

5.2 Laboratory Procedures

The following three laboratory experiments were carried out at the Laboratory of PVT and Core Analysis located at the School of Mineral Resources Engineering, Technical University of Crete:

- Constant Composition Expansion (CCE)
- Differential Liberation (DL)
- Separator Test

The above procedures and the results they yield are outlined in the following sub-sections.

5.2.1 Constant Composition Expansion

A reservoir fluid sample of known mass is placed in a laboratory cell. The pressure of the cell is set to a value equal to or greater than reservoir pressure –to ensure the fluid is single-phase– and its temperature is set equal to reservoir temperature. The pressure of the cell is reduced in steps by increasing its volume while temperature is held constant. At each pressure step, the fluid’s total volume ($V_t = V_o + V_g$) is measured. No gas or liquid is removed from the cell throughout the process; hence, the overall fluid composition remains unaltered. A typical CCE experiment is shown in Figure 5.2.

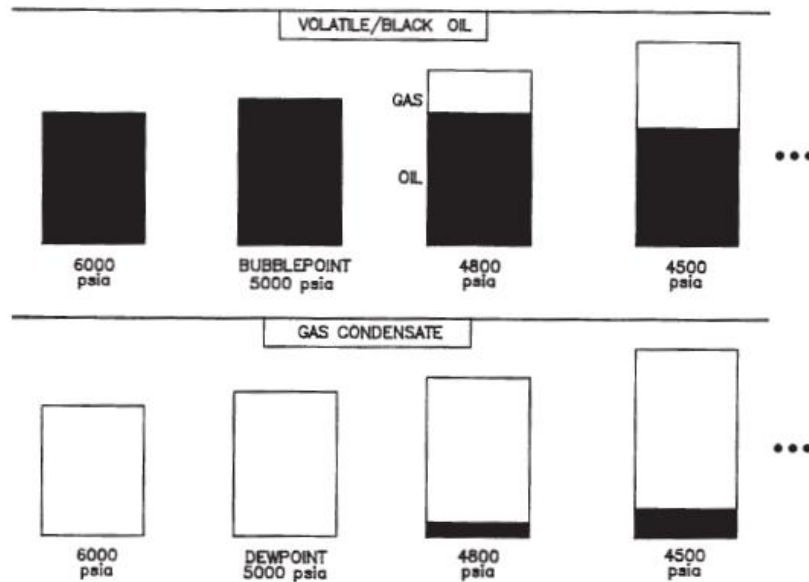


Figure 5.2: CCE for a volatile/black oil vs. a gas condensate (Source: Whitson & Brule [2])

Starting from a pressure of 4992.2 psia, the offshore Greek reservoir fluid underwent the CCE experiment at fixed temperature $T_{res}=134.6^{\circ}\text{F}$. The derived experimental PVT data include the bubble-point pressure (p_{sat}) and the fluid’s relative total volume (V_{rt}) –also known as ROV– at each pressure step (Table 5.2). Relative total volume is a dimensionless quantity defined as follows:

$$V_{rt} = \frac{V_t}{V_{ob}} \quad (5.1)$$

where V_t is the fluid’s total volume at each step and V_{ob} is oil volume at the bubble-point condition.

Table 5.2: Experimental CCE data at 134.6°F

Pressure (psia)	Experimental ROV
4992.20	0.9902
4636.86	0.9931
4281.51	0.9960
3926.17	0.9990
3826.10	1.0000
3286.56	1.0291
2858.69	1.0655
2432.28	1.1216
2005.87	1.2117
1437.32	1.4586

As shown in Table 5.2, the experimental value of the bubble-point pressure is $p_{\text{sat}}=3826.1$ psia.

5.2.2 Differential Liberation

This experiment is carried out in order to simulate reservoir performance throughout production. Similarly to the CCE procedure, a single-phase fluid sample is put in a lab cell with pressure and temperature equal to their reservoir values. Cell pressure is isothermally decreased in steps by increasing the volume until the bubble-point is reached, where the bubble-point oil volume (V_{ob}) is measured. Through this point, the DL procedure is identical to the CCE. Pressure is then decreased in a similar manner below the bubble-point until atmospheric pressure is reached. At each interval, the total gas liberated is removed from the cell while pressure is held constant. The volume (V_{g}) and specific gravity (γ_{g}) of the gas, as well as the remaining oil volume (V_{o}) are measured. Throughout this whole process, the remaining oil inside the cell changes in composition, becoming richer in heavier hydrocarbon components. After atmospheric pressure (14.7 psia) is reached, the temperature of the cell is reduced to ambient temperature (60°F or 15.6°C) where the residual oil volume (V_{or}) and the oil specific gravity (γ_{o}) are measured. A typical DL experiment is shown in Figure 5.3.

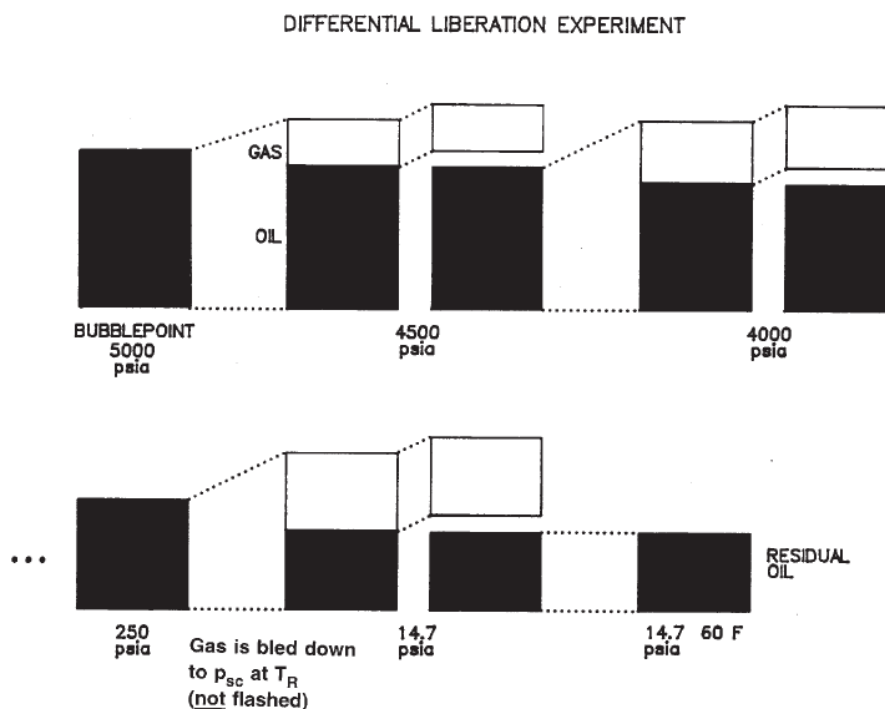


Figure 5.3: DL experiment for a typical oil sample (Source: Whitson & Brule [2])

Starting from a pressure of 4992.21 psia, the DL experiment was carried out for the offshore Greek reservoir fluid at fixed temperature $T_{res}=134.6^{\circ}\text{F}$. Reported PVT data at each pressure step include: oil FVF (B_o), solution GOR (R_s), oil SG (γ_o) and oil and gas viscosities (η_o , η_g) (Table 5.3).

Table 5.3: Experimental DL data at 134.6°F

Pressure (psia)	Oil FVF (RB/STB)	Solution GOR (scf/STB)	Oil SG	Oil Viscosity (cP)	Gas Viscosity (cP)
4992.21	1.2893	724.23	0.7811	1.05	-
4636.86	1.2931	724.23	0.7788	1.03	-
4281.52	1.2969	724.23	0.7765	1.00	-
3926.18	1.3008	724.23	0.7742	0.94	-
3826.10	1.3021	724.23	0.7734	0.92	-
3428.70	1.2747	654.16	0.7813	1.00	0.02400
3002.29	1.2515	584.87	0.7869	1.12	0.02215
2574.42	1.2268	515.19	0.7936	1.30	0.01999
1721.60	1.1764	369.05	0.8076	1.61	0.01630
868.78	1.1213	209.70	0.8239	1.83	0.01280
298.78	1.0742	87.92	0.8389	2.54	0.01016
114.58	1.0538	38.40	0.8449	2.91	0.00869
14.50	1.0320	0.00	0.8529	3.66	0.00726

Oil FVF corresponds to the value of oil volume at each pressure step per unit of residual oil volume, namely:

$$B_o = \frac{V_o}{V_{or}} \quad (5.2)$$

Solution GOR corresponds to the total volume of gas liberated at each pressure per unit of residual oil volume:

$$R_s = \frac{V_g}{V_{or}} \quad (5.3)$$

5.2.3 Separator Test

The multi-stage separator test (Figure 5.4) is usually done in two or three stages, with the last stage corresponding to a stock tank condition (STC: atmospheric pressure and ambient temperature). During the separator test, a reservoir fluid of known bubble-point oil volume (V_{ob}) initially at saturation pressure and reservoir temperature is placed in the first separator stage where pressure and temperature are selected. The liberated gas is removed and its volume (V_g) is measured. The remaining oil volume (V_{osp}) is also measured and is then brought to the next separator stage. The above process is repeated until the fluid reaches the stock tank stage (14.7 psia & 60°F), where stock tank oil volume (V_{STO}) and stock tank oil SG (γ_{STO}) are measured.

Three values of experimental data are derived in total: overall solution GOR (R_{st}), separator oil FVF (B_{osp}) and stock tank oil API gravity. The overall solution GOR is computed as the sum of gas volume removed at every stage divided by the stock tank oil volume:

$$R_{st} = \frac{\sum V_g}{V_{STO}} \quad (5.4)$$

Separator oil FVF is computed as the ratio of separator oil volume at each stage per stock tank oil volume, namely:

$$B_{osp} = \frac{V_{osp}}{V_{STO}} \quad (5.5)$$

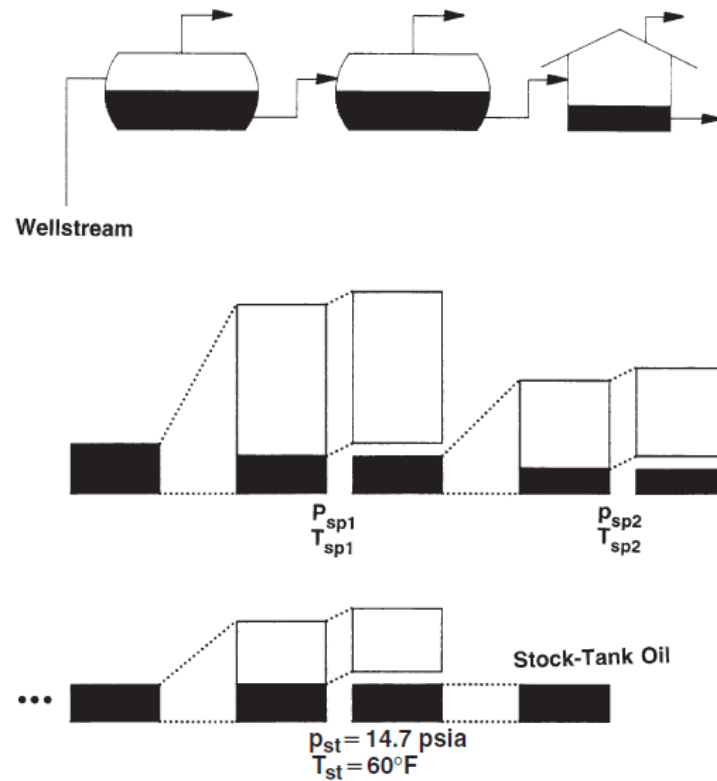


Figure 5.4: Multi-stage separator test for a typical oil sample (Source: Whitson & Brule [2])

A single-stage separator test was conducted on the offshore Greek reservoir fluid (Table 5.4). The derived experimental PVT data are given in Table 5.5.

Table 5.4: Single-stage separator test for the offshore Greek reservoir fluid

	Initial	Stage #1	Stock Tank
Press. (psia)	3826.1	185.6	14.7
Temp. (°F)	134.6	71.6	60

Table 5.5: Experimental single-stage separator data

Data Type	Experimental Value
GOR (scf/STB)	710
FVF (RB/STB)	1.283
API (°API)	29.4

5.3 Simulation Procedures using Commercial Software

Using commercial phase behavior software, the following procedures were simulated for the offshore Greek reservoir fluid:

- Constant Composition Expansion Calculation
- Differential Liberation Calculation
- Separator Test Calculation
- Saturation Pressure Calculation
- Two-Phase Envelope Calculation
- Two-Phase Flash Calculation
- Compositional Gradient Calculation

Two different fluid characterizations were developed: one using the SRK-EOS [20] and one using the PR-EOS [19]. The cubic EOS's were tuned to match the experimental PVT data provided in Sec. 5.2 by modifying their properties using Agarwal et al.'s non-linear regression method [37]. The critical pressure and temperature, acentric factor and molecular weight of the "heavy" fraction (C₁₃₊) were used as regression variables for both fluid characterizations.

Initially, the properties of the C₁₃₊ fraction were calculated by the commercial PVT software using the measured values of molecular weight ($MW_{C_{13+}}=313$) and specific gravity ($SG_{C_{13+}}=0.855$) as input data. Physical and critical properties of the C₁₃₊ fraction were computed using the Twu correlation [70], whereas C₁₃₊ acentric factor was computed using the Lee-Kesler correlation [71]. The modified along with the initially correlated (non-modified) properties of the C₁₃₊ fraction are given in Table 5.6.

Table 5.6: Modified vs. initially correlated properties of the C₁₃₊ fraction

EOS	p_c (atm)	T_c (K)	ω	MW
tuned SRK	19.80	891.5	0.4439	320.287
tuned PR	17.96	963.7	0.4688	325.526
un-tuned EOS	11.32	822.9	0.92361	313.000

For the rest of the fluid's components (H₂S through FC₁₂), their properties were taken from the software's available database, which uses the Lee-Kesler correlation [71] to calculate component critical properties and Whitson's method [72] to calculate molecular weights and specific gravities. All component properties and binary interaction coefficients of the SRK and PR EOS fluid characterizations are provided in Tables A.1 through A.3, Appendix A. The aforementioned commercial software calculations were also carried out using the un-tuned EOS models. Their respective results are all provided in Appendix A.

5.3.1 Constant Composition Expansion Calculation

The CCE experiment was simulated at $T_{\text{res}}=134.6^{\circ}\text{F}$ using the data of Table 5.2 as input data and the experimental value of 3826.1 psia as the saturation pressure estimate. Experimental vs. calculated ROV's are given in Table 5.7 and are plotted vs. pressure in Figure 5.5. The rest of the calculated PVT data from the simulated CCE experiment and their respective plots are given in Tables A.4 through A.7 and Figures A.2 through A.7 of Appendix A.

Table 5.7: CCE experimental vs. calculated ROV's using commercial software

Pressure (psia)	Experimental	Calculated ROV	
	ROV	SRK EOS	PR EOS
4992.20	0.9902	0.9879	0.9903
4636.86	0.9931	0.9914	0.9931
4281.51	0.9960	0.9950	0.9960
3926.17	0.9990	0.9989	0.9991
3826.10	1.0000	1.0000	1.0000
p_{sat}^*	-	1.0000	1.0000
3286.56	1.0291	1.0292	1.0276
2858.69	1.0655	1.0645	1.0613
2432.28	1.1216	1.1183	1.1131
2005.87	1.2117	1.2055	1.1979
1437.32	1.4586	1.4342	1.4230

*Calculated value: $p_{\text{sat}}=3826.07$ psia (SRK-EOS), $p_{\text{sat}}=3825.57$ psia (PR-EOS).

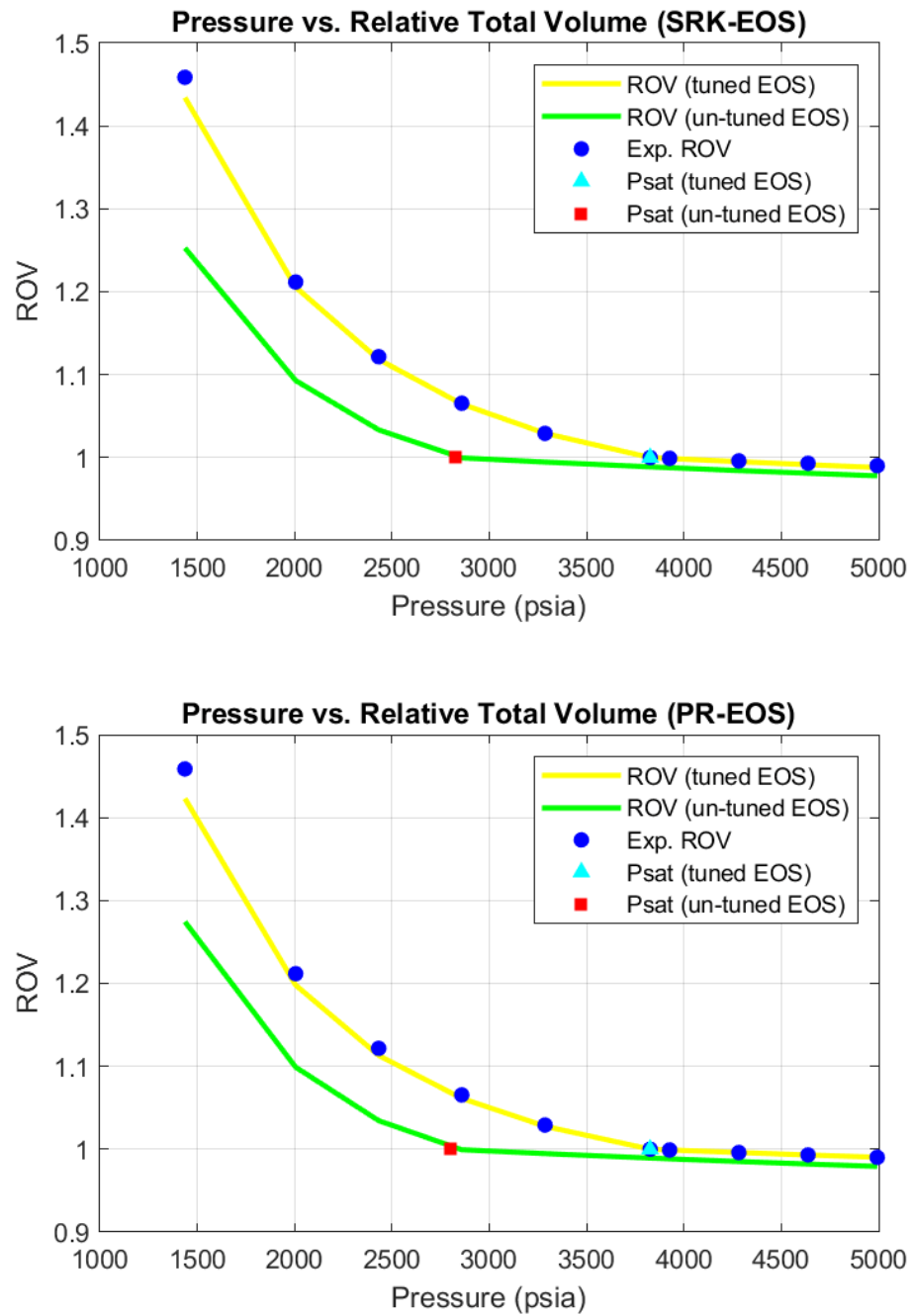


Figure 5.5: ROV plots using commercial software

5.3.2 Differential Liberation Calculation

The DL experiment was simulated at $T_{res}=134.6^{\circ}\text{F}$ using the data of Table 5.3 as input data and the experimental value of 3826.1 psia as the saturation pressure estimate. Experimental vs. calculated oil FVF's and solution GOR's are given in Table 5.8 and are plotted vs. pressure in Figure 5.6 and Figure 5.7 respectively. Experimental vs. calculated oil SG's are given in Table A.8 and are plotted vs. pressure in Figure A.8 of Appendix A. Experimental vs. calculated oil and gas viscosities are given in Table A.9 and are plotted vs. pressure in Figures A.9 and A.10 of Appendix A. The rest of the calculated PVT data from the DL experiment and their respective plots are given in Tables A.10 through A.13 and Figures A.11 through A.16 of Appendix A.

Table 5.8: DL experimental vs. calculated FVF's and GOR's using commercial PVT software

Pressure (psia)	Exp. Oil FVF (RB/STB)	Calc. Oil FVF (RB/STB)		Exp. Solution GOR (scf/STB)	Calc. Solution GOR (scf/STB)	
		SRK EOS	PR EOS		SRK EOS	PR EOS
4992.21	1.2893	1.29127	1.25704	724.23	720.96	706.57
4636.86	1.2931	1.29577	1.26058	724.23	720.96	706.57
4281.52	1.2969	1.30053	1.26430	724.23	720.96	706.57
3926.18	1.3008	1.30556	1.26823	724.23	720.96	706.57
3826.10	1.3021	1.30704	1.26938	724.23	720.96	706.57
p_{sat} *	-	1.30704	1.26938	-	720.96	706.57
3428.70	1.2747	1.28406	1.24909	654.16	657.12	644.78
3002.29	1.2515	1.25938	1.22722	584.87	589.26	578.83
2574.42	1.2268	1.23439	1.20505	515.19	521.51	512.75
1721.60	1.1764	1.18271	1.15911	369.05	384.84	378.67
868.78	1.1213	1.12609	1.10847	209.70	241.22	236.09
298.78	1.0742	1.07824	1.06569	87.92	125.83	120.67
114.58	1.0538	1.05407	1.04454	38.40	70.40	66.03
14.50	1.0320	1.01886	1.01526	0.00	0.00	0.00

*Calculated value: $p_{sat}=3826.07$ psia (SRK-EOS), $p_{sat}=3825.57$ psia (PR-EOS).

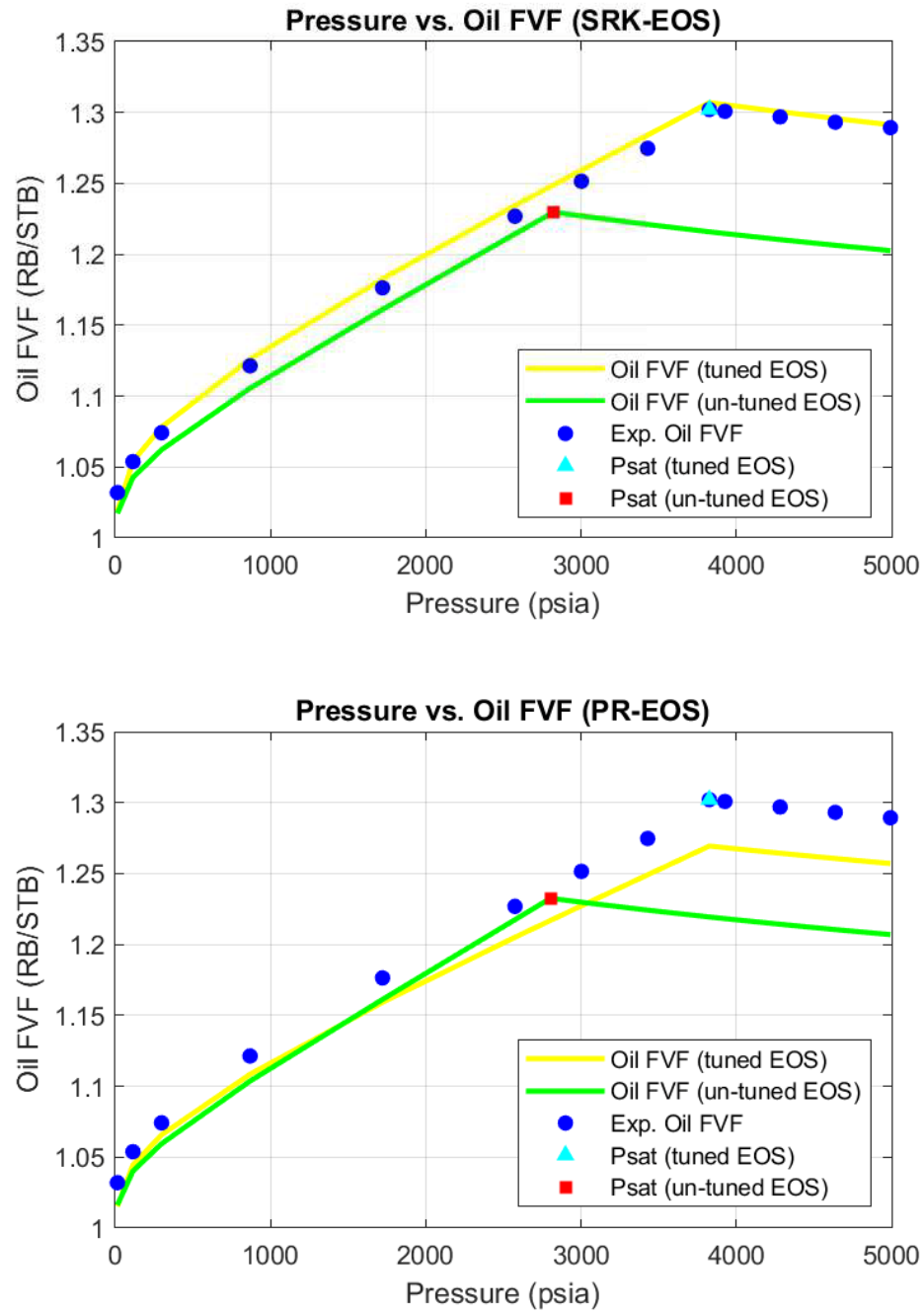


Figure 5.6: Oil FVF plots using commercial software

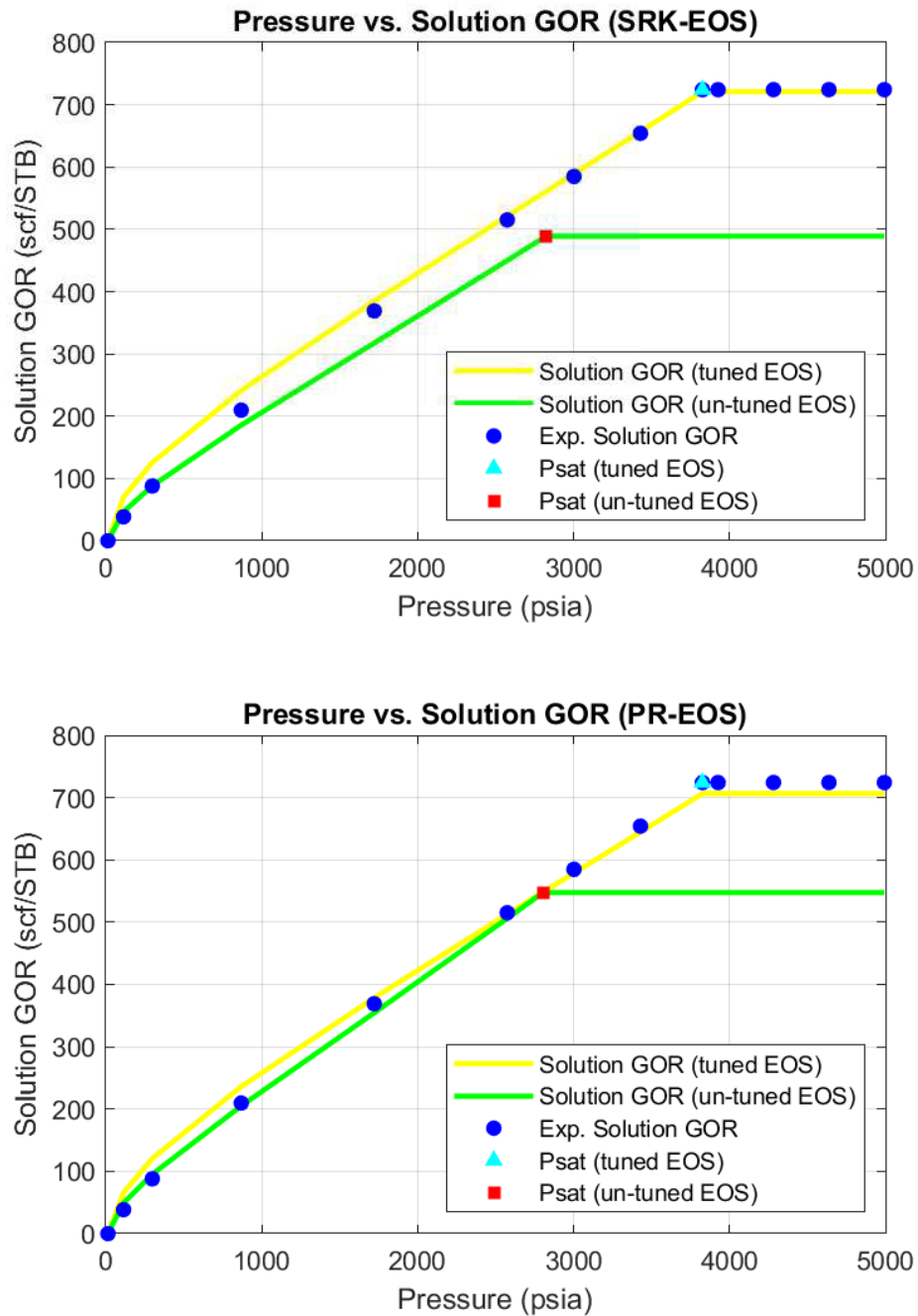


Figure 5.7: Solution GOR plots using commercial software

5.3.3 Separator Test Calculation

The single-stage separator test of Table 5.4 was simulated using the data of Table 5.5 as experimental data. Experimental vs. calculated single-stage separator data are shown in Table 5.9. Tables 5.10 and 5.11 show the calculated results using the developed SRK and PR EOS models respectively.

Table 5.9: Experimental vs. calculated single-stage separator data using commercial software

Data Type	Experimental Value	Calculated Value	
		SRK EOS	PR EOS
GOR (scf/STB)	710	695.66	683.82
FVF (RB/STB)	1.283	1.292	1.257
API (°API)	29.4	29.53	30.62

Table 5.10: Separator test calculation results for the SRK-EOS using commercial software

	Initial	Stage #1	Stock Tank
Press. (psia)	$p_{\text{sat}}=3826.07$	185.6	14.7
Temp. (°F)	134.6	71.6	60
Gas Vol. (mole)	-	240.5859	28.1155
Oil Vol. (litre)	-	53.0803	51.3778
GOR (scf/RB)*	-	602.89	72.79
GOR (scf/STB)**	-	622.87	72.79
Separator Volume Factor (RB/STB)***	-	1.033	1.000
Gas Z-factor	-	0.965	0.994
Gas SG	-	0.7783	1.1514

*Gas volume @STC / oil volume @p,T

**Gas volume @STC / oil volume @STC

***Oil volume @p,T / oil volume @STC

Table 5.11: Separator test calculation results for the PR-EOS using commercial software

	Initial	Stage #1	Stock Tank
Press. (psia)	p_{sat}=3825.57	185.6	14.7
Temp. (°F)	134.6	71.6	60
Gas Vol. (mole)	-	241.1774	28.1975
Oil Vol. (litre)	-	53.9070	52.3986
GOR (scf/RB)	-	595.11	71.58
GOR (scf/STB)	-	612.24	71.58
Separator			
Volume Factor (RB/STB)	-	1.029	1.000
Gas Z-factor	-	0.958	0.993
Gas SG	-	0.7802	1.1472

5.3.4 Saturation Pressure Calculation

A saturation pressure calculation was performed at $T_{res}=134.6^{\circ}\text{F}$. The commercial PVT software uses the saturation pressure calculation technique proposed by Nghiem et al. [73]. The experimental value of 3826.1 psia was used as the saturation pressure estimate with a weight factor of 50. The calculated values of saturation pressure were $p_{sat}=3826.068$ psia for the SRK-EOS and $p_{sat}=3825.570$ psia for the PR-EOS. Saturation pressure calculation results are given in Tables 5.12 through 5.15.

5.3.5 Two-Phase Envelope Calculation

The two-phase envelope calculation involves the construction of the p-T mixture diagram for the studied offshore Greek reservoir fluid. The bubble-point and dew-point curves represent the boundary between the single-phase and two-phase regions (two-phase boundary). Both curves intersect at the critical point. The area encased by the envelope corresponds to the two-phase region. Quality lines inside the envelope (10%, 20% and 40%) correspond to equal volumes of liquid and vapor within the mixture and all converge at the critical point. The phase envelopes constructed using the developed SRK and PR EOS models are given in Figures 5.8 and 5.9 respectively.

Table 5.12: Saturation pressure calculation results for the SRK-EOS using commercial software

Component	Composition (mole percent)		K-values (y_i/z_i)	$\ln f_i$ (atm)
	Dominant phase (z_i)	Incipient phase (y_i)		
H ₂ S	11.245	5.67274	0.5045	1.7587
CO ₂	7.010	5.81610	0.8297	2.1758
N ₂	1.172	3.39103	2.8934	2.4491
CH ₄	38.698	81.49933	2.1060	5.1930
C ₂ H ₆	1.522	1.69357	1.1127	0.6333
C ₃ H ₈	0.687	0.49234	0.7167	-1.1037
IC ₄	0.248	0.13342	0.5380	-2.7624
NC ₄	0.479	0.21985	0.4590	-2.4022
IC ₅	0.340	0.11436	0.3363	-3.4176
NC ₅	0.319	0.09680	0.3035	-3.6929
FC ₆	1.056	0.21168	0.2005	-3.3016
FC ₇	0.900	0.11885	0.1321	-4.2859
FC ₈	2.010	0.18218	0.0906	-4.2333
FC ₉	2.585	0.15738	0.0609	-4.7889
FC ₁₀	2.088	0.08404	0.0402	-5.8322
FC ₁₁	1.768	0.05044	0.0285	-6.7120
FC ₁₂	2.058	0.03975	0.0193	-7.3496
C ₁₃ +	25.815	0.02615	0.0010	-10.2323

Table 5.13: Saturation pressure calculation properties for the SRK-EOS using commercial software

	Dominant phase (z_i)	Incipient phase (y_i)
Z-factor	1.4061	0.9070
Molar Vol. (m³/mol)	0.14632	0.09438
MW (g/mol)	113.56	20.62
Density (lb/ft³)	48.4486	13.6372
Viscosity (cP)	0.9804	0.0256
IFT (dyn/cm)	0.0000	1.9956
Phase Vol. percent	100.0000	0.0000
Phase mole percent	100.0000	0.0000

Table 5.14: Saturation pressure calculation results for the PR-EOS using commercial software

Component	Composition (mole percent)		K-values (y_i/z_i)	$\ln f_i$ (atm)
	Dominant phase (z_i)	Incipient phase (y_i)		
H ₂ S	11.245	6.15886	0.5477	1.7435
CO ₂	7.010	5.85094	0.8347	2.0861
N ₂	1.172	3.19203	2.7236	2.3292
CH ₄	38.698	80.93374	2.0914	5.1021
C ₂ H ₆	1.522	1.74713	1.1479	0.5448
C ₃ H ₈	0.687	0.51496	0.7496	-1.2114
IC ₄	0.248	0.14018	0.5653	-2.8919
NC ₄	0.479	0.23456	0.4897	-2.5215
IC ₅	0.340	0.12314	0.3622	-3.5539
NC ₅	0.319	0.10498	0.3291	-3.8261
FC ₆	1.056	0.23531	0.2228	-3.4243
FC ₇	0.900	0.13525	0.1503	-4.4045
FC ₈	2.010	0.21158	0.1053	-4.3498
FC ₉	2.585	0.18665	0.0722	-4.9042
FC ₁₀	2.088	0.10215	0.0489	-5.9406
FC ₁₁	1.768	0.06253	0.0354	-6.8167
FC ₁₂	2.058	0.05061	0.0246	-7.4416
C ₁₃₊	25.815	0.01538	0.0006	-12.4227

Table 5.15: Saturation pressure calculation properties for the PR-EOS using commercial software

	Dominant phase (z_i)	Incipient phase (y_i)
Z-factor	1.3949	0.8413
Molar Vol. (m ³ /mol)	0.14518	0.08756
MW (g/mol)	114.91	20.83
Density (lb/ft ³)	49.4118	14.8523
Viscosity (cP)	1.0542	0.0277
IFT (dyn/cm)	0.0000	1.6509
Phase Vol. percent	100.0000	0.0000
Phase mole percent	100.0000	0.0000

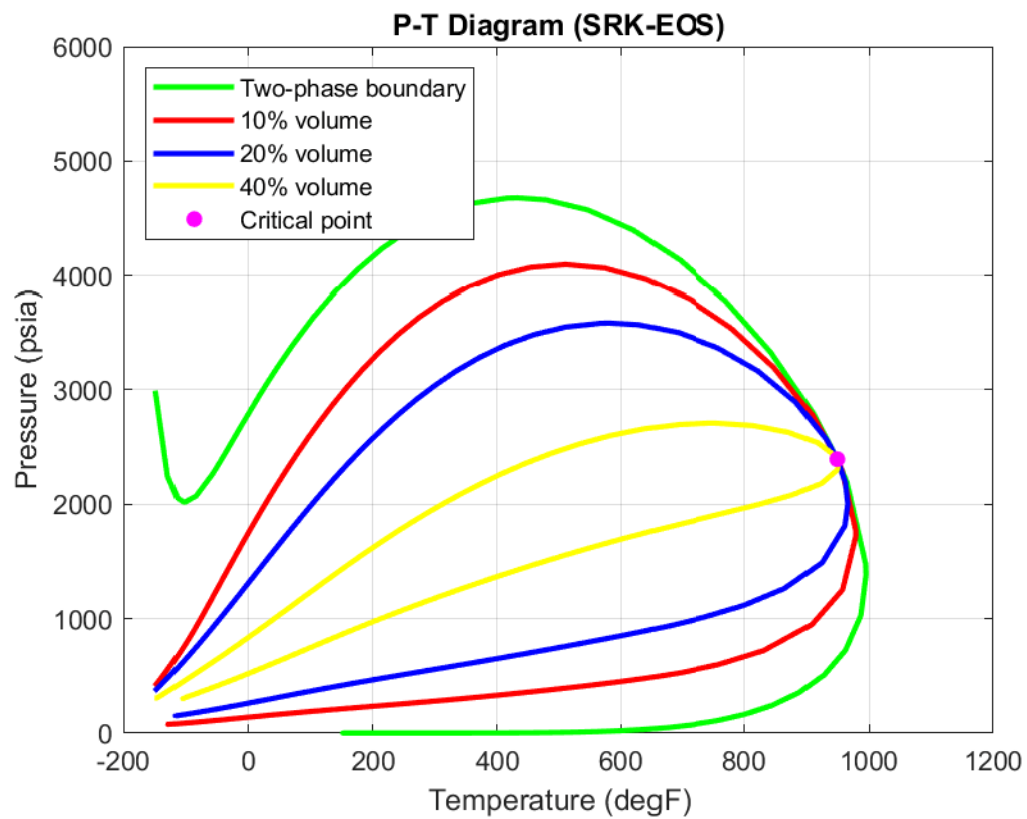


Figure 5.8: Two-phase envelope of the offshore Greek reservoir fluid (SRK-EOS)

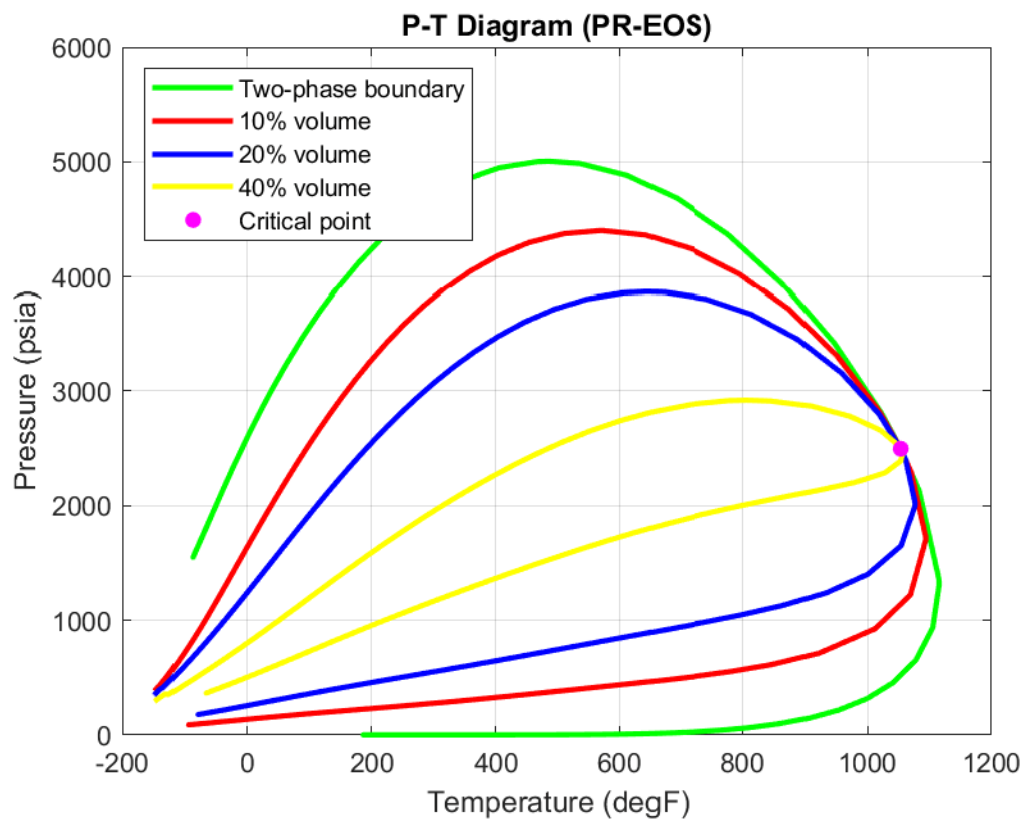


Figure 5.9: Two-phase envelope of the offshore Greek reservoir fluid (PR-EOS)

5.3.6 Two-Phase Flash Calculation

An isothermal two-phase flash calculation was performed at reference conditions $p_{\text{res}}=3826.1$ psia and $T_{\text{res}}=134.6^\circ\text{F}$. The mixture was found to be borderline single-phase at the above conditions, signifying that mixture liquid phase composition equals the overall feed composition and no vapor phase exists, i.e. $x_i=z_i$ and $y_i=0$. Two-phase flash calculation results are given in Tables 5.16 and 5.17.

Table 5.16: Two-phase flash calculation results using commercial software

Component	Composition (mole percent)	$\ln f_i$ (atm)	
	Liquid phase (x_i)	SRK EOS	PR EOS
H ₂ S	11.245	1.7587	1.7436
CO ₂	7.010	2.1758	2.0862
N ₂	1.172	2.4491	2.3293
CH ₄	38.698	5.1930	5.1021
C ₂ H ₆	1.522	0.6333	0.5449
C ₃ H ₈	0.687	-1.1037	-1.2113
IC ₄	0.248	-2.7624	-2.8917
NC ₄	0.479	-2.4022	-2.5214
IC ₅	0.340	-3.4176	-3.5537
NC ₅	0.319	-3.6929	-3.8260
FC ₆	1.056	-3.3016	-3.4241
FC ₇	0.900	-4.2859	-4.4043
FC ₈	2.010	-4.2333	-4.3496
FC ₉	2.585	-4.7888	-4.9040
FC ₁₀	2.088	-5.8322	-5.9404
FC ₁₁	1.768	-6.7120	-6.8165
FC ₁₂	2.058	-7.3496	-7.4413
C ₁₃₊	25.815	-10.2323	-12.4222

Table 5.17: Two-phase flash calculation properties using commercial software

	Liquid phase (x_i)	
	SRK EOS	PR EOS
Z-factor	1.4061	1.3951
Molar Vol. (m ³ /mol)	0.14632	0.14518
MW (g/mol)	113.56	114.91
Density (lb/ft ³)	48.4486	49.4121
Viscosity (cP)	0.9804	1.0543
Phase Vol. percent	100.0000	100.0000
Phase mole percent	100.0000	100.0000

5.3.7 Compositional Gradient Calculation

An isothermal compositional gradient calculation was performed at reference conditions $p_{\text{res}}=3826.1$ psia and $T_{\text{res}}=134.6^{\circ}\text{F}$. The calculation was initiated at reference depth $h_{\text{ref}}=8134$ ft, splitting the reservoir in 10 calculation intervals of 90 ft from top depth $h_{\text{top}}=7800$ ft to bottom depth $h_{\text{bot}}=8700$ ft. The GOC was located at 8133 ft. Reported compositional gradient calculation results include the variation from top to bottom in: reservoir pressure, saturation pressure, reservoir fluid density and component composition.

For the gradient calculation, the commercial PVT software uses the isothermal GCE algorithm developed by Whitson and Belery [59] and optionally incorporates the volume translation method of Peneloux et al. [21], the constant volume shift parameters of which are computed using the correlation of Jhaveri and Youngren [24]. Constant volume shift parameters for the SRK and PR EOS fluid characterizations are given in Table 5.18.

Table 5.18: Constant volume shift parameters for the SRK and PR EOS fluid characterizations

Component	Constant Volume Shift (S_i)	
	SRK EOS	PR EOS
H ₂ S	0.0466	-0.1288
CO ₂	0.0833	-0.0817
N ₂	-0.0079	-0.1927
CH ₄	0.0234	-0.1595
C ₂ H ₆	0.0605	-0.1134
C ₃ H ₈	0.0825	-0.0863
IC ₄	0.0830	-0.0844
NC ₄	0.0975	-0.0675
IC ₅	0.1022	-0.0608
NC ₅	0.1209	-0.0390
FC ₆	0.0830	-0.0592
FC ₇	0.1138	-0.0192
FC ₈	0.1257	-0.0021
FC ₉	0.1360	0.0127
FC ₁₀	0.1499	0.0310
FC ₁₁	0.1699	0.0553
FC ₁₂	0.1814	0.0695
C ₁₃₊ (tuned EOS)	0.2112	0.2135
C ₁₃₊ (un-tuned EOS)	0.2079	0.2079

Reservoir pressure, saturation pressure and fluid density gradient results are given in Table 5.19 and are plotted in Figures 5.10 and 5.11. Compositional gradient results for the three most prominent components (i.e. H₂S, CH₄ and C₁₃+) are given in Table 5.20 and are plotted in Figures 5.12 through 5.14.

Table 5.19: Reservoir pressure, saturation pressure and reservoir fluid density gradient results for the tuned SRK and PR EOS models with volume shift using commercial software

Depth (ft)	Reservoir Pressure (psia)		Saturation Pressure (psia)		Reservoir Fluid Density (lb/ft ³)	
	SRK EOS	PR EOS	SRK EOS	PR EOS	SRK EOS	PR EOS
7800	3794.30	3793.20	3700.85	3708.15	13.615	14.004
7890	3802.83	3801.97	3733.91	3739.29	13.662	14.055
7980	3811.38	3810.77	3767.46	3770.90	13.711	14.106
8070	3819.96	3819.60	3801.54	3802.97	13.760	14.157
8133	3825.99	3825.80	3825.71	3825.72	13.795	14.193
8134	3826.10	3826.10	3826.07	3825.57	56.725	55.955
8160	3836.35	3836.21	3815.33	3815.47	56.782	56.002
8250	3871.90	3871.26	3778.77	3781.02	56.979	56.163
8340	3907.57	3906.41	3743.10	3747.35	57.172	56.321
8430	3943.36	3941.66	3708.28	3714.41	57.360	56.475
8520	3979.27	3977.00	3674.27	3682.17	57.544	56.627
8610	4015.29	4012.44	3641.02	3650.61	57.724	56.775
8700	4051.42	4047.97	3608.51	3619.69	57.901	56.920

Table 5.20: H₂S, CH₄, C₁₃+ compositional gradient results for the tuned SRK and PR EOS models with volume shift using commercial software

Depth (ft)	H ₂ S (mole fraction)		CH ₄ (mole fraction)		C ₁₃ + (mole fraction)	
	SRK EOS	PR EOS	SRK EOS	PR EOS	SRK EOS	PR EOS
7800	0.0560	0.0608	0.8172	0.8117	0.0002	0.0001
7890	0.0562	0.0610	0.8166	0.8111	0.0002	0.0001
7980	0.0564	0.0612	0.8160	0.8104	0.0002	0.0001
8070	0.0566	0.0614	0.8154	0.8098	0.0003	0.0001
8133	0.0567	0.0616	0.8150	0.8093	0.0003	0.0002
8134	0.1124	0.1124	0.3870	0.3870	0.2581	0.2581
8160	0.1124	0.1124	0.3863	0.3863	0.2590	0.2590
8250	0.1124	0.1124	0.3838	0.3841	0.2621	0.2617
8340	0.1123	0.1123	0.3813	0.3819	0.2651	0.2645
8430	0.1123	0.1123	0.3789	0.3798	0.2681	0.2672
8520	0.1122	0.1122	0.3766	0.3776	0.2711	0.2699
8610	0.1122	0.1121	0.3743	0.3756	0.2740	0.2726
8700	0.1121	0.1121	0.3720	0.3735	0.2769	0.2752

Compositional gradient results for the rest of the fluid's components are given in Tables A.23 through A.27 and are plotted in Figures A.19 through A.33 of Appendix A. Compositional gradient results for the EOS models without volume shift –including tuned and un-tuned EOS models– are also provided in Appendix A.

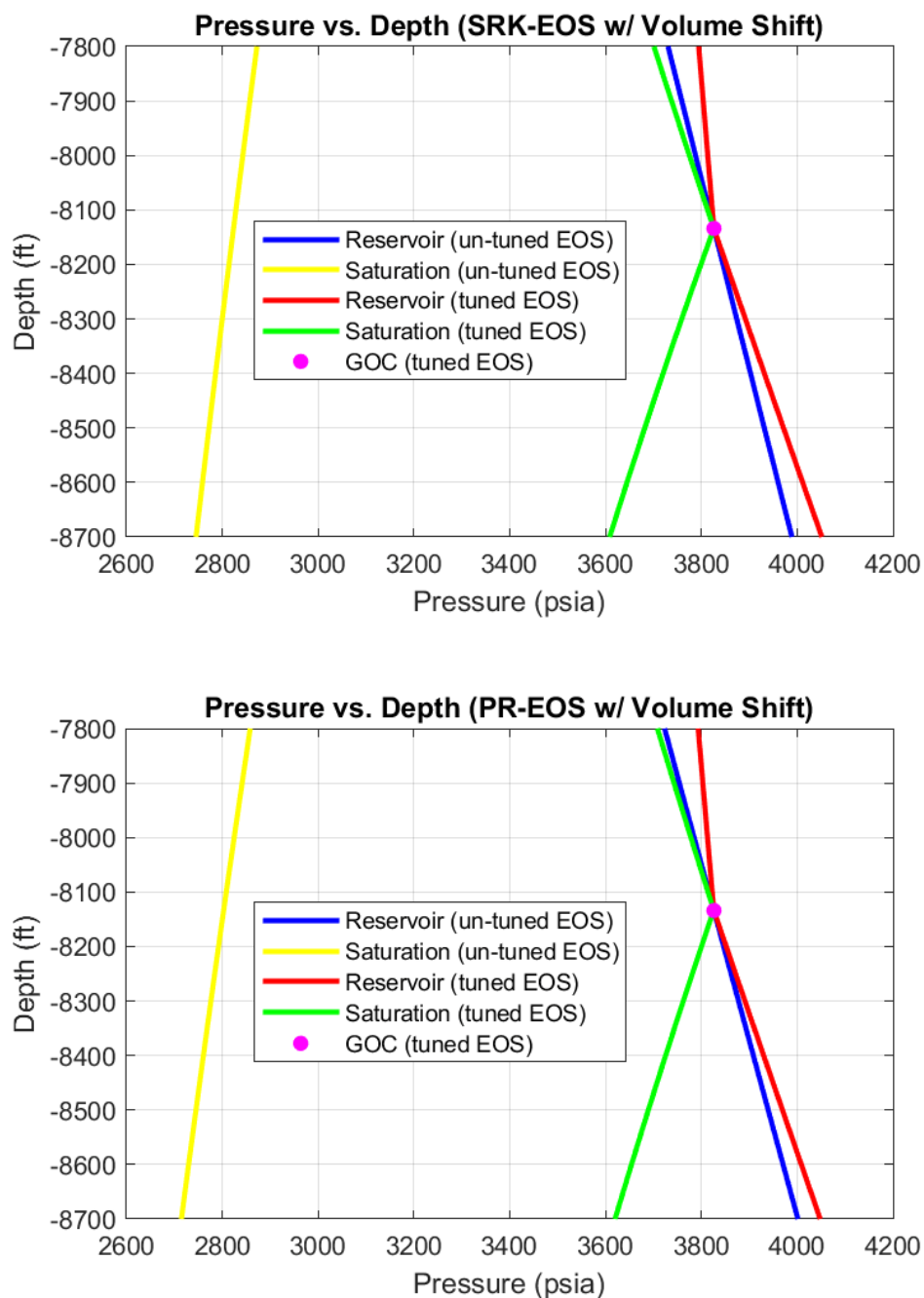


Figure 5.10: Pressure plots with volume shift using commercial software

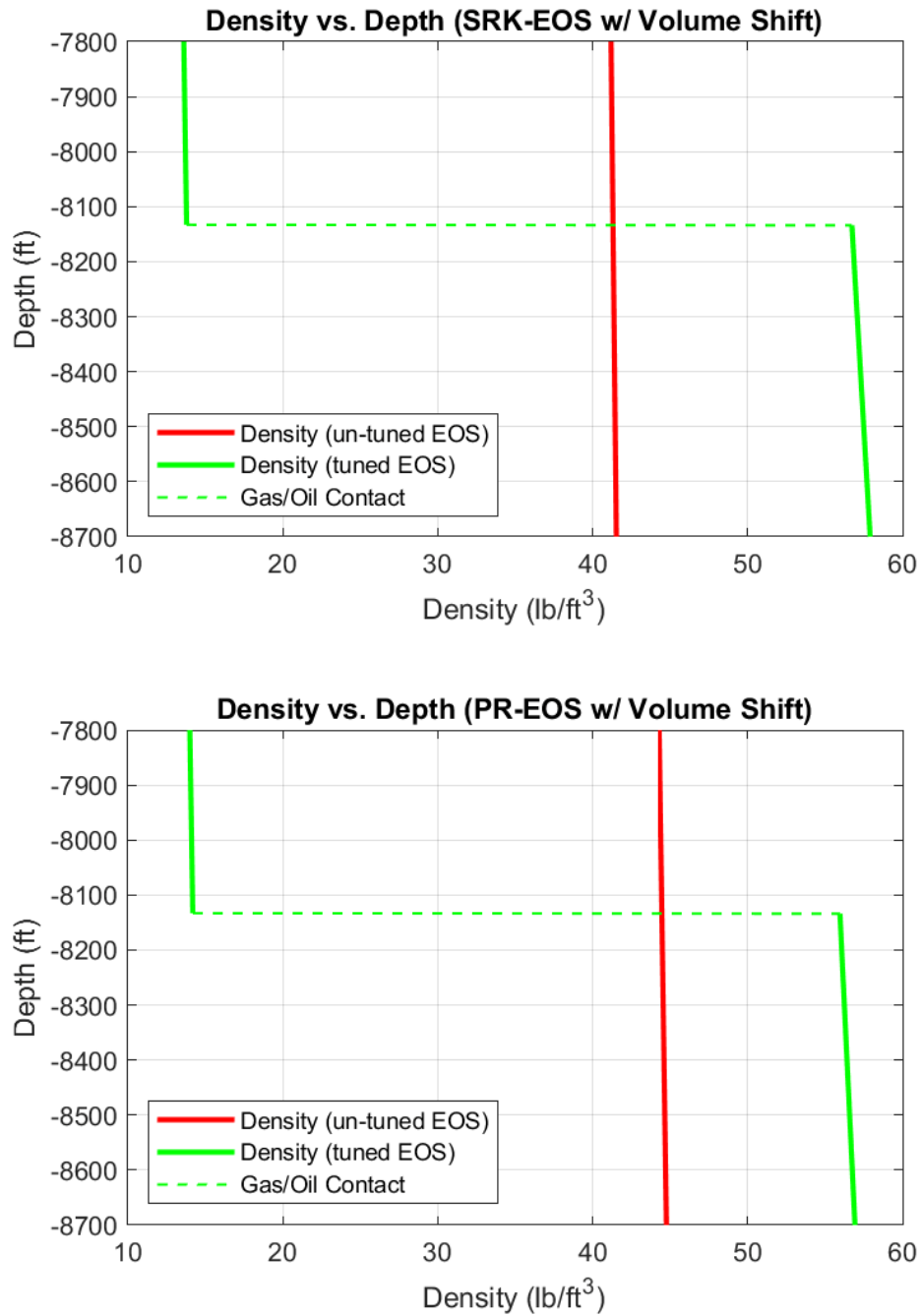
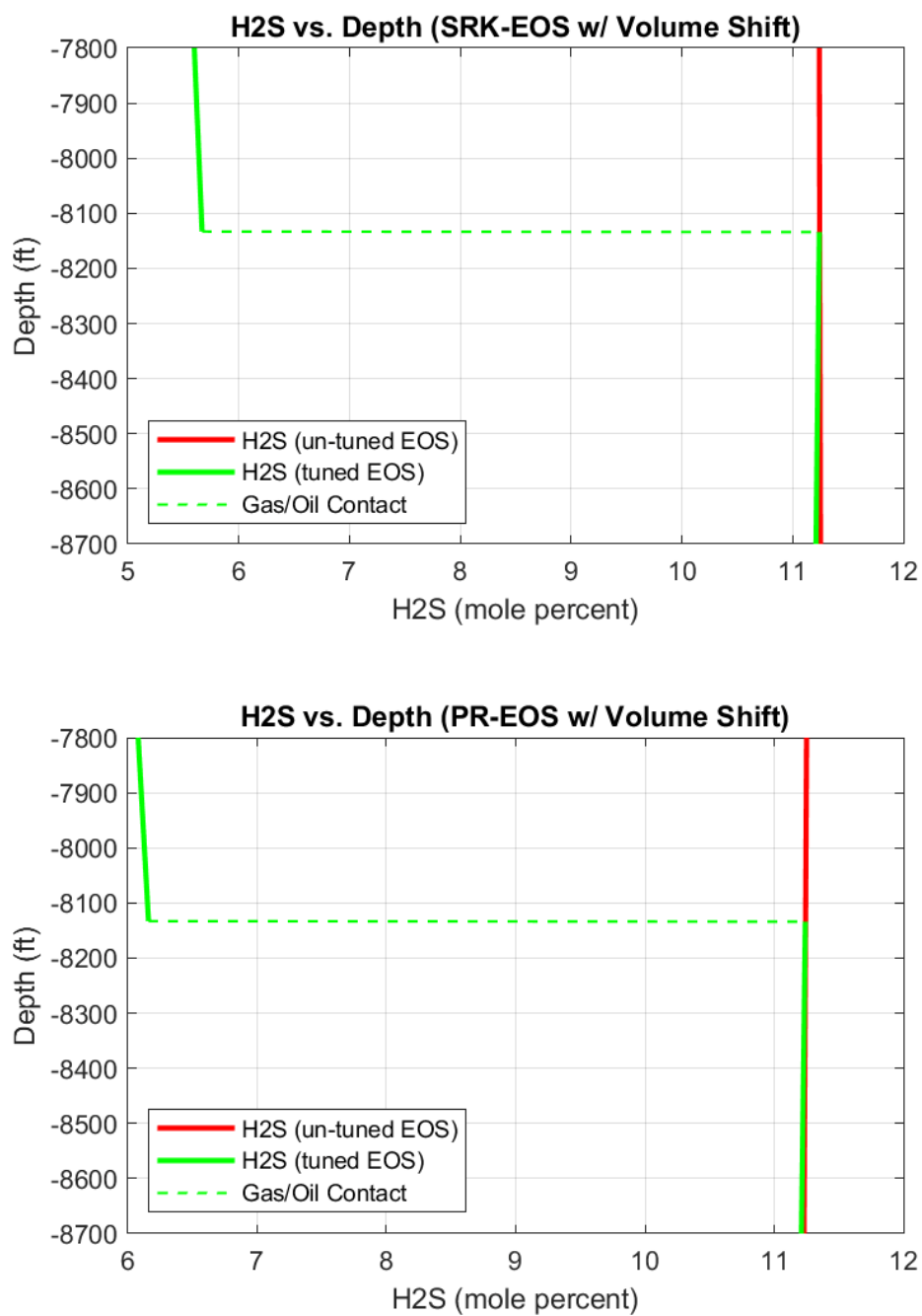
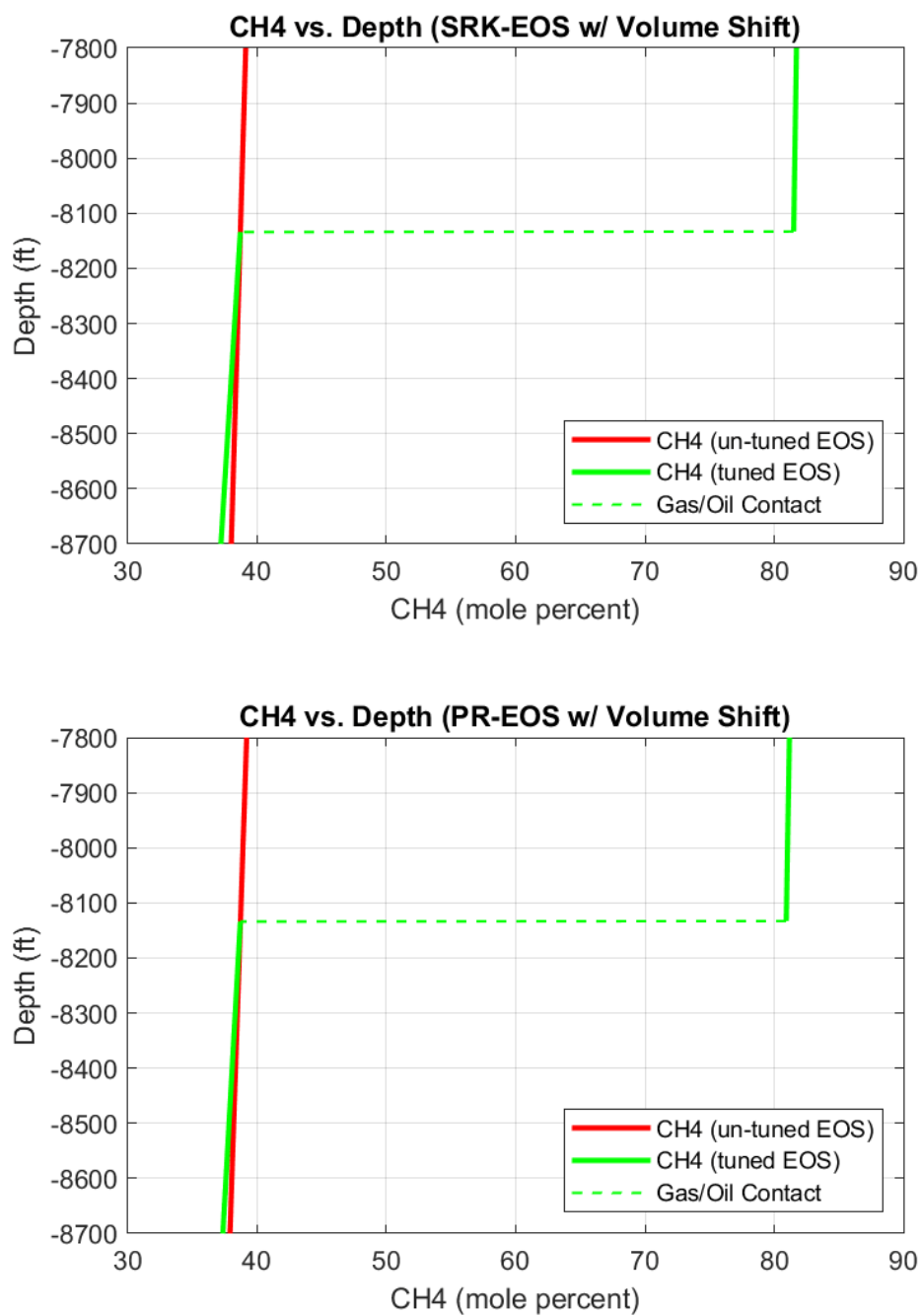
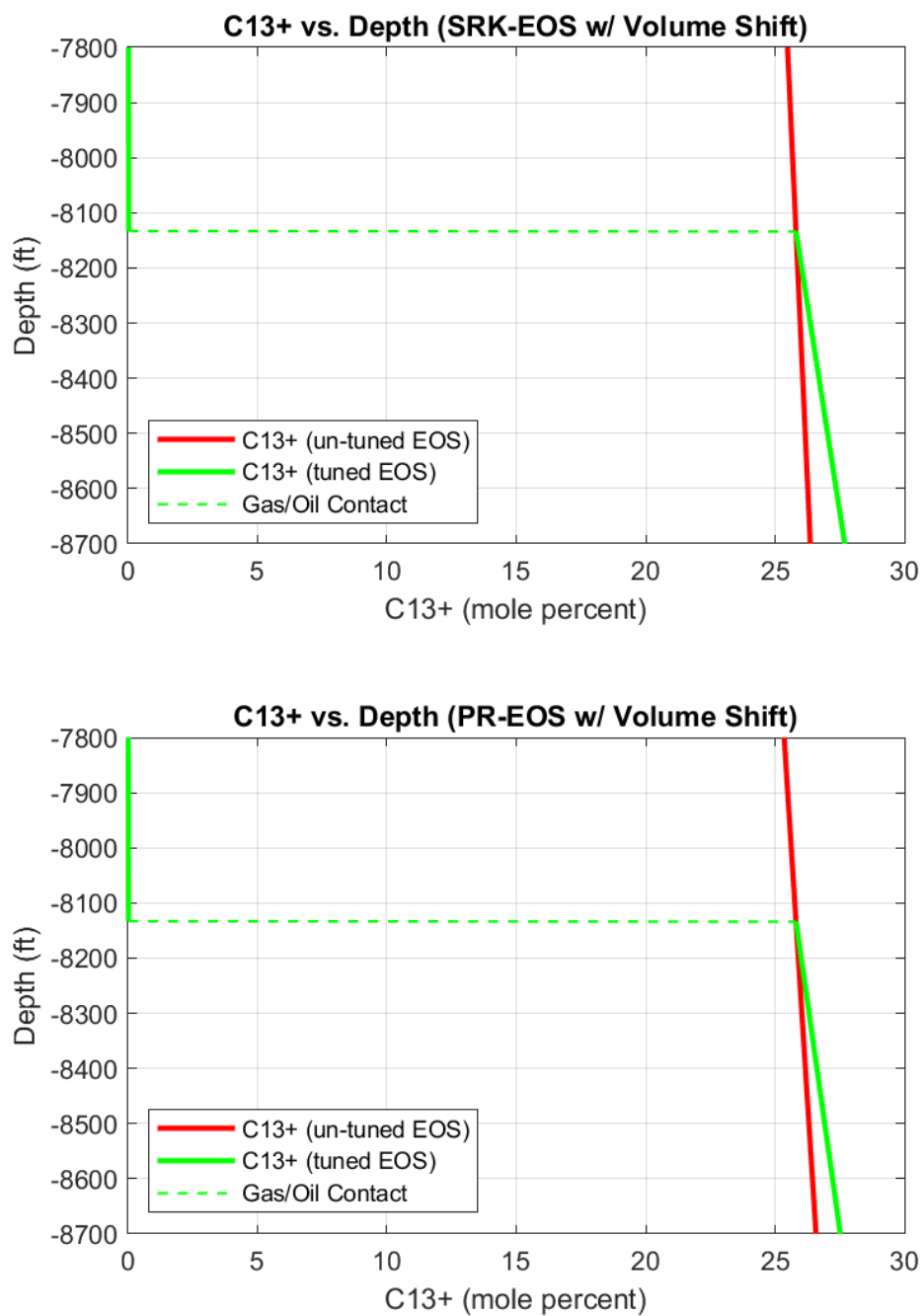


Figure 5.11: Reservoir fluid density plots with volume shift using commercial software

Figure 5.12: H₂S composition plots with volume shift using commercial software

Figure 5.13: CH₄ composition plots with volume shift using commercial software

Figure 5.14: C₁₃₊ composition plots with volume shift using commercial software

5.4 Simulation Procedures using MATLAB®

Open-source code was developed using the MATLAB® programming language for the case of the offshore Greek reservoir fluid in order to accurately predict the fluid's compositional variation with depth. In order to do so, the following EOS calculations were simulated in the MATLAB® computing environment:

- Stability Analysis
- Saturation Pressure Calculation
- Two-Phase Flash Calculation
- Compositional Gradient Calculation

The SRK and PR EOS fluid characterizations developed using the commercial PVT software and their respective component properties and binary interaction coefficients were incorporated as input data. The above calculations were also performed for the un-tuned SRK and PR EOS models. The source code for all MATLAB® scripts and functions developed for the offshore Greek reservoir fluid case study is provided in Appendix B.

5.4.1 Stability Analysis

Two different stability tests were run at reference conditions $p_{\text{res}}=3826.1$ psia and $T_{\text{res}}=134.6^\circ\text{F}$: one searching for a vapor-like second phase and one searching for a liquid-like second phase. The algorithm developed for this calculation was based on the stability test algorithm provided in Chap. 3, Sec. 3.2.2. Stability analysis results for each test are given in Table 5.21.

Table 5.21: Stability analysis results using MATLAB®

Second Phase	tuned EOS model		un-tuned EOS model	
	SRK	PR	SRK	PR
Vapor-like (S_v)	1.0000	1.0000	0.8982	0.8996
Liquid-like (S_L)	0.9999	1.0000	1.0000	1.0000

Both tests indicate $S \leq 1$; hence, the mixture is stable at reference conditions.

5.4.2 Saturation Pressure Calculation

A saturation pressure calculation was performed at $T_{\text{res}}=134.6^\circ\text{F}$ with an initial saturation pressure estimate 500 psia below reference pressure. The calculated saturation pressure values were $p_{\text{sat}}=3826.05$ psia for the SRK-EOS and $p_{\text{sat}}=3825.54$ psia for the PR-EOS. The algorithm developed for this calculation was based on the saturation pressure calculation algorithm provided in Chap. 3, Sec. 3.2.3. Saturation pressure calculation results are given in Tables 5.22 and 5.23.

Table 5.22: Saturation pressure calculation results for the SRK-EOS using MATLAB®

Component	Composition (mole fraction)		K-values (y_i/z_i)	$\ln f_i$ (atm)
	Dominant phase (z_i)	Incipient phase (y_i)		
H ₂ S	0.1124	0.0567	0.5045	1.7587
CO ₂	0.0701	0.0582	0.8297	2.1758
N ₂	0.0117	0.0339	2.8934	2.4491
CH ₄	0.3870	0.8150	2.1060	5.1929
C ₂ H ₆	0.0152	0.0169	1.1127	0.6333
C ₃ H ₈	0.0069	0.0049	0.7167	-1.1037
IC ₄	0.0025	0.0013	0.5380	-2.7624
NC ₄	0.0048	0.0022	0.4590	-2.4022
IC ₅	0.0034	0.0011	0.3363	-3.4176
NC ₅	0.0032	0.0010	0.3035	-3.6929
FC ₆	0.0106	0.0021	0.2005	-3.3016
FC ₇	0.0090	0.0012	0.1321	-4.2859
FC ₈	0.0201	0.0018	0.0906	-4.2333
FC ₉	0.0259	0.0016	0.0609	-4.7888
FC ₁₀	0.0209	0.0008	0.0402	-5.8322
FC ₁₁	0.0177	0.0005	0.0285	-6.7120
FC ₁₂	0.0206	0.0004	0.0193	-7.3496
C ₁₃ +	0.2581	0.0003	0.0010	-10.2323
Z-factor	1.4061	0.9070		

Table 5.23: Saturation pressure calculation results for the PR-EOS using MATLAB®

Component	Composition (mole fraction)		K-values (y_i/z_i)	$\ln f_i$ (atm)
	Dominant phase (z_i)	Incipient phase (y_i)		
H ₂ S	0.1124	0.0616	0.5477	1.7435
CO ₂	0.0701	0.0585	0.8347	2.0861
N ₂	0.0117	0.0319	2.7236	2.3292
CH ₄	0.3870	0.8093	2.0914	5.1021
C ₂ H ₆	0.0152	0.0175	1.1479	0.5448
C ₃ H ₈	0.0069	0.0051	0.7496	-1.2114
IC ₄	0.0025	0.0014	0.5653	-2.8919
NC ₄	0.0048	0.0023	0.4897	-2.5215
IC ₅	0.0034	0.0012	0.3622	-3.5539
NC ₅	0.0032	0.0010	0.3291	-3.8261
FC ₆	0.0106	0.0024	0.2228	-3.4243
FC ₇	0.0090	0.0014	0.1503	-4.4045
FC ₈	0.0201	0.0021	0.1053	-4.3498
FC ₉	0.0259	0.0019	0.0722	-4.9042
FC ₁₀	0.0209	0.0010	0.0489	-5.9406
FC ₁₁	0.0177	0.0006	0.0354	-6.8168
FC ₁₂	0.0206	0.0005	0.0246	-7.4416
C ₁₃₊	0.2581	0.0002	0.0006	-12.4227
Z-factor	1.3949	0.8413		

5.4.3 Two-Phase Flash Calculation

An isothermal two-phase flash calculation was performed at $p_{\text{res}}=3826.1$ psia and $T_{\text{res}}=134.6^\circ\text{F}$. The algorithm developed for this calculation was based on the two-phase flash calculation algorithm provided in Chap. 3, Sec. 3.2.1. Calculated vapor phase molar fractions for each two-phase flash calculation are given in Table 5.24. Two-phase flash calculation results are given in Table 5.25.

Table 5.24: Calculated vapor phase molar fractions using MATLAB®

Vapor phase molar fraction (β)			
tuned EOS model		un-tuned EOS model	
SRK	PR	SRK	PR
-7.6088×10^{-6}	-7.4432×10^{-5}	-0.2008	-0.2151

All calculations indicate $\beta < 0$ (negative flash); therefore, the mixture remains single-phase at reference conditions and no vapor phase exists ($x_i = z_i$ and $y_i = 0$).

Table 5.25: Two-phase flash calculation results using MATLAB®

Component	Composition (mole fraction)	$\ln f_i$ (atm)	
	Liquid phase (x_i)	SRK EOS	PR EOS
H ₂ S	0.1124	1.7587	1.7436
CO ₂	0.0701	2.1758	2.0862
N ₂	0.0117	2.4491	2.3293
CH ₄	0.3870	5.1930	5.1021
C ₂ H ₆	0.0152	0.6333	0.5449
C ₃ H ₈	0.0069	-1.1037	-1.2113
IC ₄	0.0025	-2.7624	-2.8917
NC ₄	0.0048	-2.4022	-2.5214
IC ₅	0.0034	-3.4176	-3.5537
NC ₅	0.0032	-3.6929	-3.8260
FC ₆	0.0106	-3.3016	-3.4241
FC ₇	0.0090	-4.2859	-4.4043
FC ₈	0.0201	-4.2333	-4.3496
FC ₉	0.0259	-4.7888	-4.9040
FC ₁₀	0.0209	-5.8322	-5.9404
FC ₁₁	0.0177	-6.7120	-6.8165
FC ₁₂	0.0206	-7.3496	-7.4413
C ₁₃₊	0.2581	-10.2323	-12.4222
Z-factor	SRK EOS	PR EOS	
	1.4061	1.3951	

5.4.4 Compositional Gradient Calculation

An isothermal compositional gradient calculation was performed at reference conditions $p_{\text{res}}=3826.1$ psia and $T_{\text{res}}=134.6^\circ\text{F}$. The calculation was initiated at reference depth $h_{\text{ref}}=8134$ ft and the reservoir was split in 10 calculation intervals of 90 ft from top depth $h_{\text{top}}=7800$ ft to bottom depth $h_{\text{bot}}=8700$ ft. The GOC was located at 8133.98 ft using interval halving. Calculated results include the variation from top to bottom in: reservoir pressure, saturation pressure, and component composition. The algorithms developed for this calculation were based on the GCE and GOC algorithms provided in Chap. 4, Sec. 4.3. The volume translation method of Peneloux et al. [21] was also incorporated, in which the constant volume shift parameters were taken from Table 5.18.

The variation in reservoir and saturation pressure is given in Table 5.26 and is plotted in Figure 5.15. Compositional variation of the three most prominent components is given in Table 5.27 and is plotted in Figures 5.16 through 5.18.

Table 5.26: Reservoir and saturation pressure gradient results for the tuned SRK and PR EOS models with volume shift using MATLAB®

Depth (ft)	Reservoir Pressure (psia)		Saturation Pressure (psia)	
	SRK EOS	PR EOS	SRK EOS	PR EOS
7800	3794.28	3793.18	3700.53	3704.58
7890	3802.81	3801.95	3733.60	3735.58
7980	3811.37	3810.76	3767.09	3767.04
8070	3819.95	3819.59	3801.46	3799.32
8133.98	3826.07	3825.89	3822.43	3823.21
8134	3826.10	3826.10	3826.05	3825.54
8160	3836.35	3836.21	3815.30	3815.44
8250	3871.91	3871.28	3779.00	3780.97
8340	3907.60	3906.44	3743.27	3747.29
8430	3943.40	3941.70	3708.40	3714.34
8520	3979.33	3977.06	3674.32	3682.09
8610	4015.36	4012.51	3641.02	3650.52
8700	4051.51	4048.05	3608.45	3619.59

Table 5.27: H₂S, CH₄, C₁₃+ compositional gradient results for the tuned SRK and PR EOS models with volume shift using MATLAB®

Depth (ft)	H ₂ S (mole fraction)		CH ₄ (mole fraction)		C ₁₃ + (mole fraction)	
	SRK EOS	PR EOS	SRK EOS	PR EOS	SRK EOS	PR EOS
7800	0.0560	0.0608	0.8172	0.8117	0.0002	0.0001
7890	0.0562	0.0610	0.8166	0.8111	0.0002	0.0001
7980	0.0564	0.0612	0.8160	0.8104	0.0002	0.0001
8070	0.0566	0.0614	0.8154	0.8098	0.0003	0.0001
8133.98	0.0568	0.0616	0.8149	0.8093	0.0003	0.0002
8134	0.1124	0.1124	0.3870	0.3870	0.2581	0.2581
8160	0.1124	0.1124	0.3863	0.3863	0.2590	0.2590
8250	0.1124	0.1124	0.3838	0.3841	0.2621	0.2617
8340	0.1123	0.1123	0.3813	0.3819	0.2651	0.2645
8430	0.1123	0.1123	0.3789	0.3798	0.2681	0.2672
8520	0.1122	0.1122	0.3766	0.3776	0.2711	0.2699
8610	0.1122	0.1121	0.3743	0.3756	0.2740	0.2726
8700	0.1121	0.1121	0.3720	0.3735	0.2769	0.2752

Compositional gradient results for the rest of the fluid's components are given in Tables A.52 through A.56 and are plotted in Figures A.54 through A.68 of Appendix A. Compositional gradient results for the EOS models without volume shift are also given in Appendix A.

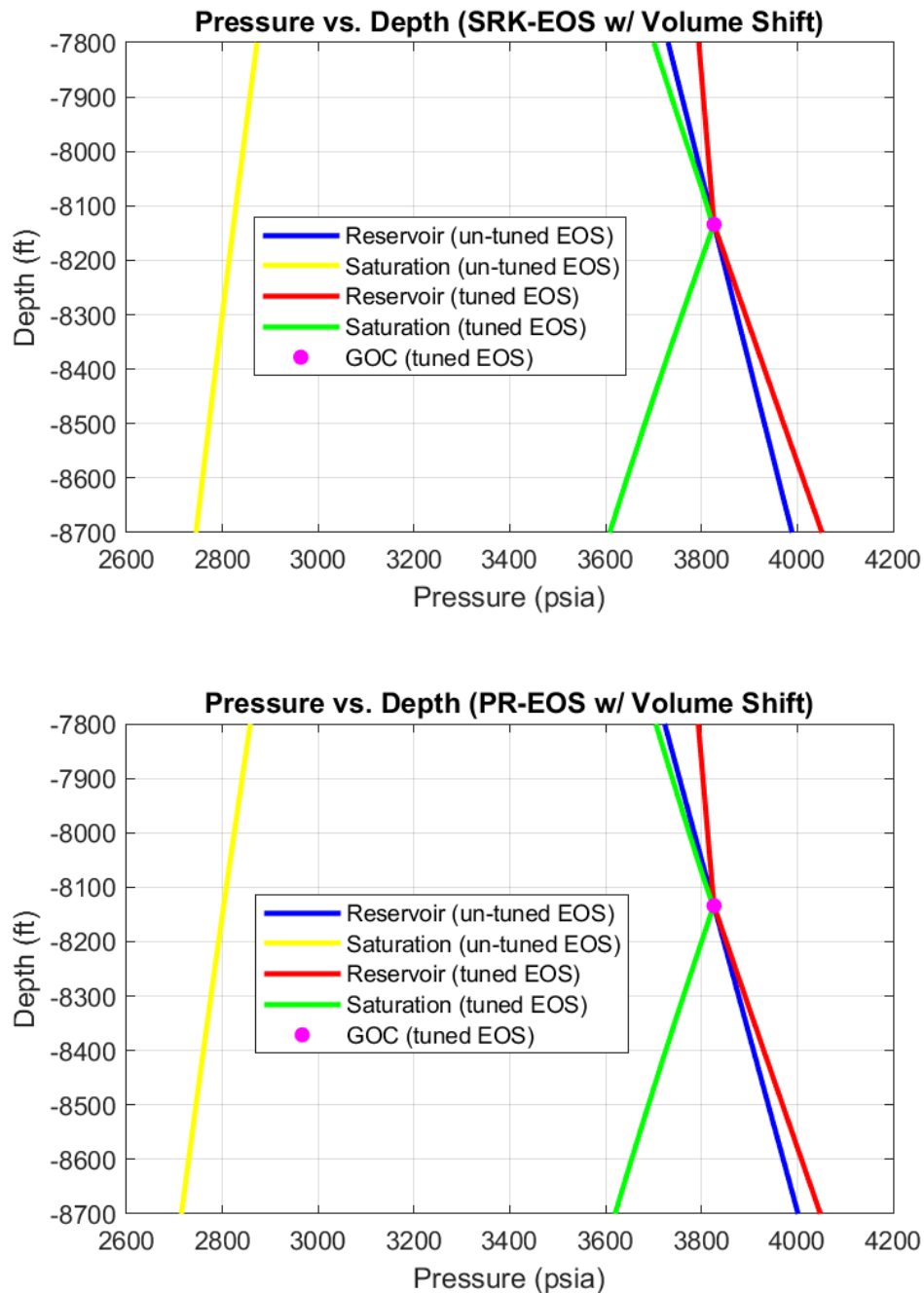


Figure 5.15: Pressure plots with volume shift using MATLAB®

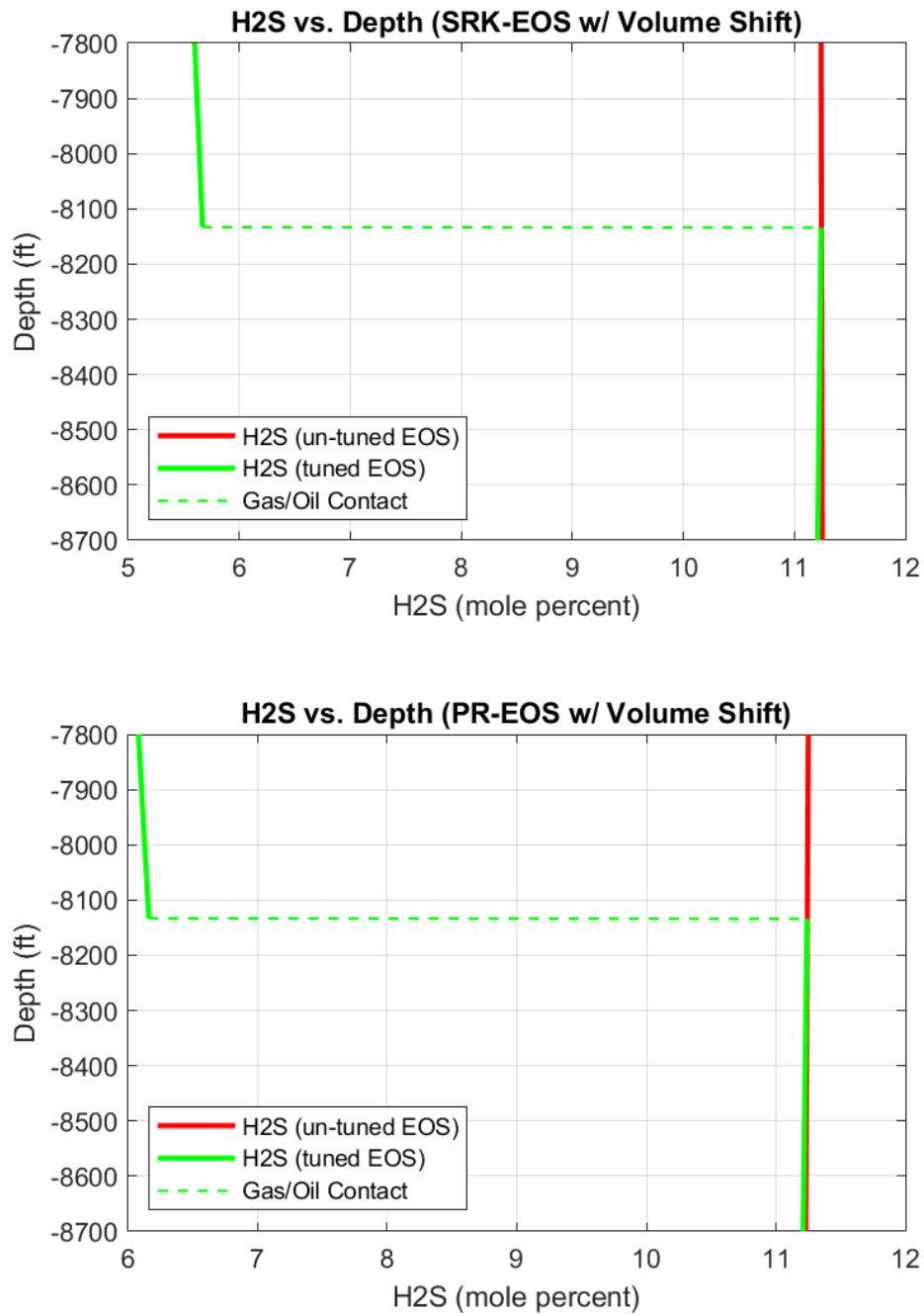


Figure 5.16: H₂S composition plots with volume shift using MATLAB®

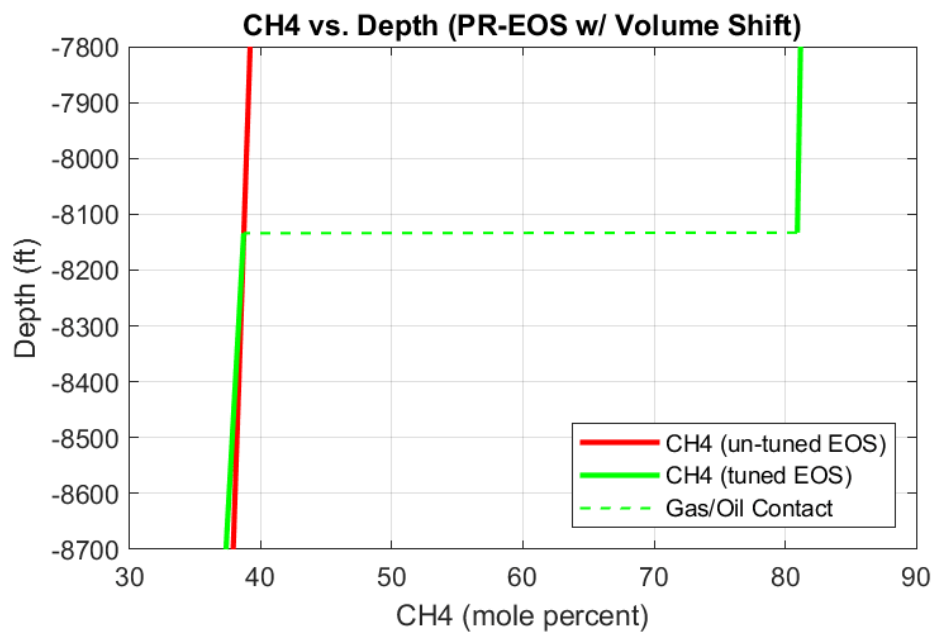
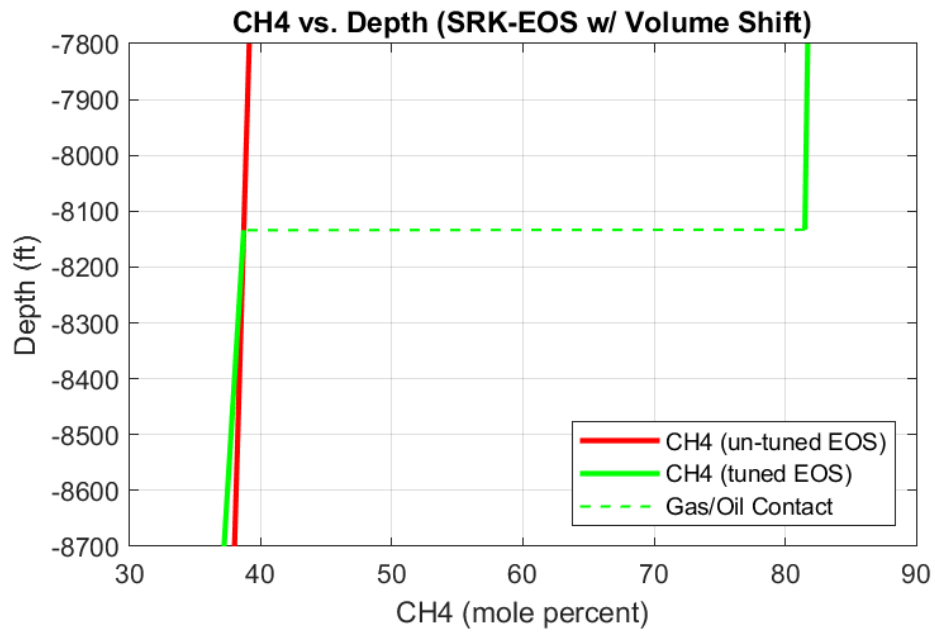
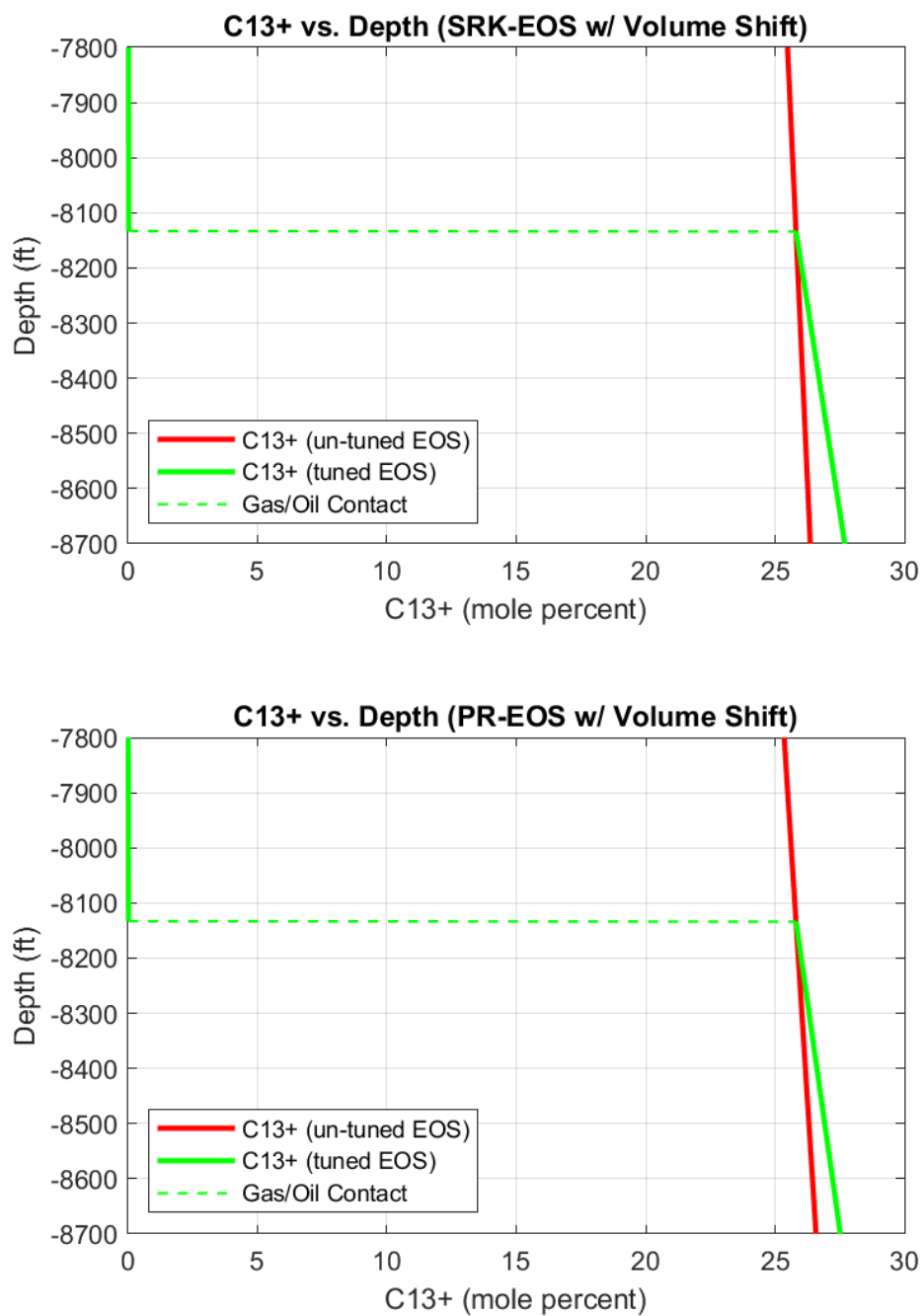


Figure 5.17: CH₄ composition plots with volume shift using MATLAB®

Figure 5.18: C₁₃₊ composition plots with volume shift using MATLAB®

Chapter 6

Conclusions and Recommendations

6.1 Conclusions

6.1.1 Software Comparison

A comparison between the commercial PVT software and MATLAB® compositional gradient calculation results indicated the following:

1. Deviations in calculated reservoir pressures are negligible (not bigger than ± 0.09 psia).
2. MATLAB® under-predicts saturation pressures at the GOC and the depths above –especially the PR-EOS– compared to the commercial PVT software. At the GOC, deviations in calculated saturation pressures are as high as ~ 4 psia for the SRK-EOS and ~ 4.5 psia for the PR-EOS. Above the GOC, deviations in calculated saturation pressures (dew-point pressures) are not bigger than ~ 0.4 psia for the SRK-EOS; however, they are as high as ~ 4 psia for the PR-EOS. Deviations in calculated saturation pressures below the GOC are negligible (up to ~ 0.2 psia).
3. The only deviations in calculated component compositions are observed at the GOC, namely ± 0.0001 mole fraction for: H₂S and CH₄ (SRK-EOS); C₃H₈ and NC₅ (PR-EOS without volume shift).
4. For the un-tuned EOS models, deviations in calculated reservoir and saturation pressures are negligible (up to ± 0.06 psia); while no deviations in calculated component compositions have been observed at any depth along the reservoir.

Non-negligible deviations in calculated saturation pressures and component compositions at the GOC are probably being reported due to the commercial software predicting the GOC 0.98 ft shallower than MATLAB® (8133 ft vs. 8133.98 ft), leading the two softwares to predict different saturation pressures and compositions at their respective GOC depths. The fact that the mixture is highly unstable at the GOC might also contribute to these deviations. Non-negligible deviations in calculated saturation pressures above the GOC (dew-point pressures) using the PR-EOS conclude that the developed MATLAB® dew-point pressure calculation algorithm (Appendix B) might be slightly weaker with the PR-EOS compared to the SRK-EOS. Figure 6.1 compares the calculated dew-point pressures between the two softwares.

Based on the above observations, one can conclude that the developed software in the MATLAB® environment is able to accurately predict variations in pressure and composition.

6.1.2 EOS Comparison

According to the literature, the PR-EOS under-predicts saturation pressures compared to the SRK-EOS. Although this seems to apply for the un-tuned EOS models, tuned EOS gradient results indicate the exact opposite, namely the SRK-EOS under-predicts saturation pressures compared to the PR-EOS.

The literature also claims that the SRK-EOS under-predicts liquid phase densities compared to the PR-EOS. This does apply for the un-tuned EOS models and the tuned EOS models without volume shift. For the tuned EOS models with volume shift however, the PR-EOS seems to be the one which under-predicts liquid densities.

For the tuned EOS models, the SRK-EOS predicts a larger variation with depth in liquid phase CH₄ and C₁₃₊ compositions compared to the PR-EOS. For the rest of the fluid's components, their compositional variation with depth is more or less identical in both EOS models.

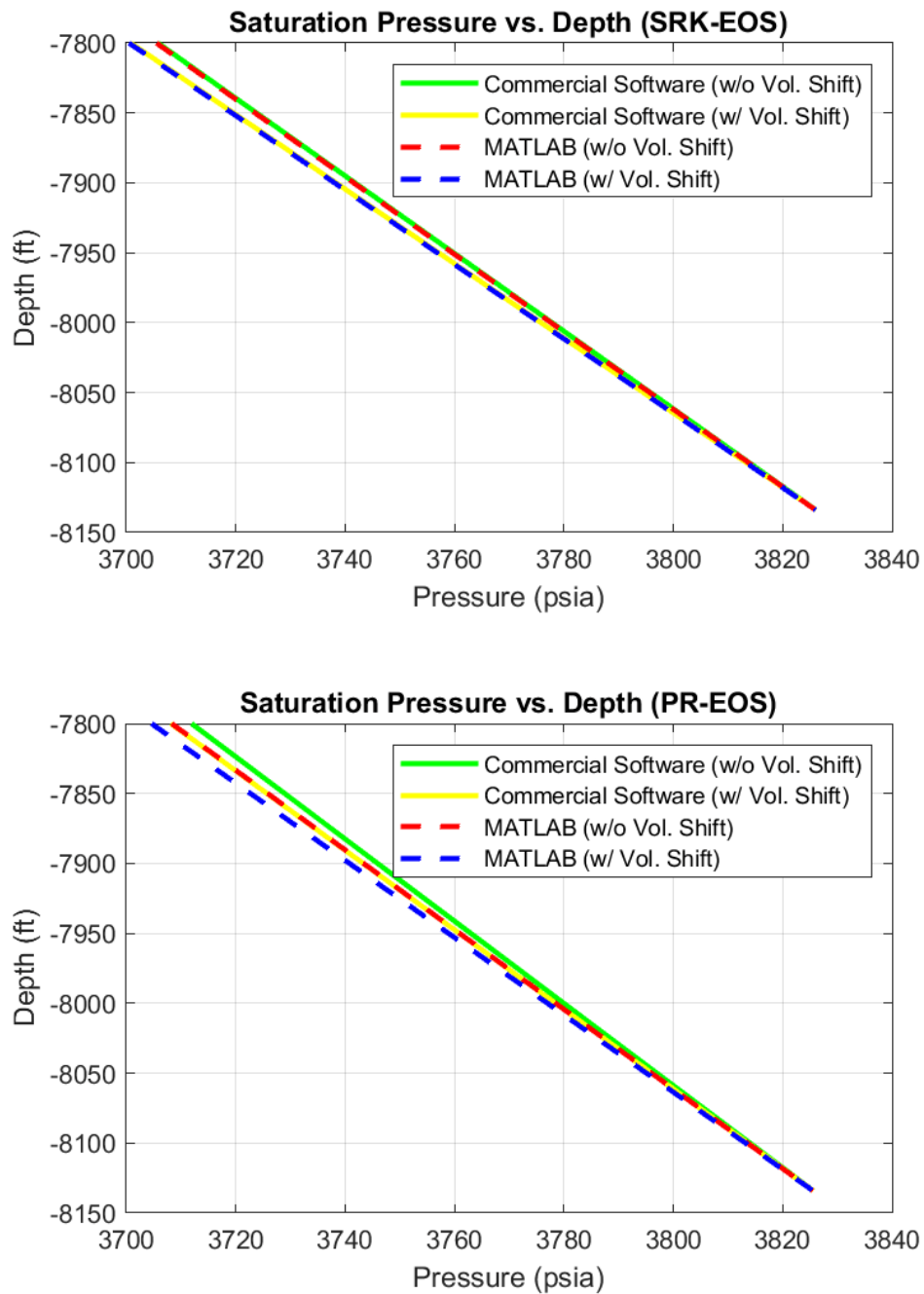


Figure 6.1: Software comparison of the calculated dew-point pressures for the SRK and PR EOS models with and without volume shift

6.1.3 EOS Tuning

EOS tuning to match experimental PVT data is crucial for all EOS calculations. As seen from the un-tuned EOS compositional gradient calculation results, a single-phase system would be predicted if no EOS tuning was performed. This would yield major inconsistencies when estimating the amount of hydrocarbons initially in place and would also lead to the selection of incorrect exploitation methods.

6.1.4 Volume Shift

A comparison between the EOS models that incorporated volume shift and those that did not indicated the following:

1. The EOS models without volume shift under-predict reservoir pressures and over-predict saturation pressures.
2. The EOS models without volume shift under-predict liquid phase densities.
3. Without volume shift, the SRK-EOS under-predicts vapor phase densities while the PR-EOS over-predicts them.
4. The EOS models without volume shift over-predict liquid phase component compositions, except for the C₁₃₊ composition which is under-predicted.
5. Vapor phase component compositions are not affected by volume shift.
6. Volume shift moderates deviations between the commercial software and MATLAB® in reported gradient data at the GOC.
7. Volume shift moderates deviations between the SRK-EOS and PR-EOS in calculated component compositions –mainly C₁₃₊ and CH₄– of the liquid phase.

Based on the above observations, incorporating volume shift in compositional gradient calculations is highly suggested.

6.1.5 Offshore Greek Reservoir Fluid Classification

Taking into consideration the reported data from the experimental and simulation procedures run on the offshore Greek reservoir fluid, as well as the calculated p-T diagram (Figures 5.8 and 5.9, Chap. 5), the fluid can be classified as a volatile oil.

6.2 Recommendations for Future Work

In the future, a non-isothermal GCE algorithm could be developed in the MATLAB® environment where the effect of a thermal gradient would be incorporated into the compositional gradient calculation. This way, compositional gradient analysis using the developed MATLAB® software could be performed on a potential fluid sampled from a reservoir exhibiting a vertical temperature gradient.

A potential three-phase mixture or even a single-phase vapor one could also be studied in the future, where the developed MATLAB® software could be adjusted and/or modified for such applications.

References

- [1] Kassinis, S. (2015). *About Oil & Gas*. Kassinis International Consulting.
- [2] Whitson, C. H., & Brule, M. R. (2000). *Phase Behavior (Digital Edition)*. SPE Monograph Series Vol. 20.
- [3] Railsback, L. B. (2011-2017). *Petroleum Geoscience and Subsurface Geology*. <http://railsback.org/PGSG/PGSGmain.html>
- [4] Coats, K. H. (1980). An Equation of State Compositional Model. *Society of Petroleum Engineers Journal*, 20(5), 363-376. <https://doi.org/10.2118/8284-PA>
- [5] Young, L. C., & Stephenson, R. E. (1983). A Generalized Compositional Approach for Reservoir Simulation. *Society of Petroleum Engineers Journal*, 23(5), 727-742. <https://doi.org/10.2118/10516-PA>
- [6] Gibbs, J. W. (1906). *The Scientific Papers of J. Willard Gibbs, Vol. 1: Thermodynamics*. Longmans, Green, and Co.
- [7] Sage, B. H., & Lacey, W. N. (1939). Gravitational Concentration Gradients in Static Columns of Hydrocarbon Fluids. *Transactions of the AIME*, 132(1), 120-131. <https://doi.org/10.2118/939120-G>
- [8] Ramey Jr., H. J. (1964). Rapid Methods for Estimating Reservoir Compressibilities. *Journal of Petroleum Technology*, 16(4), 447-454. <https://doi.org/10.2118/772-PA>
- [9] Standing, M. B. (1977). *Volumetric and Phase Behavior of Oil Field Hydrocarbon Systems* (9th ed.). Society of Petroleum Engineers of AIME.
- [10] Ahmed, T. (2010). *Reservoir Engineering Handbook* (4th ed.). Gulf Professional Publishing.
- [11] Kuenen, J. P. (1895). On the Condensation and the Critical Phenomena of Mixtures of Ethane and Nitrous Oxide. *The London, Edinburgh, and Dublin Philosophical Magazine and Journal of Science*, 40(243), 173-194. <http://doi.org/10.1080/14786449508620759>
- [12] Taftan Data. (1998). *Amagat's Law of Additive Volumes*. Taftan Data. <https://www.taftan.com/thermodynamics/AMAGAT.HTM>

- [13] Kay, W. (1936). Density of Hydrocarbon Gases and Vapors at High Temperature and Pressure. *Industrial & Engineering Chemistry*, 28(9), 1014-1019. <https://doi.org/10.1021/ie50321a008>
- [14] Daintith, J. (Ed.). (2008). *A Dictionary of Chemistry* (6th ed.). Oxford University Press.
- [15] Standing, M. B., & Katz, D. L. (1942). Density of Natural Gases. *Transactions of the AIME*, 146(1), 140-149. <https://doi.org/10.2118/942140-G>
- [16] Poling, B. E., Prausnitz, J. M., & O'Connell, J. P. (2000). *The Properties of Gases and Liquids* (5th ed.). McGraw-Hill Education.
- [17] van der Waals, J. D. (2004). *On the Continuity of the Gaseous and Liquid States (Phoenix Edition)*. Dover Publications.
- [18] Redlich, O., & Kwong, J. N. S. (1949). On the Thermodynamics of Solutions. V. An Equation of State. Fugacities of Gaseous Solutions. *Chemical Reviews*, 44(1), 233-244. <https://doi.org/10.1021/cr60137a013>
- [19] Peng, D.-Y., & Robinson, D. B. (1976). A New Two-Constant Equation of State. *Industrial & Engineering Chemistry Fundamentals*, 15(1), 59-64. <https://doi.org/10.1021/i160057a011>
- [20] Soave, G. (1972). Equilibrium Constants from a Modified Redlich-Kwong Equation of State. *Chemical Engineering Science*, 27(6), 1197-1203. [https://doi.org/10.1016/0009-2509\(72\)80096-4](https://doi.org/10.1016/0009-2509(72)80096-4)
- [21] Peneloux, A., Rauzy, E., & Freze, R. (1982). A Consistent Correction for Redlich-Kwong-Soave Volumes. *Fluid Phase Equilibria*, 8(1), 7-23. [https://doi.org/10.1016/0378-3812\(82\)80002-2](https://doi.org/10.1016/0378-3812(82)80002-2)
- [22] Martin, J. (1979). Cubic Equations of State—Which? *Industrial & Engineering Chemistry Fundamentals*, 18(2), 81-97. <https://doi.org/10.1021/i160070a001>
- [23] Rackett, H. G. (1970). Equation of State for Saturated Liquids. *Journal of Chemical and Engineering Data*, 15(4), 514-517. <https://doi.org/10.1021/jc60047a012>
- [24] Jhaveri, B. S., & Youngren, G. K. (1988). Three-Parameter Modification of the Peng-Robinson Equation of State to Improve Volumetric Predictions. *SPE Reservoir Engineering*, 3(3), 1033-1040. <https://doi.org/10.2118/13118-PA>

- [25] Pitzer, K. S., Lippmann, D. Z., Curl Jr., R. F., Huggins, C. M., & Petersen, D. E. (1955). The Volumetric and Thermodynamic Properties of Fluids. II. Compressibility Factor, Vapor Pressure and Entropy of Vaporization. *Journal of the American Chemical Society*, 77(13), 3433-3440. <https://doi.org/10.1021/ja01618a002>
- [26] Li, Y.-K., Nghiem, L. X., & Siu, A. (1985). Phase Behaviour Computations for Reservoir Fluids: Effect of Pseudo-Components on Phase Diagrams and Simulation Results. *Journal of Canadian Petroleum Technology*, 24(6), 29-36. <https://doi.org/10.2118/85-06-02>
- [27] Nghiem, L. X., Aziz, K., & Li, Y.-K. (1983). A Robust Iterative Method for Flash Calculations Using the Soave-Redlich-Kwong or the Peng-Robinson Equation of State. *Society of Petroleum Engineers Journal*, 23(3), 521-530. <https://doi.org/10.2118/8285-PA>
- [28] Rachford, H. H., & Rice, J. D. (1952). Procedure for Use of Electronic Digital Computers in Calculating Flash Vaporization Hydrocarbon Equilibrium. *Journal of Petroleum Technology*, 4(10), 327-328. <https://doi.org/10.2118/952327-G>
- [29] Whitson, C. H., & Michelsen, M. L. (1989). The Negative Flash. *Fluid Phase Equilibria*, 53, 51-71. [https://doi.org/10.1016/0378-3812\(89\)80072-X](https://doi.org/10.1016/0378-3812(89)80072-X)
- [30] Michelsen, M. L. (1982). The Isothermal Flash Problem. Part II. Phase-Split Calculation. *Fluid Phase Equilibria*, 9(1), 21-40. [https://doi.org/10.1016/0378-3812\(82\)85002-4](https://doi.org/10.1016/0378-3812(82)85002-4)
- [31] Wilson, G. (1968). *A Modified Redlich-Kwong Equation of State, Application to General Physical Data Calculations* [Paper presentation]. American Institute of Chemical Engineers 65th National Meeting, Cleveland, OH, United States.
- [32] Michelsen, M. L. (1982). The Isothermal Flash Problem. Part I. Stability. *Fluid Phase Equilibria*, 9(1), 1-19. [https://doi.org/10.1016/0378-3812\(82\)85001-2](https://doi.org/10.1016/0378-3812(82)85001-2)
- [33] Baker, L. E., Pierce, A. C., & Luks, K. D. (1982). Gibbs Energy Analysis of Phase Equilibria. *Society of Petroleum Engineers Journal*, 22(5), 731-742. <https://doi.org/10.2118/9806-PA>

- [34] Crowe, C. M., & Nishio, M. (1975). Convergence Promotion in the Simulation of Chemical Processes—The General Dominant Eigenvalue Method. *American Institute of Chemical Engineers Journal*, 21(3), 528-533. <https://doi.org/10.1002/aic.690210314>
- [35] Michelsen, M. L. (1985). Saturation Point Calculations. *Fluid Phase Equilibria*, 23(2-3), 181-192. [https://doi.org/10.1016/0378-3812\(85\)90005-6](https://doi.org/10.1016/0378-3812(85)90005-6)
- [36] Coats, K. H., & Smart, G. T. (1986). Application of a Regression-Based EOS PVT Program to Laboratory Data. *SPE Reservoir Engineering*, 1(3), 277-299. <https://doi.org/10.2118/11197-PA>
- [37] Agarwal, R. K., Li, Y.-K., & Nghiem, L. (1990). A Regression Technique with Dynamic Parameter Selection for Phase-Behavior Matching. *SPE Reservoir Engineering*, 5(1), 115-120. <https://doi.org/10.2118/16343-PA>
- [38] Lee, S.-T. (1989, October 8-11). *Capillary-Gravity Equilibria for Hydrocarbon Fluids in Porous Media* [Paper presentation]. SPE Annual Technical Conference and Exhibition, San Antonio, Texas, USA. <https://doi.org/10.2118/SPE-19650-MS>
- [39] Høier, L., & Whitson, C. H. (2001). Compositional Grading—Theory and Practice. *SPE Reservoir Evaluation & Engineering*, 4(6), 525-535. <https://doi.org/10.2118/74714-PA>
- [40] Muskat, M. (1930). Distribution of Non-Reacting Fluids in the Gravitational Field. *Physical Reviews*, 35, 1384-1393. <https://doi.org/10.1103/PhysRev.35.1384>
- [41] Leverett, M. C. (1941). Capillary Behavior in Porous Solids. *Transactions of the AIME*, 142(1), 152-169. <https://doi.org/10.2118/941152-G>
- [42] Espach, R. H., & Fry, J. (1951). Variable Characteristics of the Oil in the Tensleep Sandstone Reservoir, Elk Basin Field, Wyoming and Montana. *Journal of Petroleum Technology*, 3(3), 75-82. <https://doi.org/10.2118/951075-G>
- [43] McCord, D. R. (1953). Performance Predictions Incorporating Gravity Drainage and Gas Cap Pressure Maintenance - LL-370 Area, Bolivar Coastal Field. *Journal of Petroleum Technology*, 5(9), 231-248. <https://doi.org/10.2118/953231-G>

- [44] Clinton, G. W., & Ruiz, J. (1968). Performance of Payoa Basal Eocene Block A Reservoir. *Journal of Petroleum Technology*, 20(1), 31-35.
<https://doi.org/10.2118/1909-PA>
- [45] Havlena, D. (1968). Dynamic Reservoir Data: Part II – Interpretation, Averaging and Use of the Basic Geological-Engineering Data. *Journal of Canadian Petroleum Technology*, 7(3), 128-144. <https://doi.org/10.2118/68-03-o6>
- [46] Evans, C. R., Rogers, M. A., & Bailey, N. J. L. (1971). Evolution and Alteration of Petroleum in Western Canada. *Chemical Geology*, 8(3), 147-170.
[https://doi.org/10.1016/0009-2541\(71\)90002-7](https://doi.org/10.1016/0009-2541(71)90002-7)
- [47] Wadman, D. H., Lamprecht, D. E., & Mrosovsky, I. (1979). Joint Geologic/Engineering Analysis of the Sadlerochit Reservoir, Prudhoe Bay Field. *Journal of Petroleum Technology*, 31(7), 933-940.
<https://doi.org/10.2118/7531-PA>
- [48] Schulte, A. M. (1980, September 21-24). *Compositional Variations within a Hydrocarbon Column Due To Gravity* [Paper presentation]. SPE Annual Technical Conference and Exhibition, Dallas, Texas, USA.
<https://doi.org/10.2118/9235-MS>
- [49] Bath, P. G., Fowler, W. N., & Russell, M. P. (1980, October 21-24). *The Brent Field, a Reservoir Engineering Review* [Paper presentation]. European Offshore Technology Conference and Exhibition, London, United Kingdom.
<https://doi.org/10.2118/164-1980-MS>
- [50] Bath, P. G., van der Burgh, J., & Ypma, G. J. (1983, August 28-September 2). *Enhanced Oil Recovery in the North Sea* [Paper presentation]. 11th World Petroleum Congress London, United Kingdom.
- [51] Holt, T., Lindeberg, E., & Ratkje, S. K. (1983). *The Effect of Gravity and Temperature Gradients on Methane Distribution in Oil Reservoirs*. [Unsolicited Paper SPE 11761].
- [52] Montel, F., & Gouel, P. L. (1985, September 22-26). *Prediction of Compositional Grading in a Reservoir Fluid Column* [Paper presentation]. SPE Annual Technical Conference and Exhibition, Las Vegas, Nevada, USA.
<https://doi.org/10.2118/14410-MS>

- [53] Creek, J. L., & Schrader, M. L. (1985, September 22-26). *East Painter Reservoir: an Example of a Compositional Gradient from a Gravitational Field* [Paper presentation]. SPE Annual Technical Conference and Exhibition, Las Vegas, Nevada, USA. <https://doi.org/10.2118/14411-MS>
- [54] Riemens, W. G., Schulte, A. M., & de Jong, L. N. J. (1988). Birba Field PVT Variations along the Hydrocarbon Column and Confirmatory Field Tests. *Journal of Petroleum Technology*, 40(1), 83-88. <https://doi.org/10.2118/13719-PA>
- [55] Hirschberg, A. (1988). Role of Asphaltenes in Compositional Grading of a Reservoir's Fluid Column. *Journal of Petroleum Technology*, 40(1), 89-94. <https://doi.org/10.2118/13171-PA>
- [56] Metcalfe, R. S., Vogel, J. L., & Morris, R. W. (1988). Compositional Gradients in the Anschutz Ranch East Field. *SPE Reservoir Engineering*, 3(3), 1025-1032. <https://doi.org/10.2118/14412-PA>
- [57] Jacqmin, D. (1990). Interaction of Natural Convection and Gravity Segregation in Oil/Gas Reservoirs. *SPE Reservoir Engineering*, 5(2), 233-238. <https://doi.org/10.2118/16703-PA>
- [58] Wheaton, R. J. (1991). Treatment of Variations of Composition with Depth in Gas-Condensate Reservoirs. *SPE Reservoir Engineering*, 6(2), 239-244. <https://doi.org/10.2118/18267-PA>
- [59] Whitson, C. H., & Belery, P. (1994, August 29-31). *Compositional Gradients in Petroleum Reservoirs* [Paper presentation]. University of Tulsa Centennial Petroleum Engineering Symposium, Tulsa, Oklahoma, USA. <https://doi.org/10.2118/28000-MS>
- [60] Temeng, K. O., Al-Sadeg, M. J., & Al-Mulhim, W. A. (1998, September 27-30). *Compositional Grading in the Ghawar Khuff Reservoirs* [Paper presentation]. SPE Annual Technical Conference and Exhibition, New Orleans, Louisiana, USA. <https://doi.org/10.2118/49270-MS>
- [61] Biswas, D., & Carey, G. F. (1998). Least-Squares Finite-Element Method to Predict Areal Composition Variations in Large Hydrocarbon Reservoirs. *SPE Journal*, 3(4), 307-315. <https://doi.org/10.2118/51321-PA>

- [62] Padua, K. G. O. (1999). Non-isothermal Gravitational Composition Variation in a Large Deep-water Field. *SPE Journal*, 4(2), 109-117. <https://doi.org/10.2118/56407-PA>
- [63] Pedersen, K. S., & Lindeloff, N. (2003, October 5-8). *Simulations of Compositional Gradients in Hydrocarbon Reservoirs under the Influence of a Temperature Gradient* [Paper presentation]. SPE Annual Technical Conference and Exhibition, Denver, Colorado, USA. <https://doi.org/10.2118/84364-MS>
- [64] Barrufet, M. A., & Jaramillo, J. M. (2004). Effects in the Determination of Oil Reserves Due to Gravitational Compositional Gradients in Near-Critical Reservoirs. *Journal of Canadian Petroleum Technology*, 43(7), 31-37. <https://doi.org/10.2118/04-07-02>
- [65] Pedersen, K. S., & Hjermsstad, H. P. (2006, November 5-8). *Modeling of Large Hydrocarbon Compositional Gradient* [Paper presentation]. Abu Dhabi International Petroleum Exhibition and Conference, Abu Dhabi, UAE. <https://doi.org/10.2118/101275-MS>
- [66] Kord, S., & Zobeidi, K. (2007, June 12-14). *Effect of Compositional Grading on Reservoir Fluid Characterization in a Giant Iranian Oil Reservoir* [Paper presentation]. Canadian International Petroleum Conference, Calgary, Alberta, Canada. <https://doi.org/10.2118/2007-126>
- [67] James, B., & Patience, R. (2008). A Case Study in Using Compositional Grading to Improve Reservoir Characterization. *Journal of Canadian Petroleum Technology*, 47(7), 33-39. <https://doi.org/10.2118/08-07-33>
- [68] Pedersen, K. S., & Hjermsstad, H. P. (2015, September 28-30). *Modeling of Compositional Variation with Depth for Five North Sea Reservoirs* [Paper presentation]. SPE Annual Technical Conference and Exhibition, Houston, Texas, USA. <https://doi.org/10.2118/175085-MS>
- [69] Vinhal, A., Azeem, J., & Pedersen, K. (2021, September 21-23). *Modeling of Compositional Grading in Heavy Oil Fields* [Paper presentation]. SPE Annual Technical Conference and Exhibition, Dubai, UAE. <https://doi.org/10.2118/205887-MS>

- [70] Twu, C. H. (1984). An Internally Consistent Correlation for Predicting the Critical Properties and Molecular Weights of Petroleum and Coal-Tar Liquids. *Fluid Phase Equilibria*, 16(2), 137-150. [https://doi.org/10.1016/0378-3812\(84\)85027-X](https://doi.org/10.1016/0378-3812(84)85027-X)
- [71] Lee, B. I., & Kesler, M. G. (1975). A Generalized Thermodynamic Correlation Based on Three-Parameter Corresponding States. *American Institute of Chemical Engineers Journal*, 21(3), 510-257. <https://doi.org/10.1002/aic.690210313>
- [72] Whitson, C. H. (1983). Characterizing Hydrocarbon plus Fractions. *Society of Petroleum Engineers Journal*, 23(4), 683-694. <https://doi.org/10.2118/12233-PA>
- [73] Nghiem, L. X., Li, Y.-K., & Heidermann, R. A. (1985). Application of the Tangent Plane Criterion to Saturation Pressure and Temperature Computations. *Fluid Phase Equilibria*, 21(1-2), 39-60. [https://doi.org/10.1016/0378-3812\(85\)90059-7](https://doi.org/10.1016/0378-3812(85)90059-7)

Appendix A

Supplementary Tables and Figures

Table A.1: Component properties for the SRK and PR EOS fluid characterizations

Component	p_c (atm)	T_c (K)	ω	MW	V_c	SG
H ₂ S	88.20	373.2	0.1000	34.080	0.0985	0.801
CO ₂	72.80	304.2	0.2250	44.010	0.0940	0.818
N ₂	33.50	126.2	0.0400	28.013	0.0895	0.809
CH ₄	45.40	190.6	0.0080	16.043	0.0990	0.300
C ₂ H ₆	48.20	305.4	0.0980	30.070	0.1480	0.356
C ₃ H ₈	41.90	369.8	0.1520	44.097	0.2030	0.507
IC ₄	36.00	408.1	0.1760	58.124	0.2630	0.563
NC ₄	37.50	425.2	0.1930	58.124	0.2550	0.584
IC ₅	33.40	460.4	0.2270	72.151	0.3060	0.625
NC ₅	33.30	469.6	0.2510	72.151	0.3040	0.631
FC ₆	32.46	507.5	0.2750	86.000	0.3440	0.690
FC ₇	30.97	543.2	0.3083	96.000	0.3810	0.727
FC ₈	29.12	570.5	0.3513	107.000	0.4210	0.749
FC ₉	26.94	598.5	0.3908	121.000	0.4710	0.768
FC ₁₀	25.01	622.1	0.4438	134.000	0.5210	0.782
FC ₁₁	23.17	643.6	0.4775	147.000	0.5740	0.793
FC ₁₂	21.63	663.9	0.5223	161.000	0.6260	0.804
C ₁₃₊ (SRK)	19.80	891.5	0.4439	320.287	1.2591	0.855
C ₁₃₊ (PR)	17.96	963.7	0.4688	325.526	1.2591	0.855

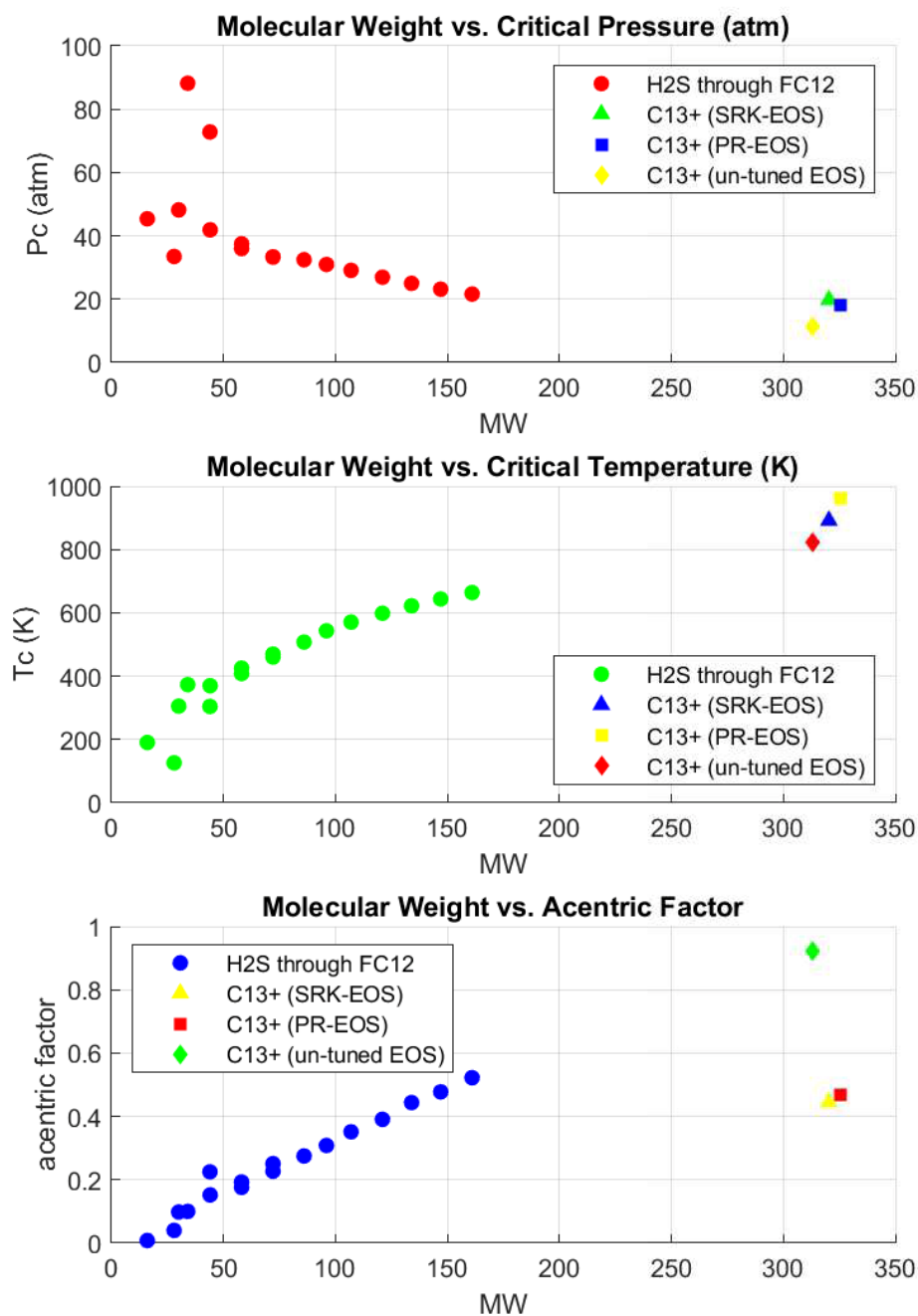


Figure A.1: Component property plot for the SRK and PR EOS fluid characterizations

Appendix A: Supplementary Tables and Figures

Table A.2: Binary interaction coefficients for the SRK-EOS fluid characterization

Comp.	H ₂ S	CO ₂	N ₂	CH ₄	C ₂ H ₆	C ₃ H ₈	IC ₄	NC ₄	IC ₅
H ₂ S	0								
CO ₂	0.12	0							
N ₂	0.12	0	0						
CH ₄	0.08	0.12	0.02	0					
C ₂ H ₆	0.07	0.15	0.06	0.003	0				
C ₃ H ₈	0.07	0.15	0.08	0.009	0.002	0			
IC ₄	0.06	0.15	0.08	0.016	0.005	0.001	0		
NC ₄	0.06	0.15	0.08	0.015	0.005	0.001	0.000	0	
IC ₅	0.06	0.15	0.08	0.021	0.009	0.003	0.000	0.001	0
NC ₅	0.06	0.15	0.08	0.021	0.009	0.003	0.000	0.001	0.000
FC ₆	0.03	0.15	0.08	0.025	0.012	0.005	0.001	0.001	0.000
FC ₇	0.03	0.15	0.08	0.030	0.015	0.007	0.002	0.003	0.001
FC ₈	0.0295	0.15	0.08	0.034	0.018	0.009	0.004	0.004	0.002
FC ₉	0.029	0.15	0.08	0.039	0.022	0.012	0.006	0.006	0.003
FC ₁₀	0.0285	0.15	0.08	0.044	0.026	0.015	0.008	0.008	0.005
FC ₁₁	0.028	0.15	0.08	0.049	0.030	0.018	0.010	0.011	0.007
FC ₁₂	0.0275	0.15	0.08	0.054	0.034	0.021	0.012	0.013	0.008
C ₁₃ +	0	0	0	0.099	0.072	0.053	0.040	0.041	0.033

Table A.2: Binary interaction coefficients for the SRK-EOS fluid characterization (cont.)

Comp.	NC ₅	FC ₆	FC ₇	FC ₈	FC ₉	FC ₁₀	FC ₁₁	FC ₁₂	C ₁₃ +
NC ₅	0								
FC ₆	0.000	0							
FC ₇	0.001	0.000	0						
FC ₈	0.002	0.001	0.000	0					
FC ₉	0.003	0.002	0.001	0.000	0				
FC ₁₀	0.005	0.003	0.002	0.001	0.000	0			
FC ₁₁	0.007	0.004	0.003	0.002	0.001	0.000	0		
FC ₁₂	0.009	0.006	0.004	0.003	0.001	0.001	0.000	0	
C ₁₃ +	0.033	0.027	0.023	0.020	0.016	0.013	0.010	0.008	0

Appendix A: Supplementary Tables and Figures

Table A.3: Binary interaction coefficients for the PR-EOS fluid characterization

Comp.	H ₂ S	CO ₂	N ₂	CH ₄	C ₂ H ₆	C ₃ H ₈	IC ₄	NC ₄	IC ₅
H ₂ S	0								
CO ₂	0.135	0							
N ₂	0.13	0	0						
CH ₄	0.07	0.105	0.025	0					
C ₂ H ₆	0.085	0.13	0.01	0.003	0				
C ₃ H ₈	0.08	0.125	0.09	0.009	0.002	0			
IC ₄	0.075	0.12	0.095	0.016	0.005	0.001	0		
NC ₄	0.075	0.115	0.095	0.015	0.005	0.001	0.000	0	
IC ₅	0.07	0.115	0.1	0.021	0.009	0.003	0.000	0.001	0
NC ₅	0.07	0.115	0.11	0.021	0.009	0.003	0.000	0.001	0.000
FC ₆	0.05	0.115	0.11	0.025	0.012	0.005	0.001	0.001	0.000
FC ₇	0.05	0.115	0.11	0.030	0.015	0.007	0.002	0.003	0.001
FC ₈	0.0495	0.115	0.11	0.034	0.018	0.009	0.004	0.004	0.002
FC ₉	0.049	0.115	0.11	0.039	0.022	0.012	0.006	0.006	0.003
FC ₁₀	0.0485	0.115	0.11	0.044	0.026	0.015	0.008	0.008	0.005
FC ₁₁	0.048	0.115	0.11	0.049	0.030	0.018	0.010	0.011	0.007
FC ₁₂	0.0475	0.115	0.11	0.054	0.034	0.021	0.012	0.013	0.008
C ₁₃₊	0	0	0	0.099	0.072	0.053	0.040	0.041	0.033

Table A.3: Binary interaction coefficients for the PR-EOS fluid characterization (cont.)

Comp.	NC ₅	FC ₆	FC ₇	FC ₈	FC ₉	FC ₁₀	FC ₁₁	FC ₁₂	C ₁₃₊
NC ₅	0								
FC ₆	0.000	0							
FC ₇	0.001	0.000	0						
FC ₈	0.002	0.001	0.000	0					
FC ₉	0.003	0.002	0.001	0.000	0				
FC ₁₀	0.005	0.003	0.002	0.001	0.000	0			
FC ₁₁	0.007	0.004	0.003	0.002	0.001	0.000	0		
FC ₁₂	0.009	0.006	0.004	0.003	0.001	0.001	0.000	0	
C ₁₃₊	0.033	0.027	0.023	0.020	0.016	0.013	0.010	0.008	0

Appendix A: Supplementary Tables and Figures

Table A.4: CCE calculated results for the SRK-EOS using commercial software

Pressure (psia)	ROV	Liquid volume (CV %)	Oil Compressibility (1/psia)	IFT (dyn/cm)	Y * function
4992.20	0.9879	100.0000	0.9542E-05	-	-
4636.86	0.9914	100.0000	0.1004E-04	-	-
4281.51	0.9950	100.0000	0.1058E-04	-	-
3926.17	0.9989	100.0000	0.1118E-04	-	-
3826.10	1.0000	100.0000	0.1136E-04	-	-
3826.07	1.0000	100.0000	0.1136E-04	1.9956	-
3286.56	1.0292	94.8424	-	2.8613	5.6158
2858.69	1.0645	89.9161	-	3.8219	5.2458
2432.28	1.1183	83.8657	-	5.1017	4.8433
2005.87	1.2055	76.1407	-	6.7838	4.4158
1437.32	1.4342	61.9999	-	9.7758	3.8279

$$* Y \text{ function} = \frac{p_{sat} - p}{p(V_{rt} - 1)}$$

Table A.4: CCE calculated results for the SRK-EOS using commercial software (cont.)

Pressure (psia)	Oil Viscosity (cp)	Gas Viscosity (cp)	Oil Z-factor	Gas Z-factor	Oil Density (lb/ft ³)	Gas Density (lb/ft ³)
4992.20	1.1123	-	1.8125	-	49.040	-
4636.86	1.0723	-	1.6894	-	48.870	-
4281.51	1.0321	-	1.5657	-	48.691	-
3926.17	0.9918	-	1.4413	-	48.503	-
3826.10	0.9804	-	1.4061	-	48.449	-
3826.07	0.9804	0.02565	1.4061	0.9070	48.449	13.63
3286.56	1.0758	0.02297	1.2716	0.8803	48.981	11.98
2858.69	1.1662	0.02089	1.1562	0.8659	49.433	10.55
2432.28	1.2739	0.01896	1.0322	0.8590	49.916	9.05
2005.87	1.4056	0.01724	0.8978	0.8606	50.441	7.47
1437.32	1.6356	0.01541	0.6991	0.8772	51.219	5.33

Appendix A: Supplementary Tables and Figures

Table A.5: CCE calculated results for the PR-EOS using commercial software

Pressure (psia)	ROV	Liquid Volume (CV %)	Oil Compressibility (1/psia)	IFT (dyn/cm)	Y function
4992.20	0.9903	100.0000	0.7725E-05	-	-
4636.86	0.9931	100.0000	0.8100E-05	-	-
4281.51	0.9960	100.0000	0.8508E-05	-	-
3926.17	0.9991	100.0000	0.8952E-05	-	-
3826.10	1.0000	100.0000	0.9084E-05	-	-
3825.57	1.0000	100.0000	0.9085E-05	1.6509	-
3286.56	1.0276	95.2022	-	2.4706	5.9418
2858.69	1.0613	90.5533	-	3.4031	5.5200
2432.28	1.1131	84.7604	-	4.6653	5.0651
2005.87	1.1979	77.2404	-	6.3393	4.5848
1437.32	1.4230	63.1784	-	9.3131	3.9277

Table A.5: CCE calculated results for the PR-EOS using commercial software (cont.)

Pressure (psia)	Oil Viscosity (cp)	Gas Viscosity (cp)	Oil Z-factor	Gas Z-factor	Oil Density (lb/ft ³)	Gas Density (lb/ft ³)
4992.20	1.1691	-	1.8026	-	49.897	-
4636.86	1.1345	-	1.6790	-	49.757	-
4281.51	1.0996	-	1.5550	-	49.610	-
3926.17	1.0643	-	1.4303	-	49.457	-
3826.10	1.0543	-	1.3951	-	49.412	-
3825.57	1.0542	0.02772	1.3949	0.8413	49.412	14.85
3286.56	1.1317	0.02451	1.2634	0.8199	49.853	12.98
2858.69	1.2038	0.02203	1.1502	0.8099	50.228	11.38
2432.28	1.2879	0.01973	1.0283	0.8076	50.628	9.70
2005.87	1.3881	0.01770	0.8961	0.8144	51.061	7.95
1437.32	1.5555	0.01560	0.7002	0.8398	51.697	5.59

Appendix A: Supplementary Tables and Figures

Table A.6: CCE calculated results for an un-tuned SRK-EOS using commercial software

Pressure (psia)	ROV	Liquid Volume (CV %)	Oil Compressibility (1/psia)	IFT (dyn/cm)	Y function
4992.20	0.9780	100.0000	0.8574E-05	-	-
4636.86	0.9810	100.0000	0.9051E-05	-	-
4281.51	0.9843	100.0000	0.9574E-05	-	-
3926.17	0.9877	100.0000	0.1015E-04	-	-
3826.10	0.9887	100.0000	0.1032E-04	-	-
3286.56	0.9945	100.0000	0.1135E-04	-	-
2858.69	0.9996	100.0000	0.1229E-04	-	-
2823.63	1.0000	100.0000	0.1237E-04	0.4735	-
2432.28	1.0334	94.8671	-	0.7003	4.8131
2005.87	1.0929	87.7266	-	1.0535	4.3898
1437.32	1.2527	74.1373	-	1.7444	3.8163

Table A.6: CCE calculated results for an un-tuned SRK-EOS using commercial software (cont.)

Pressure (psia)	Oil Viscosity (cp)	Gas Viscosity (cp)	Oil Z-factor	Gas Z-factor	Oil Density (lb/ft ³)	Gas Density (lb/ft ³)
4992.20	0.1267	-	2.4850	-	35.177	-
4636.86	0.1253	-	2.3154	-	35.067	-
4281.51	0.1237	-	2.1450	-	34.951	-
3926.17	0.1222	-	1.9739	-	34.829	-
3826.10	0.1217	-	1.9256	-	34.793	-
3286.56	0.1192	-	1.6637	-	34.590	-
2858.69	0.1171	-	1.4545	-	34.416	-
2823.63	0.1169	0.02051	1.4372	0.8704	34.401	10.23
2432.28	0.1193	0.01881	1.3136	0.8637	34.608	8.89
2005.87	0.1222	0.01715	1.1632	0.8644	34.852	7.36
1437.32	0.1260	0.01537	0.9301	0.8796	35.203	5.26

Appendix A: Supplementary Tables and Figures

Table A.7: CCE calculated results an un-tuned the PR-EOS using commercial software

Pressure (psia)	ROV	Liquid Volume (CV %)	Oil Compressibility (1/psia)	IFT (dyn/cm)	Y function
4992.20	0.9792	100.0000	0.8034E-05	-	-
4636.86	0.9821	100.0000	0.8466E-05	-	-
4281.51	0.9851	100.0000	0.8938E-05	-	-
3926.17	0.9884	100.0000	0.9458E-05	-	-
3826.10	0.9893	100.0000	0.9614E-05	-	-
3286.56	0.9947	100.0000	0.1054E-04	-	-
2858.69	0.9994	100.0000	0.1138E-04	-	-
2803.04	1.0000	100.0000	0.1150E-04	0.8335	-
2432.28	1.0344	94.7525	-	1.2003	4.4259
2005.87	1.0989	87.1155	-	1.7894	4.0172
1437.32	1.2743	72.6796	-	2.9154	3.4642

Table A.7: CCE calculated results for an un-tuned PR-EOS using commercial software (cont.)

Pressure (psia)	Oil Viscosity (cp)	Gas Viscosity (cp)	Oil Z-factor	Gas Z-factor	Oil Density (lb/ft ³)	Gas Density (lb/ft ³)
4992.20	0.2075	-	2.2311	-	39.180	-
4636.86	0.2042	-	2.0784	-	39.065	-
4281.51	0.2008	-	1.9250	-	38.945	-
3926.17	0.1973	-	1.7711	-	38.818	-
3826.10	0.1963	-	1.7276	-	38.781	-
3286.56	0.1908	-	1.4920	-	38.571	-
2858.69	0.1862	-	1.3039	-	38.391	-
2803.04	0.1856	0.02153	1.2793	0.8132	38.366	11.01
2432.28	0.1909	0.01961	1.1754	0.8112	38.612	9.57
2005.87	0.1975	0.01764	1.0416	0.8172	38.912	7.87
1437.32	0.2069	0.01557	0.8339	0.8414	39.336	5.55

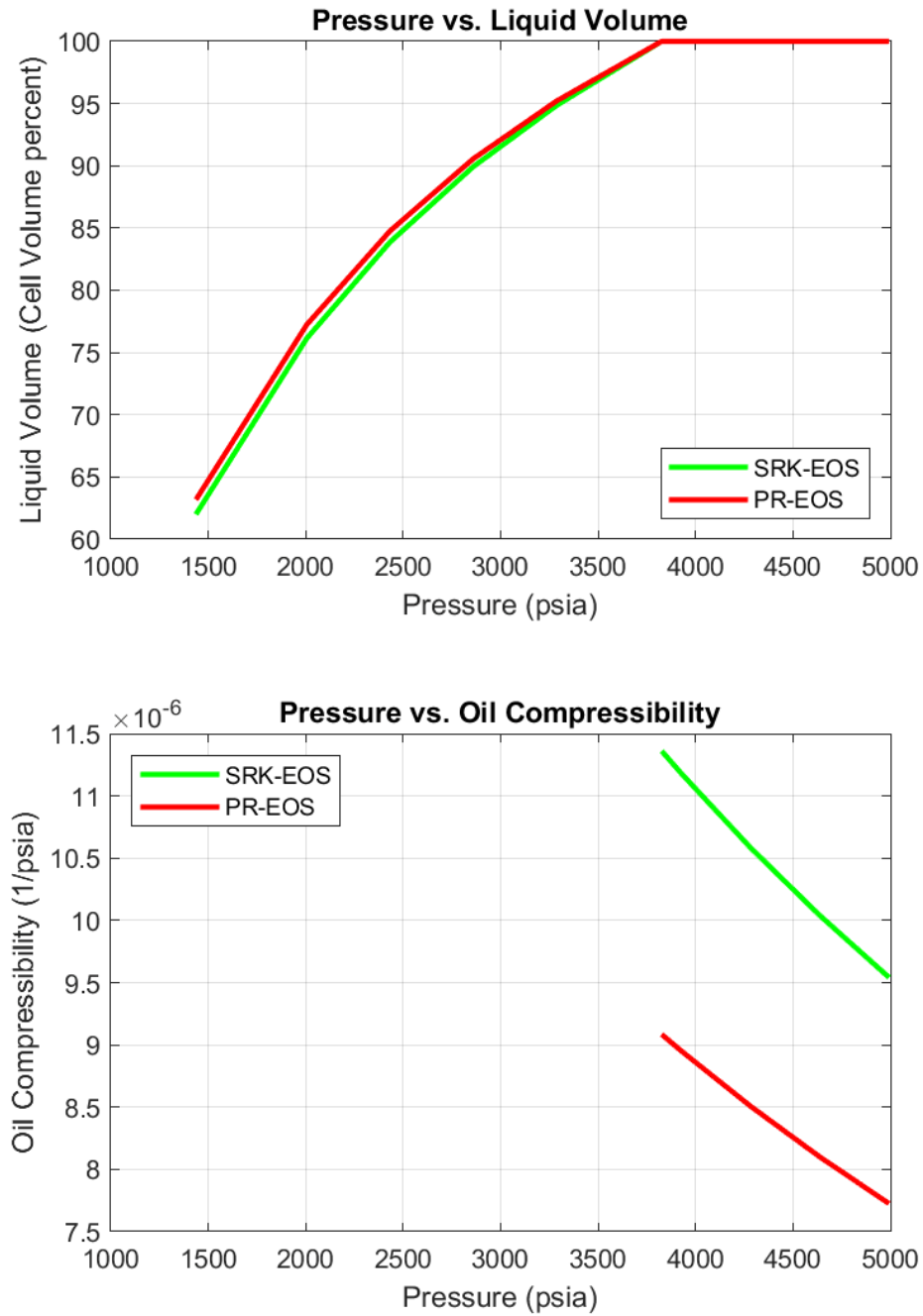


Figure A.2: Liquid volume & oil compressibility plots using commercial software

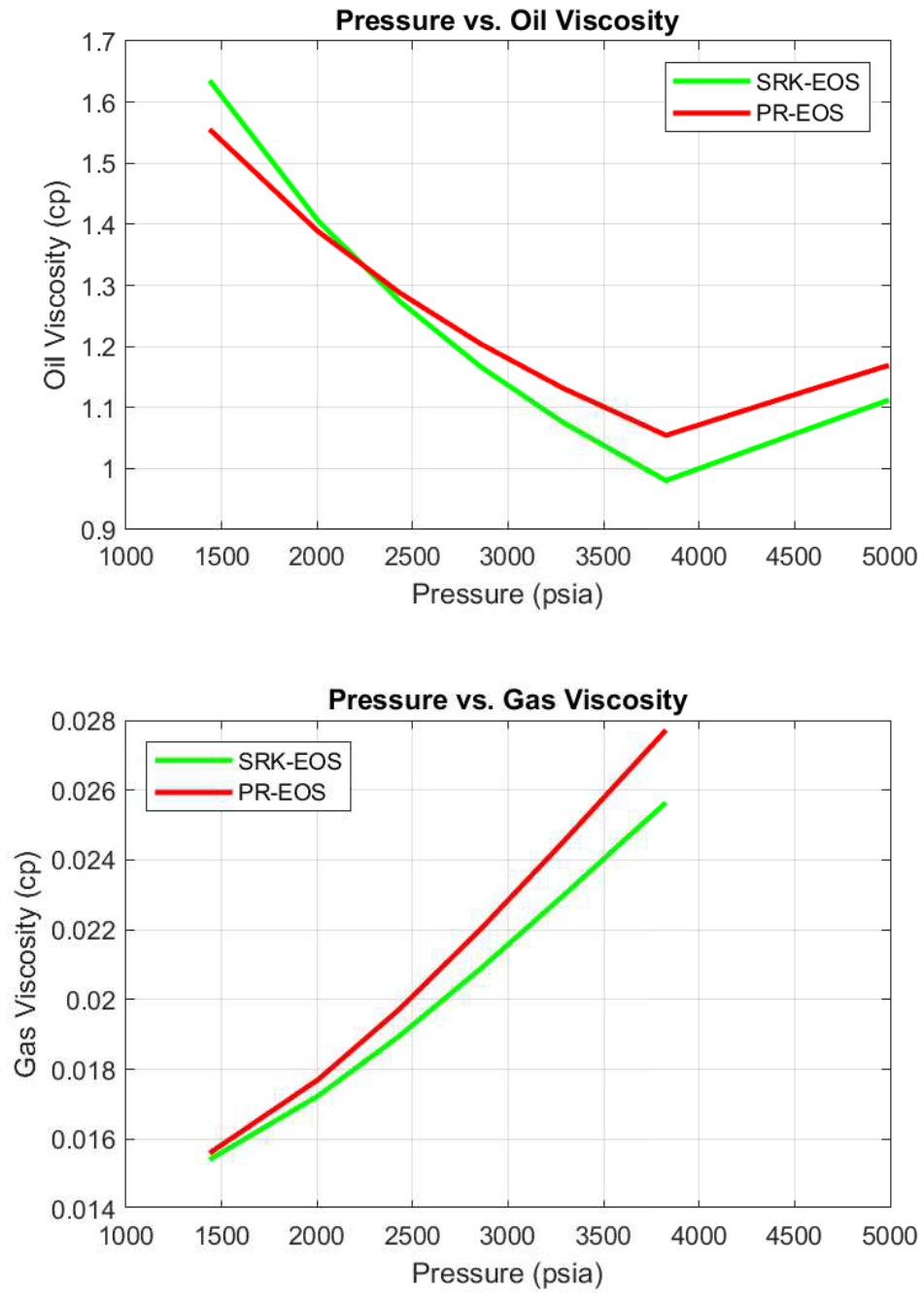


Figure A.3: Oil and gas viscosity plots using commercial software

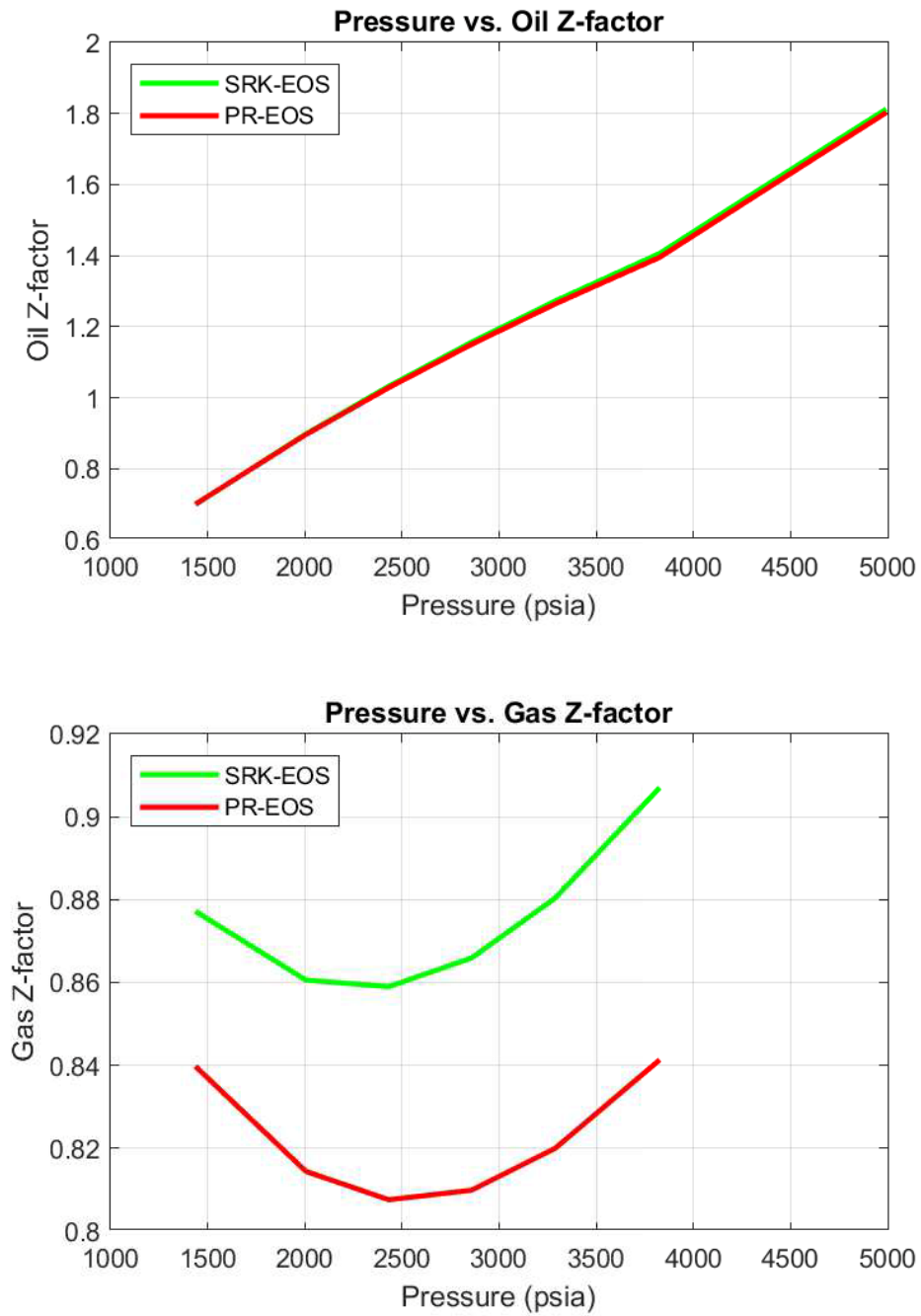


Figure A.4: Oil and gas Z-factor plots using commercial software

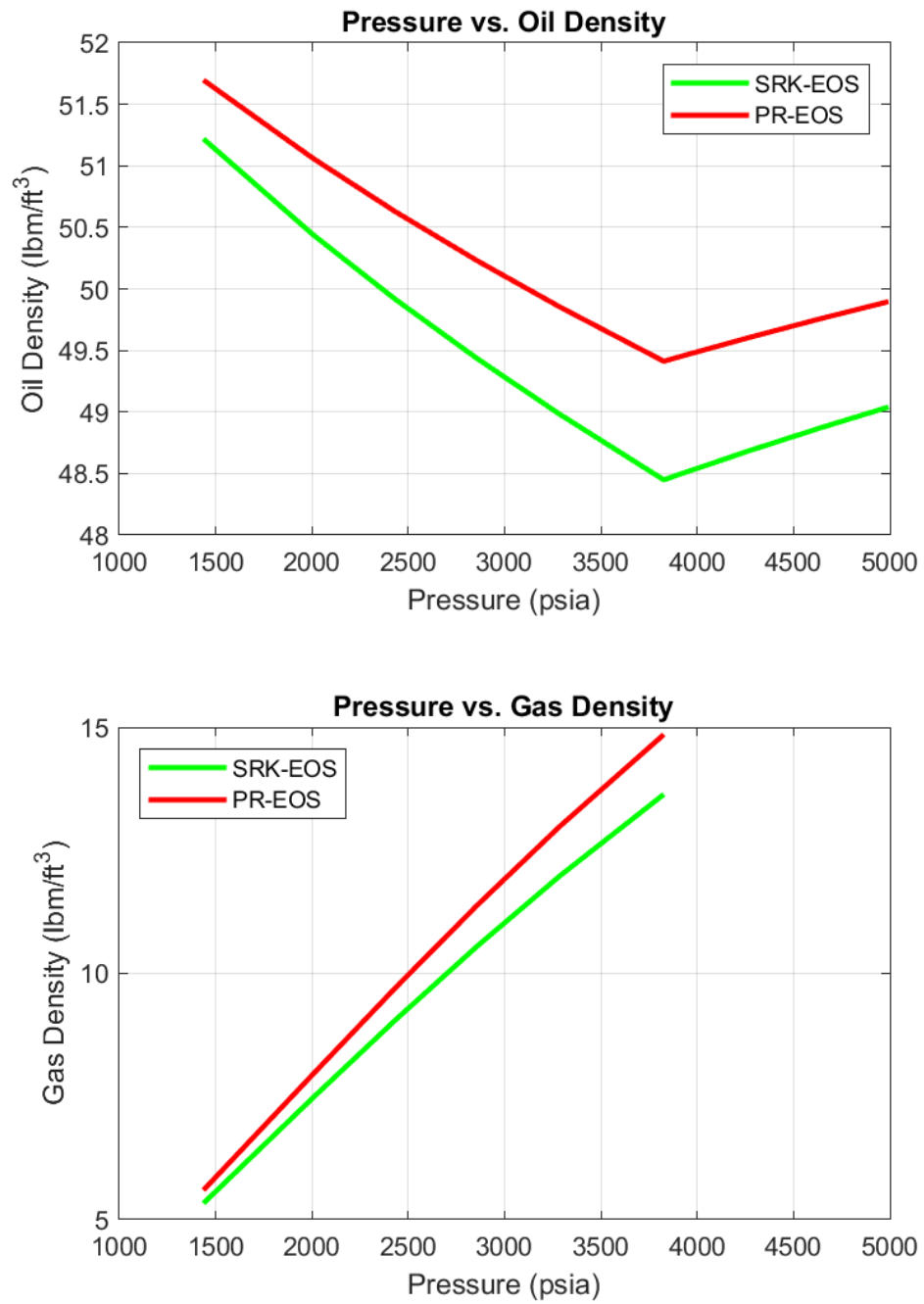


Figure A.5: Oil and gas density plots using commercial software

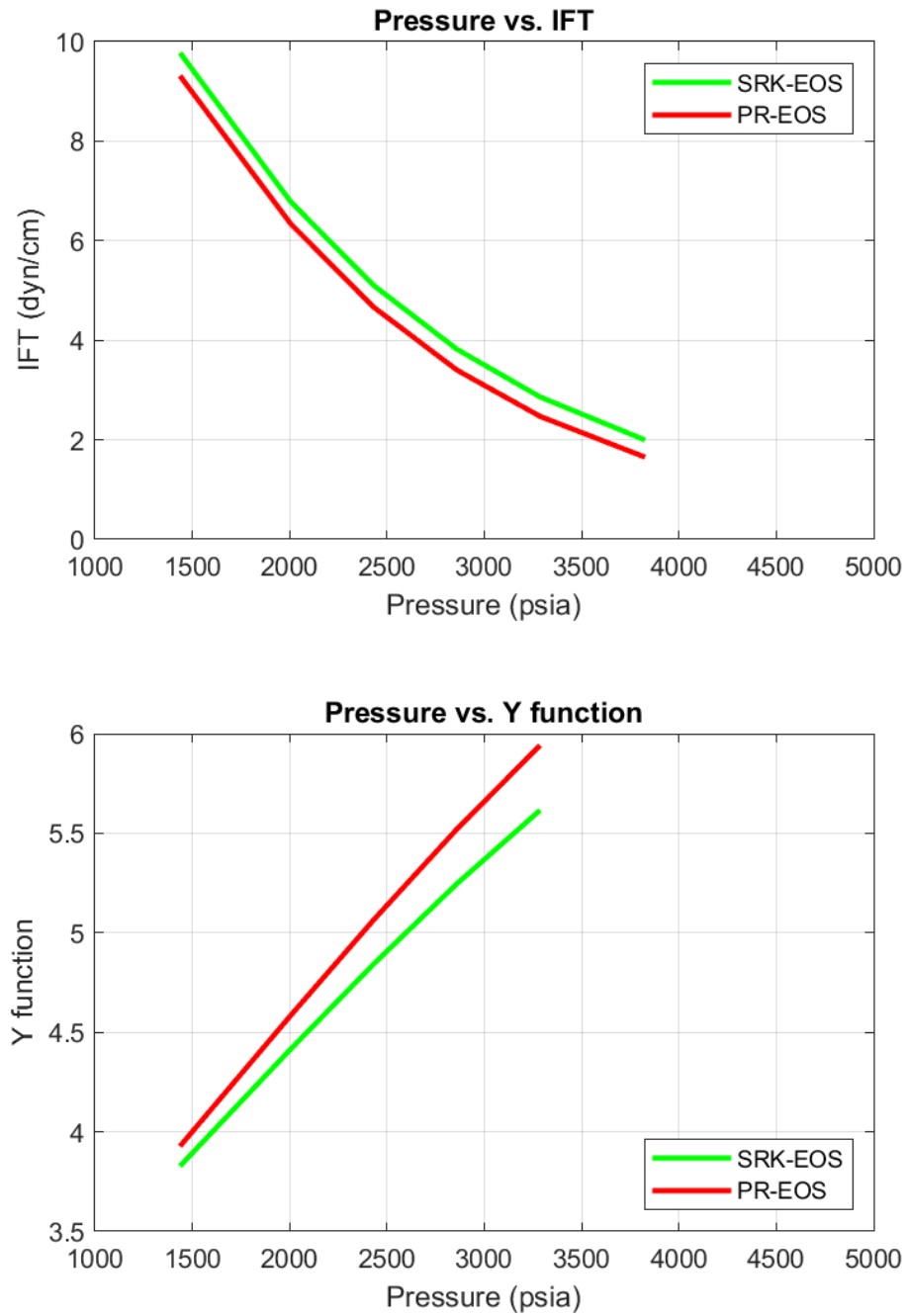


Figure A.6: IFT and Y function plots using commercial software

Appendix A: Supplementary Tables and Figures

Table A.8: DL experimental vs. calculated oil SG's using commercial software

Pressure (psia)	Experimental	Calculated Oil SG	
	Oil SG	SRK EOS	PR EOS
4992.20	0.7811	0.78555	0.79927
4636.86	0.7788	0.78282	0.79703
4281.51	0.7765	0.77996	0.79468
3926.17	0.7742	0.77695	0.79222
3826.10	0.7734	0.77607	0.79151
P_{sat}*	-	0.77607	0.79150
3428.70	0.7813	0.78229	0.79666
3002.29	0.7869	0.78936	0.80253
2574.42	0.7936	0.79693	0.80882
1721.60	0.8076	0.81381	0.82282
868.78	0.8239	0.83365	0.83908
298.78	0.8389	0.84958	0.85144
114.58	0.8449	0.85638	0.85611
14.50	0.8529	0.86521	0.86120

*Calculated value: $p_{\text{sat}}=3826.07$ psia (SRK-EOS), $p_{\text{sat}}=3825.57$ psia (PR-EOS).

Table A.9: DL experimental vs. calculated oil and gas viscosities using commercial software

Pressure (psia)	Exp. Oil Viscosity (cp)	Calc. Oil		Exp. Gas Viscosity (cp)	Calc. Gas	
		Viscosity (cP)			Viscosity (cP)	
		SRK EOS	PR EOS		SRK EOS	PR EOS
4992.21	1.05	1.1123	1.1691	-	0.0306	0.0337
4636.86	1.03	1.1123	1.1345	-	0.0292	0.0320
4281.52	1.00	1.0321	1.0996	-	0.0277	0.0301
3926.18	0.94	0.9918	1.0643	-	0.0261	0.0283
3826.10	0.92	0.9804	1.0543	-	0.0256	0.0277
P _{sat}	-	0.9804	1.0542	-	0.0256	0.0277
3428.70	1.00	1.0489	1.1100	0.02400	0.0237	0.0253
3002.29	1.12	1.1340	1.1784	0.02215	0.0216	0.0228
2574.42	1.30	1.2347	1.2578	0.01999	0.0196	0.0205
1721.60	1.61	1.5026	1.4614	0.01630	0.0163	0.0166
868.78	1.83	1.9146	1.7521	0.01280	0.0143	0.0143
298.78	2.54	2.3491	2.0129	0.01016	0.0138	0.0138
114.58	2.91	2.5508	2.0944	0.00869	0.0139	0.0139
14.50	3.66	2.7140	2.0723	0.00726	0.0130	0.0130

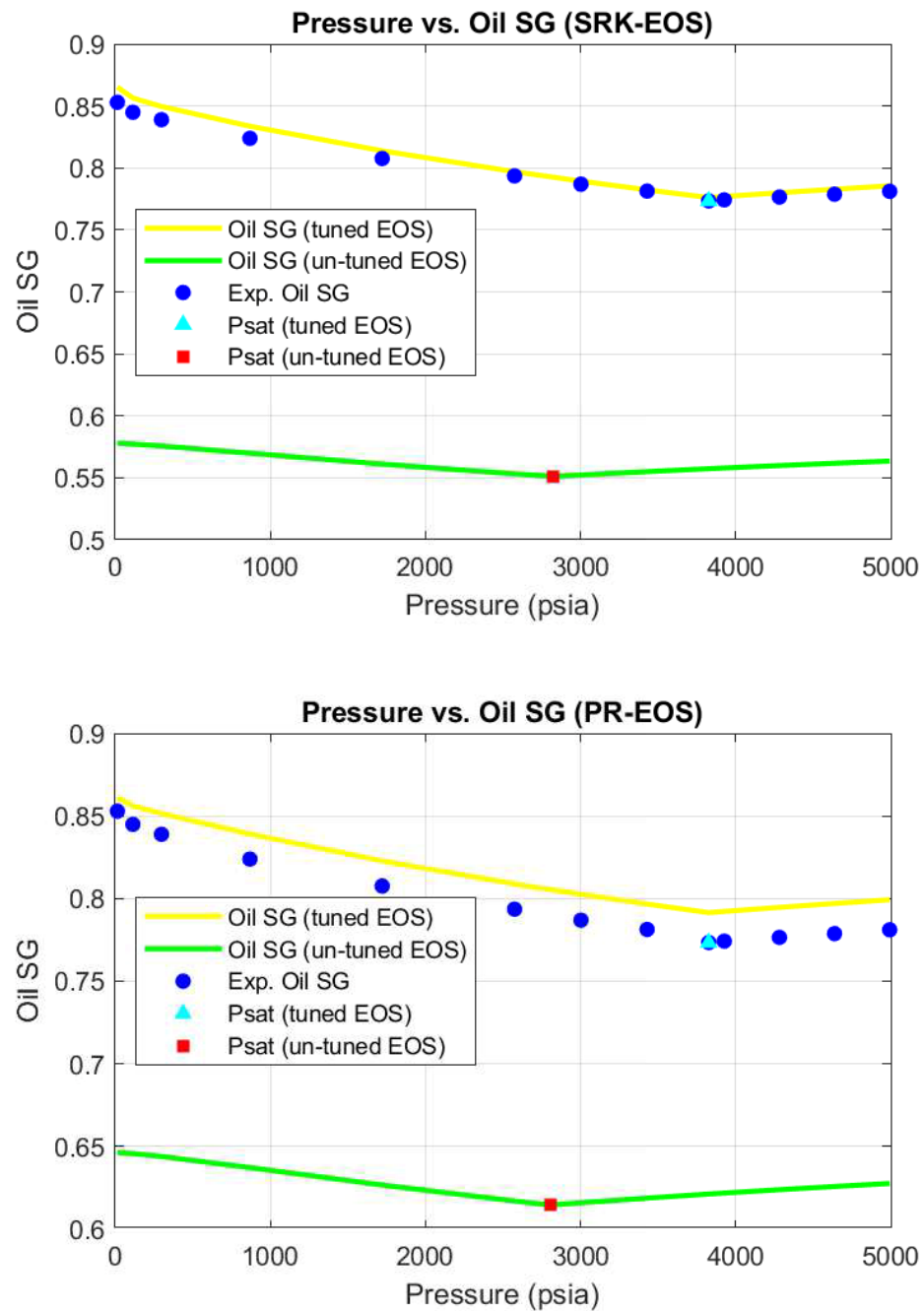


Figure A.7: Oil SG plots using commercial software

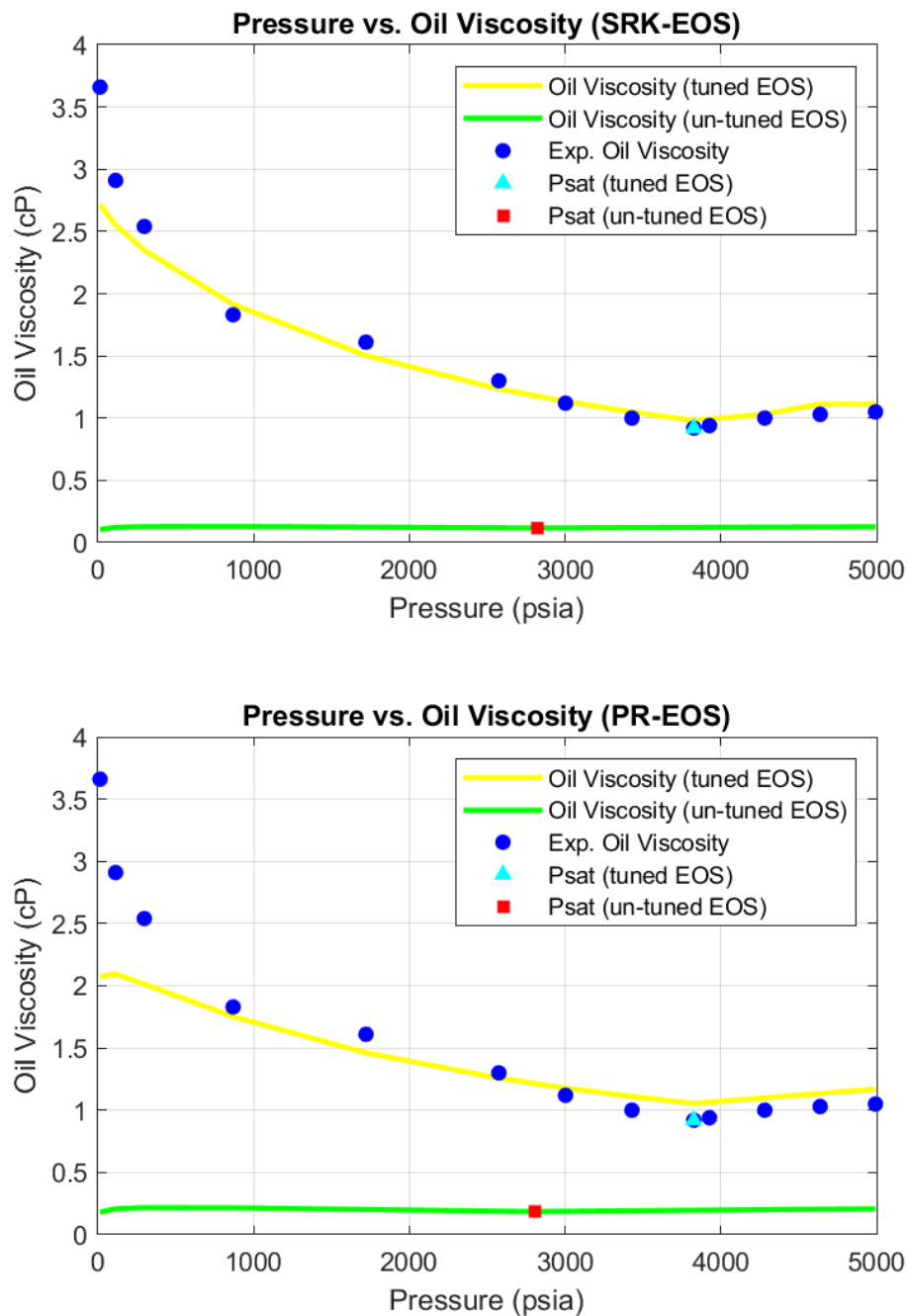


Figure A.8: Oil viscosity plots using commercial software

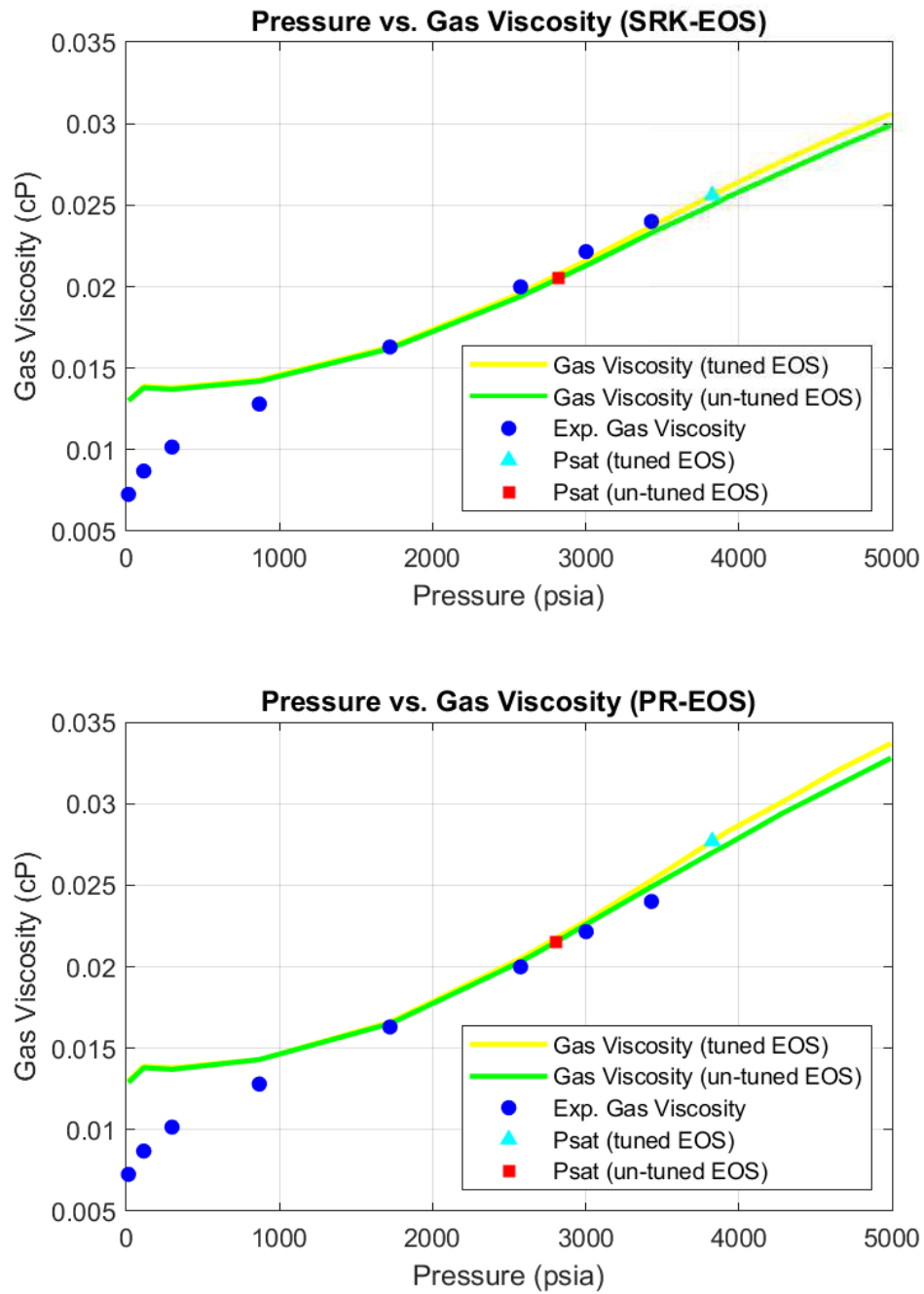


Figure A.9: Gas viscosity plots using commercial software

Appendix A: Supplementary Tables and Figures

Table A.10: DL calculated results for the SRK-EOS using commercial software

Pressure (psia)	Oil Vol. (litre)	Gas Vol. (mole)	Oil SG	Gas SG	Oil FVF (RB/STB)	Gas FVF (ft ³ /scf)
4992.21	65.5694	-	0.78555	0.7117	1.29127	0.00333
4636.86	65.7979	-	0.78282	0.7117	1.29577	0.00349
4281.52	66.0393	-	0.77996	0.7117	1.30053	0.00368
3926.18	66.2951	-	0.77695	0.7117	1.30556	0.00391
3826.10	66.3699	-	0.77607	0.7117	1.30704	0.00398
3826.07	66.3699	-	0.77607	0.7117	1.30704	0.00398
3428.70	65.2034	24.3717	0.78229	0.7076	1.28406	0.00435
3002.29	63.9497	25.9050	0.78936	0.7047	1.25938	0.00487
2574.42	62.6808	25.8648	0.79693	0.7039	1.23439	0.00561
1721.60	60.0567	52.1731	0.81381	0.7125	1.18271	0.00845
868.78	57.1817	54.8298	0.83365	0.7588	1.12609	0.01752
298.78	54.7520	44.0508	0.84958	0.9040	1.07824	0.05352
114.58	53.5246	21.1578	0.85638	1.1073	1.05407	0.14249
14.50	51.7364	26.8760	0.86521	1.3800	1.01886	1.15146

Table A.10: DL calculated results for the SRK-EOS using commercial software (cont.)

Pressure (psia)	ROV	Solution GOR (scf/STB)	Oil Viscosity (cP)	Gas Viscosity (cP)	Gas Z-factor	IFT (dyn/cm)
4992.21	1.291	720.96	1.1123	0.0306	0.9883	1.1989
4636.86	1.296	720.96	1.1123	0.0292	0.9616	1.3870
4281.52	1.301	720.96	1.0321	0.0277	0.9364	1.6176
3926.18	1.306	720.96	0.9918	0.0261	0.9131	1.9031
3826.10	1.307	720.96	0.9804	0.0256	0.9070	1.9955
3826.07	1.307	720.96	0.9804	0.0256	0.9070	1.9956
3428.70	1.333	657.12	1.0489	0.0237	0.8865	2.6005
3002.29	1.374	589.26	1.1340	0.0216	0.8699	3.4661
2574.42	1.434	521.51	1.2347	0.0196	0.8601	4.6279
1721.60	1.688	384.84	1.5026	0.0163	0.8653	8.1243
868.78	2.623	241.22	1.9146	0.0143	0.9056	13.5549
298.78	6.751	125.83	2.3491	0.0138	0.9514	18.4762
114.58	17.565	70.40	2.5508	0.0139	0.9715	20.4881
14.50	148.877	0.00	2.7140	0.0130	0.9935	22.2037

- Residual oil volume / saturated oil volume = 0.7651
- Residual oil SG @60°F = 0.8815
- Residual oil API @60°F = 29.0

Appendix A: Supplementary Tables and Figures

Table A.11: DL calculated results for the PR-EOS using commercial software

Pressure (psia)	Oil Vol. (litre)	Gas Vol. (mole)	Oil SG	Gas SG	Oil FVF (RB/STB)	Gas FVF (ft ³ /scf)
4992.21	65.2113	-	0.79927	0.7191	1.25704	0.00307
4636.86	65.3949	-	0.79703	0.7191	1.26058	0.00322
4281.52	65.5881	-	0.79468	0.7191	1.26430	0.00340
3926.18	65.7918	-	0.79222	0.7191	1.26823	0.00362
3826.10	65.8512	-	0.79151	0.7191	1.26938	0.00370
3825.57	65.8515	-	0.79150	0.7191	1.26938	0.00370
3428.70	64.7988	24.0972	0.79666	0.7147	1.24909	0.00404
3002.29	63.6644	25.7211	0.80253	0.7112	1.22722	0.00455
2574.42	62.5142	25.7707	0.80882	0.7098	1.20505	0.00527
1721.60	60.1307	52.2917	0.82282	0.7169	1.15911	0.00804
868.78	57.5036	55.6073	0.83908	0.7615	1.10847	0.01702
298.78	55.2843	45.0152	0.85144	0.9037	1.06569	0.05296
114.58	54.1876	21.3097	0.85611	1.1033	1.04454	0.14195
14.50	52.6687	25.7521	0.86120	1.3833	1.01526	1.15083

Table A.11: DL calculated results for the PR-EOS using commercial software (cont.)

Pressure (psia)	ROV	Solution GOR (scf/STB)	Oil Viscosity (cP)	Gas Viscosity (cP)	Gas Z-factor	IFT (dyn/cm)
4992.21	1.257	706.57	1.1691	0.0337	0.9124	0.8753
4636.86	1.261	706.57	1.1345	0.0320	0.8889	1.0522
4281.52	1.264	706.57	1.0996	0.0301	0.8668	1.2748
3926.18	1.268	706.57	1.0643	0.0283	0.8466	1.5575
3826.10	1.269	706.57	1.0543	0.0277	0.8414	1.6504
3826.57	1.269	706.57	1.0542	0.0277	0.8413	1.6509
3428.70	1.294	644.78	1.1100	0.0253	0.8247	2.2210
3002.29	1.331	578.83	1.1784	0.0228	0.8124	3.0562
2574.42	1.387	512.75	1.2578	0.0205	0.8072	4.1982
1721.60	1.628	378.67	1.4614	0.0166	0.8234	7.6848
868.78	2.535	236.09	1.7521	0.0143	0.8801	13.0386
298.78	6.592	120.67	2.0129	0.0138	0.9415	17.6431
114.58	17.238	66.03	2.0944	0.0139	0.9678	19.3855
14.50	145.842	0.00	2.0723	0.0130	0.9929	20.6345

- Residual oil volume / saturated oil volume = 0.7878
- Residual oil SG @60°F = 0.8743
- Residual oil API @60°F = 30.3

Appendix A: Supplementary Tables and Figures

Table A.12: DL calculated results for an un-tuned SRK-EOS using commercial software

Pressure (psia)	Oil Vol. (litre)	Gas Vol. (mole)	Oil SG	Gas SG	Oil FVF (RB/STB)	Gas FVF (ft ³ /scf)
4992.21	8989.7165	-	0.56347	0.6943	1.20260	0.00334
4636.86	9017.9008	-	0.56171	0.6943	1.20637	0.00350
4281.52	9047.7775	-	0.55986	0.6943	1.21037	0.00369
3926.18	9079.5229	-	0.55790	0.6943	1.21461	0.00393
3826.10	9088.8282	-	0.55733	0.6943	1.21586	0.00401
3428.70	9127.4989	-	0.55497	0.6943	1.22103	0.00437
3002.29	9172.3615	-	0.55225	0.6943	1.22703	0.00490
2823.63	9192.3133	-	0.55106	0.6943	1.22970	0.00518
2574.42	9077.6194	2200.1487	0.55314	0.6946	1.21436	0.00565
1721.60	8679.8435	7440.3749	0.56102	0.7035	1.16115	0.00849
868.78	8264.4985	7411.5487	0.56983	0.7460	1.10558	0.01758
298.78	7939.8185	5476.0284	0.57564	0.8758	1.06215	0.05366
114.58	7793.7926	2329.8152	0.57721	1.0637	1.04261	0.14278
14.50	7604.3261	2627.2585	0.57794	1.3643	1.01727	1.15169

Table A.12: DL calculated results for an un-tuned SRK-EOS using commercial software (cont.)

Pressure (psia)	ROV	Solution GOR (scf/STB)	Oil Viscosity (cP)	Gas Viscosity (cP)	Gas Z-factor	IFT (dyn/cm)
4992.21	1.203	489.08	0.1267	0.0299	0.9909	0.0672
4636.86	1.206	489.08	0.1253	0.0285	0.9652	0.0919
4281.52	1.210	489.08	0.1237	0.0270	0.9412	0.1261
3926.18	1.215	489.08	0.1222	0.0255	0.9190	0.1734
3826.10	1.216	489.08	0.1217	0.0250	0.9133	0.1897
3428.70	1.221	489.08	0.1199	0.0233	0.8926	0.2722
3002.29	1.227	489.08	0.1178	0.0213	0.8755	0.4021
2823.63	1.230	489.08	0.1169	0.0205	0.8704	0.4735
2574.42	1.254	449.93	0.1184	0.0194	0.8653	0.6085
1721.60	1.421	317.53	0.1241	0.0162	0.8696	1.3629
868.78	2.056	185.65	0.1294	0.0142	0.9087	2.7126
298.78	4.893	88.21	0.1280	0.0137	0.9539	3.9880
114.58	12.291	46.75	0.1218	0.0138	0.9735	4.4711
14.50	101.339	0.00	0.1049	0.0130	0.9937	4.7617

- Residual oil volume / saturated oil volume = 0.8132
- Residual oil SG @60°F = 0.5879
- Residual oil API @60°F = 109.2

Appendix A: Supplementary Tables and Figures

Table A.13: DL calculated results for an un-tuned PR-EOS using commercial software

Pressure (psia)	Oil Vol. (litre)	Gas Vol. (mole)	Oil SG	Gas SG	Oil FVF (RB/STB)	Gas FVF (ft ³ /scf)
4992.21	8071.1222	-	0.62760	0.7032	1.20691	0.00308
4636.86	8094.8085	-	0.62577	0.7032	1.21045	0.00323
4281.52	8119.8673	-	0.62384	0.7032	1.21420	0.00342
3926.18	8146.4384	-	0.62180	0.7032	1.21817	0.00365
3826.10	8154.2165	-	0.62121	0.7032	1.21933	0.00372
3428.70	8186.4901	-	0.61876	0.7032	1.22416	0.00407
3002.29	8223.8322	-	0.61595	0.7032	1.22974	0.00457
2803.04	8242.3535	-	0.61457	0.7032	1.23251	0.00488
2574.42	8141.3908	2084.5661	0.61697	0.7030	1.21742	0.00530
1721.60	7765.5352	7614.8016	0.62665	0.7104	1.16121	0.00807
868.78	7380.2909	7517.9193	0.63719	0.7515	1.10361	0.01707
298.78	7084.8780	5516.3448	0.64394	0.8785	1.05943	0.05308
114.58	6955.8345	2304.9819	0.64569	1.0618	1.04014	0.14220
14.50	6796.3041	2486.3181	0.64634	1.3689	1.01628	1.15099

Table A.13: DL calculated results for an un-tuned PR-EOS using commercial software (cont.)

Pressure (psia)	ROV	Solution GOR (scf/STB)	Oil Viscosity (cP)	Gas Viscosity (cP)	Gas Z-factor	IFT (dyn/cm)
4992.21	1.207	547.48	0.2075	0.0328	0.9149	0.1231
4636.86	1.210	547.48	0.2042	0.0311	0.8925	0.1668
4281.52	1.214	547.48	0.2008	0.0294	0.8715	0.2265
3926.18	1.218	547.48	0.1973	0.0275	0.8525	0.3086
3826.10	1.219	547.48	0.1963	0.0270	0.8475	0.3369
3428.70	1.224	547.48	0.1923	0.0249	0.8303	0.4781
3002.29	1.230	547.48	0.1878	0.0226	0.8171	0.6982
2803.04	1.233	547.48	0.1856	0.0215	0.8132	0.8335
2574.42	1.257	506.02	0.1888	0.0203	0.8112	1.0455
1721.60	1.438	354.56	0.2021	0.0165	0.8266	2.2980
868.78	2.145	205.02	0.2158	0.0143	0.8826	4.4411
298.78	5.335	95.30	0.2170	0.0137	0.9438	6.3565
114.58	13.654	49.45	0.2078	0.0138	0.9695	7.0530
14.50	113.250	0.00	0.1811	0.0129	0.9931	7.4563

- Residual oil volume / saturated oil volume = 0.8113
- Residual oil SG @60°F = 0.6569
- Residual oil API @60°F = 83.9

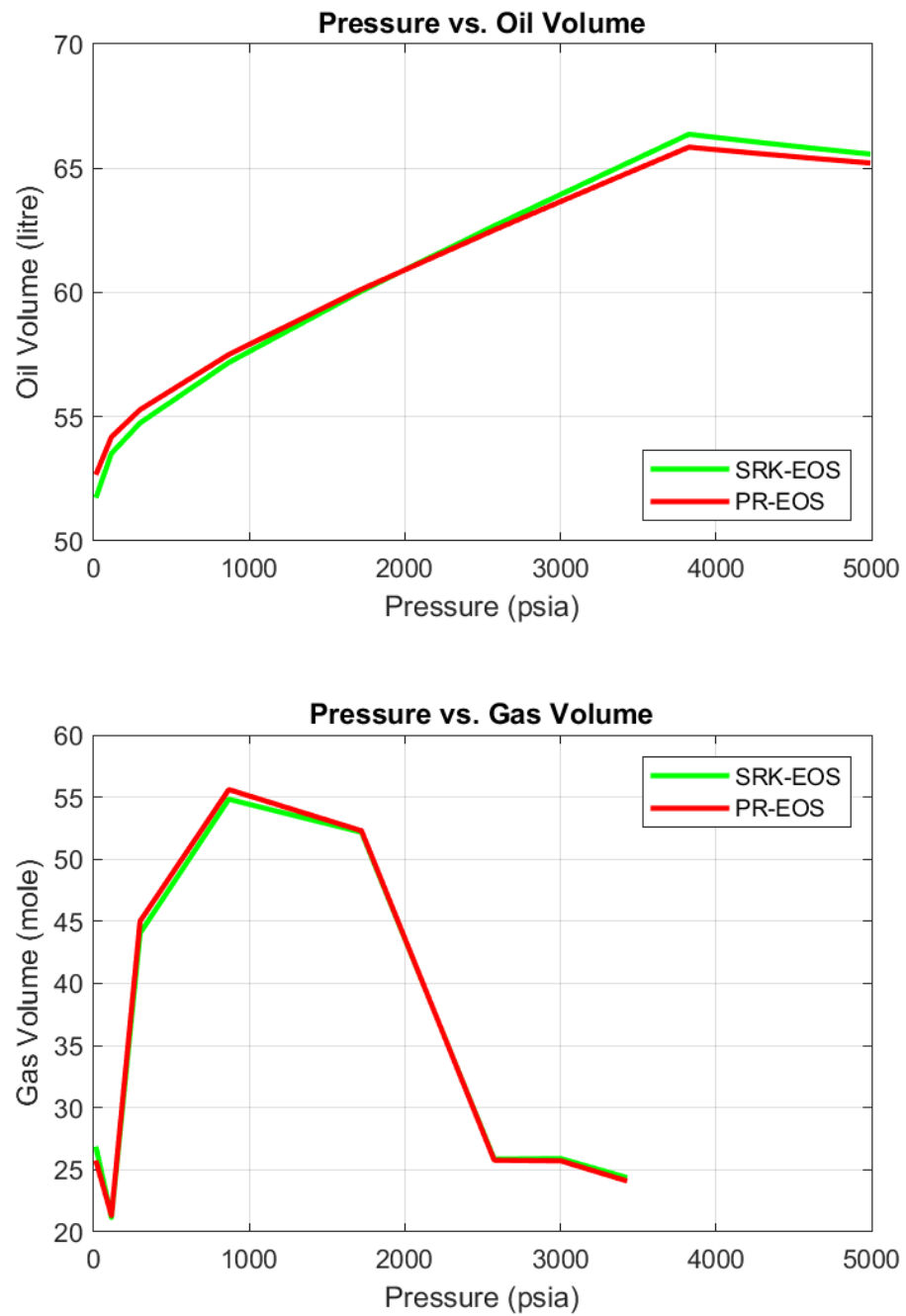


Figure A.10: Oil and gas volume plots using commercial software

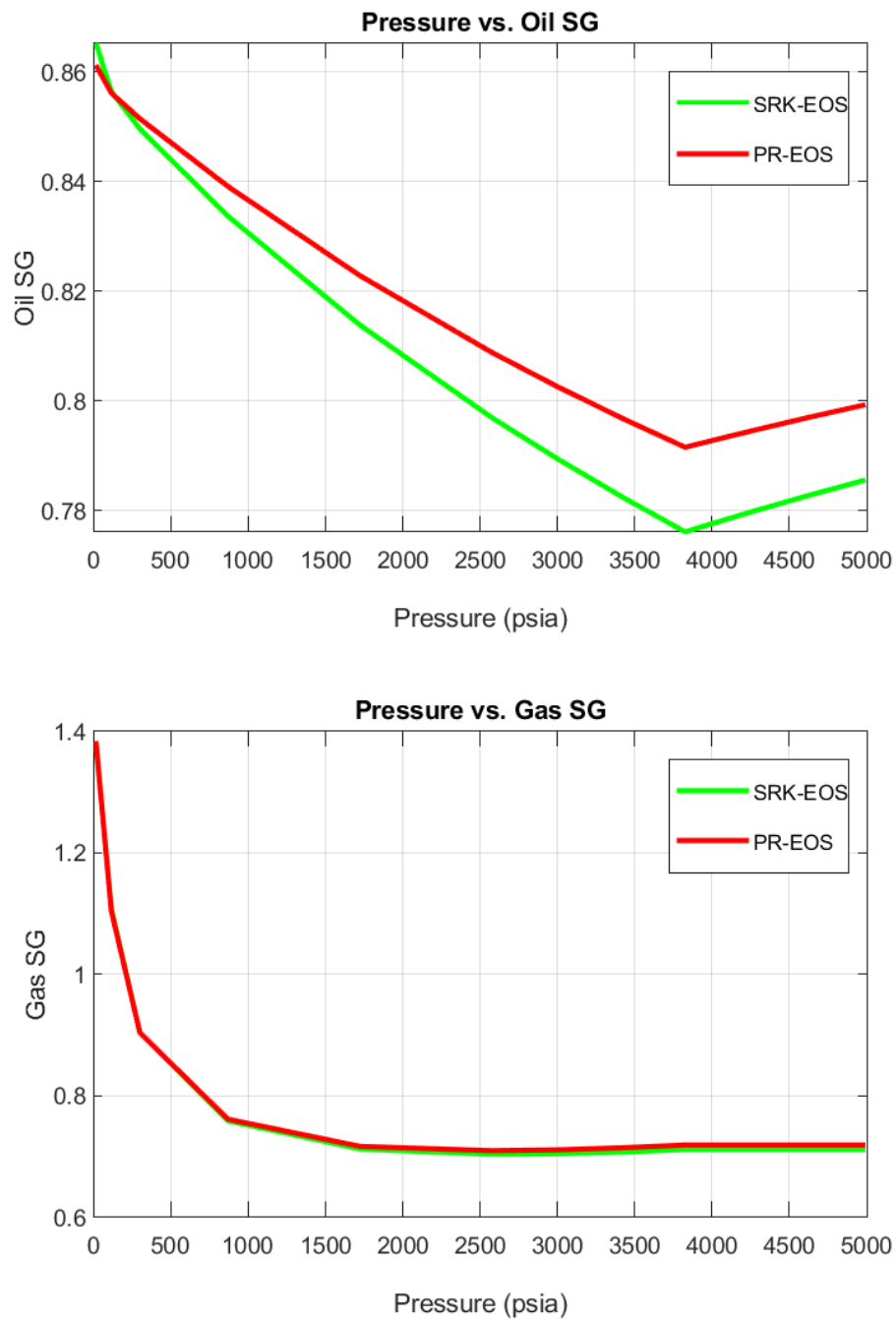


Figure A.11: Oil and gas SG plots using commercial software

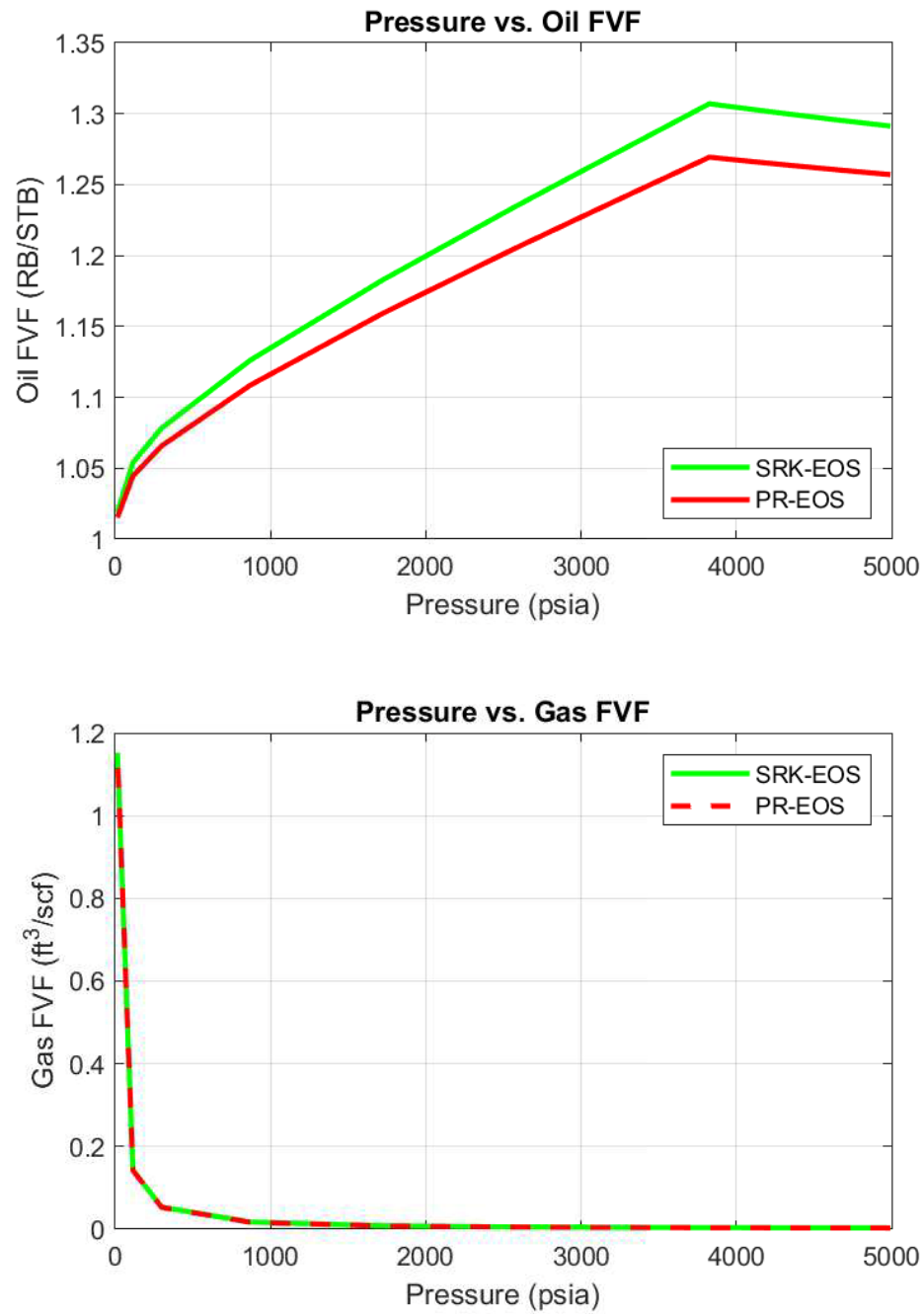


Figure A.12: Oil and gas FVF plots using commercial PVT software

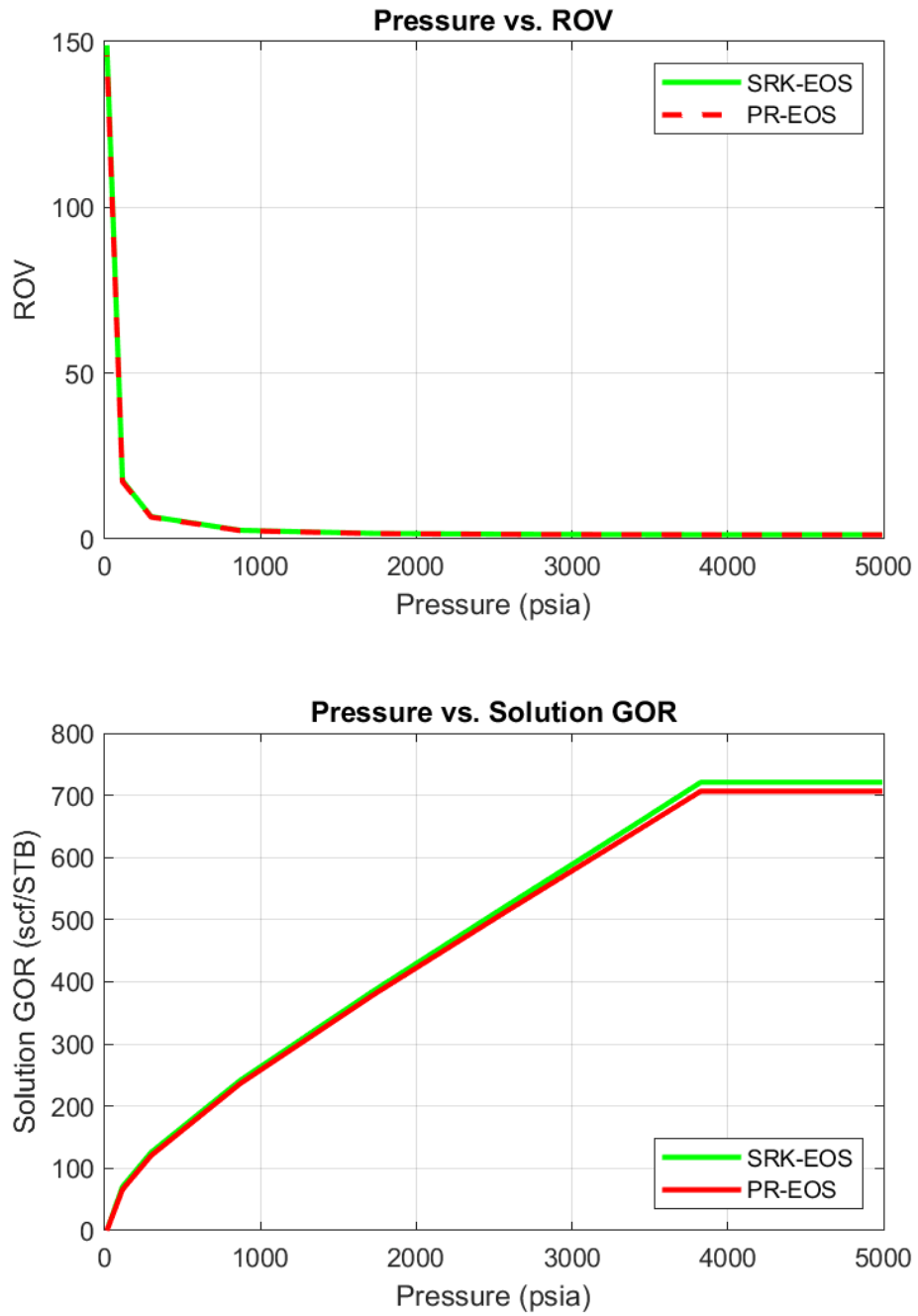


Figure A.13: ROV and solution GOR plots using commercial software

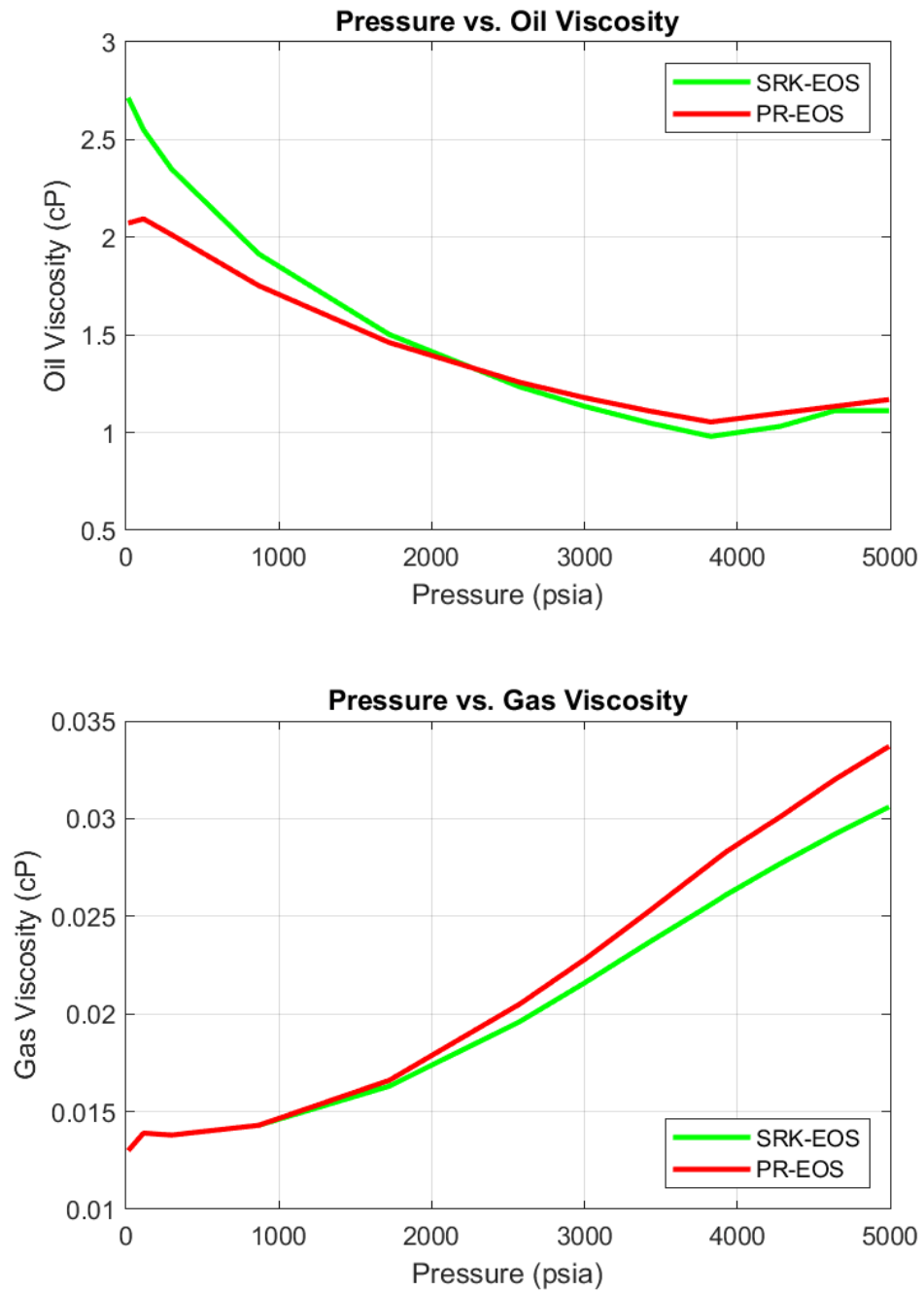


Figure A.14: Oil and gas viscosity plots using commercial software

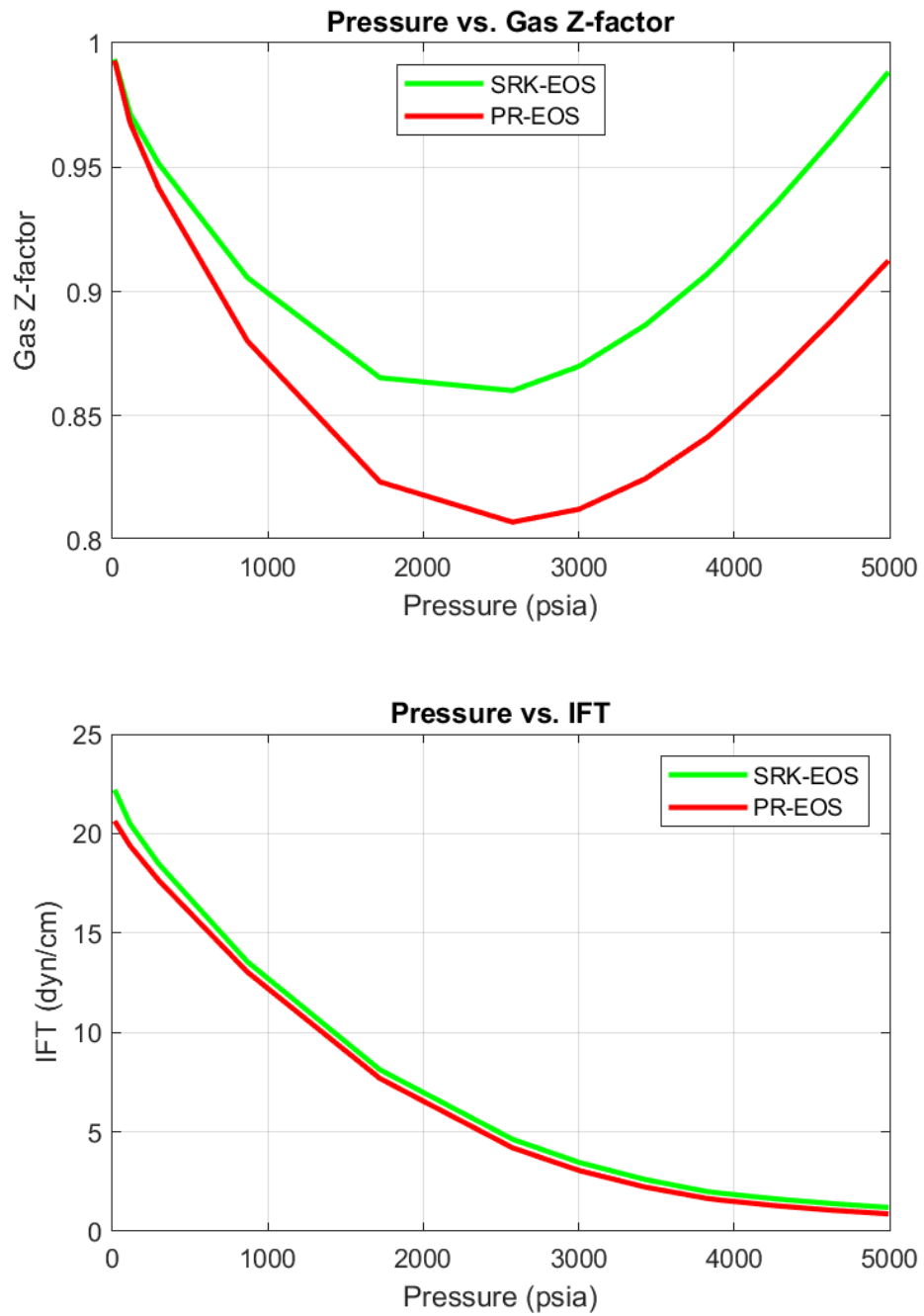


Figure A.15: Gas Z-factor and IFT plots using commercial software

Appendix A: Supplementary Tables and Figures

Table A.14: Separator test calculation results for an un-tuned SRK-EOS using commercial software

	Initial	Stage #1	Stock Tank
Press. (psia)	p_{sat}=2823.63	185.6	14.7
Temp. (°F)	134.6	71.6	60
Gas Vol. (mole)	-	238.0064	31.1489
Oil Vol. (litre)	-	77.3355	75.2909
GOR (scf/RB)	-	409.37	55.03
GOR (scf/STB)	-	420.48	55.03
Separator			
Volume Factor (RB/STB)	-	1.027	1.000
Gas Z-factor	-	0.965	0.994
Gas SG	-	0.7776	1.1288

Table A.15: Separator test calculation results for an un-tuned PR-EOS using commercial software

	Initial	Stage #1	Stock Tank
Press. (psia)	p_{sat}=2803.04	185.6	14.7
Temp. (°F)	134.6	71.6	60
Gas Vol. (mole)	-	239.3589	30.5365
Oil Vol. (litre)	-	69.1142	67.3375
GOR (scf/RB)	-	460.66	60.32
GOR (scf/STB)	-	472.82	60.32
Separator			
Volume Factor (RB/STB)	-	1.026	1.000
Gas Z-factor	-	0.958	0.993
Gas SG	-	0.7808	1.1253

Table A.16: Experimental vs. calculated single-stage separator data using commercial software
(un-tuned EOS models)

Data Type	Experimental Value	Calculated Value	
		SRK EOS	PR EOS
GOR (scf/STB)	710	475.51	533.14
FVF (RB/STB)	1.283	1.221	1.224
API (°API)	29.4	109.13	83.85

Appendix A: Supplementary Tables and Figures

Table A.17: Saturation pressure calculation results for an un-tuned SRK-EOS using commercial software

Component	Composition (mole percent)		K-values (y_i/z_i)	$\ln f_i$ (atm)
	Dominant phase (z_i)	Incipient phase (y_i)		
H ₂ S	11.245	5.7434	0.5107	1.6560
CO ₂	7.010	5.8270	0.8312	1.9731
N ₂	1.172	3.4827	2.9716	2.0962
CH ₄	38.698	82.0432	2.1201	4.9113
C ₂ H ₆	1.522	1.5720	1.0329	0.3944
C ₃ H ₈	0.687	0.4182	0.6087	-1.3530
IC ₄	0.248	0.1040	0.4192	-3.0528
NC ₄	0.479	0.1709	0.3568	-2.6638
IC ₅	0.340	0.0817	0.2404	-3.7154
NC ₅	0.319	0.0684	0.2143	-3.9829
FC ₆	1.056	0.1419	0.1344	-3.5768
FC ₇	0.900	0.0746	0.0829	-4.5616
FC ₈	2.010	0.1066	0.0530	-4.5229
FC ₉	2.585	0.0843	0.0326	-5.1109
FC ₁₀	2.088	0.0411	0.0197	-6.1864
FC ₁₁	1.768	0.0224	0.0127	-7.1194
FC ₁₂	2.058	0.0160	0.0078	-7.8040
C ₁₃₊	25.815	0.0017	0.0001	-13.9750

- Calculated saturation pressure value: $p_{\text{sat}}=2823.629$ psia.

Table A.18: Saturation pressure calculation properties for an un-tuned SRK-EOS using commercial software

	Dominant phase (z_i)	Incipient phase (y_i)
Z-factor	1.4372	0.8704
Molar Vol. (m³/mol)	0.20266	0.12273
MW (g/mol)	111.67	20.11
Density (lb/ft³)	34.4013	10.2314
Viscosity (cP)	0.1169	0.0205
IFT (dyn/cm)	0.0000	0.4735
Phase Vol. percent	100.0000	0.0000
Phase mole percent	100.0000	0.0000

Appendix A: Supplementary Tables and Figures

Table A.19: Saturation pressure calculation results for an un-tuned PR-EOS using commercial software

Component	Composition (mole percent)		K-values (y_i/z_i)	$\ln f_i$ (atm)
	Dominant phase (z_i)	Incipient phase (y_i)		
H ₂ S	11.245	6.3200	0.5620	1.6648
CO ₂	7.010	6.0237	0.8593	1.9229
N ₂	1.172	3.3028	2.8181	1.9896
CH ₄	38.698	81.2613	2.0999	4.8283
C ₂ H ₆	1.522	1.6184	1.0634	0.3185
C ₃ H ₈	0.687	0.4379	0.6374	-1.4416
IC ₄	0.248	0.1098	0.4425	-3.1574
NC ₄	0.479	0.1832	0.3824	-2.7579
IC ₅	0.340	0.0888	0.2610	-3.8204
NC ₅	0.319	0.0748	0.2344	-4.0843
FC ₆	1.056	0.1595	0.1510	-3.6650
FC ₇	0.900	0.0861	0.0957	-4.6408
FC ₈	2.010	0.1262	0.0628	-4.5951
FC ₉	2.585	0.1024	0.0396	-5.1763
FC ₁₀	2.088	0.0515	0.0247	-6.2393
FC ₁₁	1.768	0.0288	0.0163	-7.1634
FC ₁₂	2.058	0.0213	0.0103	-7.8302
C ₁₃₊	25.815	0.0038	0.0001	-13.5477

- Calculated saturation pressure value: $p_{\text{sat}}=2803.041$ psia.

Table A.20: Saturation pressure calculation properties for an un-tuned PR-EOS using commercial software

	Dominant phase (z_i)	Incipient phase (y_i)
Z-factor	1.2793	0.8132
Molar Vol. (m³/mol)	0.18171	0.11551
MW (g/mol)	111.67	20.37
Density (lb/ft³)	38.3661	11.0099
Viscosity (cP)	0.1856	0.0215
IFT (dyn/cm)	0.0000	0.8335
Phase Vol. percent	100.0000	0.0000
Phase mole percent	100.0000	0.0000

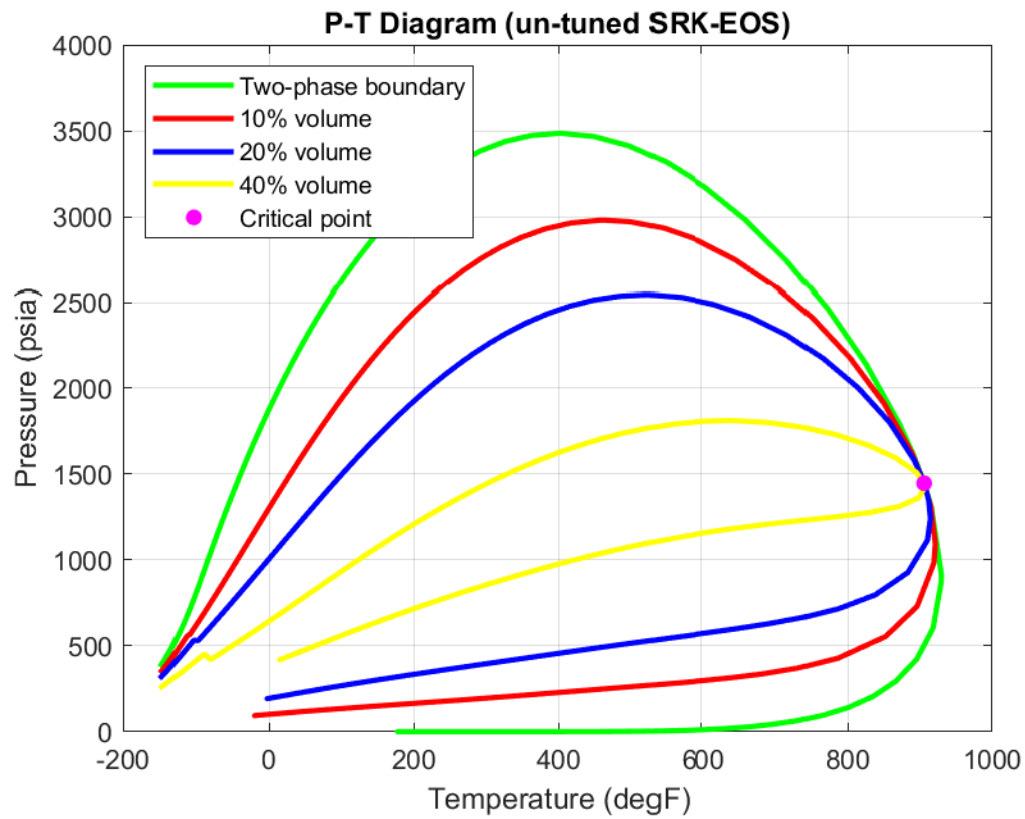


Figure A.16: Two-phase envelope of the offshore Greek reservoir fluid (un-tuned SRK-EOS)

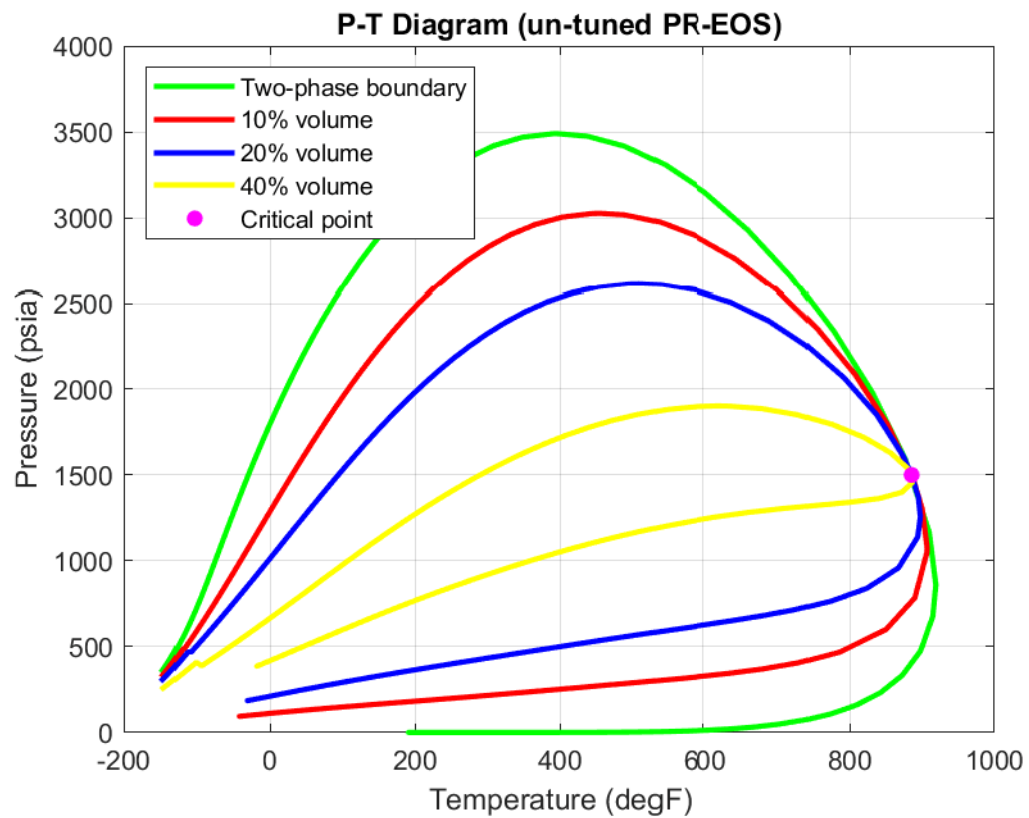


Figure A.17: Two-phase envelope of the offshore Greek reservoir fluid (un-tuned PR-EOS)

Appendix A: Supplementary Tables and Figures

Table A.21: Un-tuned EOS two-phase flash calculation results using commercial software

Component	Composition (mole percent)	$\ln f_i$ (atm)	
	Liquid phase (x_i)	SRK EOS	PR EOS
H ₂ S	11.245	1.7971	1.7946
CO ₂	7.010	2.1199	2.0580
N ₂	1.172	2.2510	2.1329
CH ₄	38.698	5.0688	4.9739
C ₂ H ₆	1.522	0.5835	0.4922
C ₃ H ₈	0.687	-1.1227	-1.2306
IC ₄	0.248	-2.7785	-2.9066
NC ₄	0.479	-2.3917	-2.5092
IC ₅	0.340	-3.4009	-3.5333
NC ₅	0.319	-3.6638	-3.7931
FC ₆	1.056	-3.2341	-3.3524
FC ₇	0.900	-4.1881	-4.3005
FC ₈	2.010	-4.1153	-4.2238
FC ₉	2.585	-4.6583	-4.7642
FC ₁₀	2.088	-5.6885	-5.7860
FC ₁₁	1.768	-6.5705	-6.6636
FC ₁₂	2.058	-7.2044	-7.2842
C ₁₃₊	25.815	-12.6173	-12.3065

Table A.22: Un-tuned EOS two-phase flash calculation properties using commercial software

	Liquid phase (x_i)	
	SRK EOS	PR EOS
Z-factor	1.9256	1.7276
Molar Vol. (m³/mol)	0.20037	0.17977
MW (g/mol)	111.67	111.67
Density (lb/ft³)	34.7930	38.7808
Viscosity (cP)	0.1217	0.1963
Phase Vol. percent	100.0000	100.0000
Phase mole percent	100.0000	100.0000

Appendix A: Supplementary Tables and Figures

Table A.23: CO₂, N₂, C₂H₆ compositional gradient results for the tuned SRK and PR EOS models with volume shift using commercial software

Depth (ft)	CO ₂ (mole fraction)		N ₂ (mole fraction)		C ₂ H ₆ (mole fraction)	
	SRK EOS	PR EOS	SRK EOS	PR EOS	SRK EOS	PR EOS
7800	0.0575	0.0578	0.0340	0.0320	0.0168	0.0173
7890	0.0577	0.0580	0.0340	0.0320	0.0168	0.0174
7980	0.0578	0.0582	0.0340	0.0320	0.0169	0.0174
8070	0.0580	0.0584	0.0339	0.0319	0.0169	0.0174
8133	0.0582	0.0585	0.0339	0.0319	0.0169	0.0175
8134	0.0701	0.0701	0.0117	0.0117	0.0152	0.0152
8160	0.0701	0.0701	0.0117	0.0117	0.0152	0.0152
8250	0.0702	0.0701	0.0116	0.0117	0.0151	0.0151
8340	0.0702	0.0702	0.0116	0.0116	0.0150	0.0150
8430	0.0702	0.0702	0.0115	0.0116	0.0149	0.0150
8520	0.0703	0.0702	0.0115	0.0115	0.0149	0.0149
8610	0.0703	0.0702	0.0114	0.0115	0.0148	0.0148
8700	0.0703	0.0703	0.0114	0.0114	0.0147	0.0147

Table A.24: C₃H₈, IC₄, NC₄ compositional gradient results for the tuned SRK and PR EOS models with volume shift using commercial software

Depth (ft)	C ₃ H ₈ (mole fraction)		IC ₄ (mole fraction)		NC ₄ (mole fraction)	
	SRK EOS	PR EOS	SRK EOS	PR EOS	SRK EOS	PR EOS
7800	0.0048	0.0051	0.0013	0.0014	0.0021	0.0023
7890	0.0049	0.0051	0.0013	0.0014	0.0022	0.0023
7980	0.0049	0.0051	0.0013	0.0014	0.0022	0.0023
8070	0.0049	0.0051	0.0013	0.0014	0.0022	0.0023
8133	0.0049	0.0051	0.0013	0.0014	0.0022	0.0023
8134	0.0069	0.0069	0.0025	0.0025	0.0048	0.0048
8160	0.0069	0.0069	0.0025	0.0025	0.0048	0.0048
8250	0.0068	0.0068	0.0025	0.0025	0.0048	0.0048
8340	0.0068	0.0068	0.0024	0.0025	0.0047	0.0047
8430	0.0068	0.0068	0.0024	0.0024	0.0047	0.0047
8520	0.0067	0.0067	0.0024	0.0024	0.0047	0.0047
8610	0.0067	0.0067	0.0024	0.0024	0.0047	0.0047
8700	0.0066	0.0067	0.0024	0.0024	0.0046	0.0047

Appendix A: Supplementary Tables and Figures

Table A.25: IC₅, NC₅, FC₆ compositional gradient results for the tuned SRK and PR EOS models with volume shift using commercial software

Depth (ft)	IC ₅ (mole fraction)		NC ₅ (mole fraction)		FC ₆ (mole fraction)	
	SRK EOS	PR EOS	SRK EOS	PR EOS	SRK EOS	PR EOS
7800	0.0011	0.0012	0.0009	0.0010	0.0020	0.0023
7890	0.0011	0.0012	0.0009	0.0010	0.0020	0.0023
7980	0.0011	0.0012	0.0010	0.0010	0.0021	0.0023
8070	0.0011	0.0012	0.0010	0.0010	0.0021	0.0023
8133	0.0011	0.0012	0.0010	0.0010	0.0021	0.0024
8134	0.0034	0.0034	0.0032	0.0032	0.0106	0.0106
8160	0.0034	0.0034	0.0032	0.0032	0.0105	0.0105
8250	0.0034	0.0034	0.0032	0.0032	0.0105	0.0105
8340	0.0034	0.0034	0.0032	0.0032	0.0105	0.0105
8430	0.0033	0.0033	0.0031	0.0031	0.0104	0.0104
8520	0.0033	0.0033	0.0031	0.0031	0.0104	0.0104
8610	0.0033	0.0033	0.0031	0.0031	0.0103	0.0103
8700	0.0033	0.0033	0.0031	0.0031	0.0103	0.0103

Table A.26: FC₇, FC₈, FC₉ compositional gradient results for the tuned SRK and PR EOS models with volume shift using commercial software

Depth (ft)	FC ₇ (mole fraction)		FC ₈ (mole fraction)		FC ₉ (mole fraction)	
	SRK EOS	PR EOS	SRK EOS	PR EOS	SRK EOS	PR EOS
7800	0.0011	0.0013	0.0017	0.0020	0.0015	0.0017
7890	0.0011	0.0013	0.0017	0.0020	0.0015	0.0018
7980	0.0012	0.0013	0.0018	0.0021	0.0015	0.0018
8070	0.0012	0.0013	0.0018	0.0021	0.0016	0.0018
8133	0.0012	0.0014	0.0018	0.0021	0.0016	0.0019
8134	0.0090	0.0090	0.0201	0.0201	0.0258	0.0258
8160	0.0090	0.0090	0.0201	0.0201	0.0258	0.0258
8250	0.0090	0.0090	0.0200	0.0200	0.0258	0.0258
8340	0.0089	0.0089	0.0200	0.0200	0.0257	0.0257
8430	0.0089	0.0089	0.0199	0.0199	0.0256	0.0256
8520	0.0089	0.0089	0.0198	0.0199	0.0255	0.0256
8610	0.0088	0.0088	0.0198	0.0198	0.0255	0.0255
8700	0.0088	0.0088	0.0197	0.0197	0.0254	0.0254

Appendix A: Supplementary Tables and Figures

Table A.27: FC₁₀, FC₁₁, FC₁₂ compositional gradient results for the tuned SRK and PR EOS models with volume shift using commercial software

Depth (ft)	FC ₁₀ (mole fraction)		FC ₁₁ (mole fraction)		FC ₁₂ (mole fraction)	
	SRK EOS	PR EOS	SRK EOS	PR EOS	SRK EOS	PR EOS
7800	0.0008	0.0009	0.0005	0.0006	0.0004	0.0005
7890	0.0008	0.0010	0.0005	0.0006	0.0004	0.0005
7980	0.0008	0.0010	0.0005	0.0006	0.0004	0.0005
8070	0.0008	0.0010	0.0005	0.0006	0.0004	0.0005
8133	0.0008	0.0010	0.0005	0.0006	0.0004	0.0005
8134	0.0209	0.0209	0.0177	0.0177	0.0206	0.0206
8160	0.0209	0.0209	0.0177	0.0177	0.0206	0.0206
8250	0.0208	0.0208	0.0176	0.0176	0.0205	0.0205
8340	0.0208	0.0208	0.0176	0.0176	0.0205	0.0205
8430	0.0207	0.0207	0.0176	0.0176	0.0205	0.0205
8520	0.0207	0.0207	0.0175	0.0175	0.0204	0.0204
8610	0.0206	0.0206	0.0175	0.0175	0.0204	0.0204
8700	0.0206	0.0206	0.0174	0.0174	0.0203	0.0203

Table A.28: Reservoir pressure, saturation pressure and reservoir fluid density gradient results for the un-tuned SRK and PR EOS models with volume shift using commercial software

Depth (ft)	Reservoir Pressure (psia)		Saturation Pressure (psia)		Reservoir Fluid Density (lb/ft ³)	
	SRK EOS	PR EOS	SRK EOS	PR EOS	SRK EOS	PR EOS
7800	3730.43	3723.17	2872.52	2858.46	41.183	44.288
7890	3756.18	3750.86	2859.13	2843.26	41.219	44.337
7980	3781.95	3778.59	2845.91	2828.26	41.254	44.386
8070	3807.74	3806.34	2832.83	2813.45	41.289	44.435
8134	3826.10	3826.10	2823.63	2803.04	41.314	44.468
8160	3833.56	3834.13	2819.91	2798.84	41.324	44.482
8250	3859.40	3861.95	2807.14	2784.40	41.359	44.529
8340	3885.26	3889.79	2794.51	2770.15	41.393	44.576
8430	3911.14	3917.67	2782.02	2756.08	41.426	44.622
8520	3937.04	3945.57	2769.67	2742.17	41.460	44.667
8610	3962.96	3973.50	2757.46	2728.43	41.493	44.712
8700	3988.91	4001.46	2745.38	2714.86	41.525	44.756

Appendix A: Supplementary Tables and Figures

Table A.29: H₂S, CO₂, N₂ compositional gradient results for the un-tuned SRK and PR EOS models with volume shift using commercial software

Depth (ft)	H ₂ S (mole fraction)		CO ₂ (mole fraction)		N ₂ (mole fraction)	
	SRK EOS	PR EOS	SRK EOS	PR EOS	SRK EOS	PR EOS
7800	0.1124	0.1125	0.0699	0.0699	0.0118	0.0118
7890	0.1124	0.1125	0.0699	0.0700	0.0118	0.0118
7980	0.1124	0.1125	0.0700	0.0700	0.0118	0.0118
8070	0.1124	0.1125	0.0701	0.0701	0.0117	0.0117
8134	0.1124	0.1124	0.0701	0.0701	0.0117	0.0117
8160	0.1125	0.1124	0.0701	0.0701	0.0117	0.0117
8250	0.1125	0.1124	0.0702	0.0702	0.0117	0.0117
8340	0.1125	0.1124	0.0702	0.0702	0.0117	0.0117
8430	0.1125	0.1124	0.0703	0.0703	0.0117	0.0116
8520	0.1125	0.1123	0.0704	0.0703	0.0116	0.0116
8610	0.1125	0.1123	0.0704	0.0704	0.0116	0.0116
8700	0.1125	0.1123	0.0705	0.0704	0.0116	0.0116

Table A.30: CH₄, C₂H₆, C₃H₈ compositional gradient results for the un-tuned SRK and PR EOS models with volume shift using commercial software

Depth (ft)	CH ₄ (mole fraction)		C ₂ H ₆ (mole fraction)		C ₃ H ₈ (mole fraction)	
	SRK EOS	PR EOS	SRK EOS	PR EOS	SRK EOS	PR EOS
7800	0.3919	0.3912	0.0153	0.0154	0.0069	0.0069
7890	0.3905	0.3901	0.0153	0.0153	0.0069	0.0069
7980	0.3892	0.3889	0.0153	0.0153	0.0069	0.0069
8070	0.3879	0.3878	0.0152	0.0152	0.0069	0.0069
8134	0.3870	0.3870	0.0152	0.0152	0.0069	0.0069
8160	0.3866	0.3867	0.0152	0.0152	0.0069	0.0069
8250	0.3853	0.3855	0.0152	0.0152	0.0069	0.0069
8340	0.3840	0.3844	0.0151	0.0151	0.0068	0.0068
8430	0.3828	0.3833	0.0151	0.0151	0.0068	0.0068
8520	0.3815	0.3822	0.0151	0.0150	0.0068	0.0068
8610	0.3802	0.3811	0.0151	0.0150	0.0068	0.0068
8700	0.3790	0.3800	0.0150	0.0150	0.0068	0.0068

Appendix A: Supplementary Tables and Figures

Table A.31: IC₄, NC₄, IC₅ compositional gradient results for the un-tuned SRK and PR EOS models with volume shift using commercial software

Depth (ft)	IC ₄ (mole fraction)		NC ₄ (mole fraction)		IC ₅ (mole fraction)	
	SRK EOS	PR EOS	SRK EOS	PR EOS	SRK EOS	PR EOS
7800	0.0025	0.0025	0.0048	0.0048	0.0034	0.0034
7890	0.0025	0.0025	0.0048	0.0048	0.0034	0.0034
7980	0.0025	0.0025	0.0048	0.0048	0.0034	0.0034
8070	0.0025	0.0025	0.0048	0.0048	0.0034	0.0034
8134	0.0025	0.0025	0.0048	0.0048	0.0034	0.0034
8160	0.0025	0.0025	0.0048	0.0048	0.0034	0.0034
8250	0.0025	0.0025	0.0048	0.0048	0.0034	0.0034
8340	0.0025	0.0025	0.0048	0.0048	0.0034	0.0034
8430	0.0025	0.0025	0.0048	0.0048	0.0034	0.0034
8520	0.0025	0.0025	0.0048	0.0048	0.0034	0.0034
8610	0.0025	0.0025	0.0048	0.0047	0.0034	0.0034
8700	0.0025	0.0024	0.0048	0.0047	0.0034	0.0034

Table A.32: NC₅, FC₆, FC₇ compositional gradient results for the un-tuned SRK and PR EOS models with volume shift using commercial software

Depth (ft)	NC ₅ (mole fraction)		FC ₆ (mole fraction)		FC ₇ (mole fraction)	
	SRK EOS	PR EOS	SRK EOS	PR EOS	SRK EOS	PR EOS
7800	0.0032	0.0032	0.0106	0.0106	0.0090	0.0090
7890	0.0032	0.0032	0.0106	0.0106	0.0090	0.0090
7980	0.0032	0.0032	0.0106	0.0106	0.0090	0.0090
8070	0.0032	0.0032	0.0106	0.0106	0.0090	0.0090
8134	0.0032	0.0032	0.0106	0.0106	0.0090	0.0090
8160	0.0032	0.0032	0.0106	0.0106	0.0090	0.0090
8250	0.0032	0.0032	0.0106	0.0106	0.0090	0.0090
8340	0.0032	0.0032	0.0106	0.0105	0.0090	0.0090
8430	0.0032	0.0032	0.0106	0.0105	0.0090	0.0090
8520	0.0032	0.0032	0.0106	0.0105	0.0090	0.0090
8610	0.0032	0.0032	0.0106	0.0105	0.0090	0.0090
8700	0.0032	0.0032	0.0106	0.0105	0.0090	0.0090

Appendix A: Supplementary Tables and Figures

Table A.33: FC8, FC9, FC10 compositional gradient results for the un-tuned SRK and PR EOS models with volume shift using commercial software

Depth (ft)	FC8 (mole fraction)		FC9 (mole fraction)		FC10 (mole fraction)	
	SRK EOS	PR EOS	SRK EOS	PR EOS	SRK EOS	PR EOS
7800	0.0200	0.0201	0.0257	0.0258	0.0207	0.0208
7890	0.0200	0.0201	0.0257	0.0258	0.0207	0.0208
7980	0.0201	0.0201	0.0258	0.0258	0.0208	0.0208
8070	0.0201	0.0201	0.0258	0.0258	0.0208	0.0209
8134	0.0201	0.0201	0.0258	0.0258	0.0209	0.0209
8160	0.0201	0.0201	0.0259	0.0259	0.0209	0.0209
8250	0.0201	0.0201	0.0259	0.0259	0.0209	0.0209
8340	0.0202	0.0201	0.0260	0.0259	0.0210	0.0209
8430	0.0202	0.0201	0.0260	0.0259	0.0210	0.0210
8520	0.0202	0.0201	0.0260	0.0259	0.0211	0.0210
8610	0.0202	0.0201	0.0261	0.0260	0.0211	0.0210
8700	0.0203	0.0201	0.0261	0.0260	0.0212	0.0211

Table A.34: FC11, FC12, C13+ compositional gradient results for the un-tuned SRK and PR EOS models with volume shift using commercial software

Depth (ft)	FC11 (mole fraction)		FC12 (mole fraction)		C13+ (mole fraction)	
	SRK EOS	PR EOS	SRK EOS	PR EOS	SRK EOS	PR EOS
7800	0.0175	0.0176	0.0203	0.0204	0.2548	0.2535
7890	0.0175	0.0176	0.0204	0.0204	0.2557	0.2547
7980	0.0176	0.0176	0.0205	0.0205	0.2566	0.2560
8070	0.0176	0.0177	0.0205	0.0205	0.2575	0.2573
8134	0.0177	0.0177	0.0206	0.0206	0.2581	0.2581
8160	0.0177	0.0177	0.0206	0.0206	0.2584	0.2585
8250	0.0177	0.0177	0.0207	0.0206	0.2593	0.2597
8340	0.0178	0.0178	0.0207	0.0207	0.2602	0.2610
8430	0.0178	0.0178	0.0208	0.0207	0.2611	0.2622
8520	0.0179	0.0178	0.0209	0.0208	0.2619	0.2634
8610	0.0179	0.0178	0.0209	0.0208	0.2628	0.2646
8700	0.0180	0.0179	0.0210	0.0209	0.2636	0.2658

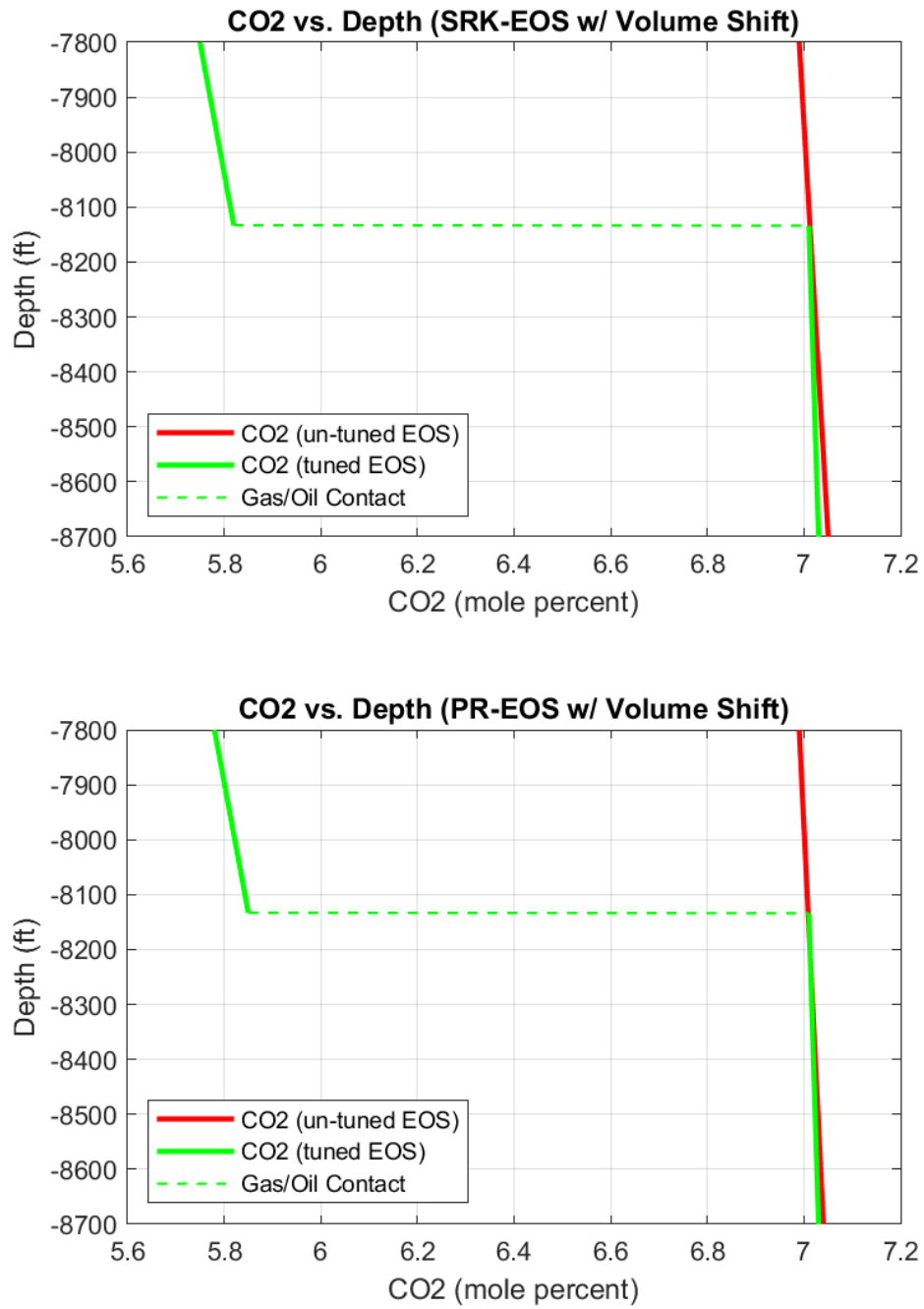


Figure A.18: CO₂ composition plots with volume shift using commercial software

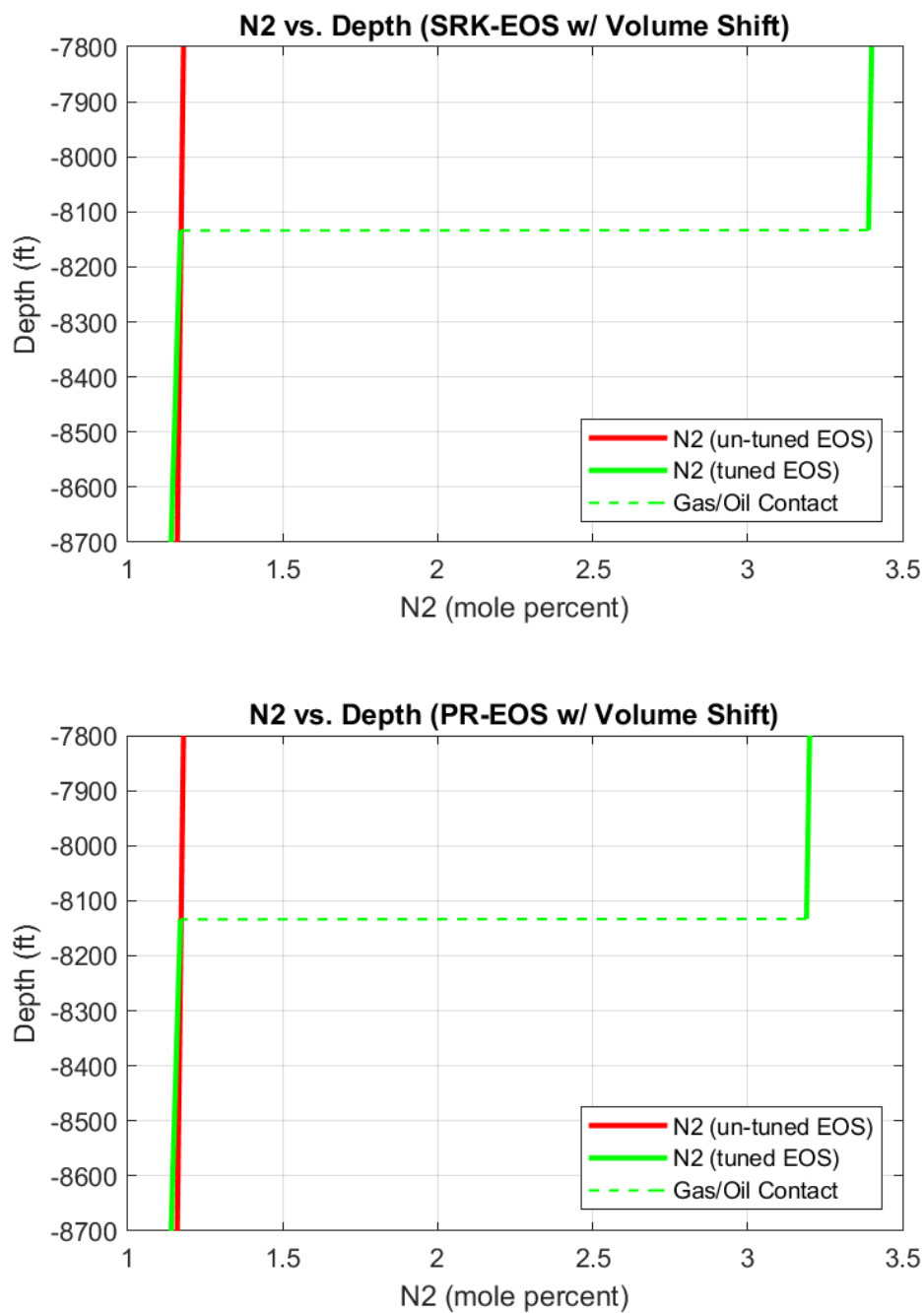


Figure A.19: N₂ composition plots with volume shift using commercial software

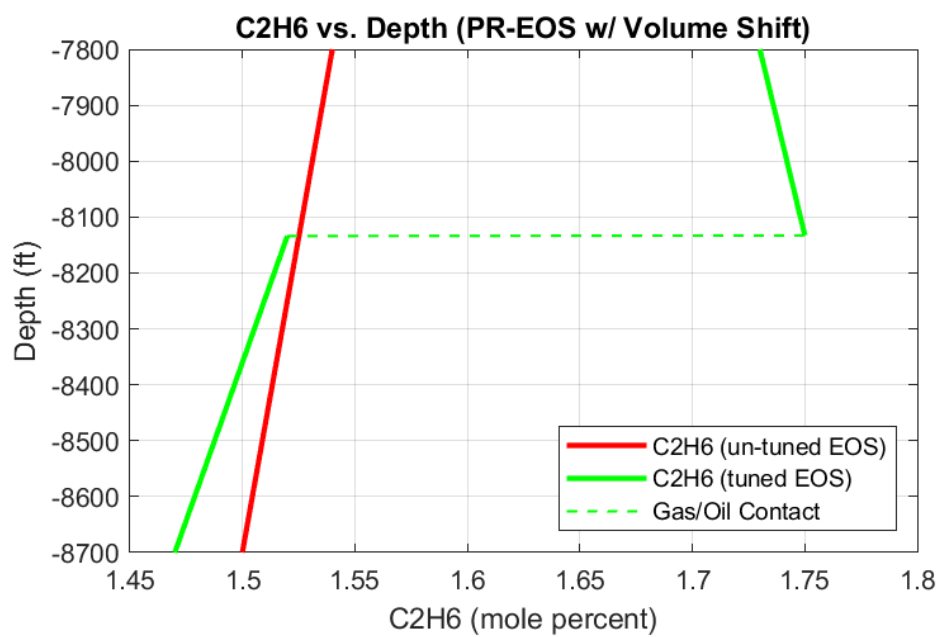
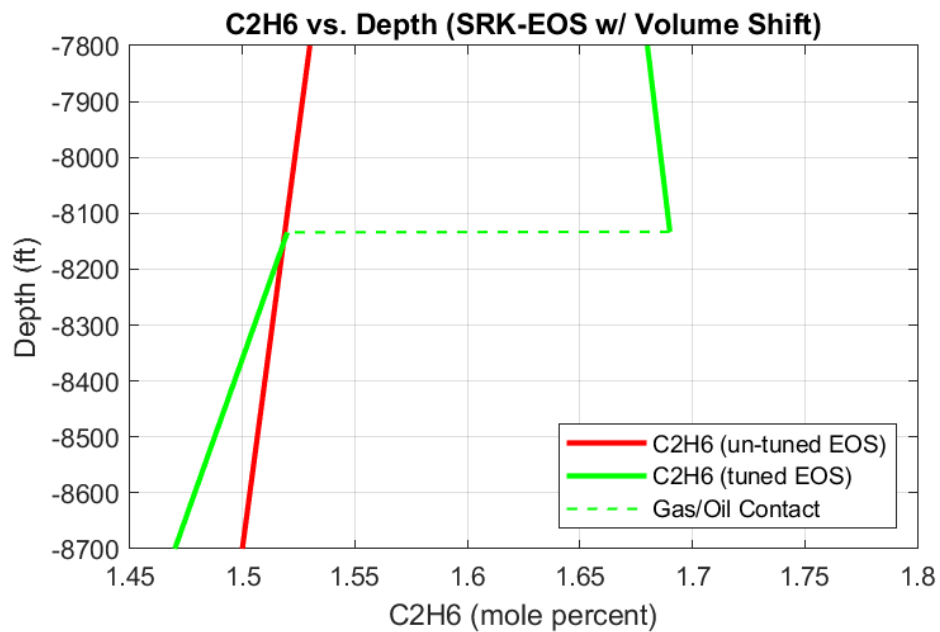


Figure A.20: C₂H₆ composition plots with volume shift using commercial software

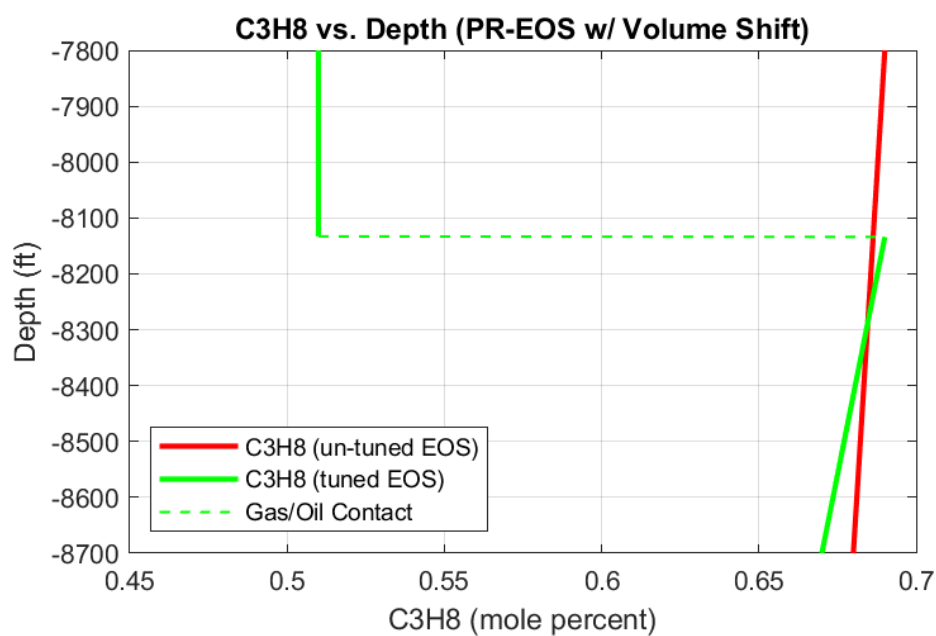
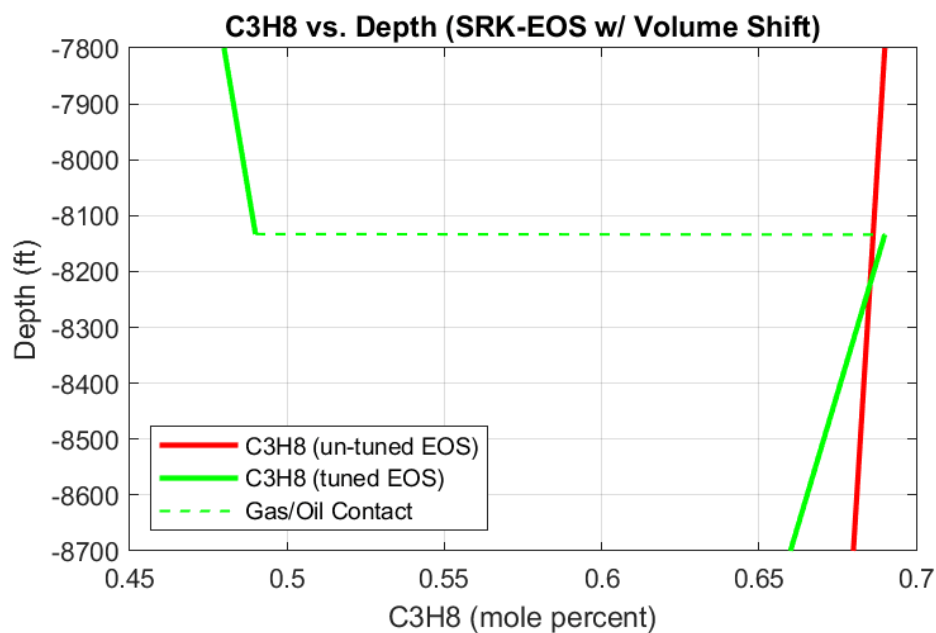


Figure A.21: C₃H₈ composition plots with volume shift using commercial software

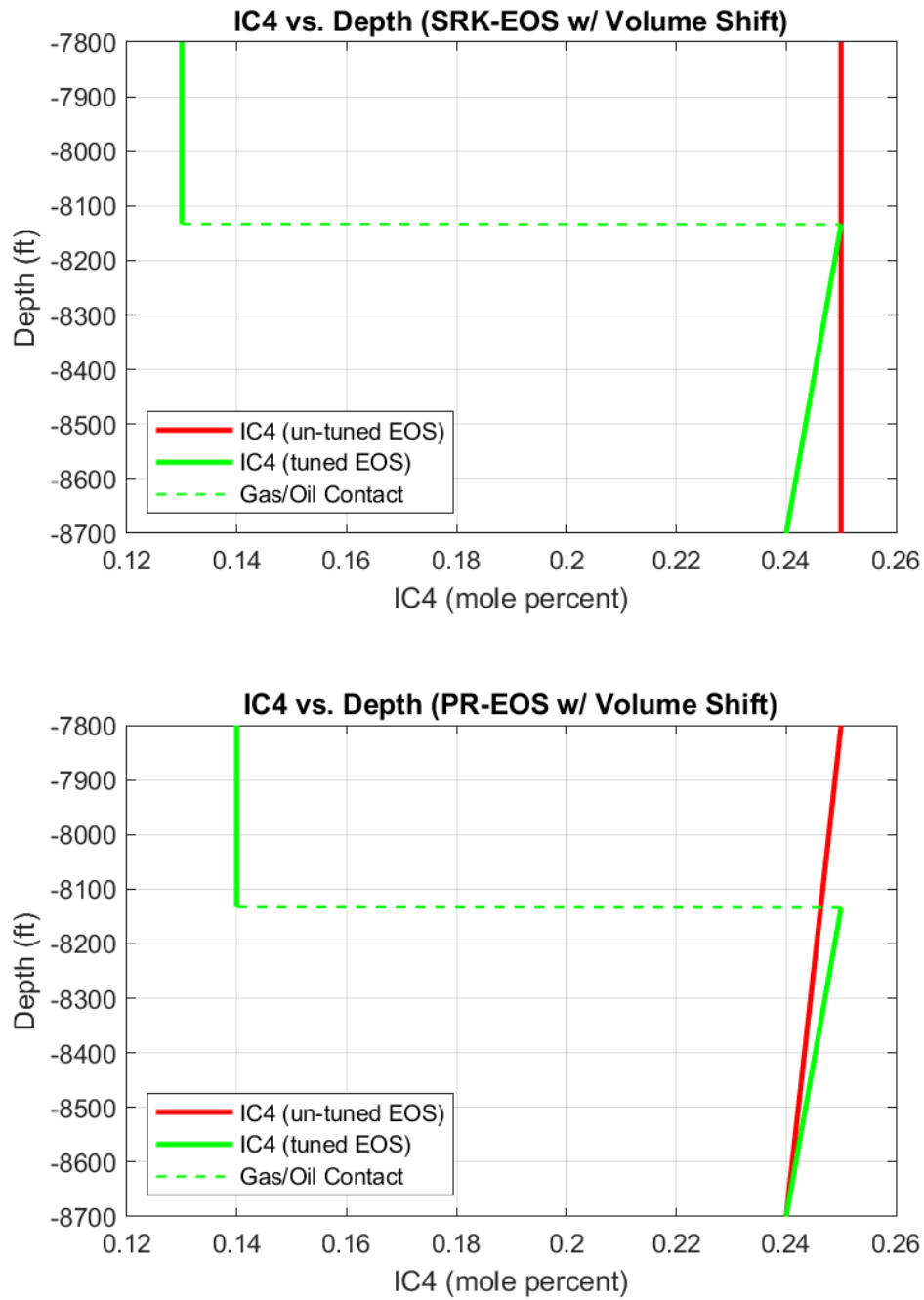


Figure A.22: IC4 composition plots with volume shift using commercial software

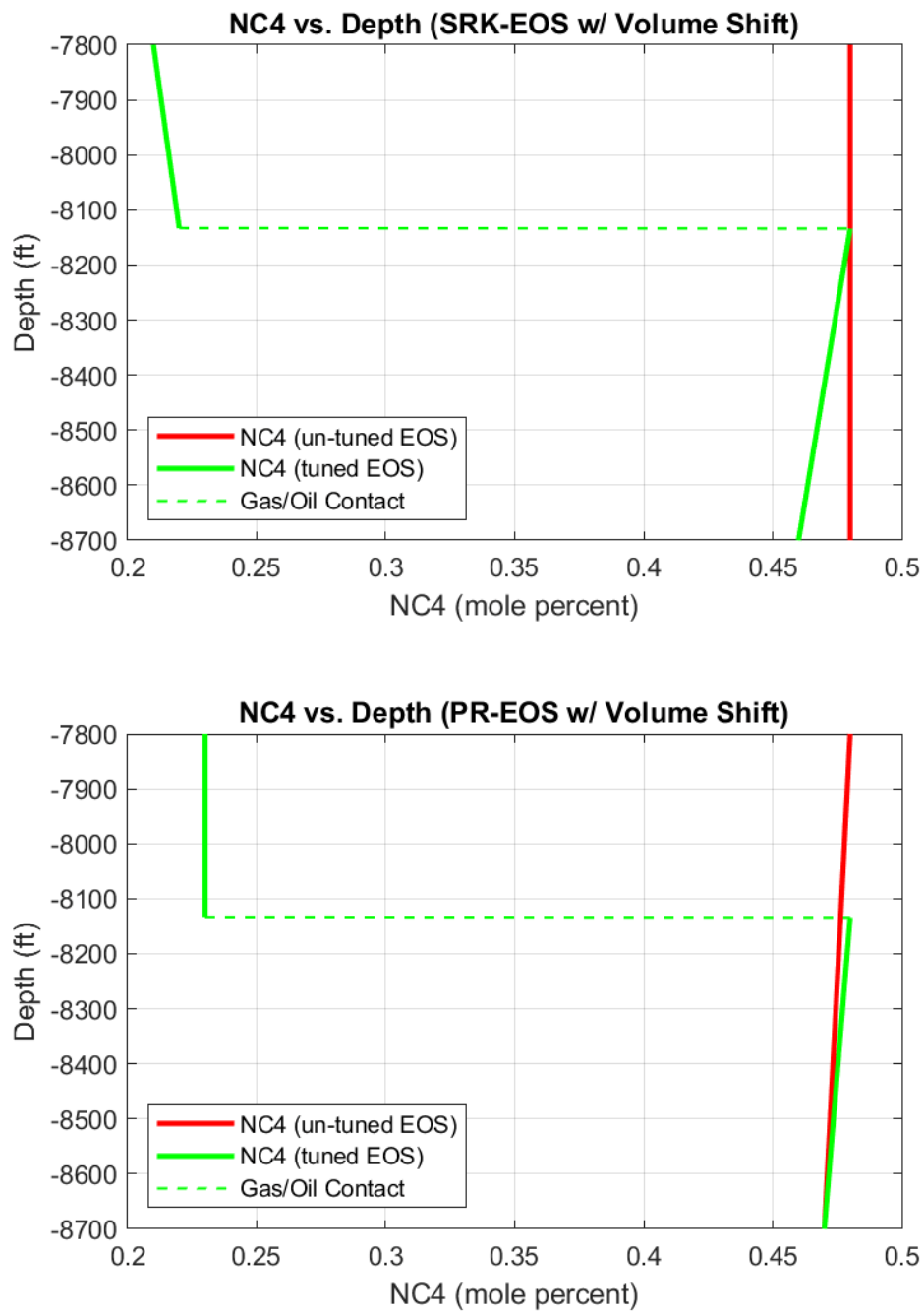


Figure A.23: NC₄ composition plots with volume shift using commercial software

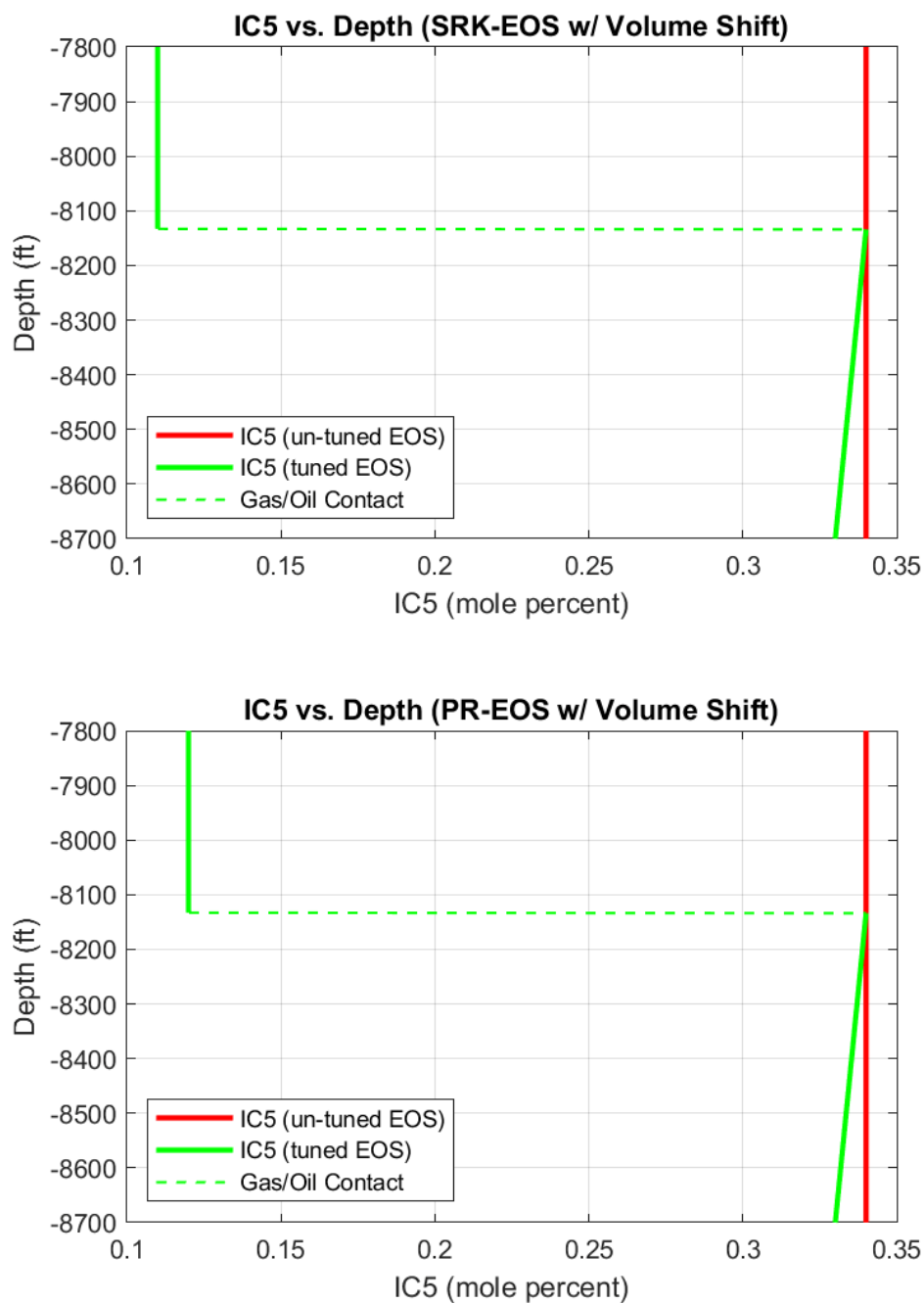


Figure A.24: IC₅ composition plots with volume shift using commercial software

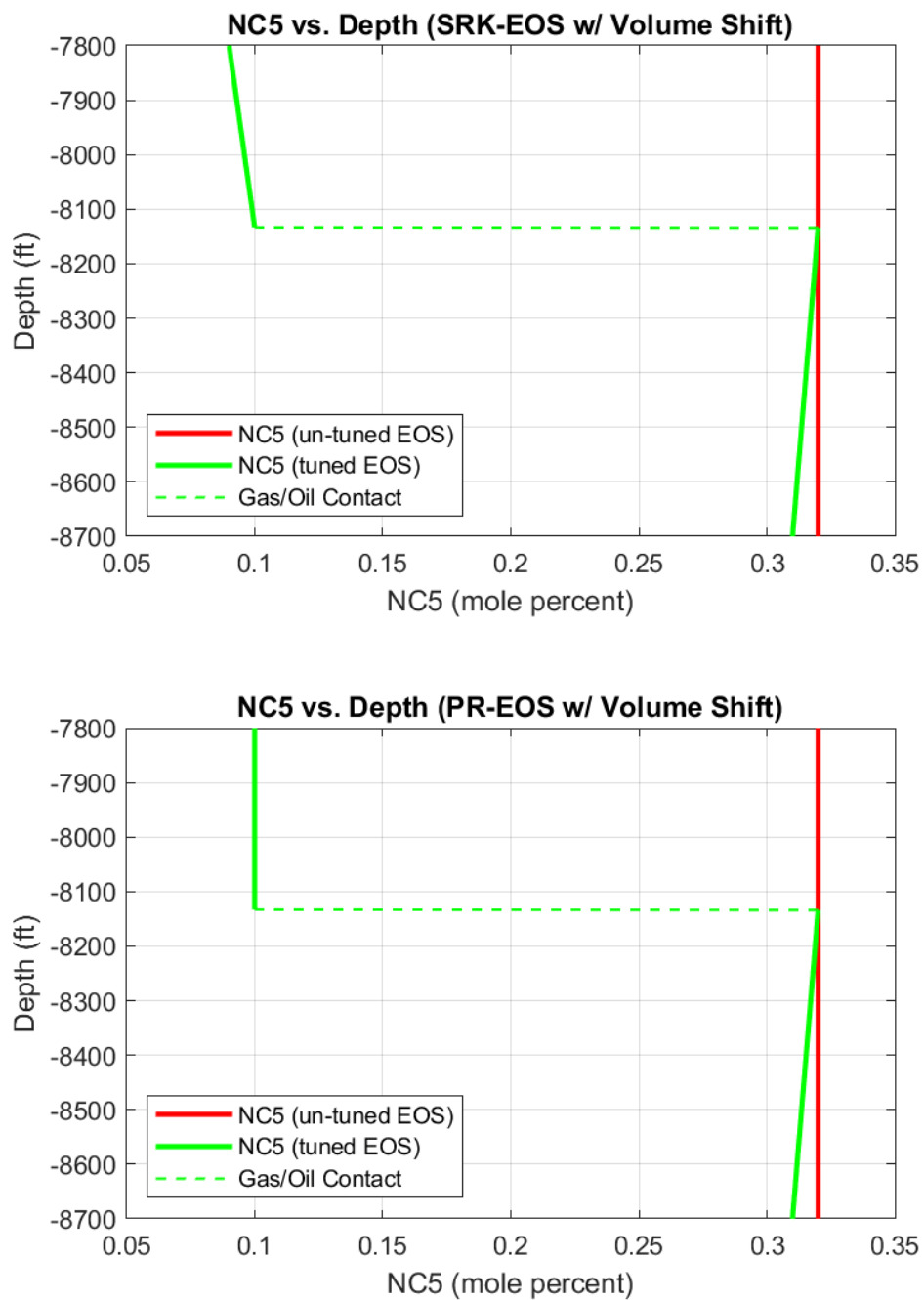


Figure A.25: NC₅ composition plots with volume shift using commercial software

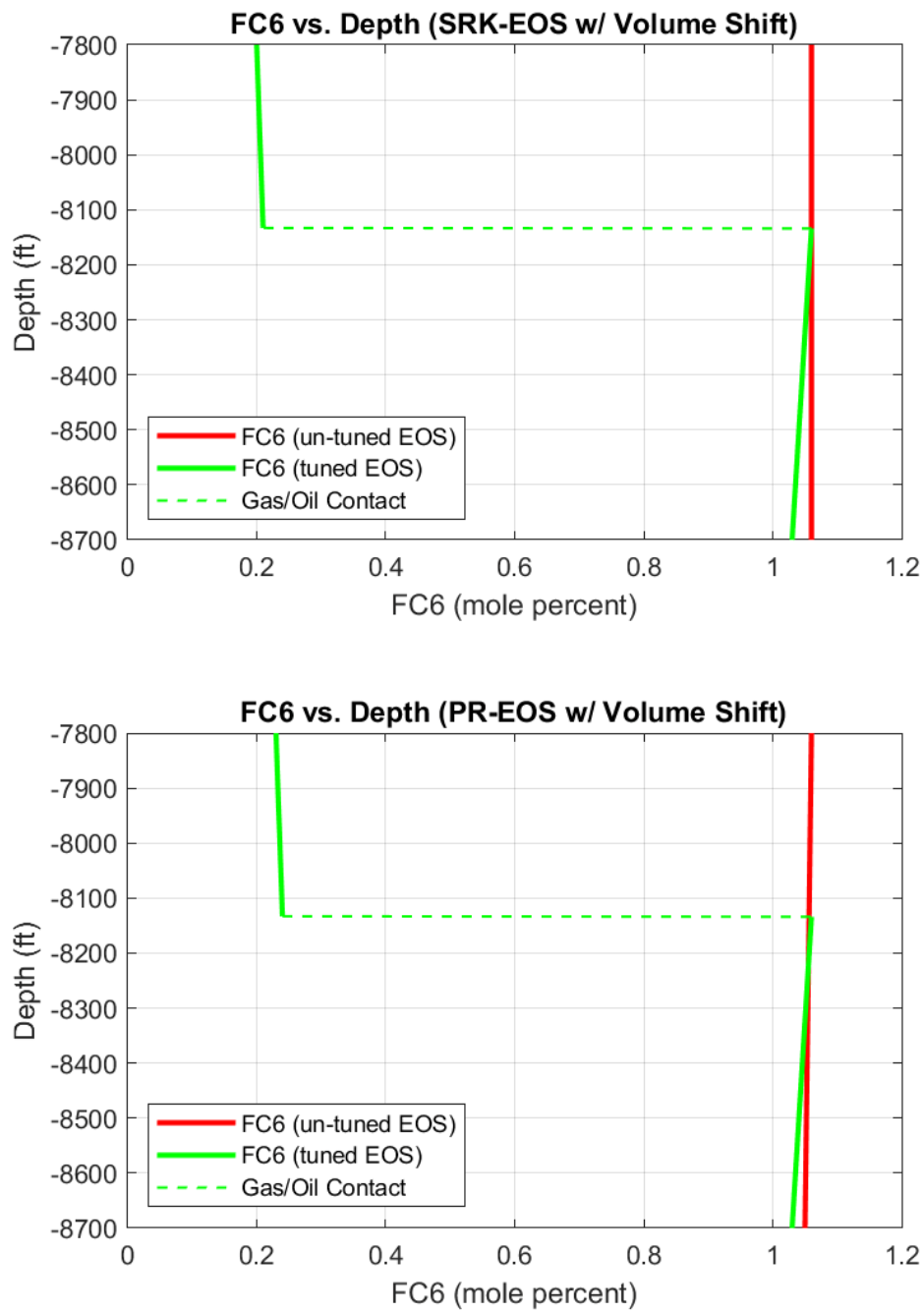


Figure A.26: FC6 composition plots with volume shift using commercial software

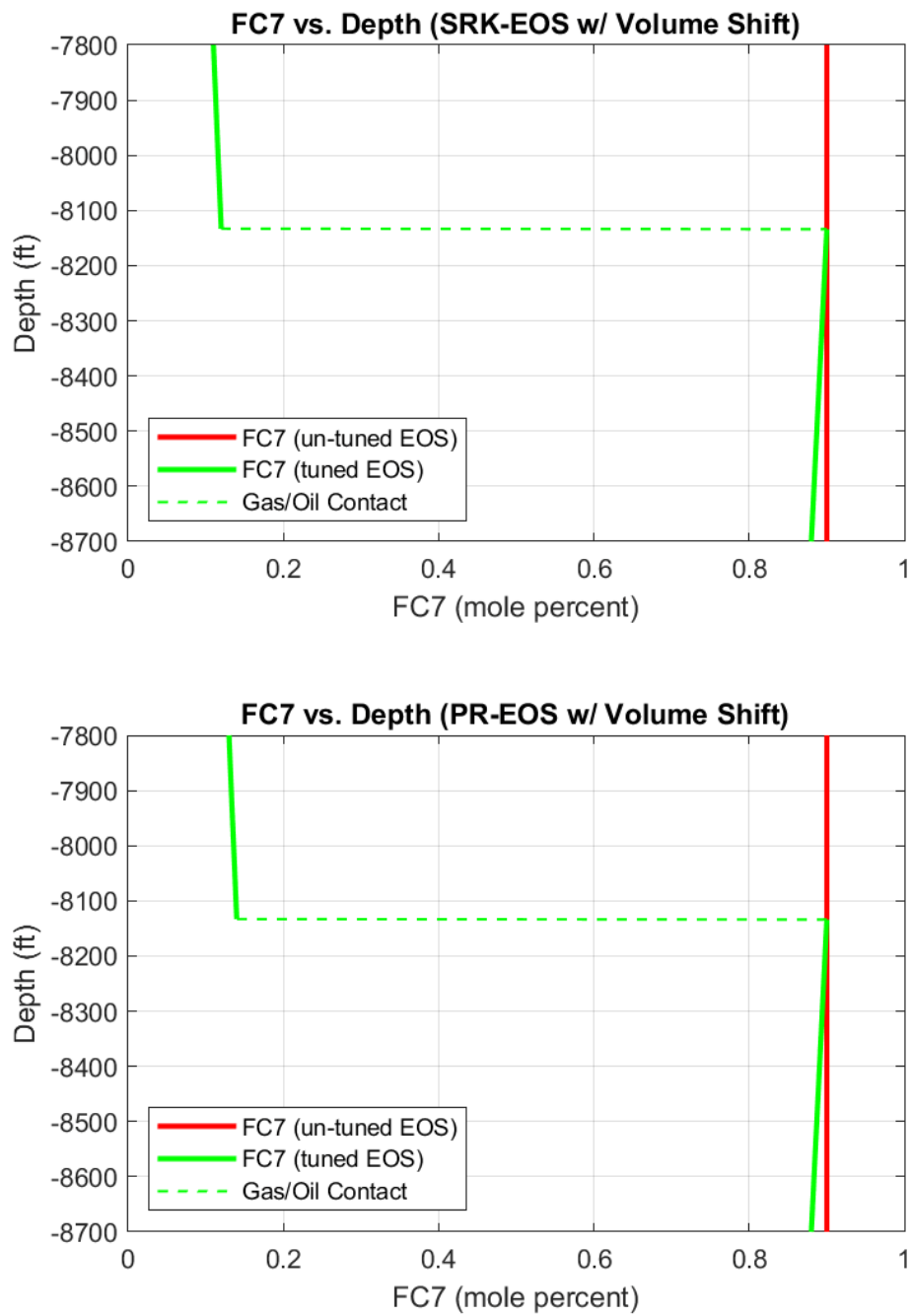


Figure A.27: FC7 composition plots with volume shift using commercial software

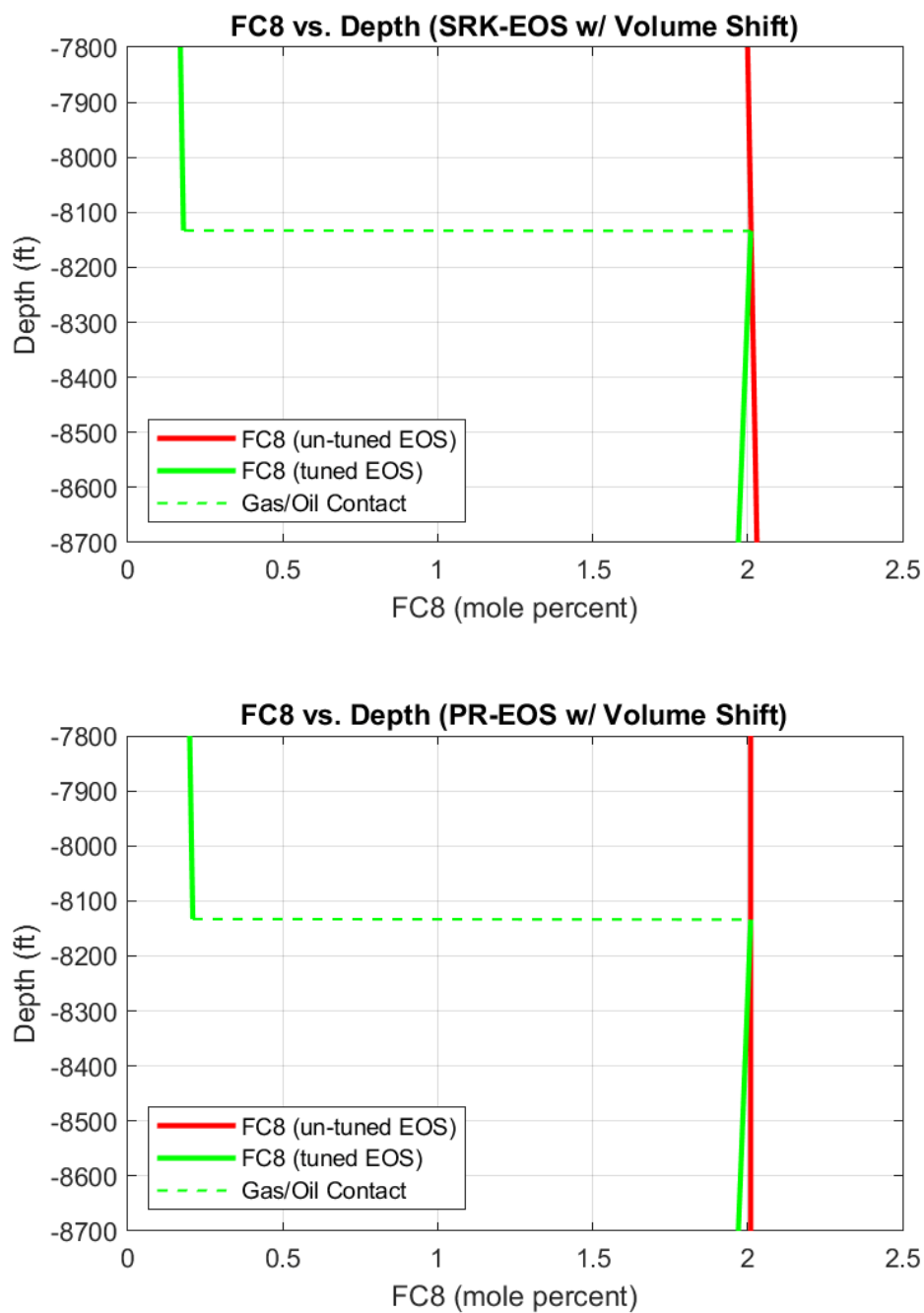


Figure A.28: FC8 composition plots with volume shift using commercial software

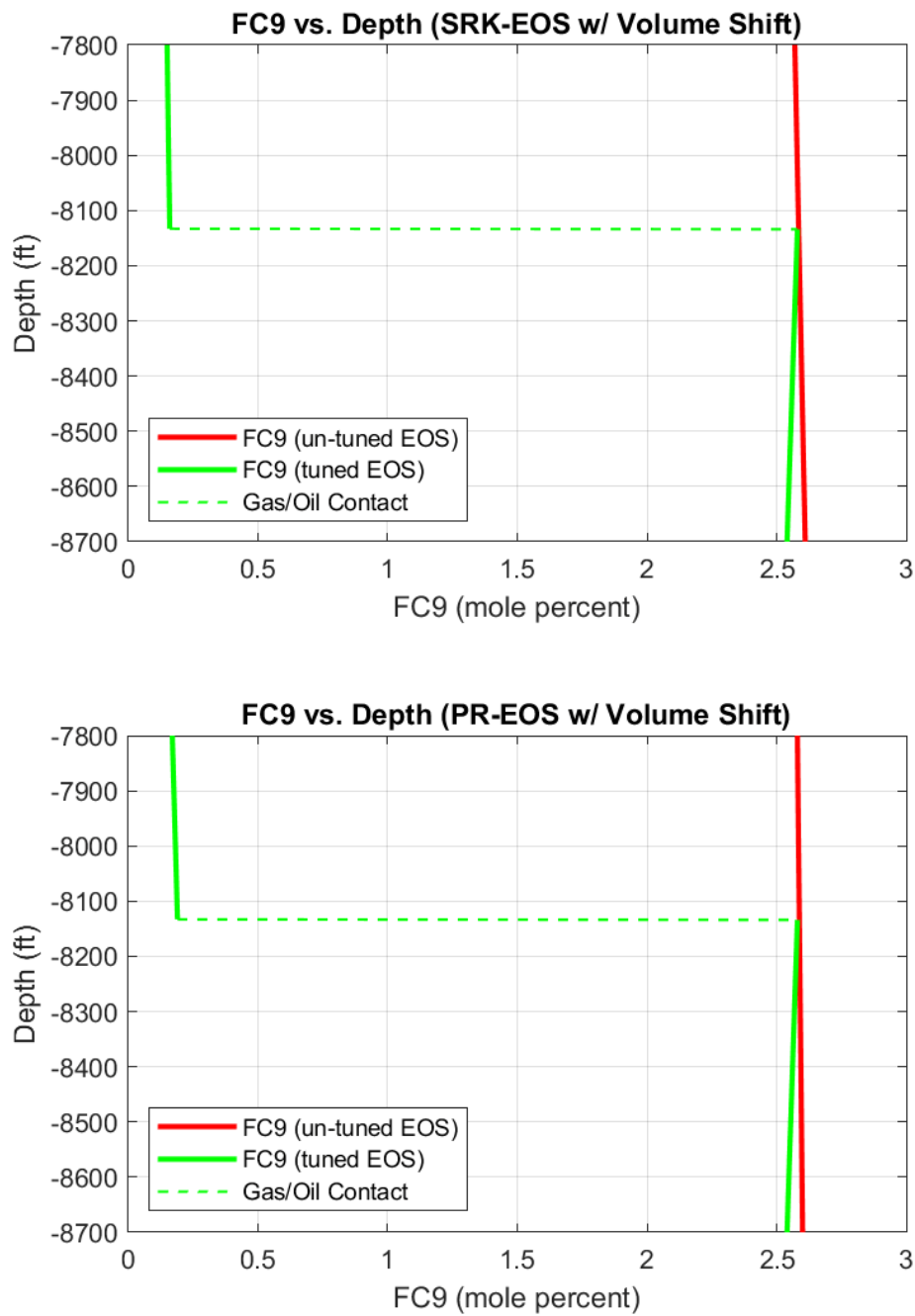


Figure A.29: FC9 composition plots with volume shift using commercial software

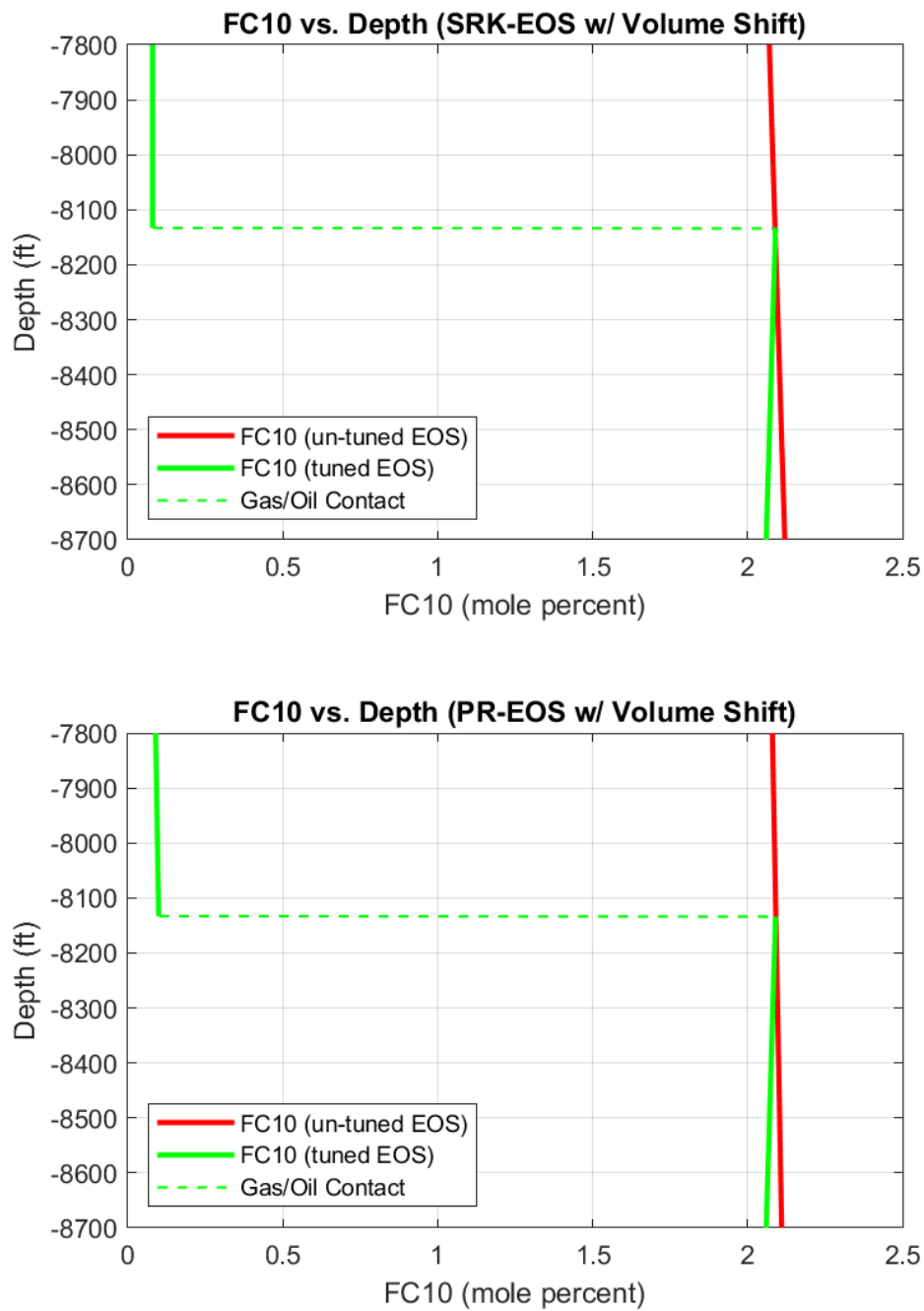


Figure A.30: FC10 composition plots with volume shift using commercial software

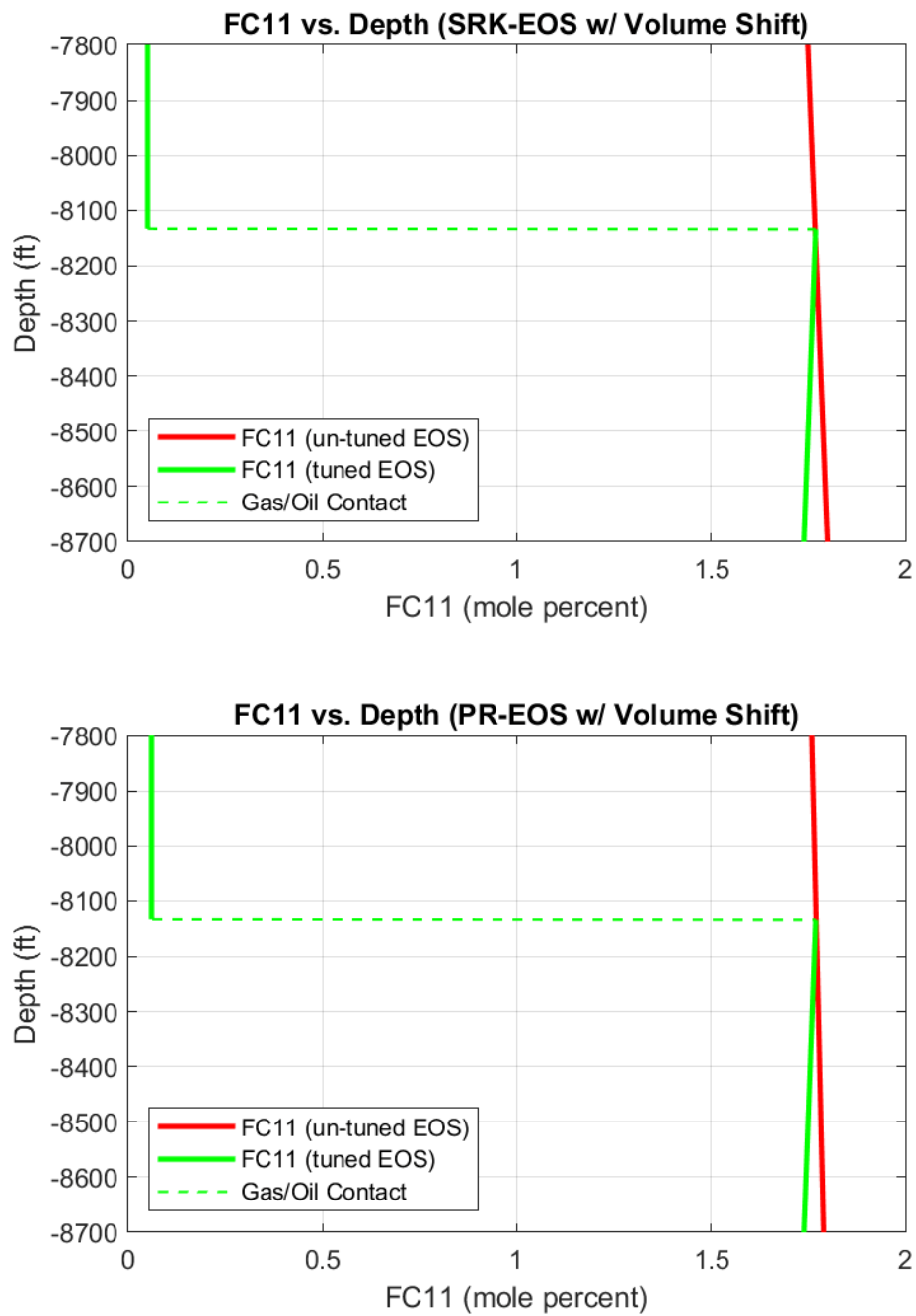


Figure A.31: FC11 composition plots with volume shift using commercial software

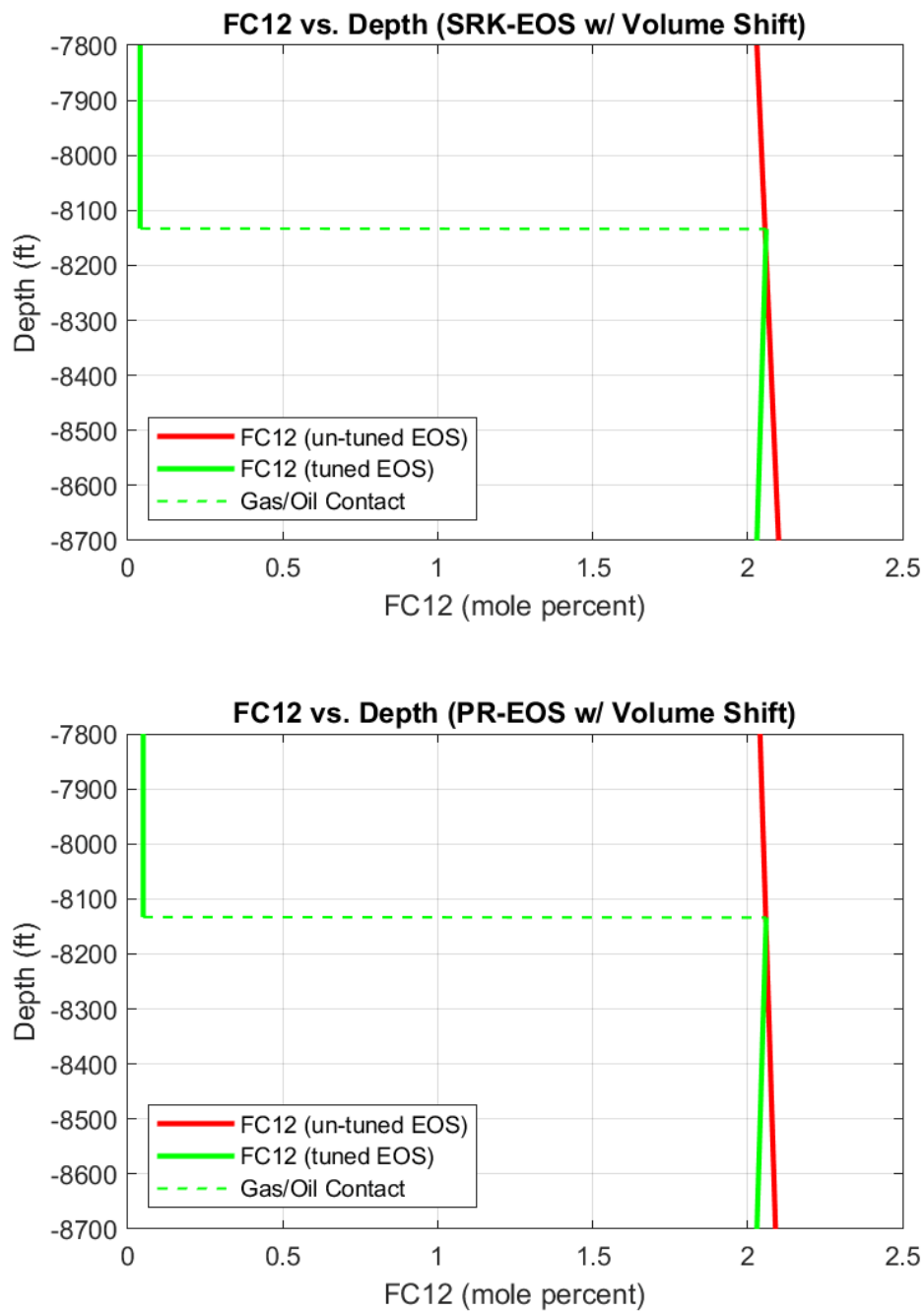


Figure A.32: FC12 composition plots with volume shift using commercial software

Appendix A: Supplementary Tables and Figures

Table A.35: Reservoir pressure, saturation pressure and reservoir fluid density gradient results for the tuned SRK and PR EOS models without volume shift using commercial software

Depth (ft)	Reservoir Pressure (psia)		Saturation Pressure (psia)		Reservoir Fluid Density (lb/ft ³)	
	SRK EOS	PR EOS	SRK EOS	PR EOS	SRK EOS	PR EOS
7800	3794.66	3791.68	3705.80	3711.93	13.466	14.646
7890	3803.09	3800.85	3737.58	3742.11	13.511	14.701
7980	3811.55	3810.06	3769.82	3772.72	13.557	14.757
8070	3820.03	3819.30	3802.54	3803.76	13.604	14.813
8133	3825.99	3825.79	3825.73	3825.76	13.637	14.853
8134	3826.10	3826.10	3826.07	3825.57	48.449	49.412
8160	3834.85	3835.02	3817.60	3818.51	48.480	49.431
8250	3865.18	3865.94	3788.69	3794.34	48.588	49.496
8340	3895.58	3896.89	3760.37	3770.60	48.693	49.559
8430	3926.05	3927.89	3732.62	3747.26	48.796	49.622
8520	3956.58	3958.92	3705.41	3724.33	48.897	49.683
8610	3987.17	3989.99	3678.72	3701.78	48.996	49.744
8700	4017.82	4021.10	3652.53	3679.59	49.094	49.803

Table A.36: H₂S, CO₂, N₂ compositional gradient results for the tuned SRK and PR EOS models without volume shift using commercial software

Depth (ft)	H ₂ S (mole fraction)		CO ₂ (mole fraction)		N ₂ (mole fraction)	
	SRK EOS	PR EOS	SRK EOS	PR EOS	SRK EOS	PR EOS
7800	0.0560	0.0608	0.0575	0.0578	0.0340	0.0320
7890	0.0562	0.0610	0.0577	0.0580	0.0340	0.0320
7980	0.0564	0.0612	0.0578	0.0582	0.0339	0.0320
8070	0.0566	0.0614	0.0580	0.0584	0.0339	0.0319
8133	0.0567	0.0616	0.0582	0.0585	0.0339	0.0319
8134	0.1124	0.1124	0.0701	0.0701	0.0117	0.0117
8160	0.1125	0.1125	0.0701	0.0701	0.0117	0.0117
8250	0.1125	0.1125	0.0702	0.0702	0.0117	0.0117
8340	0.1124	0.1125	0.0702	0.0702	0.0116	0.0117
8430	0.1124	0.1125	0.0703	0.0703	0.0116	0.0116
8520	0.1124	0.1125	0.0704	0.0703	0.0115	0.0116
8610	0.1124	0.1125	0.0704	0.0704	0.0115	0.0116
8700	0.1124	0.1125	0.0705	0.0705	0.0115	0.0115

Appendix A: Supplementary Tables and Figures

Table A.37: CH₄, C₂H₆, C₃H₈ compositional gradient results for the tuned SRK and PR EOS models without volume shift using commercial software

Depth (ft)	CH ₄ (mole fraction)		C ₂ H ₆ (mole fraction)		C ₃ H ₈ (mole fraction)	
	SRK EOS	PR EOS	SRK EOS	PR EOS	SRK EOS	PR EOS
7800	0.8172	0.8117	0.0168	0.0173	0.0048	0.0051
7890	0.8166	0.8111	0.0168	0.0174	0.0049	0.0051
7980	0.8160	0.8104	0.0169	0.0174	0.0049	0.0051
8070	0.8154	0.8098	0.0169	0.0174	0.0049	0.0051
8133	0.8150	0.8093	0.0169	0.0175	0.0049	0.0051
8134	0.3870	0.3870	0.0152	0.0152	0.0069	0.0069
8160	0.3864	0.3865	0.0152	0.0152	0.0069	0.0069
8250	0.3844	0.3850	0.0151	0.0152	0.0068	0.0068
8340	0.3825	0.3834	0.0151	0.0151	0.0068	0.0068
8430	0.3805	0.3819	0.0150	0.0151	0.0068	0.0068
8520	0.3786	0.3804	0.0149	0.0150	0.0067	0.0068
8610	0.3768	0.3790	0.0149	0.0150	0.0067	0.0068
8700	0.3749	0.3775	0.0148	0.0149	0.0067	0.0067

Table A.38: IC₄, NC₄, IC₅ compositional gradient results for the tuned SRK and PR EOS models without volume shift using commercial software

Depth (ft)	IC ₄ (mole fraction)		NC ₄ (mole fraction)		IC ₅ (mole fraction)	
	SRK EOS	PR EOS	SRK EOS	PR EOS	SRK EOS	PR EOS
7800	0.0013	0.0014	0.0021	0.0023	0.0011	0.0012
7890	0.0013	0.0014	0.0022	0.0023	0.0011	0.0012
7980	0.0013	0.0014	0.0022	0.0023	0.0011	0.0012
8070	0.0013	0.0014	0.0022	0.0023	0.0011	0.0012
8133	0.0013	0.0014	0.0022	0.0023	0.0011	0.0012
8134	0.0025	0.0025	0.0048	0.0048	0.0034	0.0034
8160	0.0025	0.0025	0.0048	0.0048	0.0034	0.0034
8250	0.0025	0.0025	0.0048	0.0048	0.0034	0.0034
8340	0.0025	0.0025	0.0047	0.0048	0.0034	0.0034
8430	0.0024	0.0025	0.0047	0.0047	0.0034	0.0034
8520	0.0024	0.0025	0.0047	0.0047	0.0033	0.0034
8610	0.0024	0.0024	0.0047	0.0047	0.0033	0.0034
8700	0.0024	0.0024	0.0047	0.0047	0.0033	0.0033

Appendix A: Supplementary Tables and Figures

Table A.39: NC₅, FC₆, FC₇ compositional gradient results for the tuned SRK and PR EOS models without volume shift using commercial software

Depth (ft)	NC ₅ (mole fraction)		FC ₆ (mole fraction)		FC ₇ (mole fraction)	
	SRK EOS	PR EOS	SRK EOS	PR EOS	SRK EOS	PR EOS
7800	0.0009	0.0010	0.0020	0.0023	0.0011	0.0013
7890	0.0009	0.0010	0.0021	0.0023	0.0011	0.0013
7980	0.0010	0.0010	0.0021	0.0023	0.0012	0.0013
8070	0.0010	0.0010	0.0021	0.0023	0.0012	0.0013
8133	0.0010	0.0010	0.0021	0.0024	0.0012	0.0014
8134	0.0032	0.0032	0.0106	0.0106	0.0090	0.0090
8160	0.0032	0.0032	0.0106	0.0106	0.0090	0.0090
8250	0.0032	0.0032	0.0105	0.0105	0.0090	0.0090
8340	0.0032	0.0032	0.0105	0.0105	0.0089	0.0090
8430	0.0031	0.0032	0.0105	0.0105	0.0089	0.0090
8520	0.0031	0.0032	0.0104	0.0105	0.0089	0.0089
8610	0.0031	0.0031	0.0104	0.0105	0.0089	0.0089
8700	0.0031	0.0031	0.0104	0.0105	0.0089	0.0089

Table A.40: FC₈, FC₉, FC₁₀ compositional gradient results for the tuned SRK and PR EOS models without volume shift using commercial software

Depth (ft)	FC ₈ (mole fraction)		FC ₉ (mole fraction)		FC ₁₀ (mole fraction)	
	SRK EOS	PR EOS	SRK EOS	PR EOS	SRK EOS	PR EOS
7800	0.0017	0.0020	0.0015	0.0017	0.0008	0.0009
7890	0.0017	0.0020	0.0015	0.0018	0.0008	0.0010
7980	0.0018	0.0021	0.0015	0.0018	0.0008	0.0010
8070	0.0018	0.0021	0.0016	0.0018	0.0008	0.0010
8133	0.0018	0.0021	0.0016	0.0019	0.0008	0.0010
8134	0.0201	0.0201	0.0258	0.0258	0.0209	0.0209
8160	0.0201	0.0201	0.0258	0.0258	0.0209	0.0209
8250	0.0200	0.0201	0.0258	0.0258	0.0208	0.0209
8340	0.0200	0.0201	0.0257	0.0258	0.0208	0.0208
8430	0.0199	0.0200	0.0257	0.0258	0.0207	0.0208
8520	0.0199	0.0200	0.0256	0.0258	0.0207	0.0208
8610	0.0198	0.0200	0.0255	0.0257	0.0206	0.0208
8700	0.0198	0.0200	0.0255	0.0257	0.0206	0.0208

Appendix A: Supplementary Tables and Figures

Table A.41: FC₁₁, FC₁₂, C₁₃₊ compositional gradient results for the tuned SRK and PR EOS models without volume shift using commercial software

Depth (ft)	FC ₁₁ (mole fraction)		FC ₁₂ (mole fraction)		C ₁₃₊ (mole fraction)	
	SRK EOS	PR EOS	SRK EOS	PR EOS	SRK EOS	PR EOS
7800	0.0005	0.0006	0.0004	0.0005	0.0002	0.0001
7890	0.0005	0.0006	0.0004	0.0005	0.0002	0.0001
7980	0.0005	0.0006	0.0004	0.0005	0.0002	0.0001
8070	0.0005	0.0006	0.0004	0.0005	0.0003	0.0001
8133	0.0005	0.0006	0.0004	0.0005	0.0003	0.0002
8134	0.0177	0.0177	0.0206	0.0206	0.2581	0.2581
8160	0.0177	0.0177	0.0206	0.0206	0.2588	0.2587
8250	0.0176	0.0177	0.0205	0.0206	0.2613	0.2604
8340	0.0176	0.0176	0.0205	0.0205	0.2636	0.2621
8430	0.0175	0.0176	0.0204	0.0205	0.2660	0.2638
8520	0.0175	0.0176	0.0204	0.0205	0.2683	0.2655
8610	0.0175	0.0176	0.0203	0.0205	0.2706	0.2672
8700	0.0174	0.0176	0.0203	0.0205	0.2729	0.2688

Table A.42: Reservoir pressure, saturation pressure and reservoir fluid density gradient results for the un-tuned SRK and PR EOS models without volume shift using commercial software

Depth (ft)	Reservoir Pressure (psia)		Saturation Pressure (psia)		Reservoir Fluid Density (lb/ft ³)	
	SRK EOS	PR EOS	SRK EOS	PR EOS	SRK EOS	PR EOS
7800	3745.47	3736.23	2858.30	2838.52	34.730	38.708
7890	3767.18	3760.43	2848.84	2828.83	34.747	38.728
7980	3788.91	3784.64	2839.47	2819.24	34.764	38.747
8070	3810.64	3808.87	2830.18	2809.74	34.781	38.767
8134	3826.10	3826.10	2823.63	2803.04	34.793	38.781
8160	3832.38	3833.10	2820.98	2800.33	34.798	38.786
8250	3854.14	3857.35	2811.86	2791.02	34.814	38.806
8340	3875.90	3881.61	2802.82	2781.79	34.831	38.825
8430	3897.67	3905.88	2793.87	2772.65	34.847	38.844
8520	3919.46	3930.16	2784.99	2763.60	34.863	38.863
8610	3941.25	3954.46	2776.19	2754.63	34.879	38.881
8700	3963.06	3978.77	2767.46	2745.74	34.895	38.900

Appendix A: Supplementary Tables and Figures

Table A.43: H₂S, CO₂, N₂ compositional gradient results for the un-tuned SRK and PR EOS models without volume shift using commercial software

Depth (ft)	H ₂ S (mole fraction)		CO ₂ (mole fraction)		N ₂ (mole fraction)	
	SRK EOS	PR EOS	SRK EOS	PR EOS	SRK EOS	PR EOS
7800	0.1123	0.1123	0.0698	0.0698	0.0118	0.0118
7890	0.1123	0.1123	0.0699	0.0699	0.0117	0.0118
7980	0.1124	0.1124	0.0700	0.0700	0.0117	0.0117
8070	0.1124	0.1124	0.0700	0.0700	0.0117	0.0117
8134	0.1124	0.1124	0.0701	0.0701	0.0117	0.0117
8160	0.1125	0.1125	0.0701	0.0701	0.0117	0.0117
8250	0.1125	0.1125	0.0702	0.0702	0.0117	0.0117
8340	0.1126	0.1125	0.0703	0.0703	0.0117	0.0117
8430	0.1126	0.1126	0.0704	0.0704	0.0117	0.0117
8520	0.1127	0.1126	0.0704	0.0704	0.0117	0.0117
8610	0.1127	0.1127	0.0705	0.0705	0.0117	0.0117
8700	0.1128	0.1127	0.0706	0.0706	0.0117	0.0117

Table A.44: CH₄, C₂H₆, C₃H₈ compositional gradient results for the un-tuned SRK and PR EOS models without volume shift using commercial software

Depth (ft)	CH ₄ (mole fraction)		C ₂ H ₆ (mole fraction)		C ₃ H ₈ (mole fraction)	
	SRK EOS	PR EOS	SRK EOS	PR EOS	SRK EOS	PR EOS
7800	0.3901	0.3902	0.0153	0.0153	0.0069	0.0069
7890	0.3892	0.3893	0.0153	0.0153	0.0069	0.0069
7980	0.3884	0.3884	0.0153	0.0153	0.0069	0.0069
8070	0.3876	0.3876	0.0152	0.0152	0.0069	0.0069
8134	0.3870	0.3870	0.0152	0.0152	0.0069	0.0069
8160	0.3867	0.3867	0.0152	0.0152	0.0069	0.0069
8250	0.3859	0.3859	0.0152	0.0152	0.0069	0.0069
8340	0.3851	0.3851	0.0152	0.0152	0.0069	0.0069
8430	0.3843	0.3842	0.0152	0.0152	0.0069	0.0069
8520	0.3835	0.3834	0.0151	0.0151	0.0068	0.0068
8610	0.3827	0.3826	0.0151	0.0151	0.0068	0.0068
8700	0.3819	0.3817	0.0151	0.0151	0.0068	0.0068

Appendix A: Supplementary Tables and Figures

Table A.45: IC₄, NC₄, IC₅ compositional gradient results for the un-tuned SRK and PR EOS models without volume shift using commercial software

Depth (ft)	IC ₄ (mole fraction)		NC ₄ (mole fraction)		IC ₅ (mole fraction)	
	SRK EOS	PR EOS	SRK EOS	PR EOS	SRK EOS	PR EOS
7800	0.0025	0.0025	0.0048	0.0048	0.0034	0.0034
7890	0.0025	0.0025	0.0048	0.0048	0.0034	0.0034
7980	0.0025	0.0025	0.0048	0.0048	0.0034	0.0034
8070	0.0025	0.0025	0.0048	0.0048	0.0034	0.0034
8134	0.0025	0.0025	0.0048	0.0048	0.0034	0.0034
8160	0.0025	0.0025	0.0048	0.0048	0.0034	0.0034
8250	0.0025	0.0025	0.0048	0.0048	0.0034	0.0034
8340	0.0025	0.0025	0.0048	0.0048	0.0034	0.0034
8430	0.0025	0.0025	0.0048	0.0048	0.0034	0.0034
8520	0.0025	0.0025	0.0048	0.0048	0.0034	0.0034
8610	0.0025	0.0025	0.0048	0.0048	0.0034	0.0034
8700	0.0025	0.0025	0.0048	0.0048	0.0034	0.0034

Table A.46: NC₅, FC₆, FC₇ compositional gradient results for the un-tuned SRK and PR EOS models without volume shift using commercial software

Depth (ft)	NC ₅ (mole fraction)		FC ₆ (mole fraction)		FC ₇ (mole fraction)	
	SRK EOS	PR EOS	SRK EOS	PR EOS	SRK EOS	PR EOS
7800	0.0032	0.0032	0.0105	0.0105	0.0090	0.0090
7890	0.0032	0.0032	0.0105	0.0105	0.0090	0.0090
7980	0.0032	0.0032	0.0105	0.0105	0.0090	0.0090
8070	0.0032	0.0032	0.0106	0.0106	0.0090	0.0090
8134	0.0032	0.0032	0.0106	0.0106	0.0090	0.0090
8160	0.0032	0.0032	0.0106	0.0106	0.0090	0.0090
8250	0.0032	0.0032	0.0106	0.0106	0.0090	0.0090
8340	0.0032	0.0032	0.0106	0.0106	0.0090	0.0090
8430	0.0032	0.0032	0.0106	0.0106	0.0090	0.0090
8520	0.0032	0.0032	0.0106	0.0106	0.0091	0.0091
8610	0.0032	0.0032	0.0106	0.0106	0.0091	0.0091
8700	0.0032	0.0032	0.0106	0.0106	0.0091	0.0091

Appendix A: Supplementary Tables and Figures

Table A.47: FC8, FC9, FC10 compositional gradient results for the un-tuned SRK and PR EOS models without volume shift using commercial software

Depth (ft)	FC8 (mole fraction)		FC9 (mole fraction)		FC10 (mole fraction)	
	SRK EOS	PR EOS	SRK EOS	PR EOS	SRK EOS	PR EOS
7800	0.0200	0.0200	0.0256	0.0256	0.0207	0.0207
7890	0.0200	0.0200	0.0257	0.0257	0.0207	0.0207
7980	0.0200	0.0200	0.0258	0.0257	0.0208	0.0208
8070	0.0201	0.0201	0.0258	0.0258	0.0208	0.0208
8134	0.0201	0.0201	0.0258	0.0258	0.0209	0.0209
8160	0.0201	0.0201	0.0259	0.0259	0.0209	0.0209
8250	0.0201	0.0201	0.0259	0.0259	0.0209	0.0210
8340	0.0202	0.0202	0.0260	0.0260	0.0210	0.0210
8430	0.0202	0.0202	0.0260	0.0260	0.0211	0.0211
8520	0.0203	0.0203	0.0261	0.0261	0.0211	0.0211
8610	0.0203	0.0203	0.0262	0.0262	0.0212	0.0212
8700	0.0203	0.0203	0.0262	0.0262	0.0212	0.0212

Table A.48: FC11, FC12, C13+ compositional gradient results for the un-tuned SRK and PR EOS models without volume shift using commercial software

Depth (ft)	FC11 (mole fraction)		FC12 (mole fraction)		C13+ (mole fraction)	
	SRK EOS	PR EOS	SRK EOS	PR EOS	SRK EOS	PR EOS
7800	0.0175	0.0175	0.0203	0.0203	0.2565	0.2563
7890	0.0175	0.0175	0.0204	0.0204	0.2569	0.2568
7980	0.0176	0.0176	0.0205	0.0205	0.2574	0.2573
8070	0.0176	0.0176	0.0205	0.0205	0.2578	0.2578
8134	0.0177	0.0177	0.0206	0.0206	0.2581	0.2581
8160	0.0177	0.0177	0.0206	0.0206	0.2583	0.2583
8250	0.0177	0.0177	0.0207	0.0207	0.2587	0.2588
8340	0.0178	0.0178	0.0207	0.0207	0.2592	0.2592
8430	0.0178	0.0178	0.0208	0.0208	0.2596	0.2597
8520	0.0179	0.0179	0.0209	0.0209	0.2600	0.2601
8610	0.0179	0.0179	0.0209	0.0209	0.2604	0.2606
8700	0.0180	0.0180	0.0210	0.0210	0.2609	0.2610

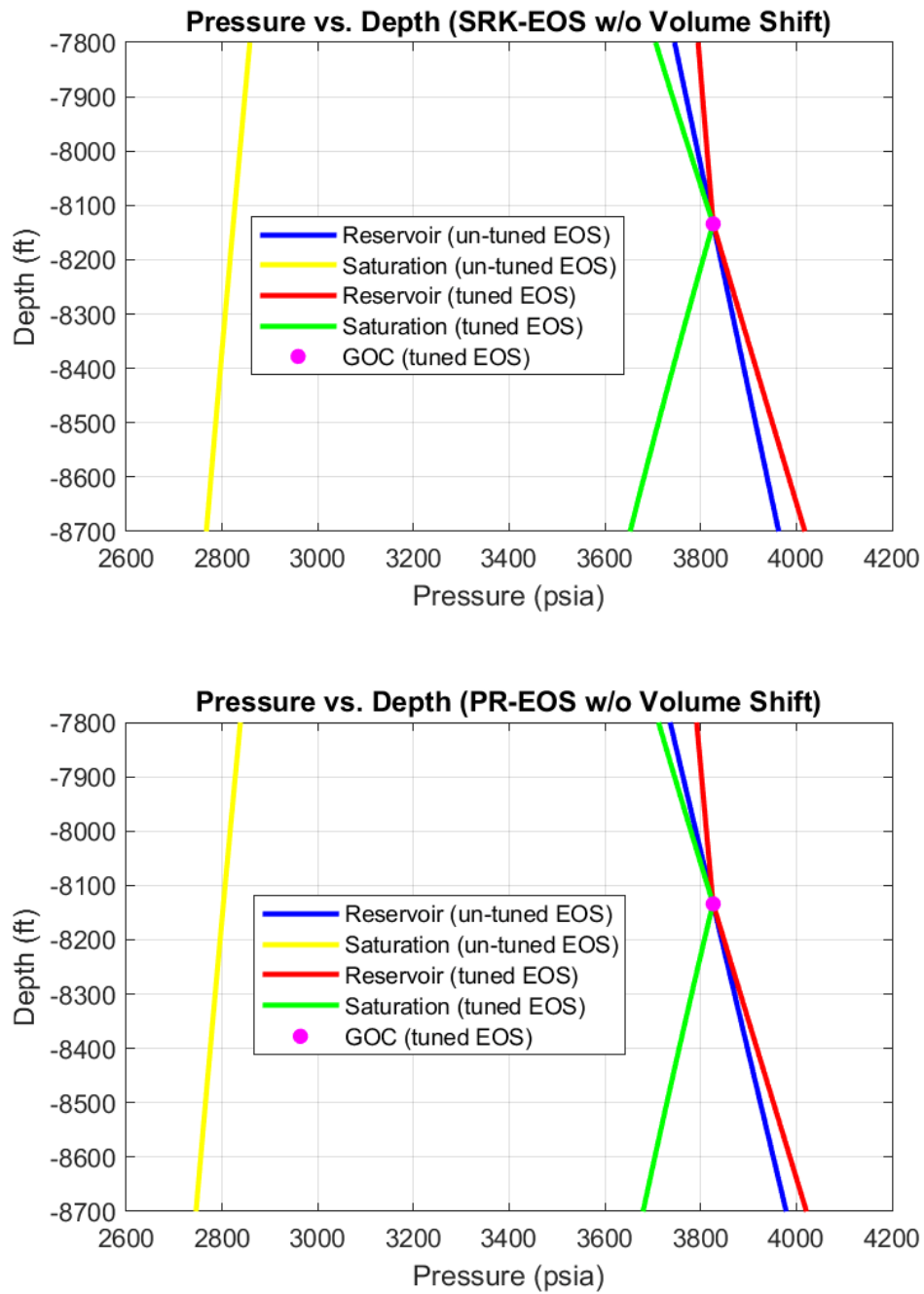


Figure A.33: Pressure plots without volume shift using commercial software

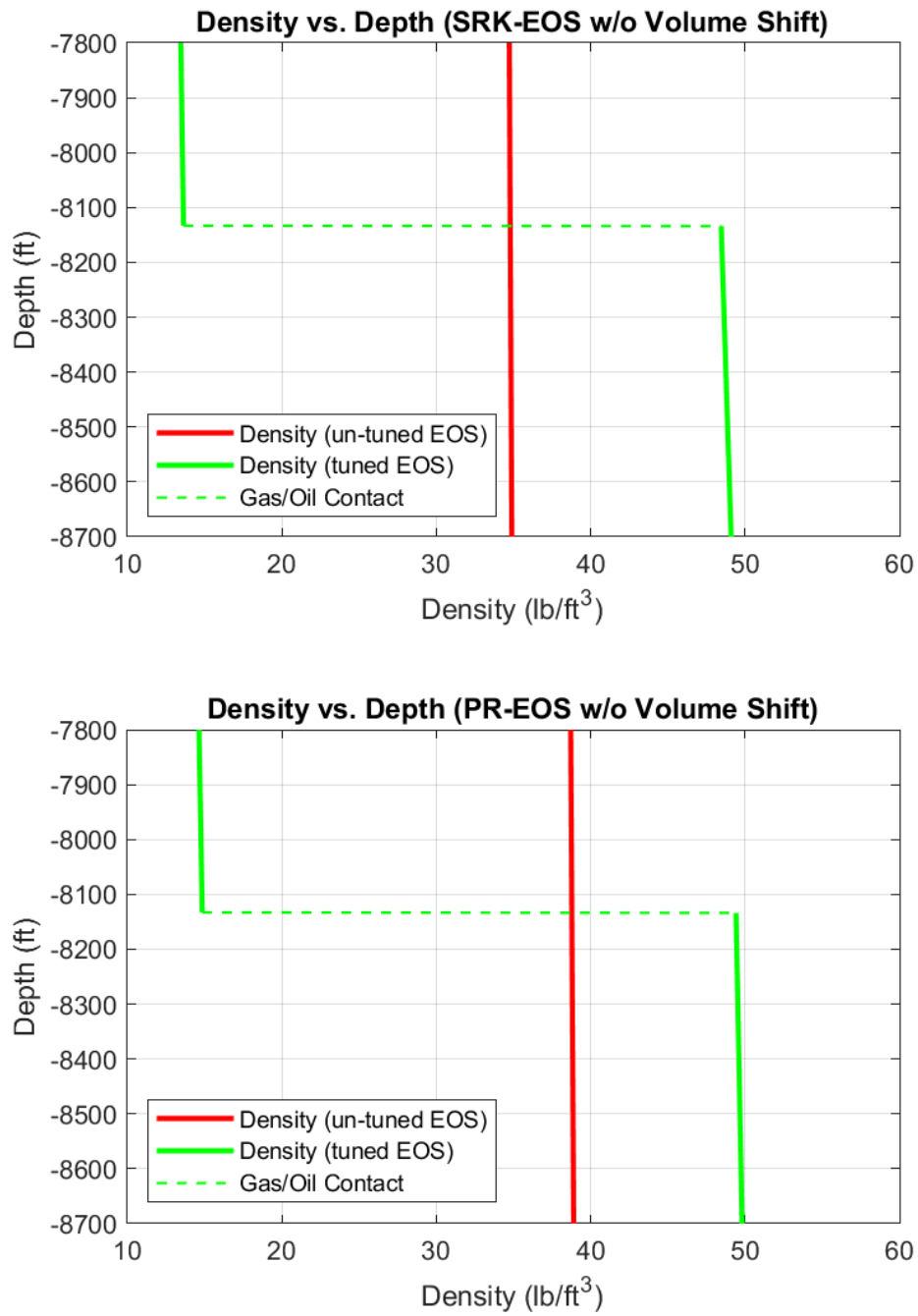


Figure A.34: Density plots without volume shift using commercial software

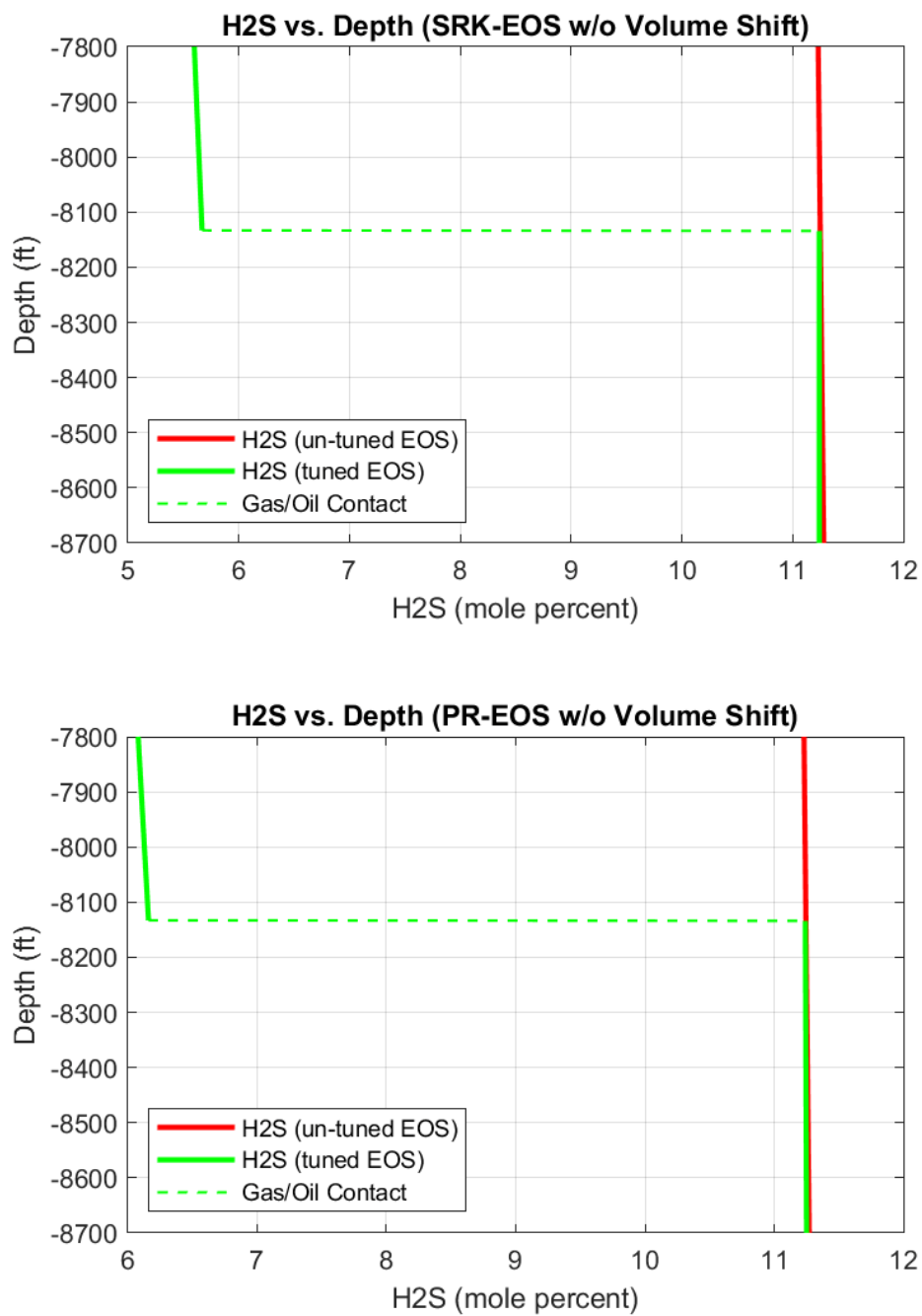


Figure A.35: H₂S composition plots without volume shift using commercial software

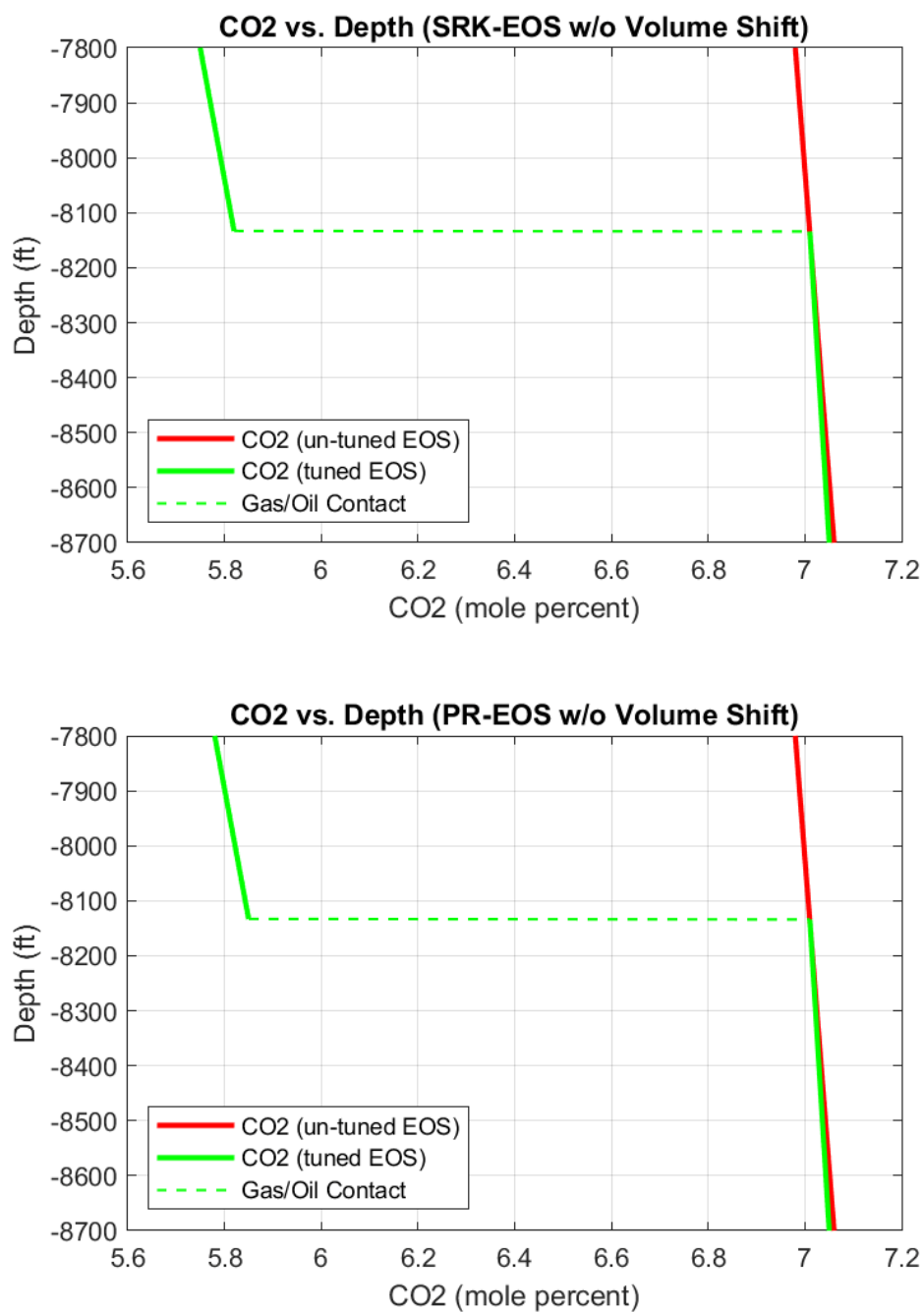


Figure A.36: CO₂ composition plots without volume shift using commercial software

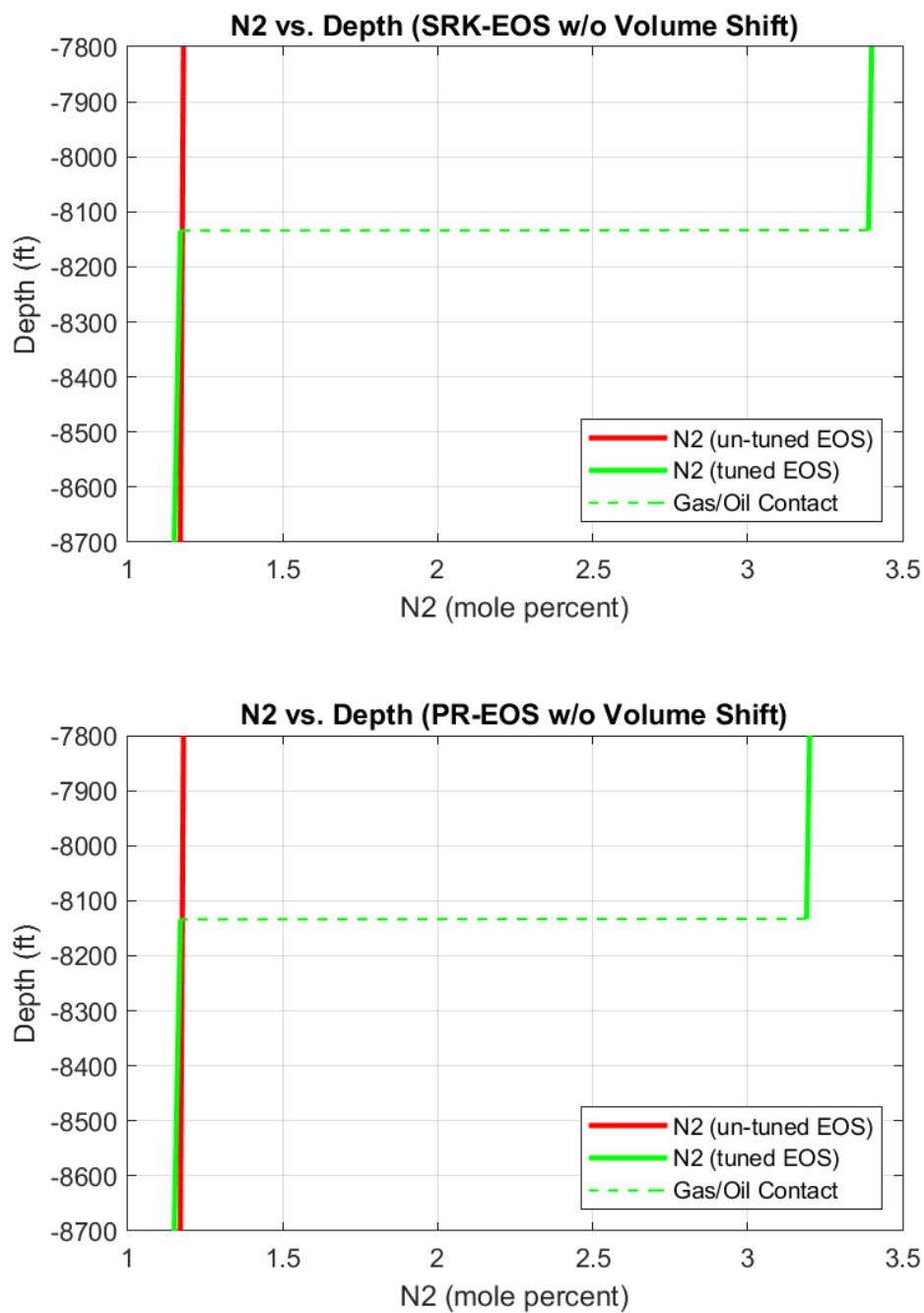


Figure A.37: N₂ composition plots without volume shift using commercial software

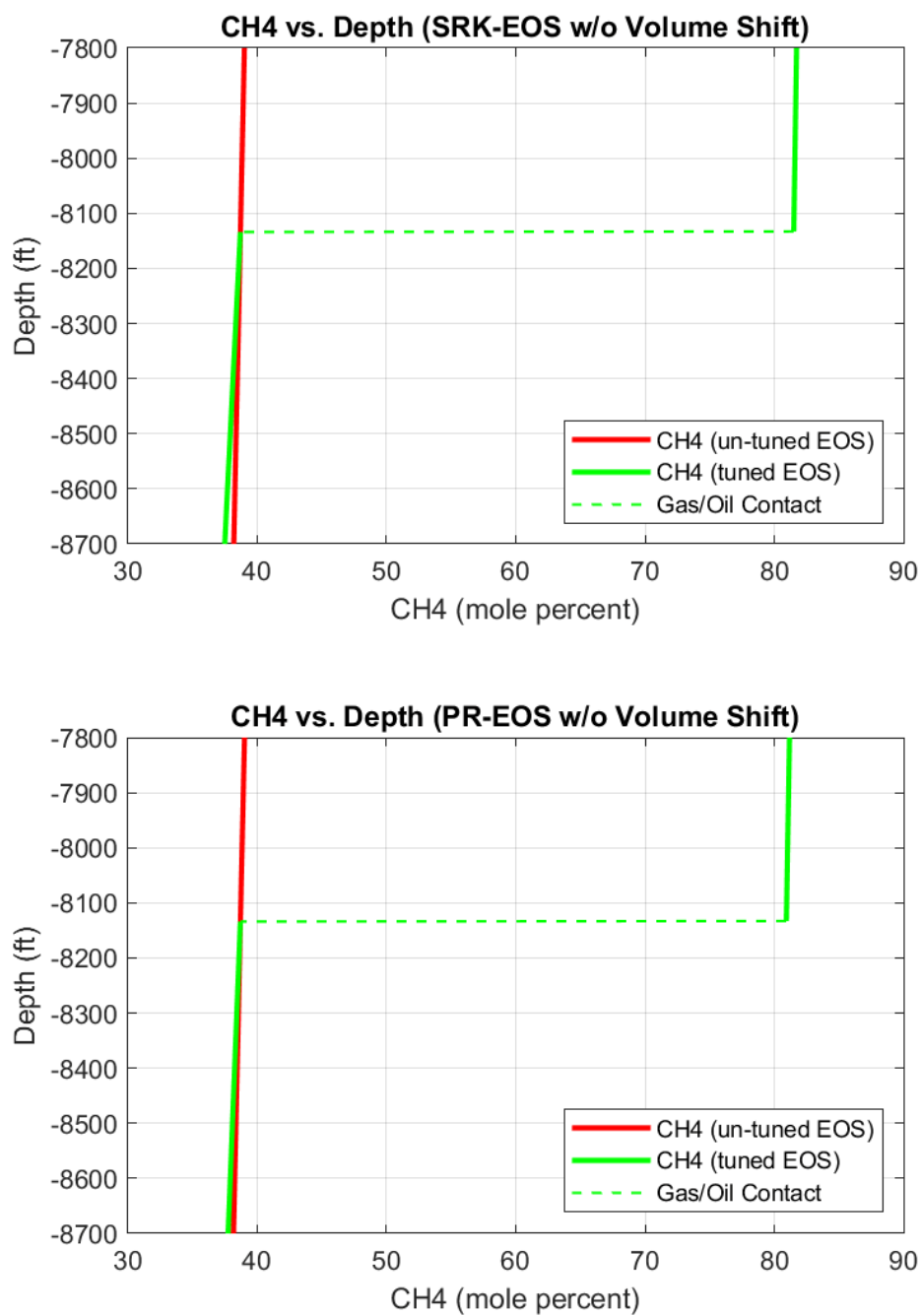


Figure A.38: CH₄ composition plots without volume shift using commercial software

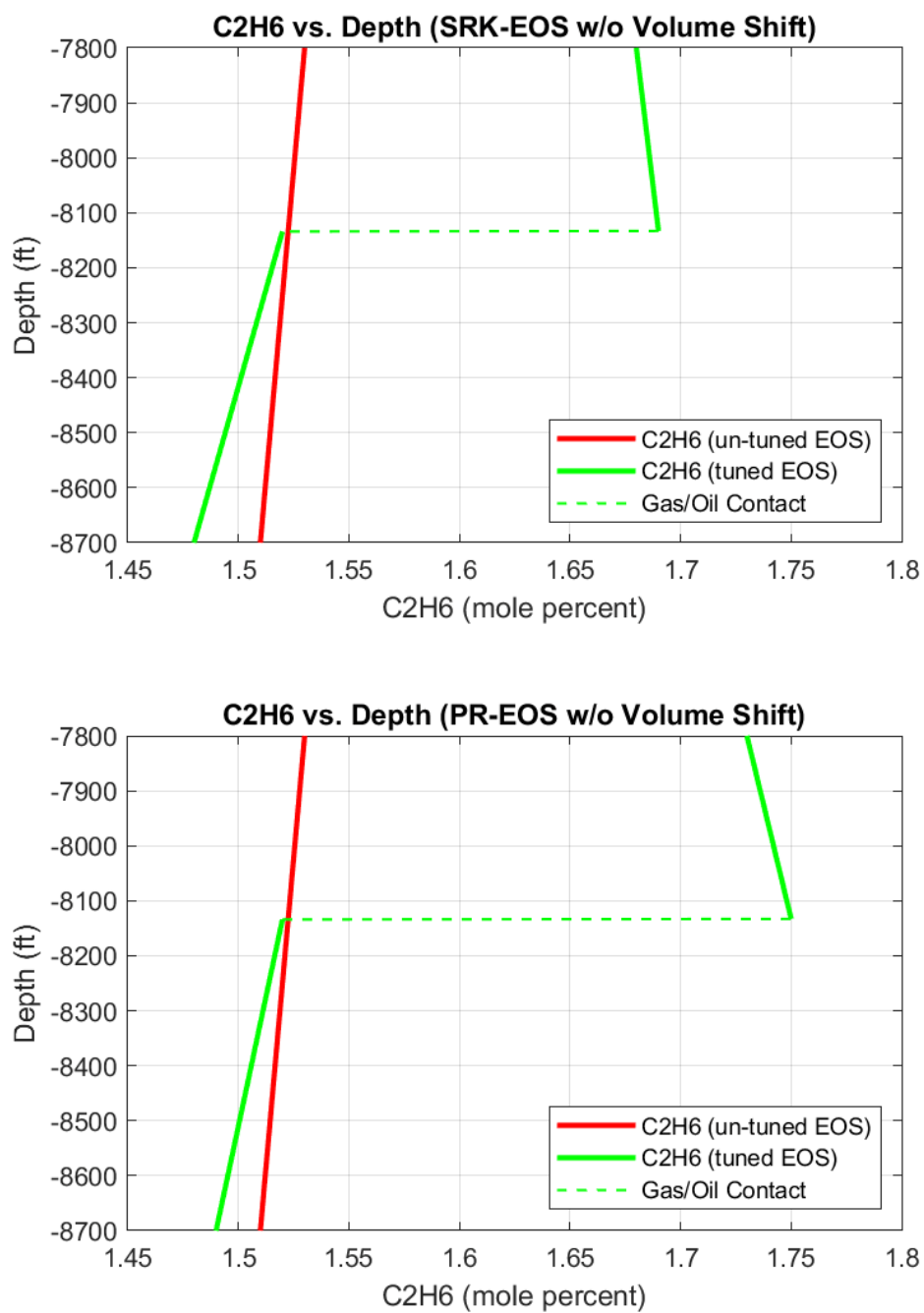


Figure A.39: C₂H₆ composition plots without volume shift using commercial software

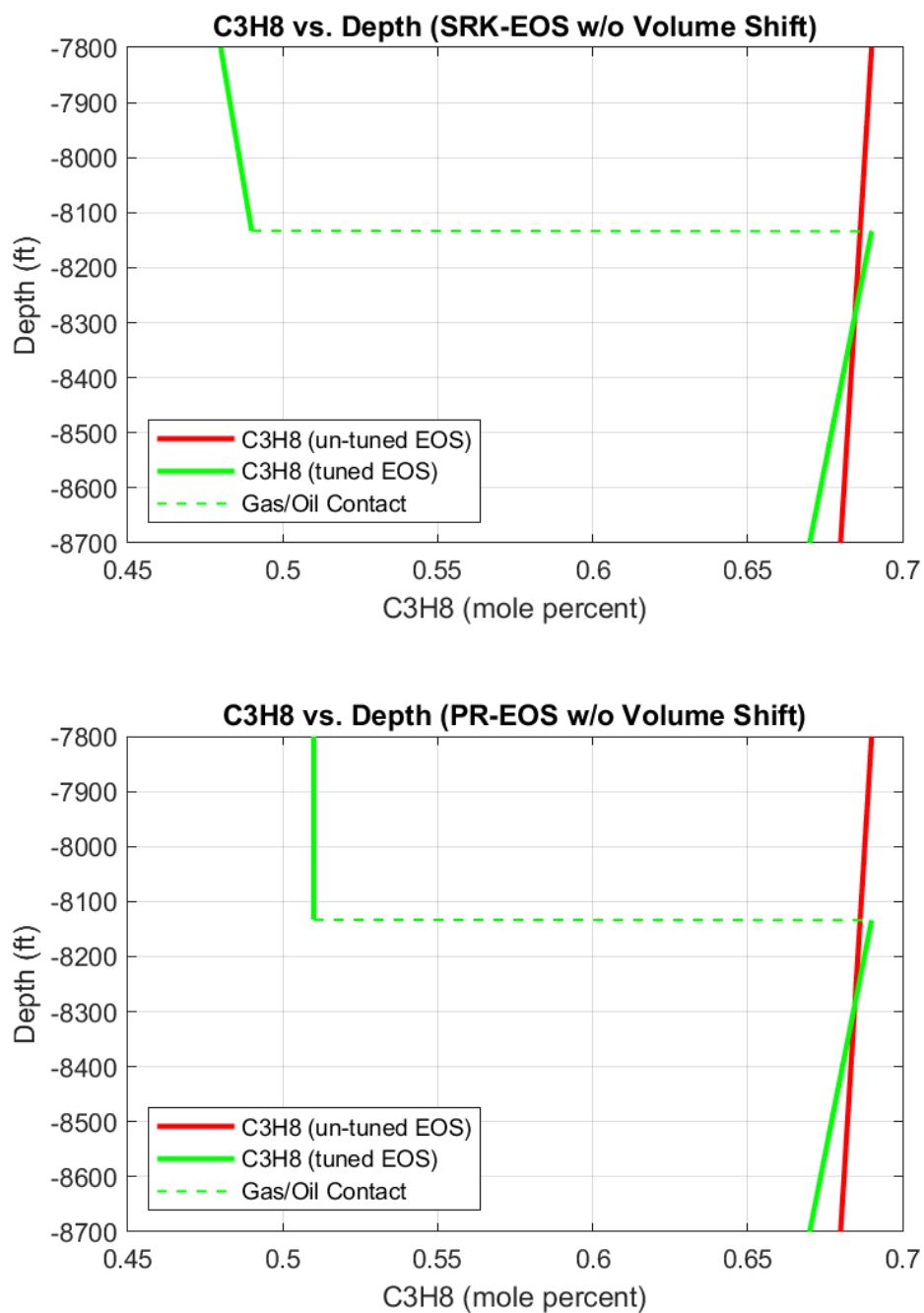


Figure A.40: C₃H₈ composition plots without volume shift using commercial software

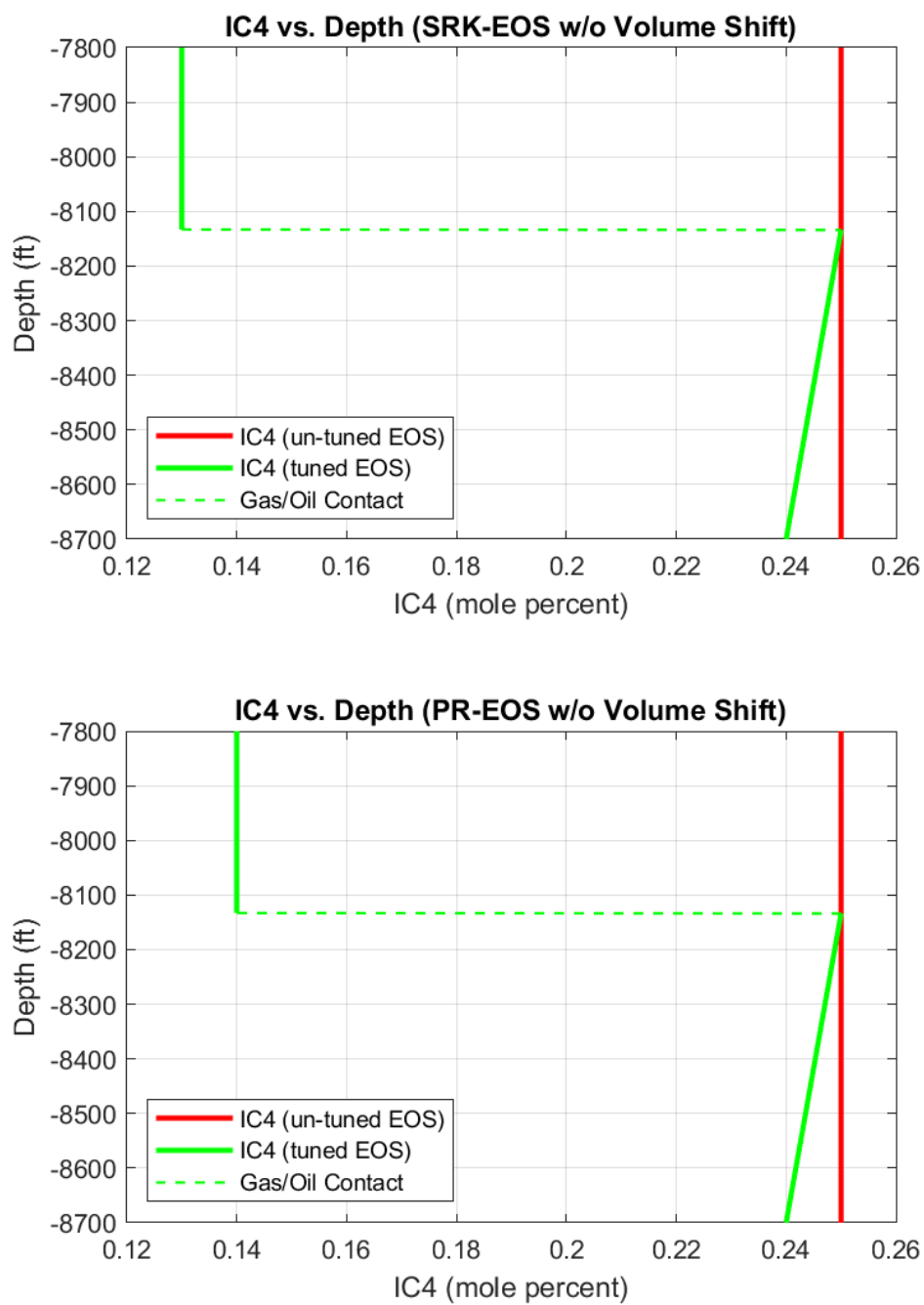


Figure A.41: IC4 composition plots without volume shift using commercial software

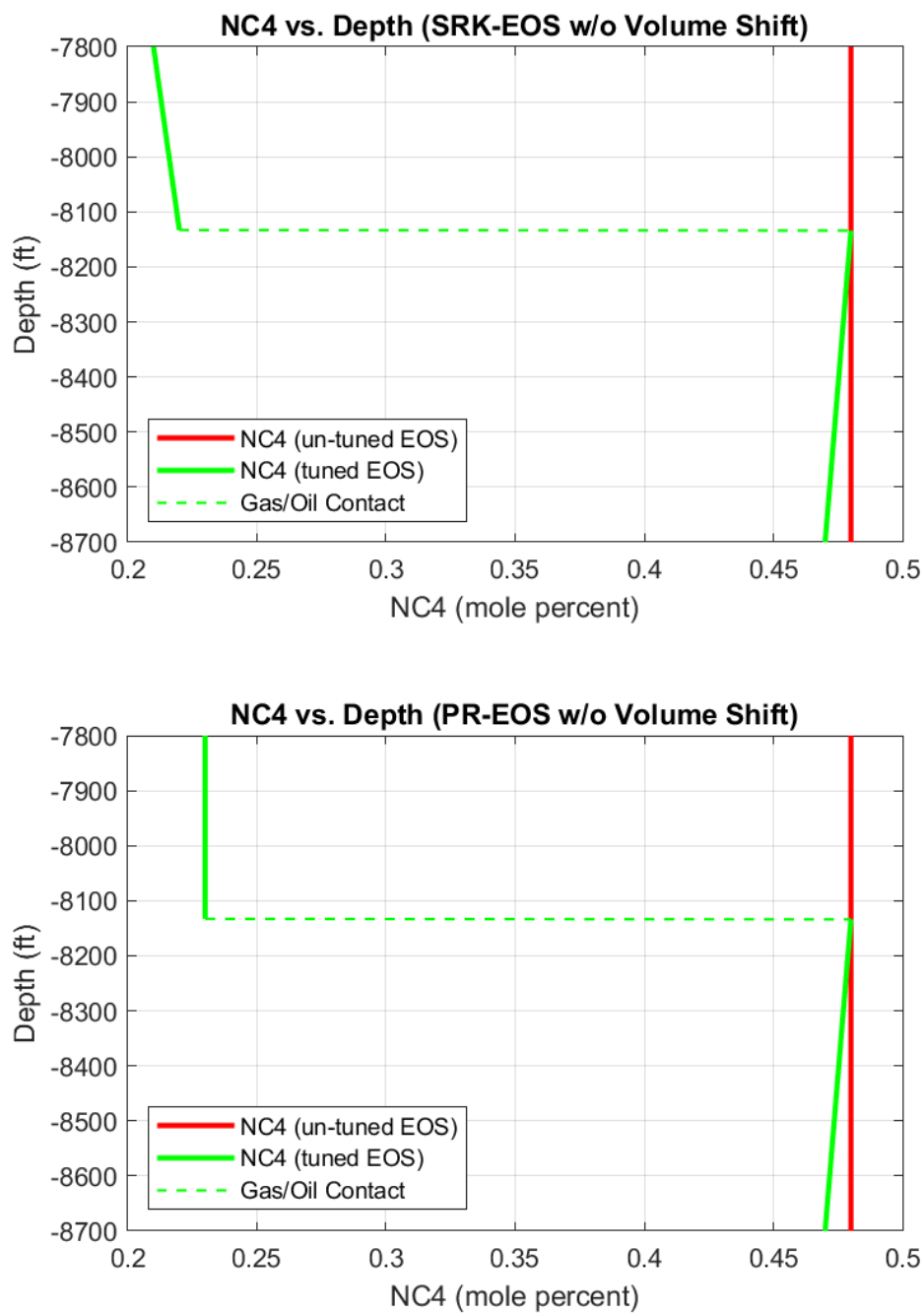


Figure A.42: NC4 composition plots without volume shift using commercial software

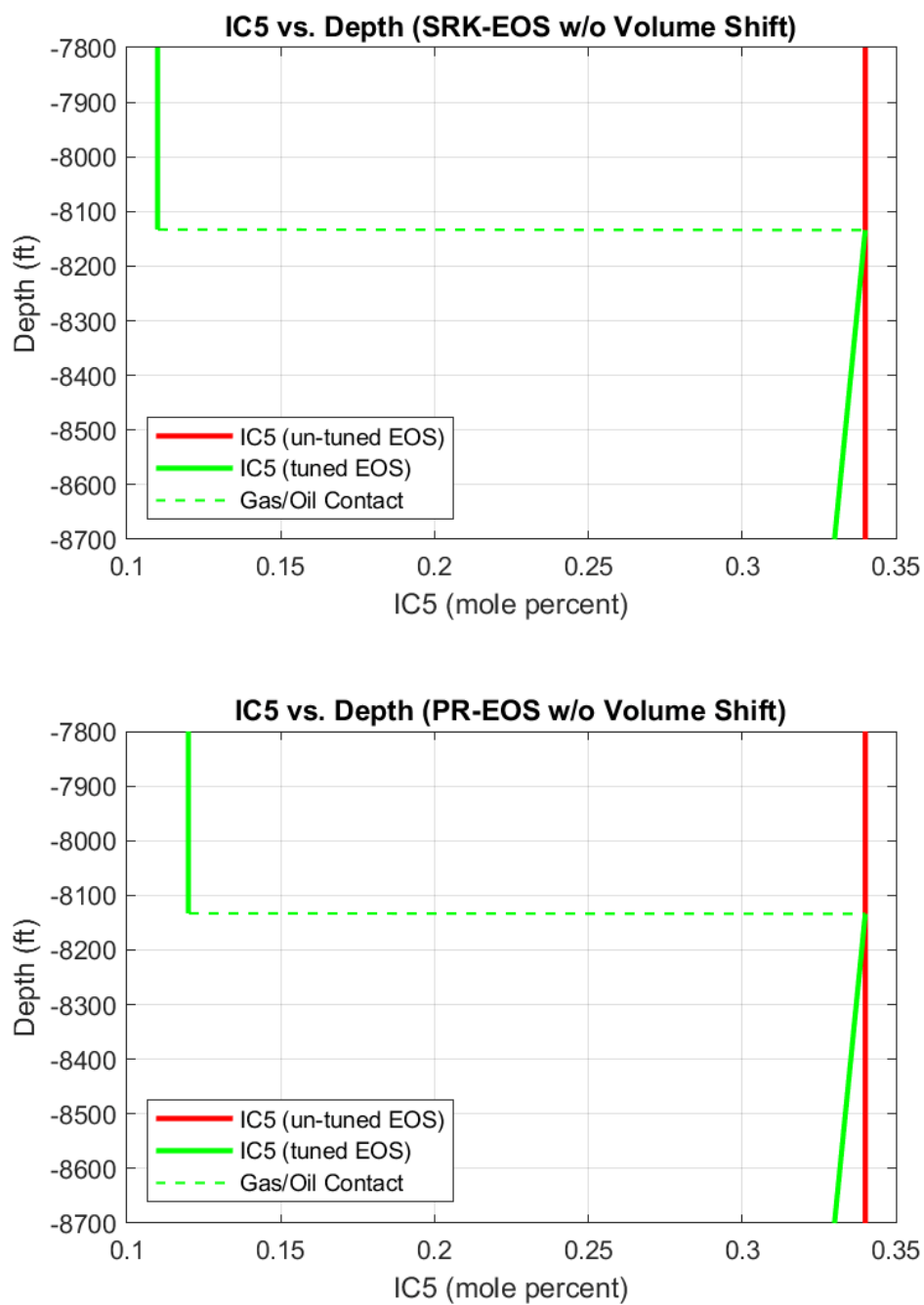


Figure A.43: IC5 composition plots without volume shift using commercial software

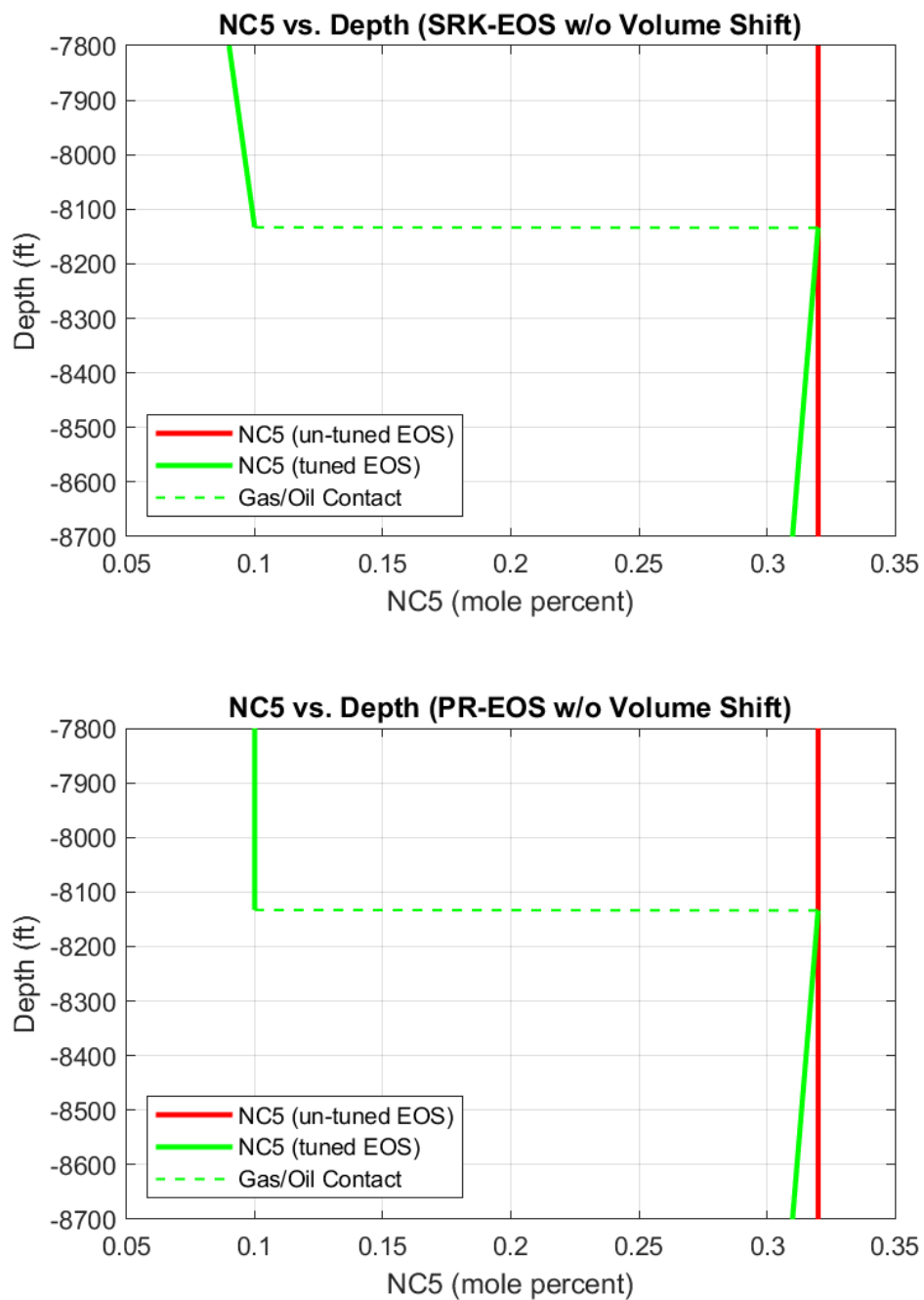


Figure A.44: NC5 composition plots without volume shift using commercial software

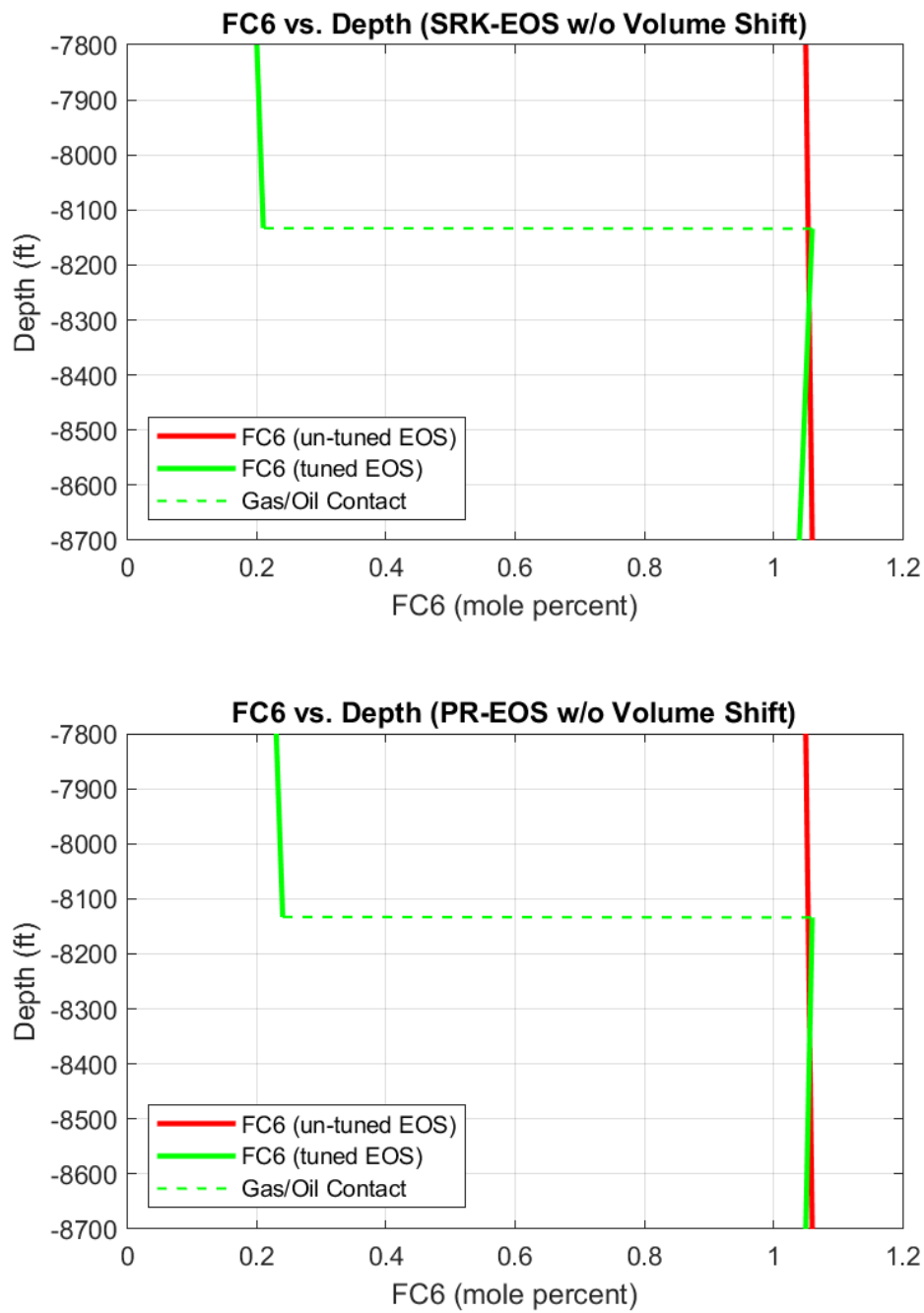


Figure A.45: FC6 composition plots without volume shift using commercial software

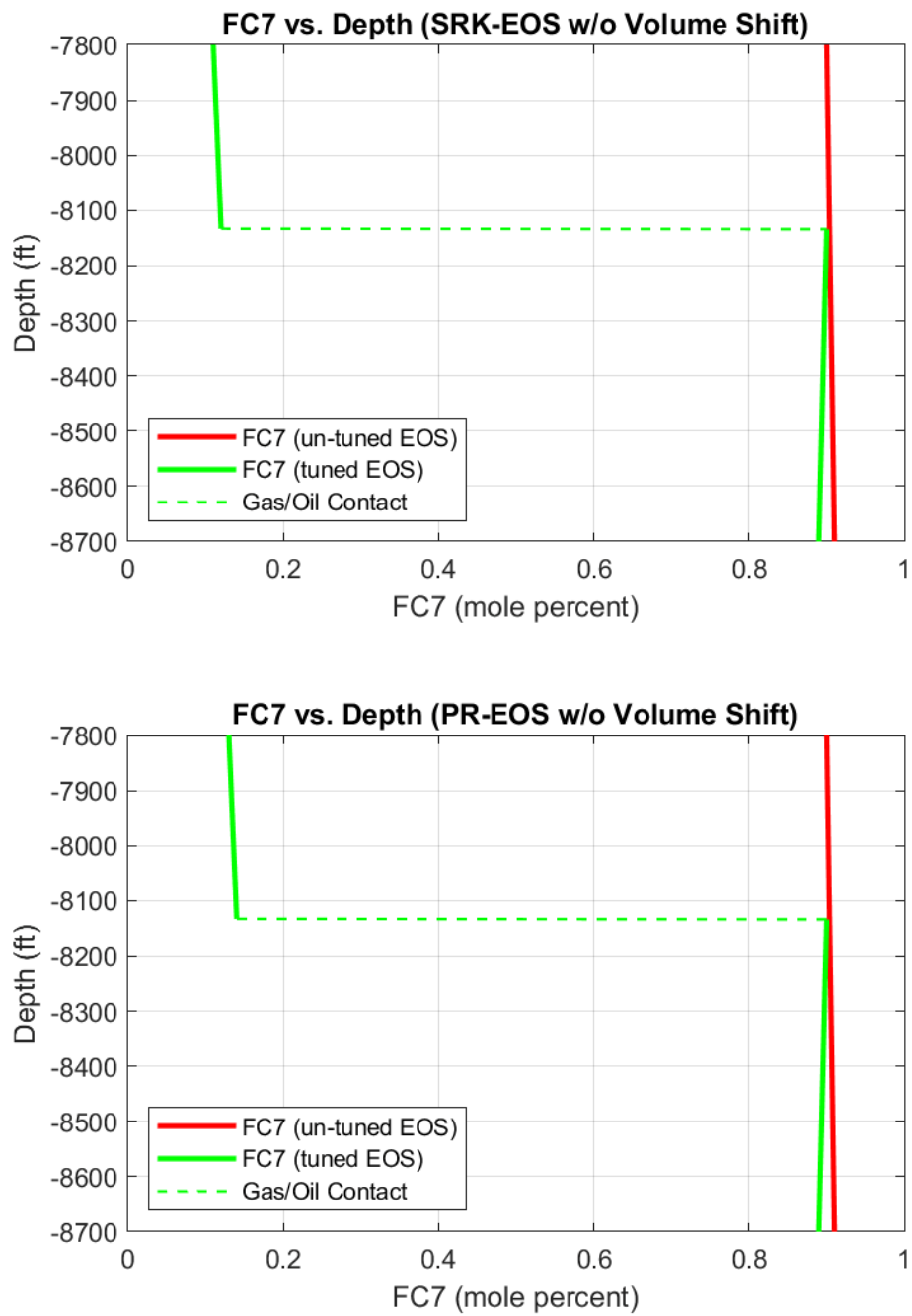


Figure A.46: FC7 composition plots without volume shift using commercial software

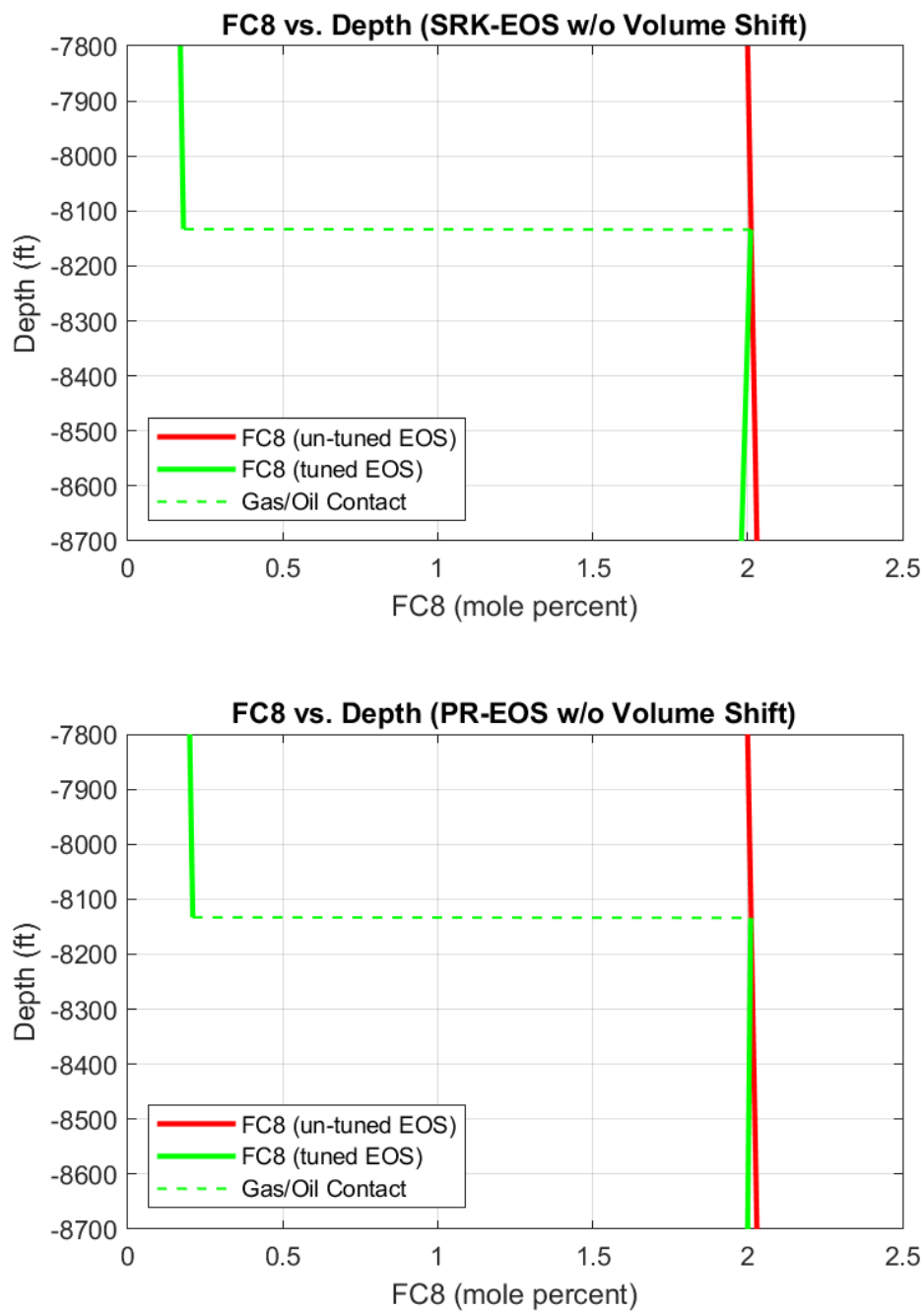


Figure A.47: FC8 composition plots without volume shift using commercial software

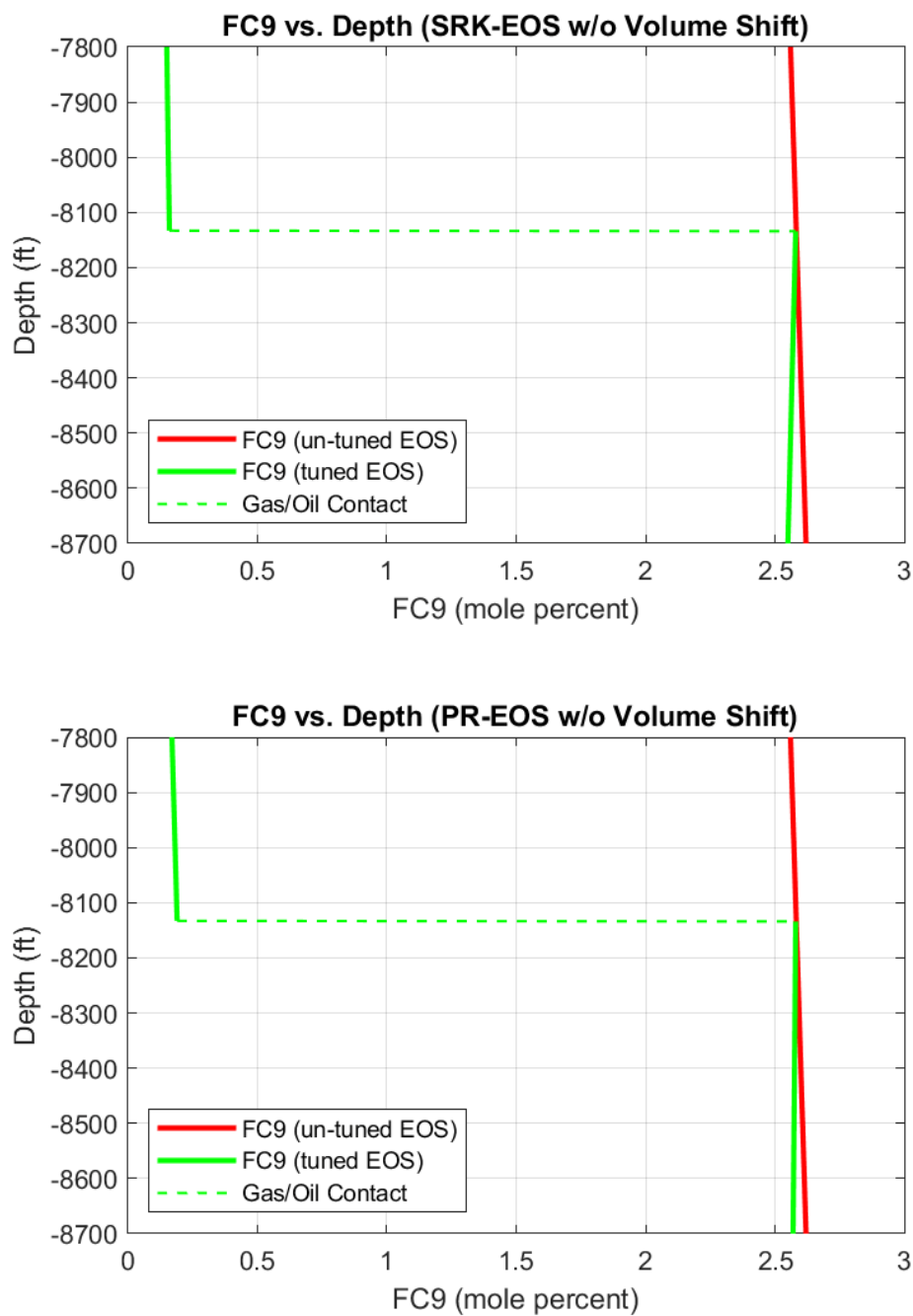


Figure A.48: FC9 composition plots without volume shift using commercial software

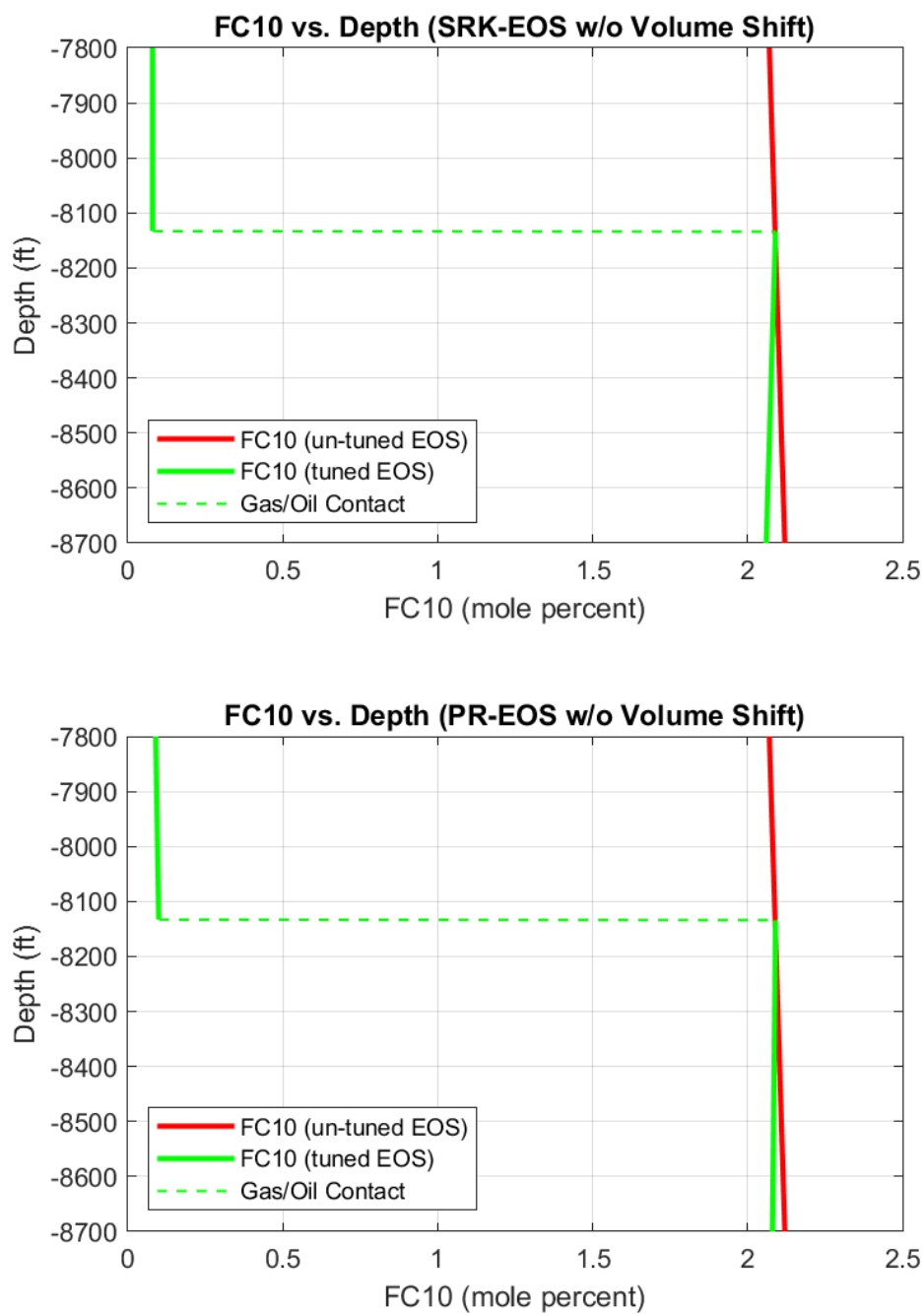


Figure A.49: FC10 composition plots without volume shift using commercial software

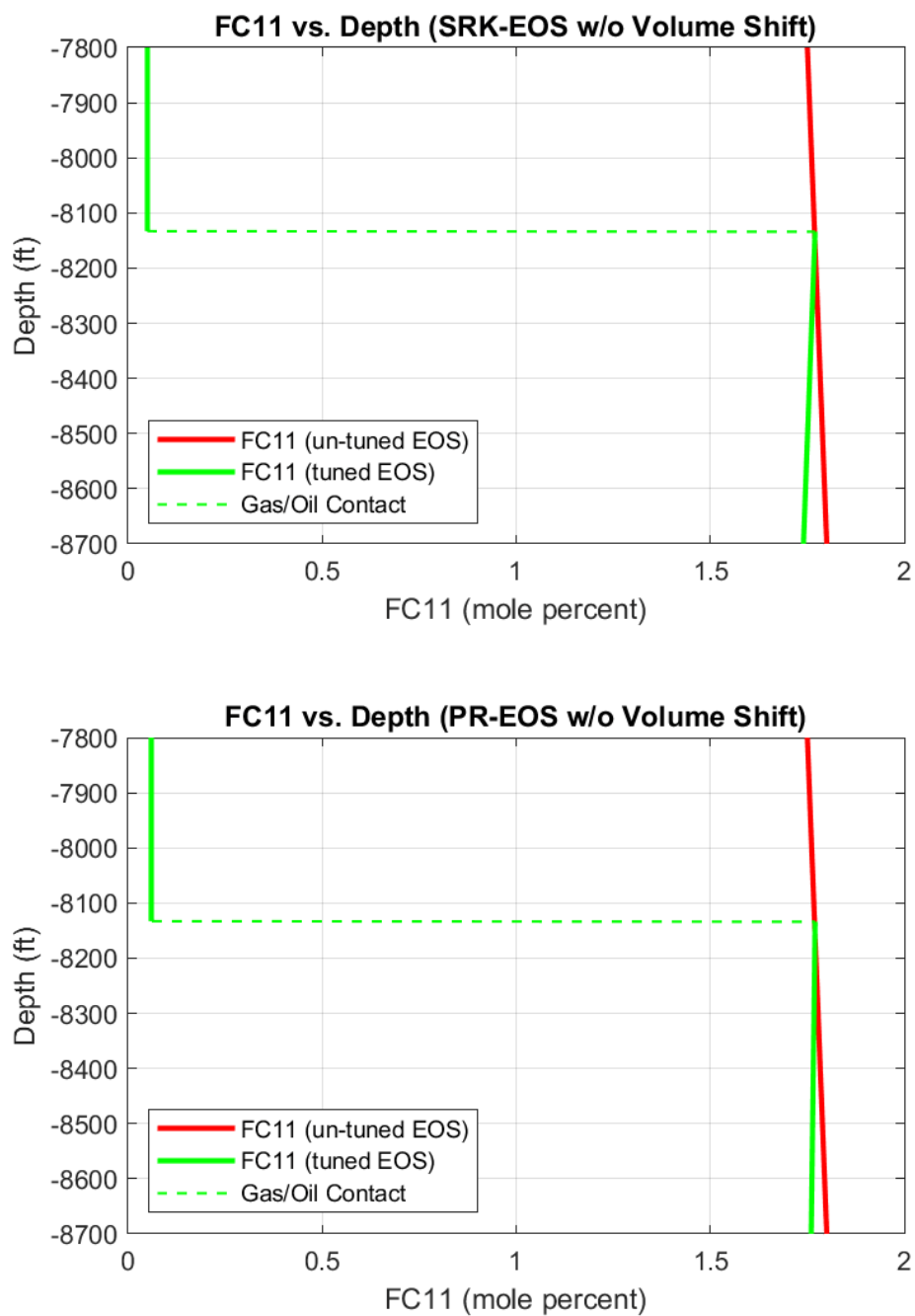


Figure A.50: FC11 composition plots without volume shift using commercial software

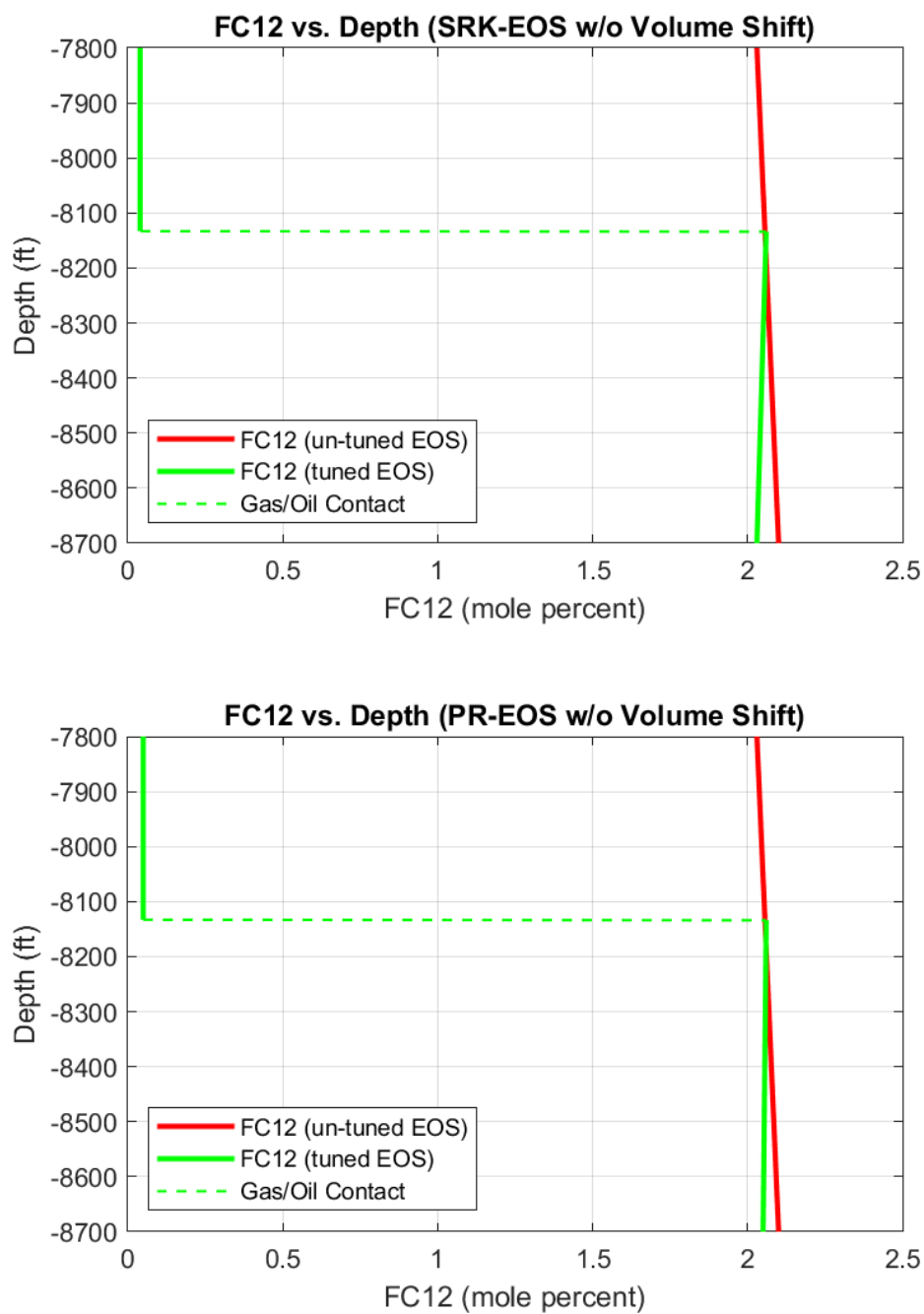


Figure A.51: FC12 composition plots without volume shift using commercial software

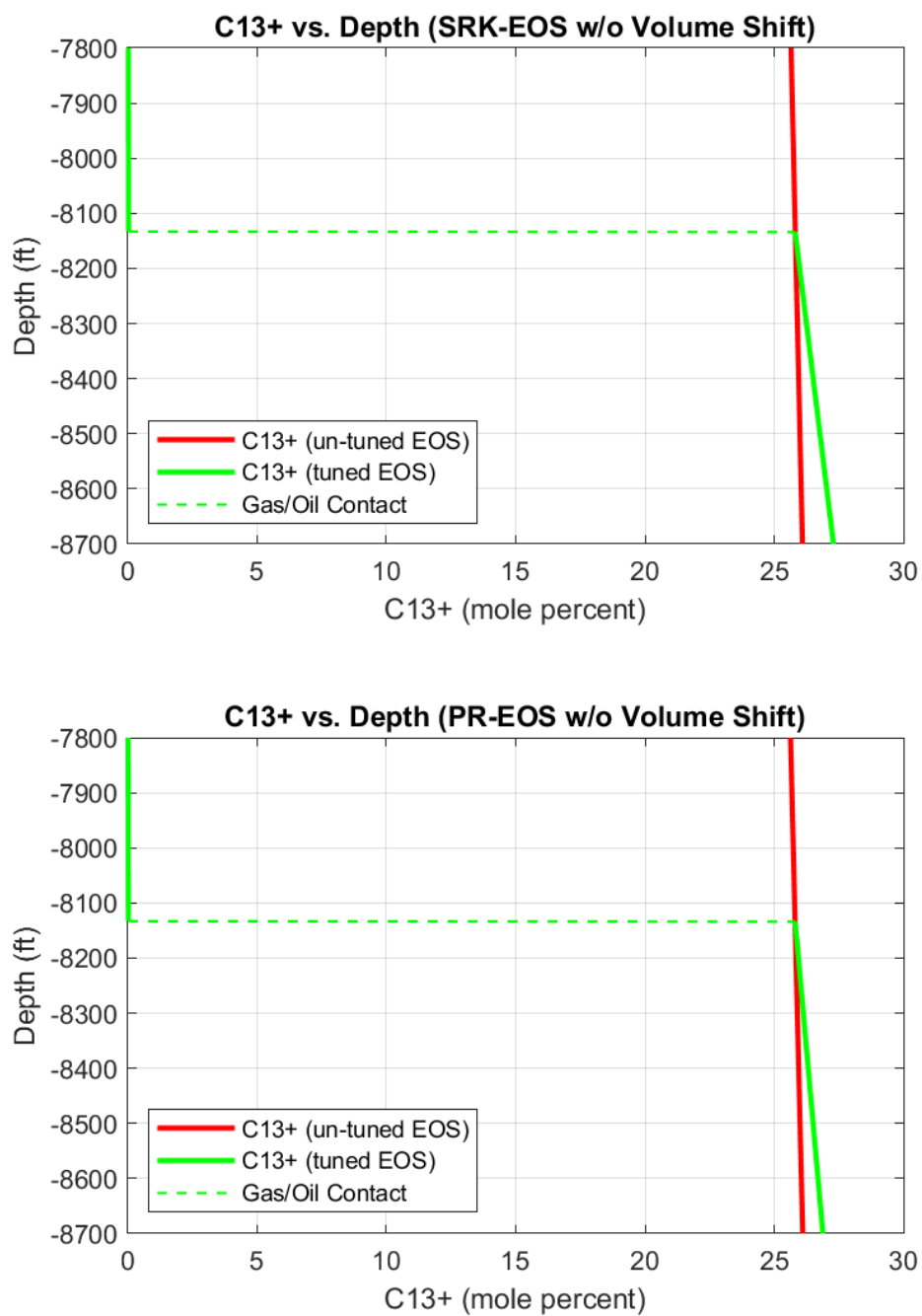


Figure A.52: C₁₃₊ composition plots without volume shift using commercial software

Table A.49: Saturation pressure calculation results for an un-tuned SRK-EOS using MATLAB®

Component	Composition (mole fraction)		K-values (y_i/z_i)	$\ln f_i$ (atm)
	Dominant phase (z_i)	Incipient phase (y_i)		
H ₂ S	0.1124	0.0574	0.5107	1.6560
CO ₂	0.0701	0.0583	0.8312	1.9731
N ₂	0.0117	0.0348	2.9716	2.0962
CH ₄	0.3870	0.8204	2.1201	4.9113
C ₂ H ₆	0.0152	0.0157	1.0329	0.3944
C ₃ H ₈	0.0069	0.0042	0.6087	-1.3530
IC ₄	0.0025	0.0010	0.4192	-3.0528
NC ₄	0.0048	0.0017	0.3568	-2.6638
IC ₅	0.0034	0.0008	0.2404	-3.7154
NC ₅	0.0032	0.0007	0.2143	-3.9829
FC ₆	0.0106	0.0014	0.1344	-3.5768
FC ₇	0.0090	0.0007	0.0829	-4.5616
FC ₈	0.0201	0.0011	0.0530	-4.5229
FC ₉	0.0259	0.0008	0.0326	-5.1109
FC ₁₀	0.0209	0.0004	0.0197	-6.1864
FC ₁₁	0.0177	0.0002	0.0127	-7.1194
FC ₁₂	0.0206	0.0002	0.0078	-7.8040
C ₁₃ +	0.2581	0.0000	0.0001	-13.9750
Z-factor	1.4372	0.8704		

- Calculated saturation pressure value: $p_{\text{sat}}=2823.6105$ psia.

Table A.50: Saturation pressure calculation results for an un-tuned PR-EOS using MATLAB®

Component	Composition (mole percent)		K-values (y_i/z_i)	$\ln f_i$ (atm)
	Dominant phase (z_i)	Incipient phase (y_i)		
H ₂ S	0.1124	0.0632	0.5620	1.6648
CO ₂	0.0701	0.0602	0.8593	1.9229
N ₂	0.0117	0.0330	2.8181	1.9896
CH ₄	0.3870	0.8126	2.0999	4.8283
C ₂ H ₆	0.0152	0.0162	1.0634	0.3185
C ₃ H ₈	0.0069	0.0044	0.6374	-1.4416
IC ₄	0.0025	0.0011	0.4425	-3.1574
NC ₄	0.0048	0.0018	0.3824	-2.7579
IC ₅	0.0034	0.0009	0.2610	-3.8204
NC ₅	0.0032	0.0007	0.2344	-4.0843
FC ₆	0.0106	0.0016	0.1510	-3.6650
FC ₇	0.0090	0.0009	0.0957	-4.6408
FC ₈	0.0201	0.0013	0.0628	-4.5951
FC ₉	0.0259	0.0010	0.0396	-5.1763
FC ₁₀	0.0209	0.0005	0.0247	-6.2393
FC ₁₁	0.0177	0.0003	0.0163	-7.1634
FC ₁₂	0.0206	0.0002	0.0103	-7.8302
C ₁₃ +	0.2581	0.0000	0.0001	-13.5478
Z-factor	1.2793	0.8132		

- Calculated saturation pressure value: $p_{\text{sat}}=2803.0249$ psia.

Appendix A: Supplementary Tables and Figures

Table A.51: Un-tuned EOS two-phase flash calculation results using MATLAB®

Component	Composition (mole fraction)	$\ln f_i$ (atm)	
	Liquid phase (x_i)	SRK EOS	PR EOS
H ₂ S	0.1124	1.7971	1.7946
CO ₂	0.0701	2.1199	2.0580
N ₂	0.0117	2.2510	2.1329
CH ₄	0.3870	5.0688	4.9739
C ₂ H ₆	0.0152	0.5835	0.4922
C ₃ H ₈	0.0069	-1.1227	-1.2306
IC ₄	0.0025	-2.7785	-2.9066
NC ₄	0.0048	-2.3917	-2.5092
IC ₅	0.0034	-3.4009	-3.5333
NC ₅	0.0032	-3.6638	-3.7931
FC ₆	0.0106	-3.2341	-3.3524
FC ₇	0.0090	-4.1881	-4.3005
FC ₈	0.0201	-4.1152	-4.2238
FC ₉	0.0259	-4.6583	-4.7642
FC ₁₀	0.0209	-5.6884	-5.7860
FC ₁₁	0.0177	-6.5705	-6.6636
FC ₁₂	0.0206	-7.2044	-7.2842
C ₁₃₊	0.2581	-12.6173	-12.3065
Z-factor	SRK EOS	PR EOS	
	1.9256	1.7276	

Appendix A: Supplementary Tables and Figures

Table A.52: CO₂, N₂, C₂H₆ compositional gradient results for the tuned SRK and PR EOS models with volume shift using MATLAB®

Depth (ft)	CO ₂ (mole fraction)		N ₂ (mole fraction)		C ₂ H ₆ (mole fraction)	
	SRK EOS	PR EOS	SRK EOS	PR EOS	SRK EOS	PR EOS
7800	0.0575	0.0578	0.0340	0.0320	0.0168	0.0173
7890	0.0577	0.0580	0.0340	0.0320	0.0168	0.0174
7980	0.0578	0.0582	0.0340	0.0320	0.0169	0.0174
8070	0.0580	0.0584	0.0339	0.0319	0.0169	0.0174
8133.98	0.0582	0.0585	0.0339	0.0319	0.0169	0.0175
8134	0.0701	0.0701	0.0117	0.0117	0.0152	0.0152
8160	0.0701	0.0701	0.0117	0.0117	0.0152	0.0152
8250	0.0702	0.0701	0.0116	0.0117	0.0151	0.0151
8340	0.0702	0.0702	0.0116	0.0116	0.0150	0.0150
8430	0.0702	0.0702	0.0115	0.0116	0.0149	0.0150
8520	0.0703	0.0702	0.0115	0.0115	0.0149	0.0149
8610	0.0703	0.0702	0.0114	0.0115	0.0148	0.0148
8700	0.0703	0.0703	0.0114	0.0114	0.0147	0.0147

Table A.53: C₃H₈, IC₄, NC₄ compositional gradient results for the tuned SRK and PR EOS models with volume shift using MATLAB®

Depth (ft)	C ₃ H ₈ (mole fraction)		IC ₄ (mole fraction)		NC ₄ (mole fraction)	
	SRK EOS	PR EOS	SRK EOS	PR EOS	SRK EOS	PR EOS
7800	0.0048	0.0051	0.0013	0.0014	0.0021	0.0023
7890	0.0049	0.0051	0.0013	0.0014	0.0022	0.0023
7980	0.0049	0.0051	0.0013	0.0014	0.0022	0.0023
8070	0.0049	0.0051	0.0013	0.0014	0.0022	0.0023
8133.98	0.0049	0.0051	0.0013	0.0014	0.0022	0.0023
8134	0.0069	0.0069	0.0025	0.0025	0.0048	0.0048
8160	0.0069	0.0069	0.0025	0.0025	0.0048	0.0048
8250	0.0068	0.0068	0.0025	0.0025	0.0048	0.0048
8340	0.0068	0.0068	0.0024	0.0025	0.0047	0.0047
8430	0.0068	0.0068	0.0024	0.0024	0.0047	0.0047
8520	0.0067	0.0067	0.0024	0.0024	0.0047	0.0047
8610	0.0067	0.0067	0.0024	0.0024	0.0047	0.0047
8700	0.0066	0.0067	0.0024	0.0024	0.0046	0.0047

Appendix A: Supplementary Tables and Figures

Table A.54: IC₅, NC₅, FC₆ compositional gradient results for the tuned SRK and PR EOS models with volume shift using MATLAB®

Depth (ft)	IC ₅ (mole fraction)		NC ₅ (mole fraction)		FC ₆ (mole fraction)	
	SRK EOS	PR EOS	SRK EOS	PR EOS	SRK EOS	PR EOS
7800	0.0011	0.0012	0.0009	0.0010	0.0020	0.0023
7890	0.0011	0.0012	0.0009	0.0010	0.0020	0.0023
7980	0.0011	0.0012	0.0010	0.0010	0.0021	0.0023
8070	0.0011	0.0012	0.0010	0.0010	0.0021	0.0023
8133.98	0.0011	0.0012	0.0010	0.0010	0.0021	0.0024
8134	0.0034	0.0034	0.0032	0.0032	0.0106	0.0106
8160	0.0034	0.0034	0.0032	0.0032	0.0105	0.0105
8250	0.0034	0.0034	0.0032	0.0032	0.0105	0.0105
8340	0.0034	0.0034	0.0032	0.0032	0.0105	0.0105
8430	0.0033	0.0033	0.0031	0.0031	0.0104	0.0104
8520	0.0033	0.0033	0.0031	0.0031	0.0104	0.0104
8610	0.0033	0.0033	0.0031	0.0031	0.0103	0.0103
8700	0.0033	0.0033	0.0031	0.0031	0.0103	0.0103

Table A.55: FC₇, FC₈, FC₉ compositional gradient results for the tuned SRK and PR EOS models with volume shift using MATLAB®

Depth (ft)	FC ₇ (mole fraction)		FC ₈ (mole fraction)		FC ₉ (mole fraction)	
	SRK EOS	PR EOS	SRK EOS	PR EOS	SRK EOS	PR EOS
7800	0.0011	0.0013	0.0017	0.0020	0.0015	0.0017
7890	0.0011	0.0013	0.0017	0.0020	0.0015	0.0018
7980	0.0012	0.0013	0.0018	0.0021	0.0015	0.0018
8070	0.0012	0.0013	0.0018	0.0021	0.0016	0.0018
8133.98	0.0012	0.0014	0.0018	0.0021	0.0016	0.0019
8134	0.0090	0.0090	0.0201	0.0201	0.0258	0.0258
8160	0.0090	0.0090	0.0201	0.0201	0.0258	0.0258
8250	0.0090	0.0090	0.0200	0.0200	0.0258	0.0258
8340	0.0089	0.0089	0.0200	0.0200	0.0257	0.0257
8430	0.0089	0.0089	0.0199	0.0199	0.0256	0.0256
8520	0.0089	0.0089	0.0198	0.0199	0.0255	0.0256
8610	0.0088	0.0088	0.0198	0.0198	0.0255	0.0255
8700	0.0088	0.0088	0.0197	0.0197	0.0254	0.0254

Appendix A: Supplementary Tables and Figures

Table A.56: FC₁₀, FC₁₁, FC₁₂ compositional gradient results for the tuned SRK and PR EOS models with volume shift using MATLAB®

Depth (ft)	FC ₁₀ (mole fraction)		FC ₁₁ (mole fraction)		FC ₁₂ (mole fraction)	
	SRK EOS	PR EOS	SRK EOS	PR EOS	SRK EOS	PR EOS
7800	0.0008	0.0009	0.0005	0.0006	0.0004	0.0005
7890	0.0008	0.0010	0.0005	0.0006	0.0004	0.0005
7980	0.0008	0.0010	0.0005	0.0006	0.0004	0.0005
8070	0.0008	0.0010	0.0005	0.0006	0.0004	0.0005
8133.98	0.0008	0.0010	0.0005	0.0006	0.0004	0.0005
8134	0.0209	0.0209	0.0177	0.0177	0.0206	0.0206
8160	0.0209	0.0209	0.0177	0.0177	0.0206	0.0206
8250	0.0208	0.0208	0.0176	0.0176	0.0205	0.0205
8340	0.0208	0.0208	0.0176	0.0176	0.0205	0.0205
8430	0.0207	0.0207	0.0176	0.0176	0.0205	0.0205
8520	0.0207	0.0207	0.0175	0.0175	0.0204	0.0204
8610	0.0206	0.0206	0.0175	0.0175	0.0204	0.0204
8700	0.0206	0.0206	0.0174	0.0174	0.0203	0.0203

Table 5.57: Reservoir and saturation pressure gradient results for the un-tuned SRK and PR EOS models with volume shift using MATLAB®

Depth (ft)	Reservoir Pressure (psia)		Saturation Pressure (psia)	
	SRK EOS	PR EOS	SRK EOS	PR EOS
7800	3730.39	3723.13	2872.52	2858.47
7890	3756.15	3750.83	2859.14	2843.26
7980	3781.93	3778.57	2845.90	2828.26
8070	3807.74	3806.34	2832.82	2813.44
8134	3826.10	3826.10	2823.63	2803.04
8160	3833.56	3834.13	2819.89	2798.82
8250	3859.41	3861.96	2807.11	2784.38
8340	3885.28	3889.81	2794.50	2770.13
8430	3911.17	3917.70	2781.99	2756.05
8520	3937.08	3945.61	2769.65	2742.14
8610	3963.01	3973.55	2757.43	2728.39
8700	3988.97	4001.52	2745.35	2714.81

Appendix A: Supplementary Tables and Figures

Table A.58: H₂S, CO₂, N₂ compositional gradient results for the un-tuned SRK and PR EOS models with volume shift using MATLAB®

Depth (ft)	H ₂ S (mole fraction)		CO ₂ (mole fraction)		N ₂ (mole fraction)	
	SRK EOS	PR EOS	SRK EOS	PR EOS	SRK EOS	PR EOS
7800	0.1124	0.1125	0.0699	0.0699	0.0118	0.0118
7890	0.1124	0.1125	0.0699	0.0700	0.0118	0.0118
7980	0.1124	0.1125	0.0700	0.0700	0.0118	0.0118
8070	0.1124	0.1125	0.0701	0.0701	0.0117	0.0117
8134	0.1124	0.1124	0.0701	0.0701	0.0117	0.0117
8160	0.1125	0.1124	0.0701	0.0701	0.0117	0.0117
8250	0.1125	0.1124	0.0702	0.0702	0.0117	0.0117
8340	0.1125	0.1124	0.0702	0.0702	0.0117	0.0117
8430	0.1125	0.1124	0.0703	0.0703	0.0117	0.0116
8520	0.1125	0.1123	0.0704	0.0703	0.0116	0.0116
8610	0.1125	0.1123	0.0704	0.0704	0.0116	0.0116
8700	0.1125	0.1123	0.0705	0.0704	0.0116	0.0116

Table A.59: CH₄, C₂H₆, C₃H₈ compositional gradient results for the un-tuned SRK and PR EOS models with volume shift using MATLAB®

Depth (ft)	CH ₄ (mole fraction)		C ₂ H ₆ (mole fraction)		C ₃ H ₈ (mole fraction)	
	SRK EOS	PR EOS	SRK EOS	PR EOS	SRK EOS	PR EOS
7800	0.3919	0.3912	0.0153	0.0154	0.0069	0.0069
7890	0.3905	0.3901	0.0153	0.0153	0.0069	0.0069
7980	0.3892	0.3889	0.0153	0.0153	0.0069	0.0069
8070	0.3879	0.3878	0.0152	0.0152	0.0069	0.0069
8134	0.3870	0.3870	0.0152	0.0152	0.0069	0.0069
8160	0.3866	0.3867	0.0152	0.0152	0.0069	0.0069
8250	0.3853	0.3855	0.0152	0.0152	0.0069	0.0069
8340	0.3840	0.3844	0.0151	0.0151	0.0068	0.0068
8430	0.3828	0.3833	0.0151	0.0151	0.0068	0.0068
8520	0.3815	0.3822	0.0151	0.0150	0.0068	0.0068
8610	0.3802	0.3811	0.0151	0.0150	0.0068	0.0068
8700	0.3790	0.3800	0.0150	0.0150	0.0068	0.0068

Appendix A: Supplementary Tables and Figures

Table A.60: IC₄, NC₄, IC₅ compositional gradient results for the un-tuned SRK and PR EOS models with volume shift using MATLAB®

Depth (ft)	IC ₄ (mole fraction)		NC ₄ (mole fraction)		IC ₅ (mole fraction)	
	SRK EOS	PR EOS	SRK EOS	PR EOS	SRK EOS	PR EOS
7800	0.0025	0.0025	0.0048	0.0048	0.0034	0.0034
7890	0.0025	0.0025	0.0048	0.0048	0.0034	0.0034
7980	0.0025	0.0025	0.0048	0.0048	0.0034	0.0034
8070	0.0025	0.0025	0.0048	0.0048	0.0034	0.0034
8134	0.0025	0.0025	0.0048	0.0048	0.0034	0.0034
8160	0.0025	0.0025	0.0048	0.0048	0.0034	0.0034
8250	0.0025	0.0025	0.0048	0.0048	0.0034	0.0034
8340	0.0025	0.0025	0.0048	0.0048	0.0034	0.0034
8430	0.0025	0.0025	0.0048	0.0048	0.0034	0.0034
8520	0.0025	0.0025	0.0048	0.0048	0.0034	0.0034
8610	0.0025	0.0025	0.0048	0.0047	0.0034	0.0034
8700	0.0025	0.0024	0.0048	0.0047	0.0034	0.0034

Table A.61: NC₅, FC₆, FC₇ compositional gradient results for the un-tuned SRK and PR EOS models with volume shift using MATLAB®

Depth (ft)	NC ₅ (mole fraction)		FC ₆ (mole fraction)		FC ₇ (mole fraction)	
	SRK EOS	PR EOS	SRK EOS	PR EOS	SRK EOS	PR EOS
7800	0.0032	0.0032	0.0106	0.0106	0.0090	0.0090
7890	0.0032	0.0032	0.0106	0.0106	0.0090	0.0090
7980	0.0032	0.0032	0.0106	0.0106	0.0090	0.0090
8070	0.0032	0.0032	0.0106	0.0106	0.0090	0.0090
8134	0.0032	0.0032	0.0106	0.0106	0.0090	0.0090
8160	0.0032	0.0032	0.0106	0.0106	0.0090	0.0090
8250	0.0032	0.0032	0.0106	0.0106	0.0090	0.0090
8340	0.0032	0.0032	0.0106	0.0105	0.0090	0.0090
8430	0.0032	0.0032	0.0106	0.0105	0.0090	0.0090
8520	0.0032	0.0032	0.0106	0.0105	0.0090	0.0090
8610	0.0032	0.0032	0.0106	0.0105	0.0090	0.0090
8700	0.0032	0.0032	0.0106	0.0105	0.0090	0.0090

Appendix A: Supplementary Tables and Figures

Table A.62: FC8, FC9, FC10 compositional gradient results for the un-tuned SRK and PR EOS models with volume shift using MATLAB®

Depth (ft)	FC8 (mole fraction)		FC9 (mole fraction)		FC10 (mole fraction)	
	SRK EOS	PR EOS	SRK EOS	PR EOS	SRK EOS	PR EOS
7800	0.0200	0.0201	0.0257	0.0258	0.0207	0.0208
7890	0.0200	0.0201	0.0257	0.0258	0.0207	0.0208
7980	0.0201	0.0201	0.0258	0.0258	0.0208	0.0208
8070	0.0201	0.0201	0.0258	0.0258	0.0208	0.0209
8134	0.0201	0.0201	0.0258	0.0258	0.0209	0.0209
8160	0.0201	0.0201	0.0259	0.0259	0.0209	0.0209
8250	0.0201	0.0201	0.0259	0.0259	0.0209	0.0209
8340	0.0202	0.0201	0.0260	0.0259	0.0210	0.0209
8430	0.0202	0.0201	0.0260	0.0259	0.0210	0.0210
8520	0.0202	0.0201	0.0260	0.0259	0.0211	0.0210
8610	0.0202	0.0201	0.0261	0.0260	0.0211	0.0210
8700	0.0203	0.0201	0.0261	0.0260	0.0212	0.0211

Table A.63: FC11, FC12, C13+ compositional gradient results for the un-tuned SRK and PR EOS models with volume shift using MATLAB®

Depth (ft)	FC11 (mole fraction)		FC12 (mole fraction)		C13+ (mole fraction)	
	SRK EOS	PR EOS	SRK EOS	PR EOS	SRK EOS	PR EOS
7800	0.0175	0.0176	0.0203	0.0204	0.2548	0.2535
7890	0.0175	0.0176	0.0204	0.0204	0.2557	0.2547
7980	0.0176	0.0176	0.0205	0.0205	0.2566	0.2560
8070	0.0176	0.0177	0.0205	0.0205	0.2575	0.2573
8134	0.0177	0.0177	0.0206	0.0206	0.2581	0.2581
8160	0.0177	0.0177	0.0206	0.0206	0.2584	0.2585
8250	0.0177	0.0177	0.0207	0.0206	0.2593	0.2597
8340	0.0178	0.0178	0.0207	0.0207	0.2602	0.2610
8430	0.0178	0.0178	0.0208	0.0207	0.2611	0.2622
8520	0.0179	0.0178	0.0209	0.0208	0.2619	0.2634
8610	0.0179	0.0178	0.0209	0.0208	0.2628	0.2646
8700	0.0180	0.0179	0.0210	0.0209	0.2636	0.2658

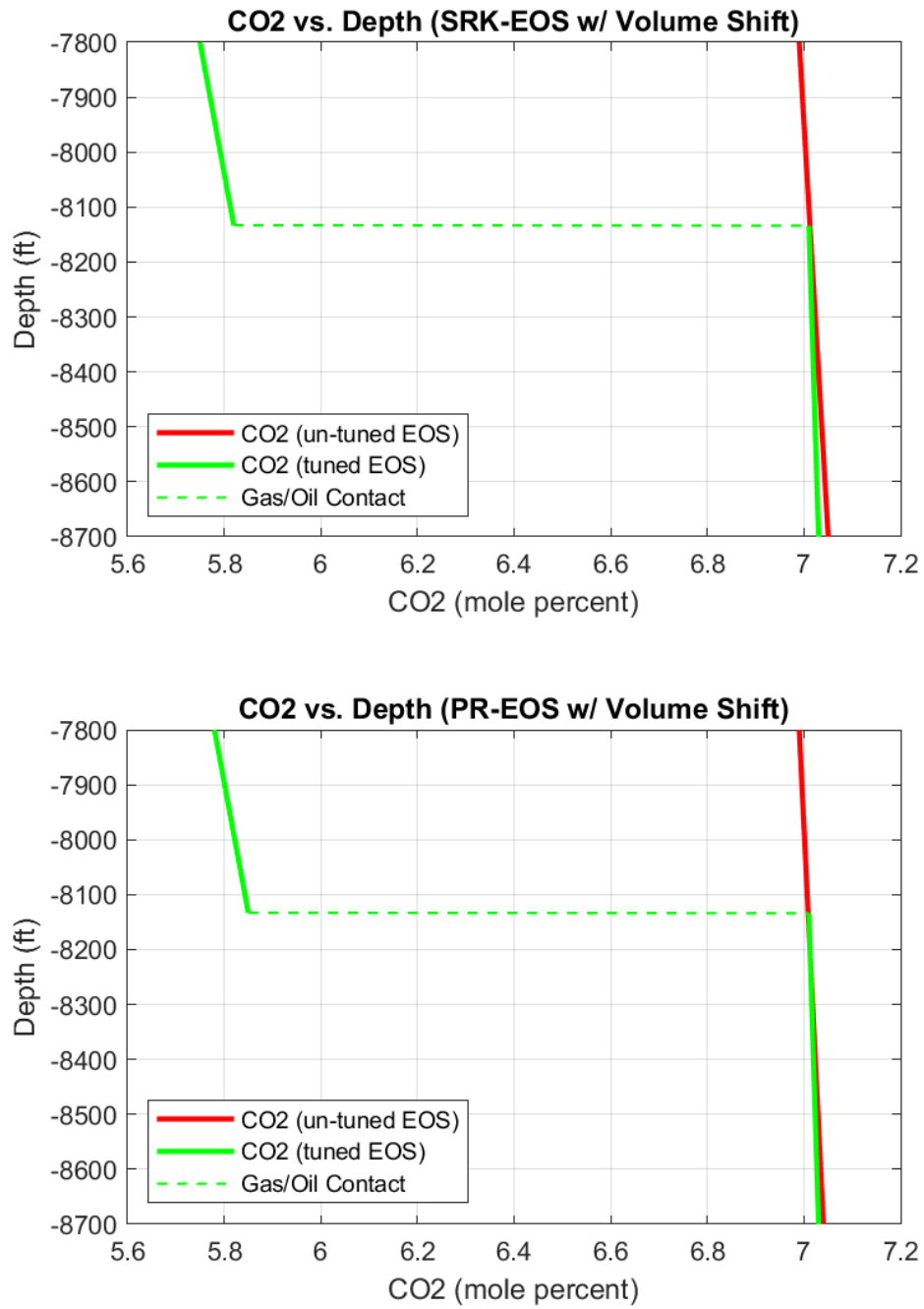


Figure A.53: CO₂ composition plots with volume shift using MATLAB®

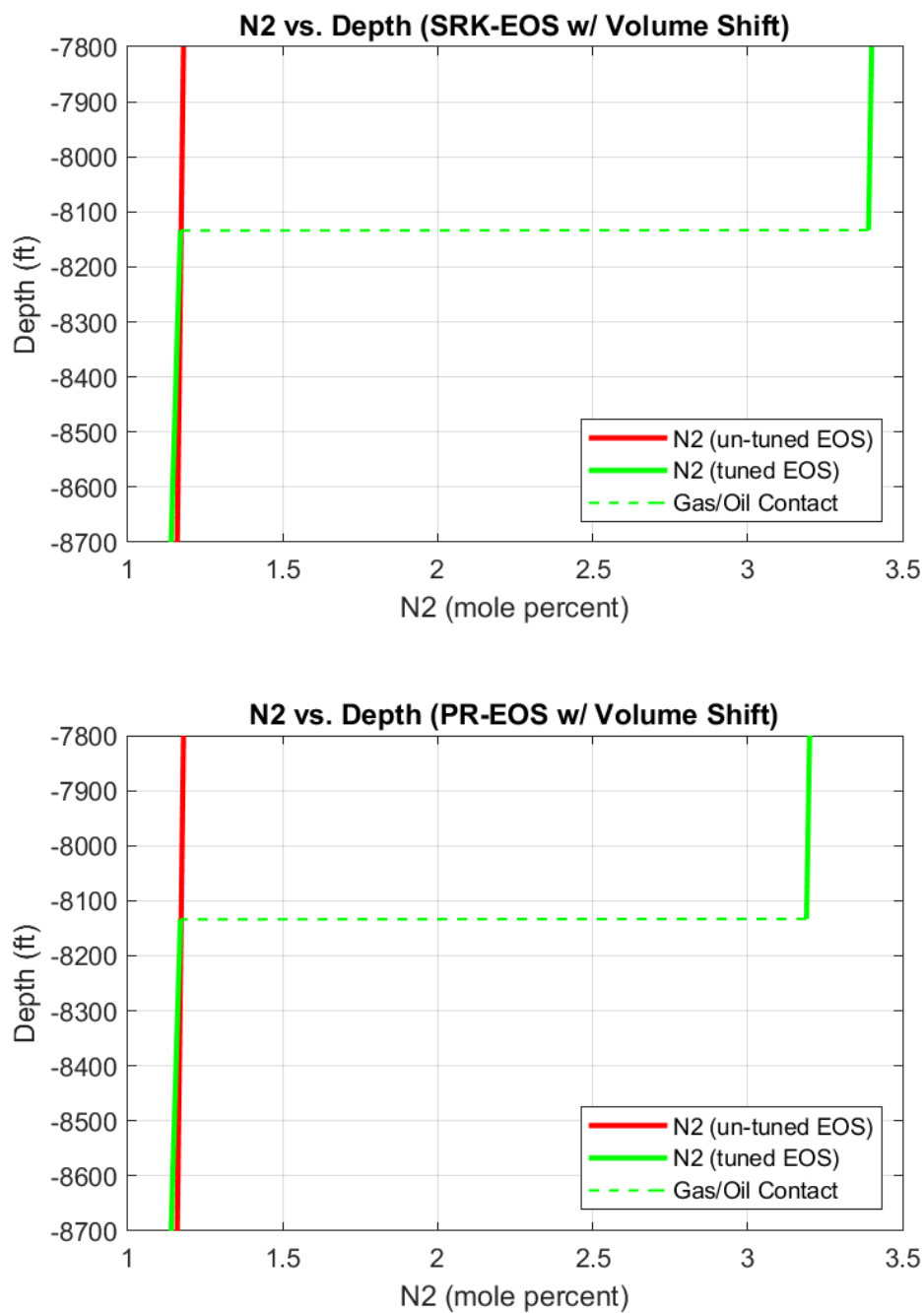


Figure A.54: N₂ composition plots with volume shift using MATLAB®

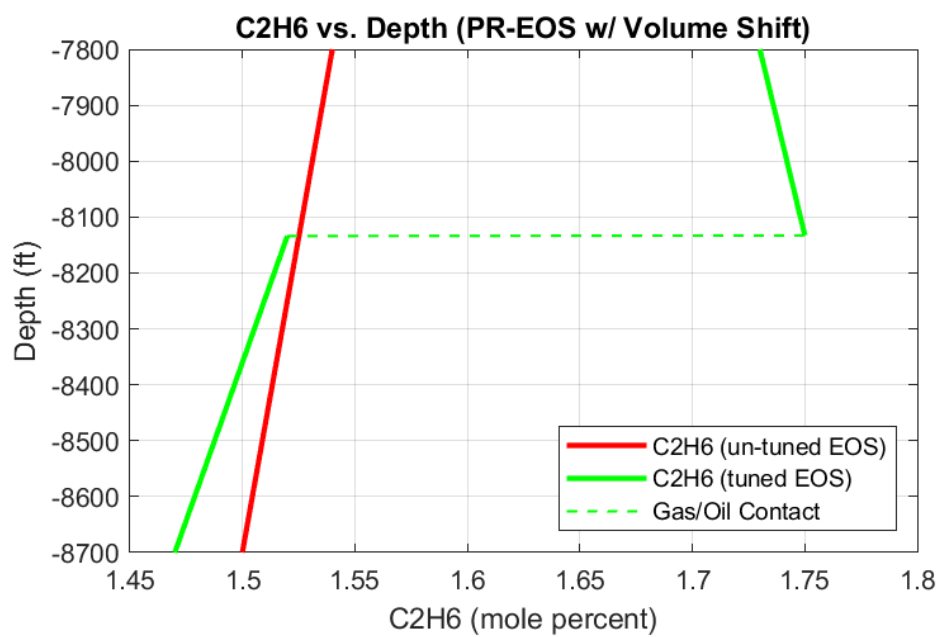
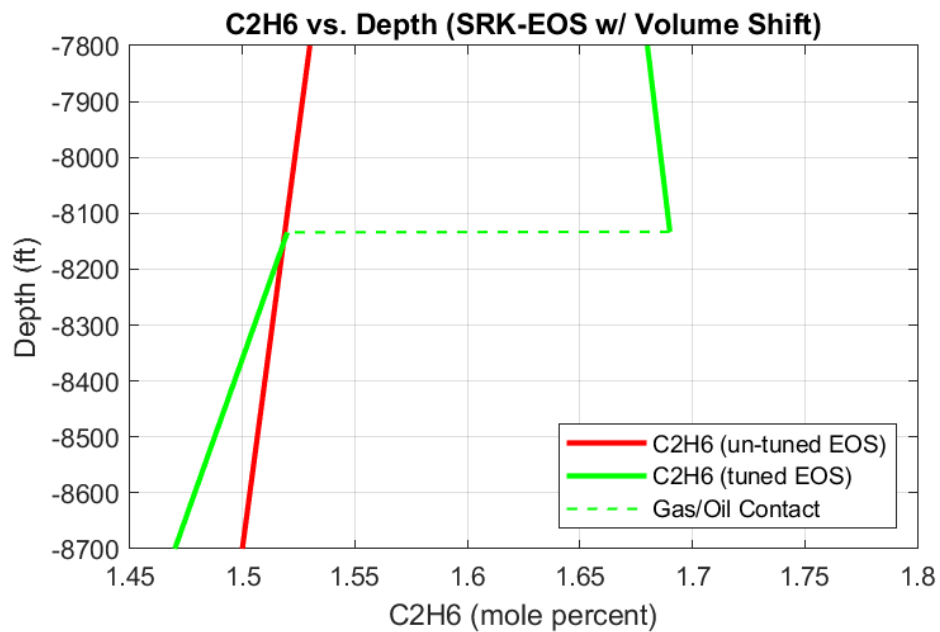


Figure A.55: C₂H₆ composition plots with volume shift using MATLAB®

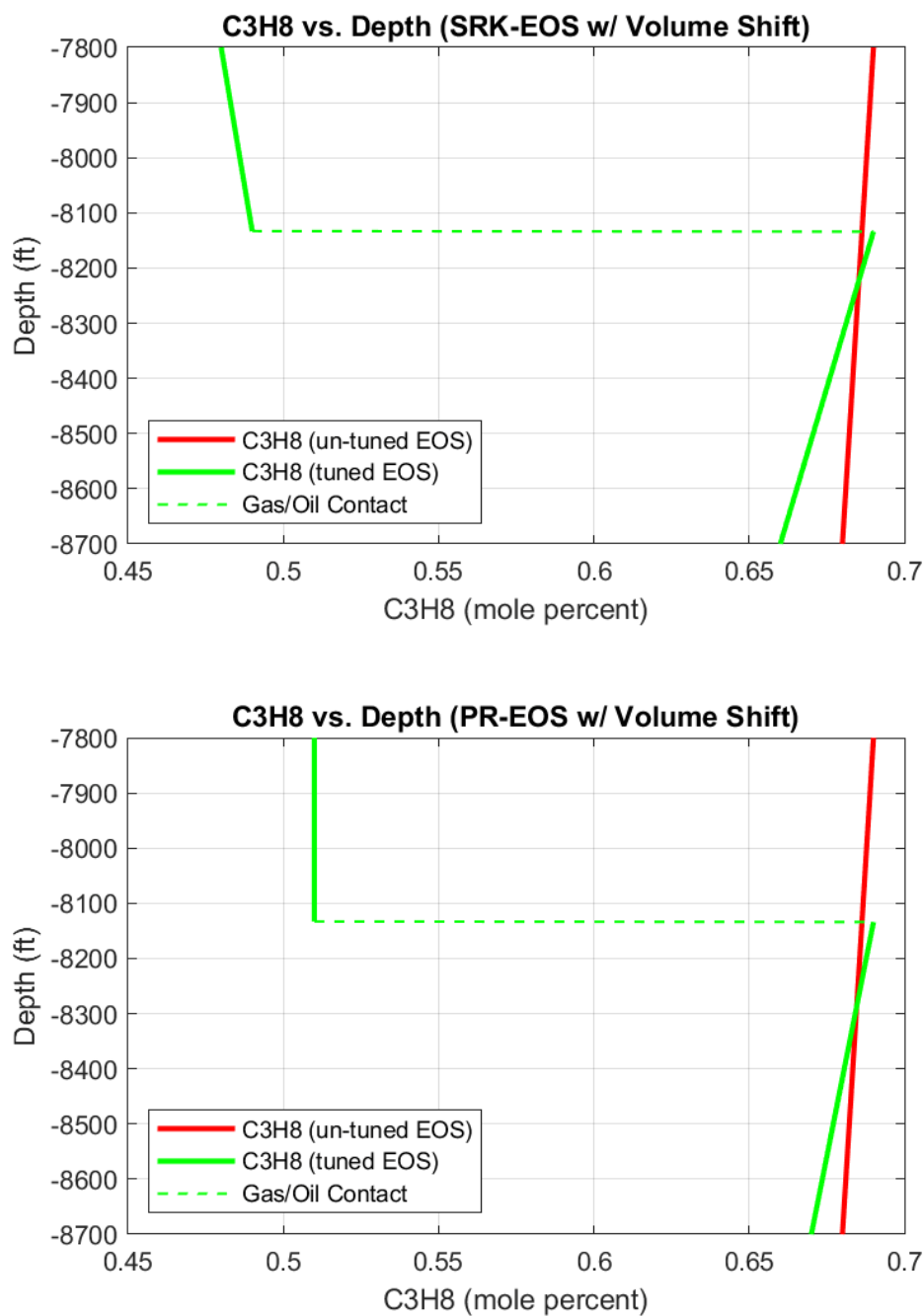


Figure A.56: C₃H₈ composition plots with volume shift using MATLAB®

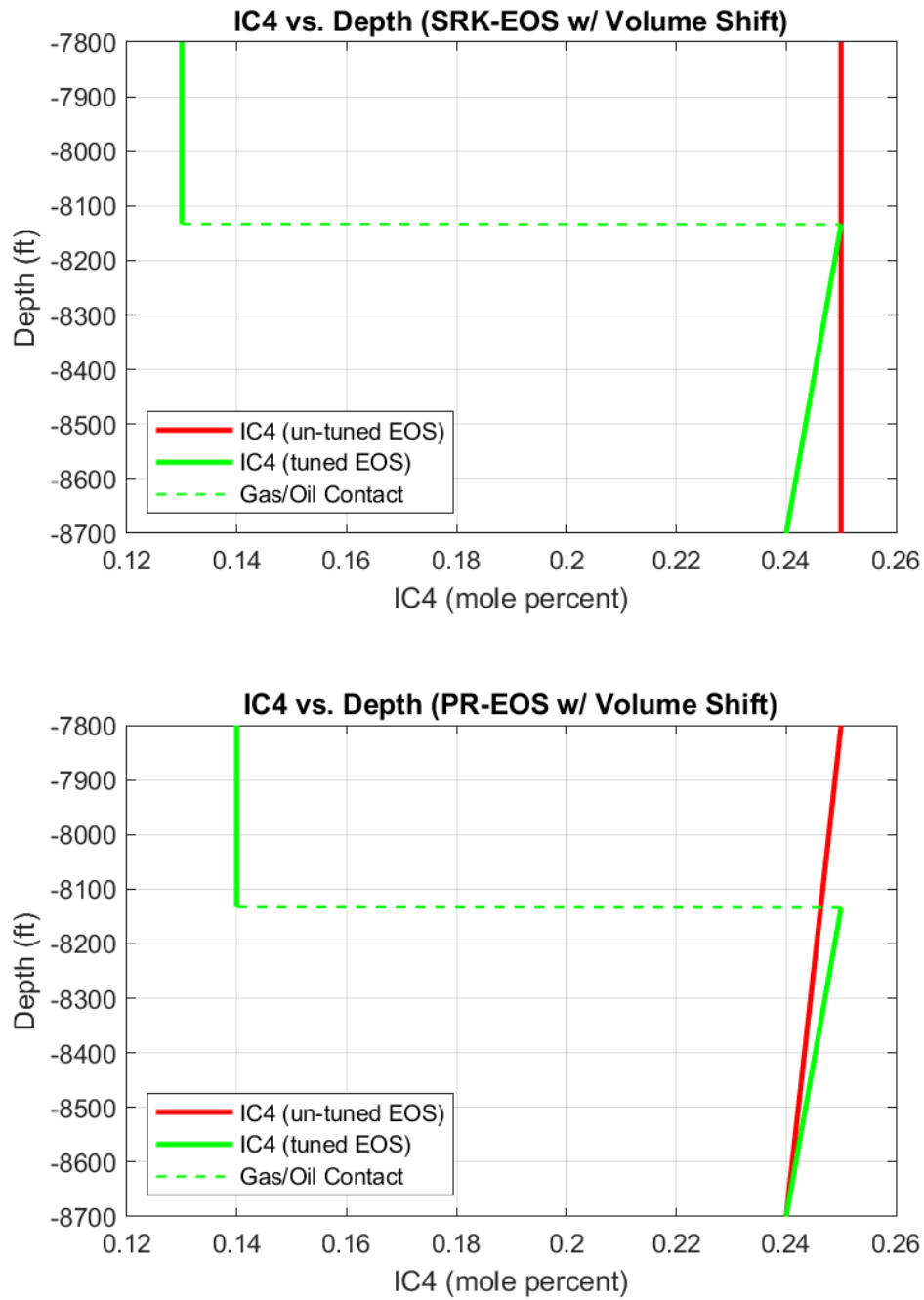


Figure A.57: IC4 composition plots with volume shift using MATLAB®

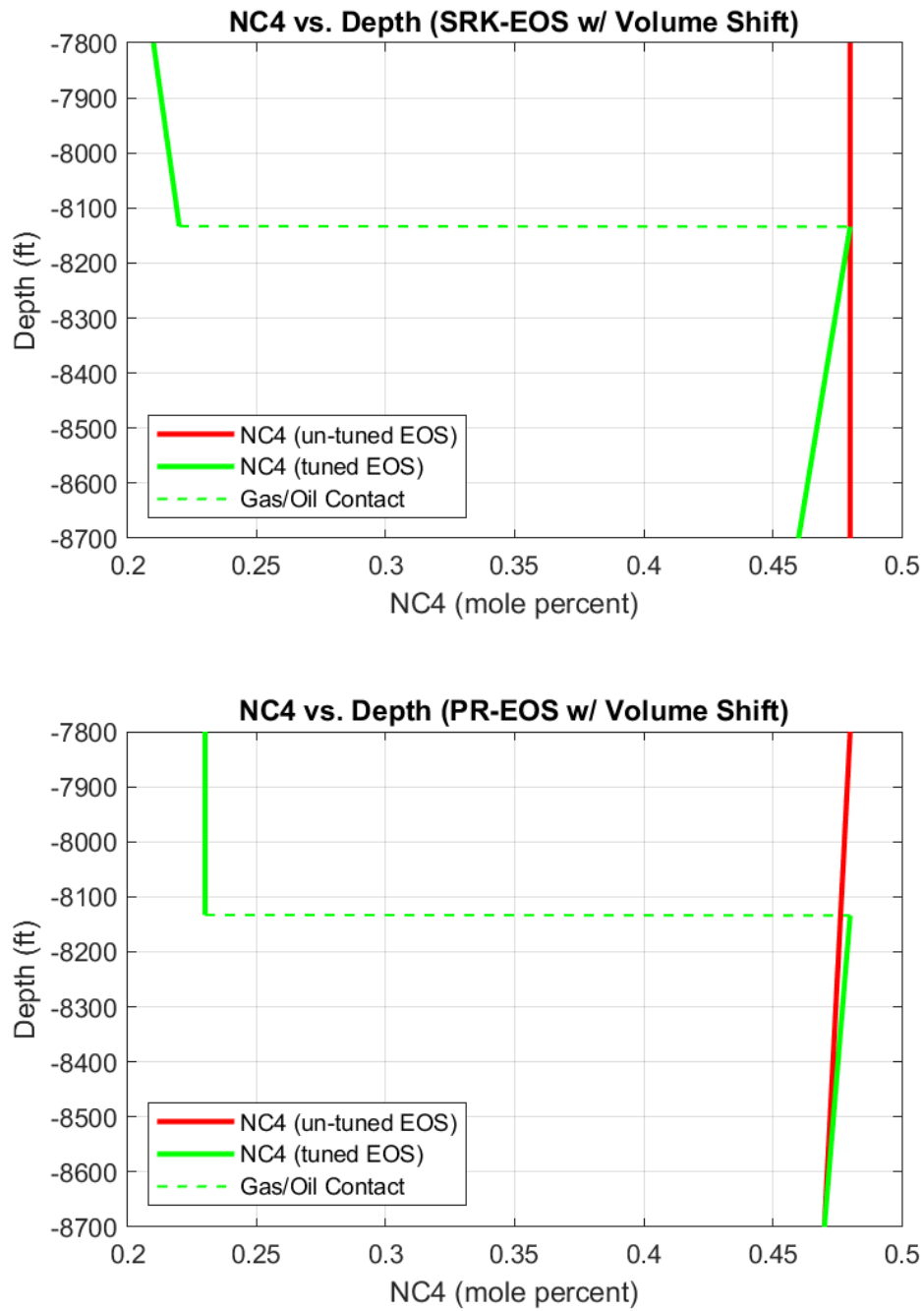


Figure A.58: NC₄ composition plots with volume shift using MATLAB®

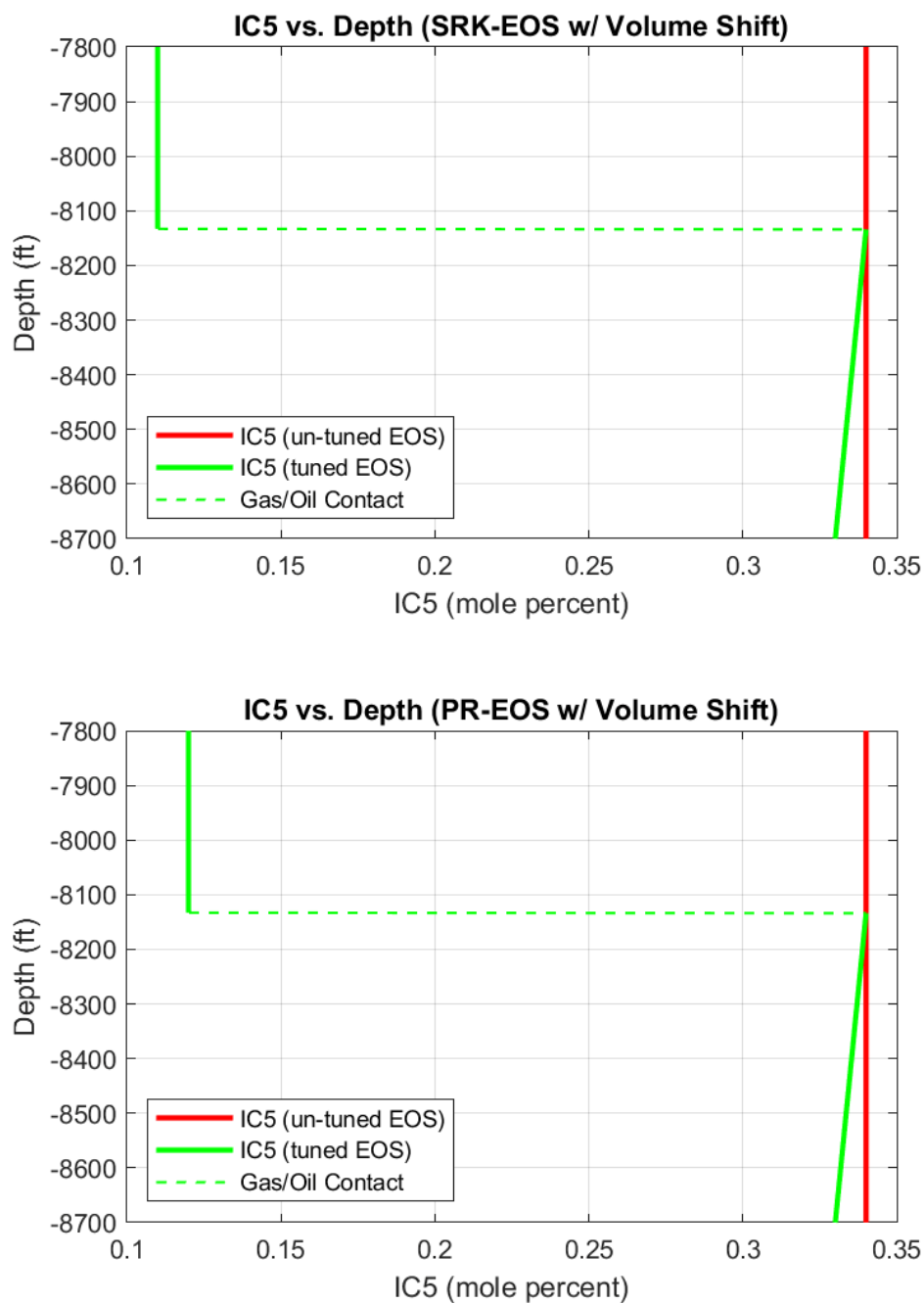


Figure A.59: IC5 composition plots with volume shift using MATLAB®

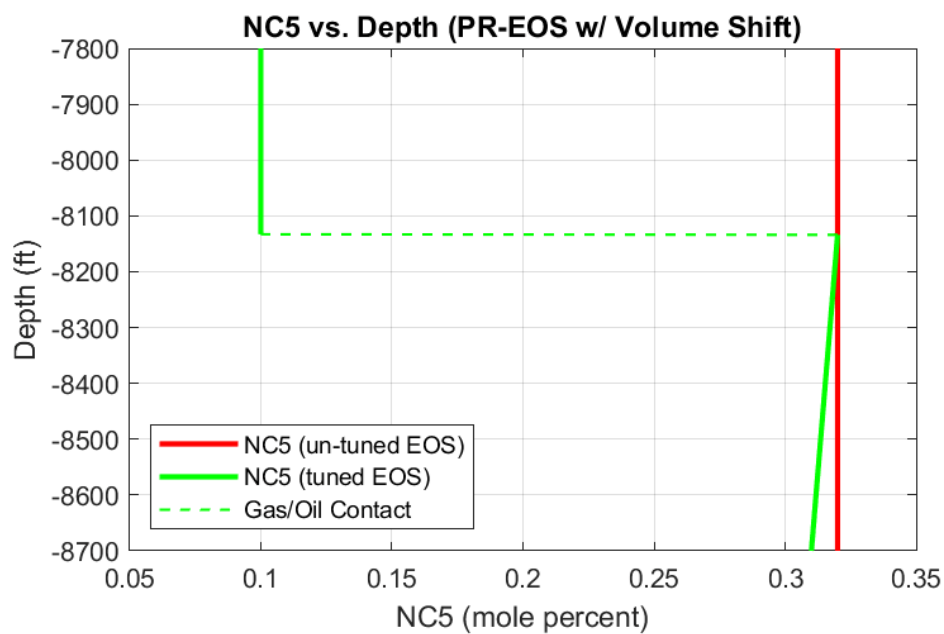
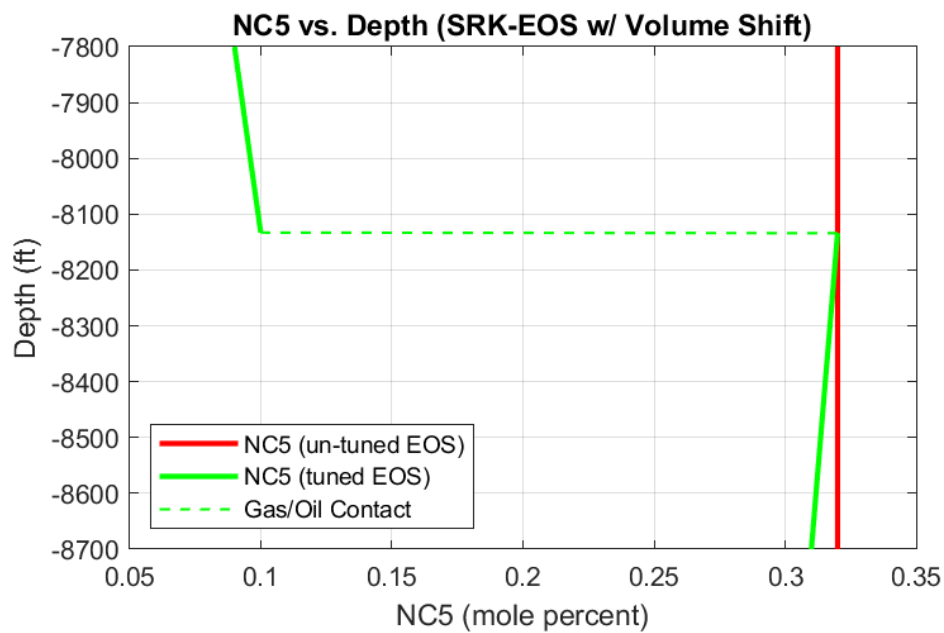


Figure A.6o: NC₅ composition plots with volume shift using MATLAB®

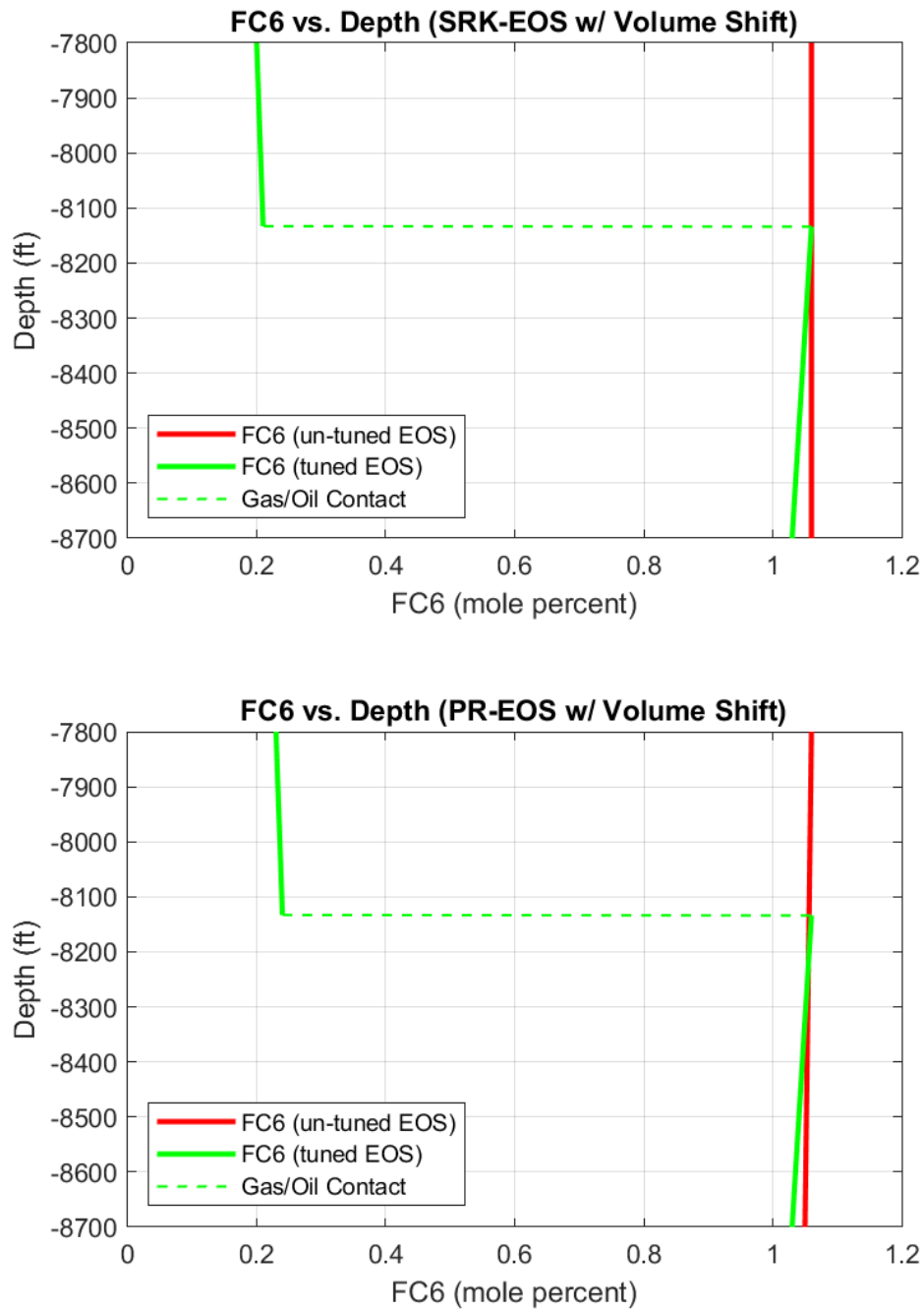


Figure A.61: FC6 composition plots with volume shift using MATLAB®

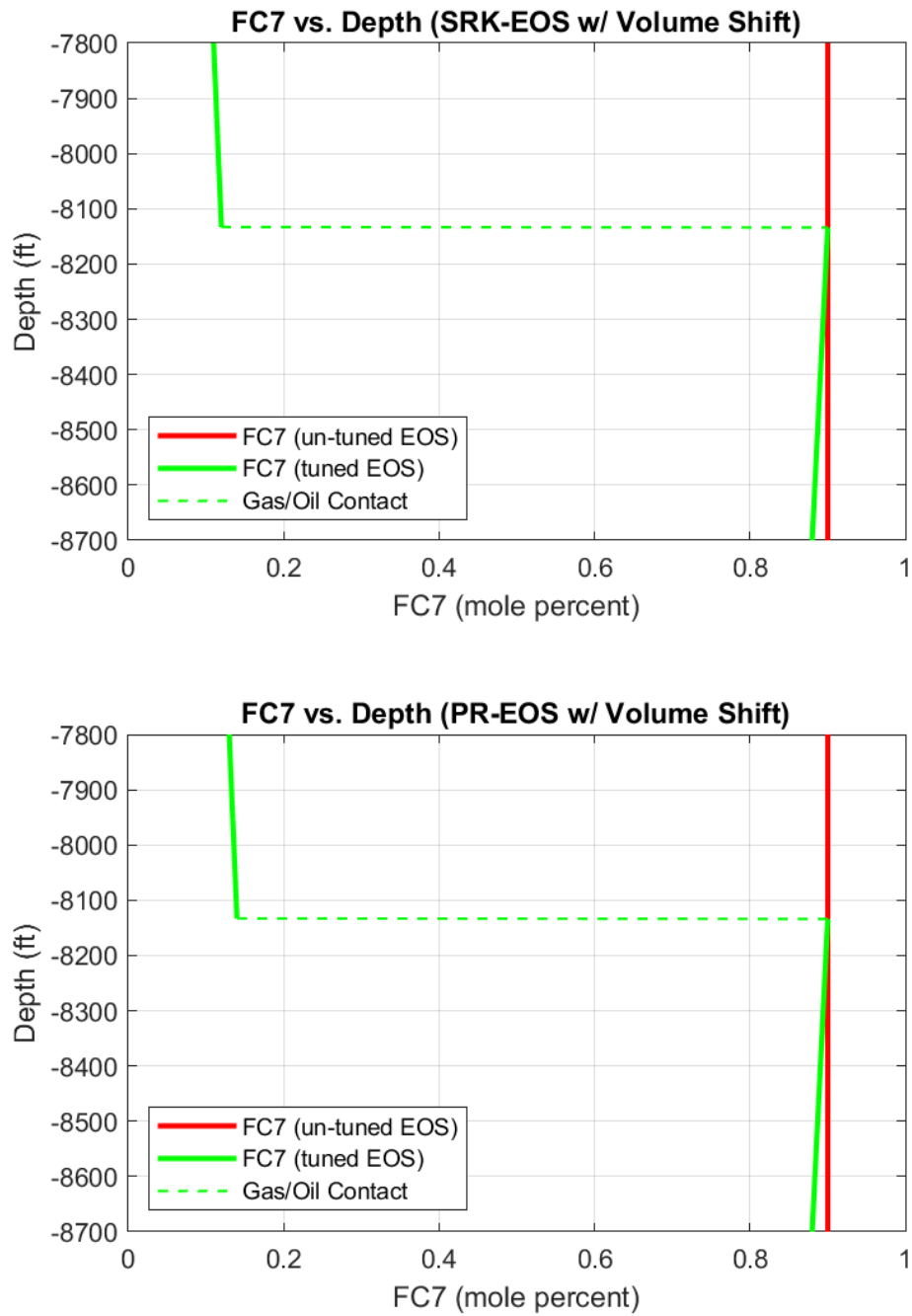


Figure A.62: FC7 composition plots with volume shift using MATLAB®

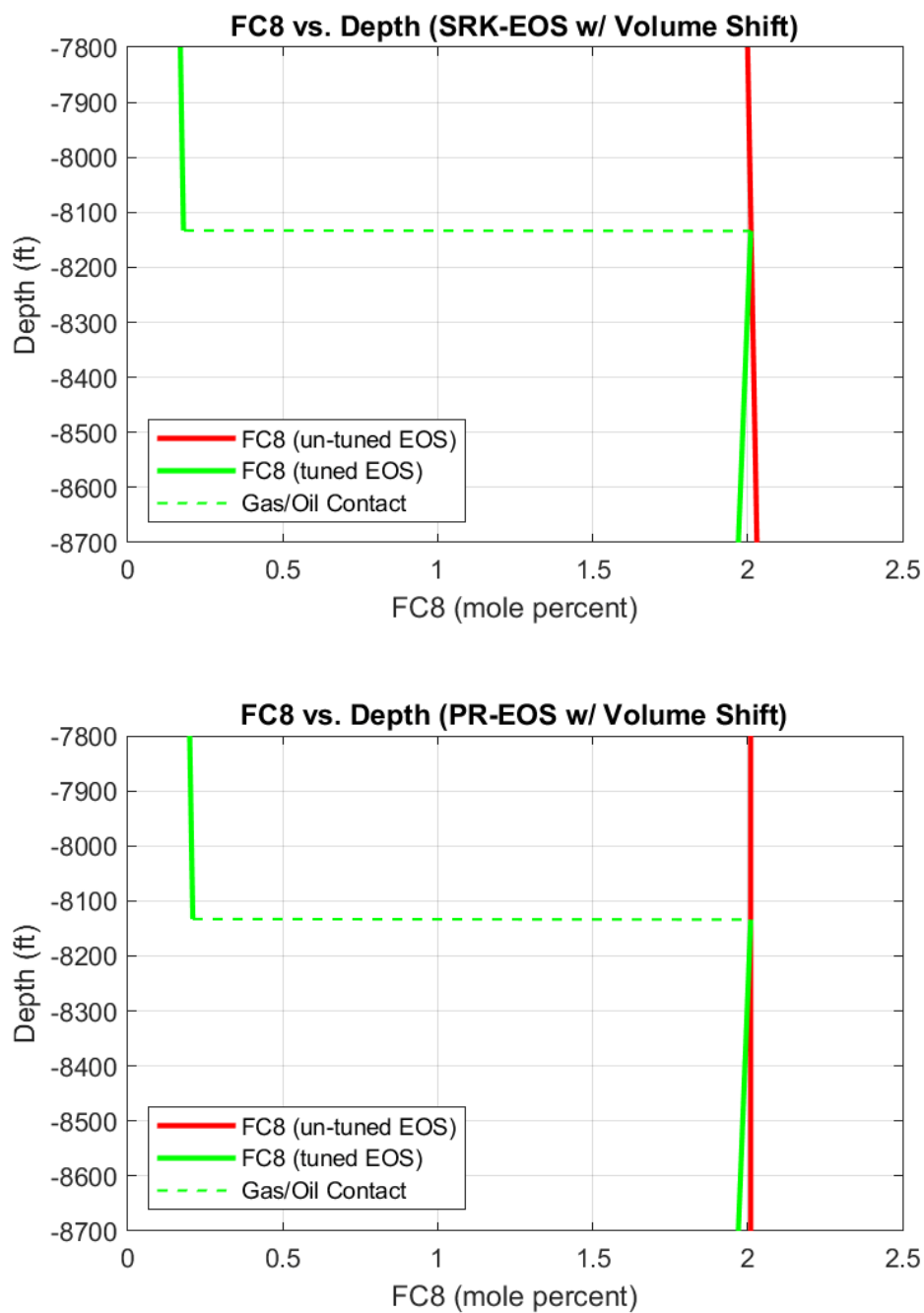


Figure A.63: FC8 composition plots with volume shift using MATLAB®

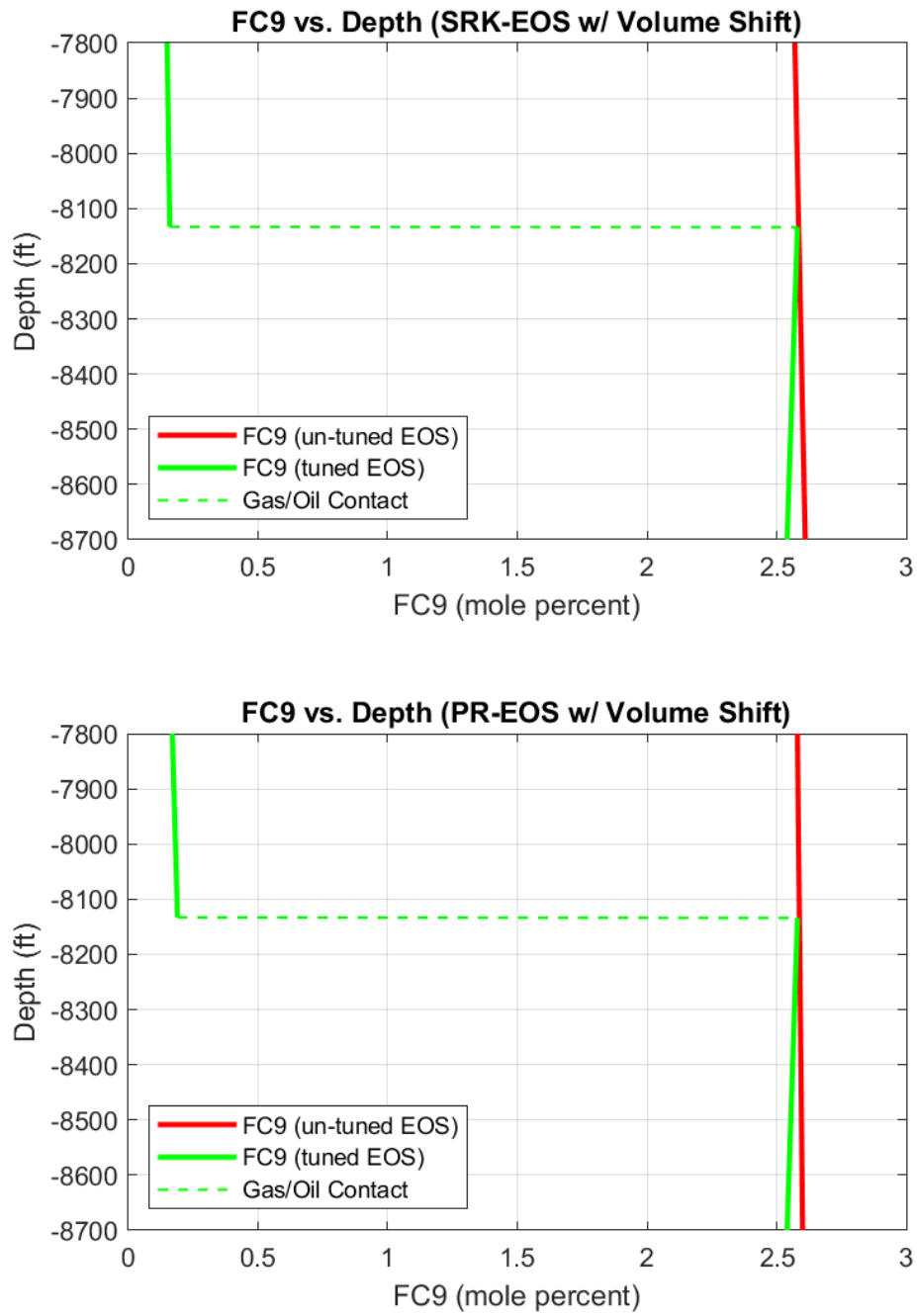


Figure A.64: FC9 composition plots with volume shift using MATLAB®

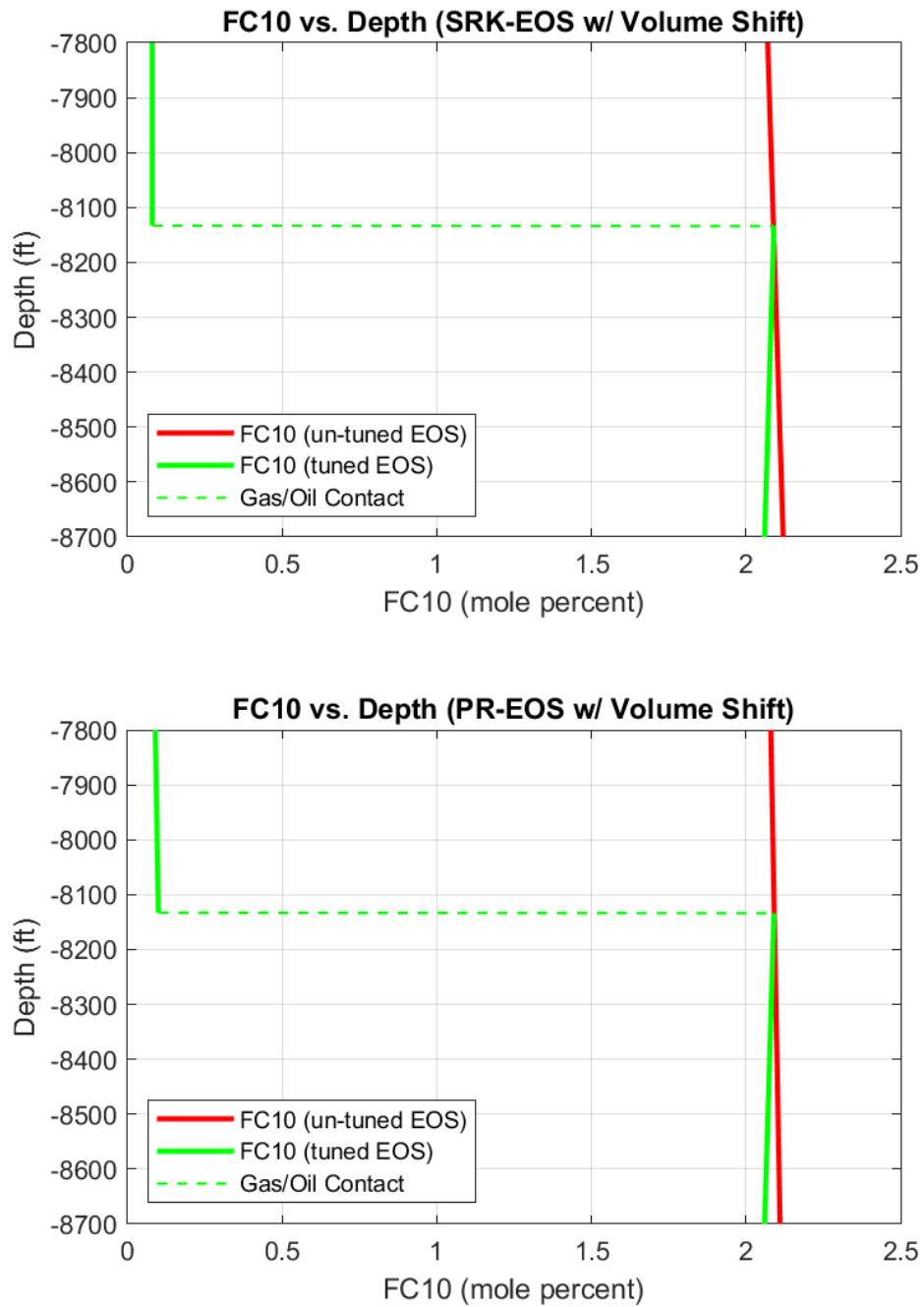


Figure A.65: FC10 composition plots with volume shift using MATLAB®

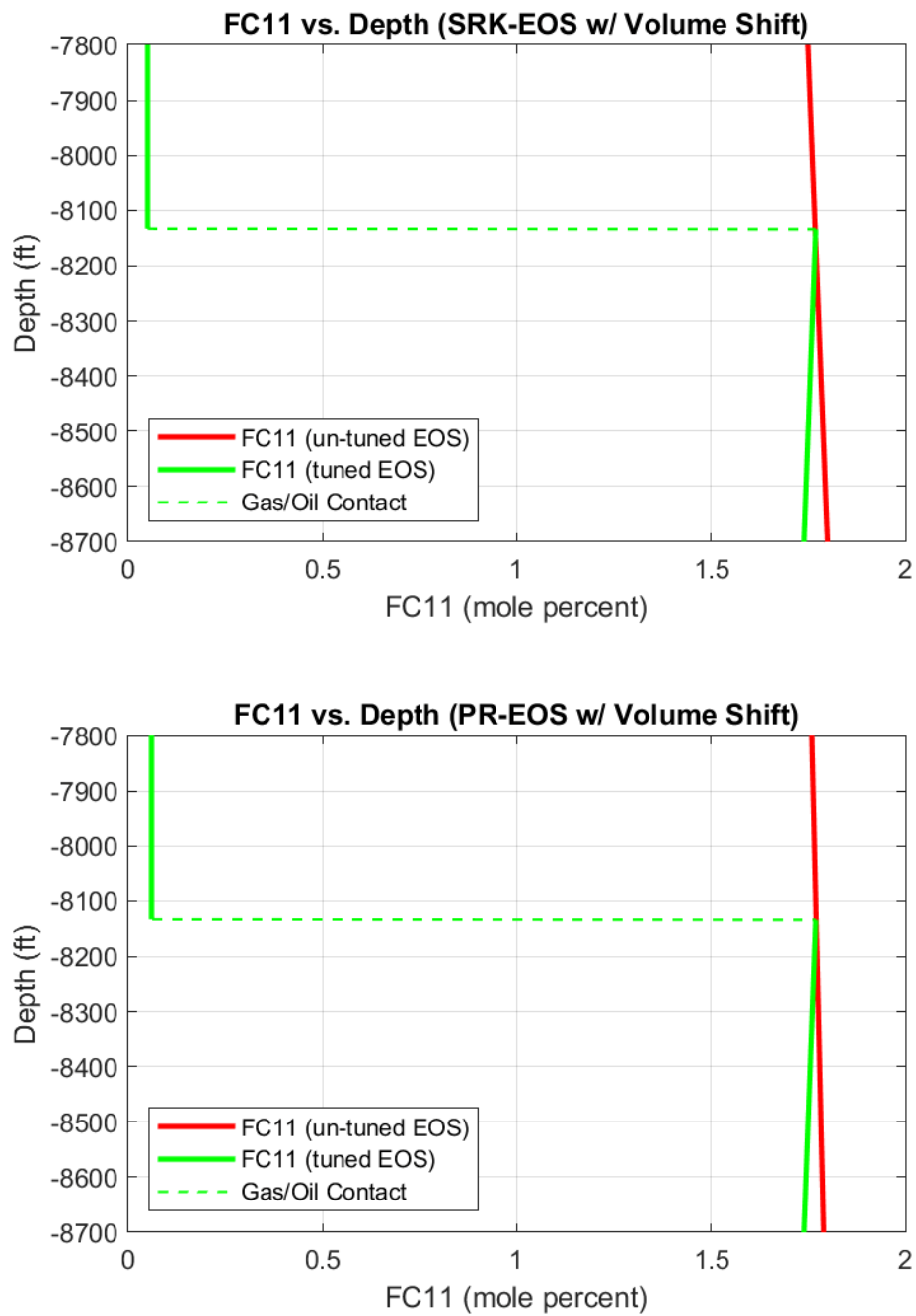


Figure A.66: FC11 composition plots with volume shift using MATLAB®

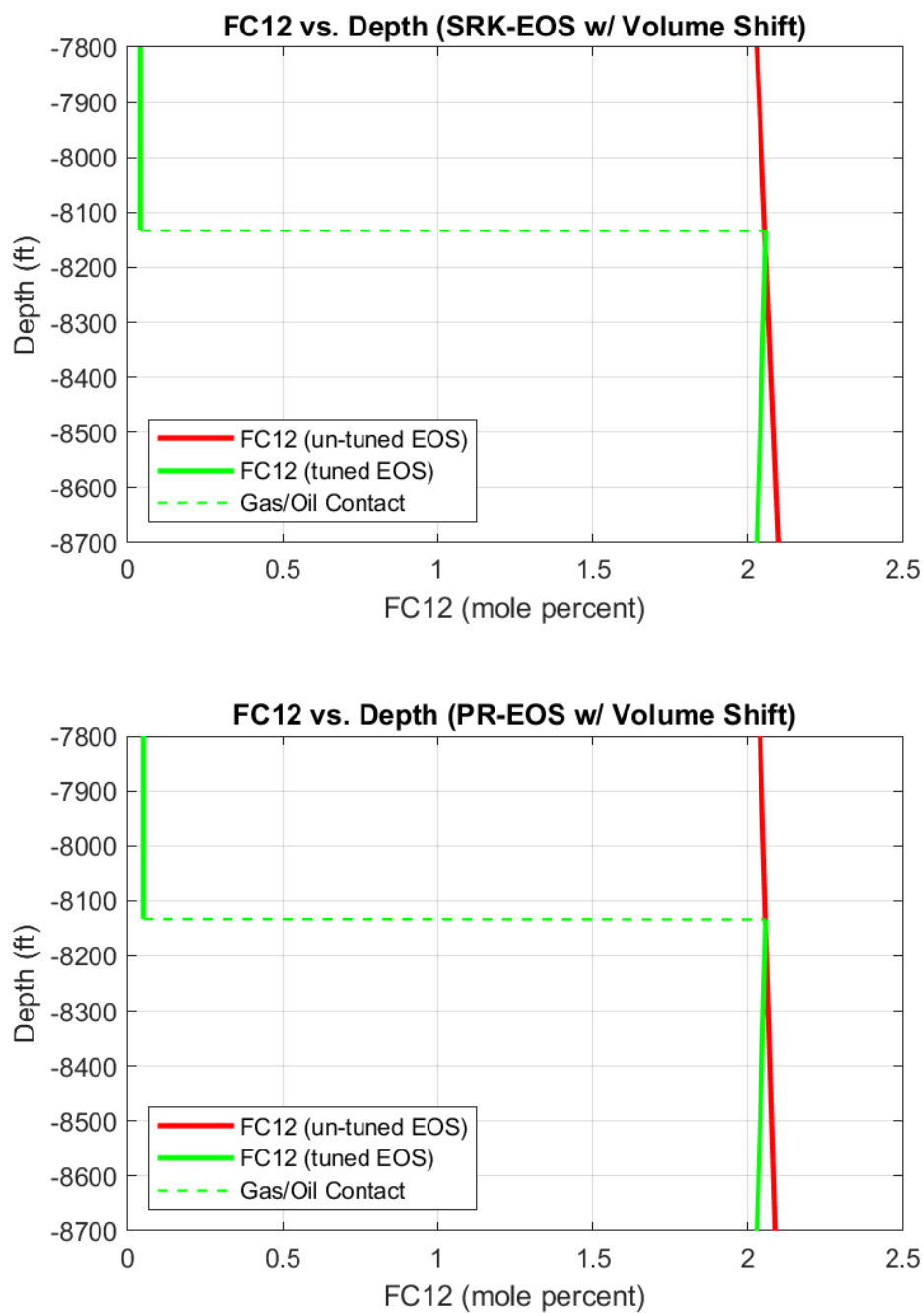


Figure A.67: FC12 composition plots with volume shift using MATLAB®

Appendix A: Supplementary Tables and Figures

Table A.64: Reservoir and saturation pressure gradient results for the tuned SRK and PR EOS models without volume shift using MATLAB®

Depth (ft)	Reservoir Pressure (psia)		Saturation Pressure (psia)	
	SRK EOS	PR EOS	SRK EOS	PR EOS
7800	3794.64	3791.66	3705.47	3708.26
7890	3803.07	3800.84	3737.25	3738.30
7980	3811.53	3810.05	3769.44	3768.75
8070	3820.02	3819.29	3802.46	3800.16
8133.98	3826.06	3825.88	3821.87	3821.33
8134	3826.10	3826.10	3826.05	3825.54
8160	3834.85	3835.03	3817.58	3818.47
8250	3865.20	3865.95	3788.65	3794.30
8340	3895.61	3896.92	3760.57	3770.54
8430	3926.09	3927.92	3732.77	3747.20
8520	3956.63	3958.97	3705.51	3724.26
8610	3987.23	3990.05	3678.64	3701.71
8700	4017.89	4021.17	3652.44	3679.51

Table A.65: H₂S, CO₂, N₂ compositional gradient results for the tuned SRK and PR EOS models without volume shift using MATLAB®

Depth (ft)	H ₂ S (mole fraction)		CO ₂ (mole fraction)		N ₂ (mole fraction)	
	SRK EOS	PR EOS	SRK EOS	PR EOS	SRK EOS	PR EOS
7800	0.0560	0.0608	0.0575	0.0578	0.0340	0.0320
7890	0.0562	0.0610	0.0577	0.0580	0.0340	0.0320
7980	0.0564	0.0612	0.0578	0.0582	0.0339	0.0320
8070	0.0566	0.0614	0.0580	0.0584	0.0339	0.0319
8133.98	0.0568	0.0616	0.0582	0.0585	0.0339	0.0319
8134	0.1124	0.1124	0.0701	0.0701	0.0117	0.0117
8160	0.1125	0.1125	0.0701	0.0701	0.0117	0.0117
8250	0.1125	0.1125	0.0702	0.0702	0.0117	0.0117
8340	0.1124	0.1125	0.0702	0.0702	0.0116	0.0117
8430	0.1124	0.1125	0.0703	0.0703	0.0116	0.0116
8520	0.1124	0.1125	0.0704	0.0703	0.0115	0.0116
8610	0.1124	0.1125	0.0704	0.0704	0.0115	0.0116
8700	0.1124	0.1125	0.0705	0.0705	0.0115	0.0115

Appendix A: Supplementary Tables and Figures

Table A.66: CH₄, C₂H₆, C₃H₈ compositional gradient results for the tuned SRK and PR EOS models without volume shift using MATLAB®

Depth (ft)	CH ₄ (mole fraction)		C ₂ H ₆ (mole fraction)		C ₃ H ₈ (mole fraction)	
	SRK EOS	PR EOS	SRK EOS	PR EOS	SRK EOS	PR EOS
7800	0.8172	0.8117	0.0168	0.0173	0.0048	0.0051
7890	0.8166	0.8111	0.0168	0.0174	0.0049	0.0051
7980	0.8160	0.8104	0.0169	0.0174	0.0049	0.0051
8070	0.8154	0.8098	0.0169	0.0174	0.0049	0.0051
8133.98	0.8149	0.8093	0.0169	0.0175	0.0049	0.0052
8134	0.3870	0.3870	0.0152	0.0152	0.0069	0.0069
8160	0.3864	0.3865	0.0152	0.0152	0.0069	0.0069
8250	0.3844	0.3850	0.0151	0.0152	0.0068	0.0068
8340	0.3825	0.3834	0.0151	0.0151	0.0068	0.0068
8430	0.3805	0.3819	0.0150	0.0151	0.0068	0.0068
8520	0.3786	0.3804	0.0149	0.0150	0.0067	0.0068
8610	0.3768	0.3790	0.0149	0.0150	0.0067	0.0068
8700	0.3749	0.3775	0.0148	0.0149	0.0067	0.0067

Table A.67: IC₄, NC₄, IC₅ compositional gradient results for the tuned SRK and PR EOS models without volume shift using MATLAB®

Depth (ft)	IC ₄ (mole fraction)		NC ₄ (mole fraction)		IC ₅ (mole fraction)	
	SRK EOS	PR EOS	SRK EOS	PR EOS	SRK EOS	PR EOS
7800	0.0013	0.0014	0.0021	0.0023	0.0011	0.0012
7890	0.0013	0.0014	0.0022	0.0023	0.0011	0.0012
7980	0.0013	0.0014	0.0022	0.0023	0.0011	0.0012
8070	0.0013	0.0014	0.0022	0.0023	0.0011	0.0012
8133.98	0.0013	0.0014	0.0022	0.0023	0.0011	0.0012
8134	0.0025	0.0025	0.0048	0.0048	0.0034	0.0034
8160	0.0025	0.0025	0.0048	0.0048	0.0034	0.0034
8250	0.0025	0.0025	0.0048	0.0048	0.0034	0.0034
8340	0.0025	0.0025	0.0047	0.0048	0.0034	0.0034
8430	0.0024	0.0025	0.0047	0.0047	0.0034	0.0034
8520	0.0024	0.0025	0.0047	0.0047	0.0033	0.0034
8610	0.0024	0.0024	0.0047	0.0047	0.0033	0.0034
8700	0.0024	0.0024	0.0047	0.0047	0.0033	0.0033

Appendix A: Supplementary Tables and Figures

Table A.68: NC₅, FC₆, FC₇ compositional gradient results for the tuned SRK and PR EOS models without volume shift using MATLAB®

Depth (ft)	NC ₅ (mole fraction)		FC ₆ (mole fraction)		FC ₇ (mole fraction)	
	SRK EOS	PR EOS	SRK EOS	PR EOS	SRK EOS	PR EOS
7800	0.0009	0.0010	0.0020	0.0023	0.0011	0.0013
7890	0.0009	0.0010	0.0021	0.0023	0.0011	0.0013
7980	0.0010	0.0010	0.0021	0.0023	0.0012	0.0013
8070	0.0010	0.0010	0.0021	0.0023	0.0012	0.0013
8133.98	0.0010	0.0011	0.0021	0.0024	0.0012	0.0014
8134	0.0032	0.0032	0.0106	0.0106	0.0090	0.0090
8160	0.0032	0.0032	0.0106	0.0106	0.0090	0.0090
8250	0.0032	0.0032	0.0105	0.0105	0.0090	0.0090
8340	0.0032	0.0032	0.0105	0.0105	0.0089	0.0090
8430	0.0031	0.0032	0.0105	0.0105	0.0089	0.0090
8520	0.0031	0.0032	0.0104	0.0105	0.0089	0.0089
8610	0.0031	0.0031	0.0104	0.0105	0.0089	0.0089
8700	0.0031	0.0031	0.0104	0.0105	0.0089	0.0089

Table A.69: FC₈, FC₉, FC₁₀ compositional gradient results for the tuned SRK and PR EOS models without volume shift using MATLAB®

Depth (ft)	FC ₈ (mole fraction)		FC ₉ (mole fraction)		FC ₁₀ (mole fraction)	
	SRK EOS	PR EOS	SRK EOS	PR EOS	SRK EOS	PR EOS
7800	0.0017	0.0020	0.0015	0.0017	0.0008	0.0009
7890	0.0017	0.0020	0.0015	0.0018	0.0008	0.0010
7980	0.0018	0.0021	0.0015	0.0018	0.0008	0.0010
8070	0.0018	0.0021	0.0016	0.0018	0.0008	0.0010
8133.98	0.0018	0.0021	0.0016	0.0019	0.0008	0.0010
8134	0.0201	0.0201	0.0258	0.0258	0.0209	0.0209
8160	0.0201	0.0201	0.0258	0.0258	0.0209	0.0209
8250	0.0200	0.0201	0.0258	0.0258	0.0208	0.0209
8340	0.0200	0.0201	0.0257	0.0258	0.0208	0.0208
8430	0.0199	0.0200	0.0257	0.0258	0.0207	0.0208
8520	0.0199	0.0200	0.0256	0.0258	0.0207	0.0208
8610	0.0198	0.0200	0.0255	0.0257	0.0206	0.0208
8700	0.0198	0.0200	0.0255	0.0257	0.0206	0.0208

Appendix A: Supplementary Tables and Figures

Table A.70: FC₁₁, FC₁₂, C₁₃₊ compositional gradient results for the tuned SRK and PR EOS models without volume shift using MATLAB®

Depth (ft)	FC ₁₁ (mole fraction)		FC ₁₂ (mole fraction)		C ₁₃₊ (mole fraction)	
	SRK EOS	PR EOS	SRK EOS	PR EOS	SRK EOS	PR EOS
7800	0.0005	0.0006	0.0004	0.0005	0.0002	0.0001
7890	0.0005	0.0006	0.0004	0.0005	0.0002	0.0001
7980	0.0005	0.0006	0.0004	0.0005	0.0002	0.0001
8070	0.0005	0.0006	0.0004	0.0005	0.0003	0.0001
8133.98	0.0005	0.0006	0.0004	0.0005	0.0003	0.0002
8134	0.0177	0.0177	0.0206	0.0206	0.2581	0.2581
8160	0.0177	0.0177	0.0206	0.0206	0.2588	0.2587
8250	0.0176	0.0177	0.0205	0.0206	0.2613	0.2604
8340	0.0176	0.0176	0.0205	0.0205	0.2636	0.2621
8430	0.0175	0.0176	0.0204	0.0205	0.2660	0.2638
8520	0.0175	0.0176	0.0204	0.0205	0.2683	0.2655
8610	0.0175	0.0176	0.0203	0.0205	0.2706	0.2672
8700	0.0174	0.0176	0.0203	0.0205	0.2729	0.2688

Table A.71: Reservoir and saturation pressure gradient results for the un-tuned SRK and PR EOS models without volume shift using MATLAB®

Depth (ft)	Reservoir Pressure (psia)		Saturation Pressure (psia)	
	SRK EOS	PR EOS	SRK EOS	PR EOS
7800	3745.44	3736.20	2858.30	2838.52
7890	3767.16	3760.41	2848.84	2828.82
7980	3788.89	3784.63	2839.46	2819.23
8070	3810.63	3808.86	2830.17	2809.73
8134	3826.10	3826.10	2823.63	2803.04
8160	3832.38	3833.11	2820.96	2800.32
8250	3854.15	3857.36	2811.83	2791.00
8340	3875.92	3881.63	2802.81	2781.77
8430	3897.70	3905.91	2793.86	2772.63
8520	3919.49	3930.20	2784.96	2763.57
8610	3941.30	3954.51	2776.16	2754.60
8700	3963.11	3978.82	2767.43	2745.71

Appendix A: Supplementary Tables and Figures

Table A.72: H₂S, CO₂, N₂ compositional gradient results for the un-tuned SRK and PR EOS models without volume shift using MATLAB®

Depth (ft)	H ₂ S (mole fraction)		CO ₂ (mole fraction)		N ₂ (mole fraction)	
	SRK EOS	PR EOS	SRK EOS	PR EOS	SRK EOS	PR EOS
7800	0.1123	0.1123	0.0698	0.0698	0.0118	0.0118
7890	0.1123	0.1123	0.0699	0.0699	0.0117	0.0118
7980	0.1124	0.1124	0.0700	0.0700	0.0117	0.0117
8070	0.1124	0.1124	0.0700	0.0700	0.0117	0.0117
8134	0.1124	0.1124	0.0701	0.0701	0.0117	0.0117
8160	0.1125	0.1125	0.0701	0.0701	0.0117	0.0117
8250	0.1125	0.1125	0.0702	0.0702	0.0117	0.0117
8340	0.1126	0.1125	0.0703	0.0703	0.0117	0.0117
8430	0.1126	0.1126	0.0704	0.0704	0.0117	0.0117
8520	0.1127	0.1126	0.0704	0.0704	0.0117	0.0117
8610	0.1127	0.1127	0.0705	0.0705	0.0117	0.0117
8700	0.1128	0.1127	0.0706	0.0706	0.0117	0.0117

Table A.73: CH₄, C₂H₆, C₃H₈ compositional gradient results for the un-tuned SRK and PR EOS models without volume shift using MATLAB®

Depth (ft)	CH ₄ (mole fraction)		C ₂ H ₆ (mole fraction)		C ₃ H ₈ (mole fraction)	
	SRK EOS	PR EOS	SRK EOS	PR EOS	SRK EOS	PR EOS
7800	0.3901	0.3902	0.0153	0.0153	0.0069	0.0069
7890	0.3892	0.3893	0.0153	0.0153	0.0069	0.0069
7980	0.3884	0.3884	0.0153	0.0153	0.0069	0.0069
8070	0.3876	0.3876	0.0152	0.0152	0.0069	0.0069
8134	0.3870	0.3870	0.0152	0.0152	0.0069	0.0069
8160	0.3867	0.3867	0.0152	0.0152	0.0069	0.0069
8250	0.3859	0.3859	0.0152	0.0152	0.0069	0.0069
8340	0.3851	0.3851	0.0152	0.0152	0.0069	0.0069
8430	0.3843	0.3842	0.0152	0.0152	0.0069	0.0069
8520	0.3835	0.3834	0.0151	0.0151	0.0068	0.0068
8610	0.3827	0.3826	0.0151	0.0151	0.0068	0.0068
8700	0.3819	0.3817	0.0151	0.0151	0.0068	0.0068

Appendix A: Supplementary Tables and Figures

Table A.74: IC₄, NC₄, IC₅ compositional gradient results for the un-tuned SRK and PR EOS models without volume shift using MATLAB®

Depth (ft)	IC ₄ (mole fraction)		NC ₄ (mole fraction)		IC ₅ (mole fraction)	
	SRK EOS	PR EOS	SRK EOS	PR EOS	SRK EOS	PR EOS
7800	0.0025	0.0025	0.0048	0.0048	0.0034	0.0034
7890	0.0025	0.0025	0.0048	0.0048	0.0034	0.0034
7980	0.0025	0.0025	0.0048	0.0048	0.0034	0.0034
8070	0.0025	0.0025	0.0048	0.0048	0.0034	0.0034
8134	0.0025	0.0025	0.0048	0.0048	0.0034	0.0034
8160	0.0025	0.0025	0.0048	0.0048	0.0034	0.0034
8250	0.0025	0.0025	0.0048	0.0048	0.0034	0.0034
8340	0.0025	0.0025	0.0048	0.0048	0.0034	0.0034
8430	0.0025	0.0025	0.0048	0.0048	0.0034	0.0034
8520	0.0025	0.0025	0.0048	0.0048	0.0034	0.0034
8610	0.0025	0.0025	0.0048	0.0048	0.0034	0.0034
8700	0.0025	0.0025	0.0048	0.0048	0.0034	0.0034

Table A.75: NC₅, FC₆, FC₇ compositional gradient results for the un-tuned SRK and PR EOS models without volume shift using MATLAB®

Depth (ft)	NC ₅ (mole fraction)		FC ₆ (mole fraction)		FC ₇ (mole fraction)	
	SRK EOS	PR EOS	SRK EOS	PR EOS	SRK EOS	PR EOS
7800	0.0032	0.0032	0.0105	0.0105	0.0090	0.0090
7890	0.0032	0.0032	0.0105	0.0105	0.0090	0.0090
7980	0.0032	0.0032	0.0105	0.0105	0.0090	0.0090
8070	0.0032	0.0032	0.0106	0.0106	0.0090	0.0090
8134	0.0032	0.0032	0.0106	0.0106	0.0090	0.0090
8160	0.0032	0.0032	0.0106	0.0106	0.0090	0.0090
8250	0.0032	0.0032	0.0106	0.0106	0.0090	0.0090
8340	0.0032	0.0032	0.0106	0.0106	0.0090	0.0090
8430	0.0032	0.0032	0.0106	0.0106	0.0090	0.0090
8520	0.0032	0.0032	0.0106	0.0106	0.0091	0.0091
8610	0.0032	0.0032	0.0106	0.0106	0.0091	0.0091
8700	0.0032	0.0032	0.0106	0.0106	0.0091	0.0091

Appendix A: Supplementary Tables and Figures

Table A.76: FC8, FC9, FC10 compositional gradient results for the un-tuned SRK and PR EOS models without volume shift using MATLAB®

Depth (ft)	FC8 (mole fraction)		FC9 (mole fraction)		FC10 (mole fraction)	
	SRK EOS	PR EOS	SRK EOS	PR EOS	SRK EOS	PR EOS
7800	0.0200	0.0200	0.0256	0.0256	0.0207	0.0207
7890	0.0200	0.0200	0.0257	0.0257	0.0207	0.0207
7980	0.0200	0.0200	0.0258	0.0257	0.0208	0.0208
8070	0.0201	0.0201	0.0258	0.0258	0.0208	0.0208
8134	0.0201	0.0201	0.0258	0.0258	0.0209	0.0209
8160	0.0201	0.0201	0.0259	0.0259	0.0209	0.0209
8250	0.0201	0.0201	0.0259	0.0259	0.0209	0.0210
8340	0.0202	0.0202	0.0260	0.0260	0.0210	0.0210
8430	0.0202	0.0202	0.0260	0.0260	0.0211	0.0211
8520	0.0203	0.0203	0.0261	0.0261	0.0211	0.0211
8610	0.0203	0.0203	0.0262	0.0262	0.0212	0.0212
8700	0.0203	0.0203	0.0262	0.0262	0.0212	0.0212

Table A.77: FC11, FC12, C13+ compositional gradient results for the un-tuned SRK and PR EOS models without volume shift using MATLAB®

Depth (ft)	FC11 (mole fraction)		FC12 (mole fraction)		C13+ (mole fraction)	
	SRK EOS	PR EOS	SRK EOS	PR EOS	SRK EOS	PR EOS
7800	0.0175	0.0175	0.0203	0.0203	0.2565	0.2563
7890	0.0175	0.0175	0.0204	0.0204	0.2569	0.2568
7980	0.0176	0.0176	0.0205	0.0205	0.2574	0.2573
8070	0.0176	0.0176	0.0205	0.0205	0.2578	0.2578
8134	0.0177	0.0177	0.0206	0.0206	0.2581	0.2581
8160	0.0177	0.0177	0.0206	0.0206	0.2583	0.2583
8250	0.0177	0.0177	0.0207	0.0207	0.2587	0.2588
8340	0.0178	0.0178	0.0207	0.0207	0.2592	0.2592
8430	0.0178	0.0178	0.0208	0.0208	0.2596	0.2597
8520	0.0179	0.0179	0.0209	0.0209	0.2600	0.2601
8610	0.0179	0.0179	0.0209	0.0209	0.2604	0.2606
8700	0.0180	0.0180	0.0210	0.0210	0.2609	0.2610

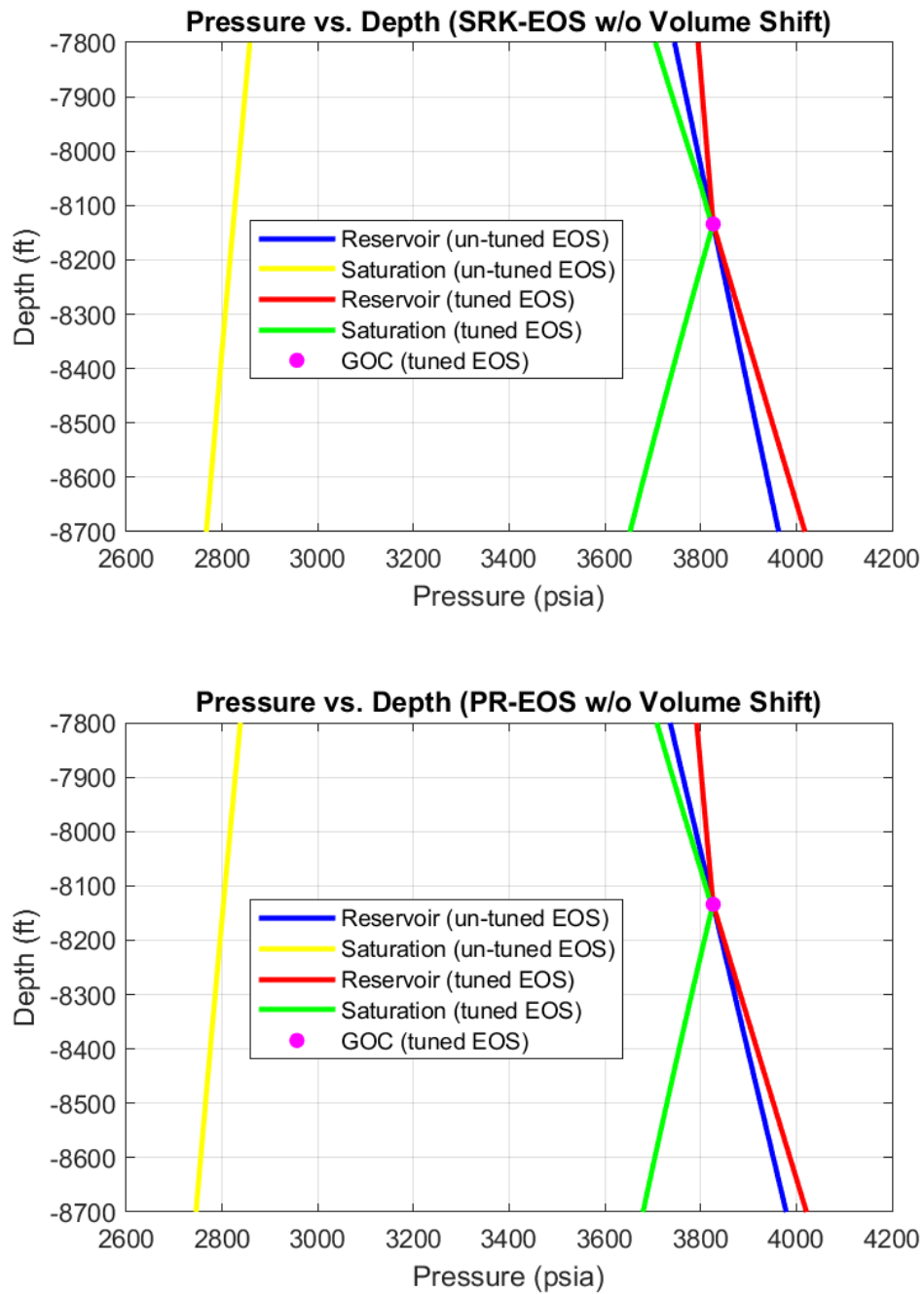


Figure A.68: Pressure plots without volume shift using MATLAB®

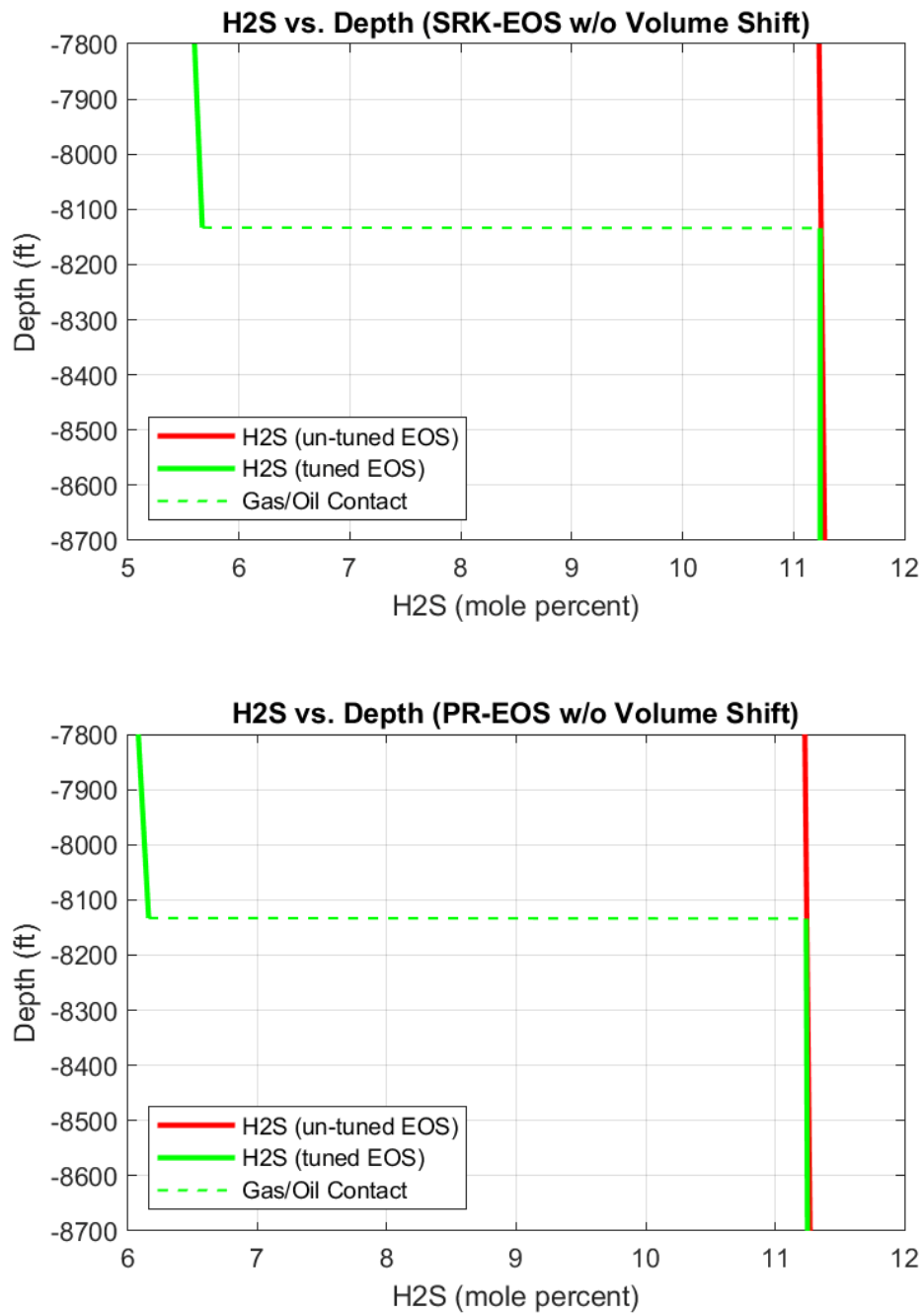


Figure A.69: H₂S composition plots without volume shift using MATLAB®

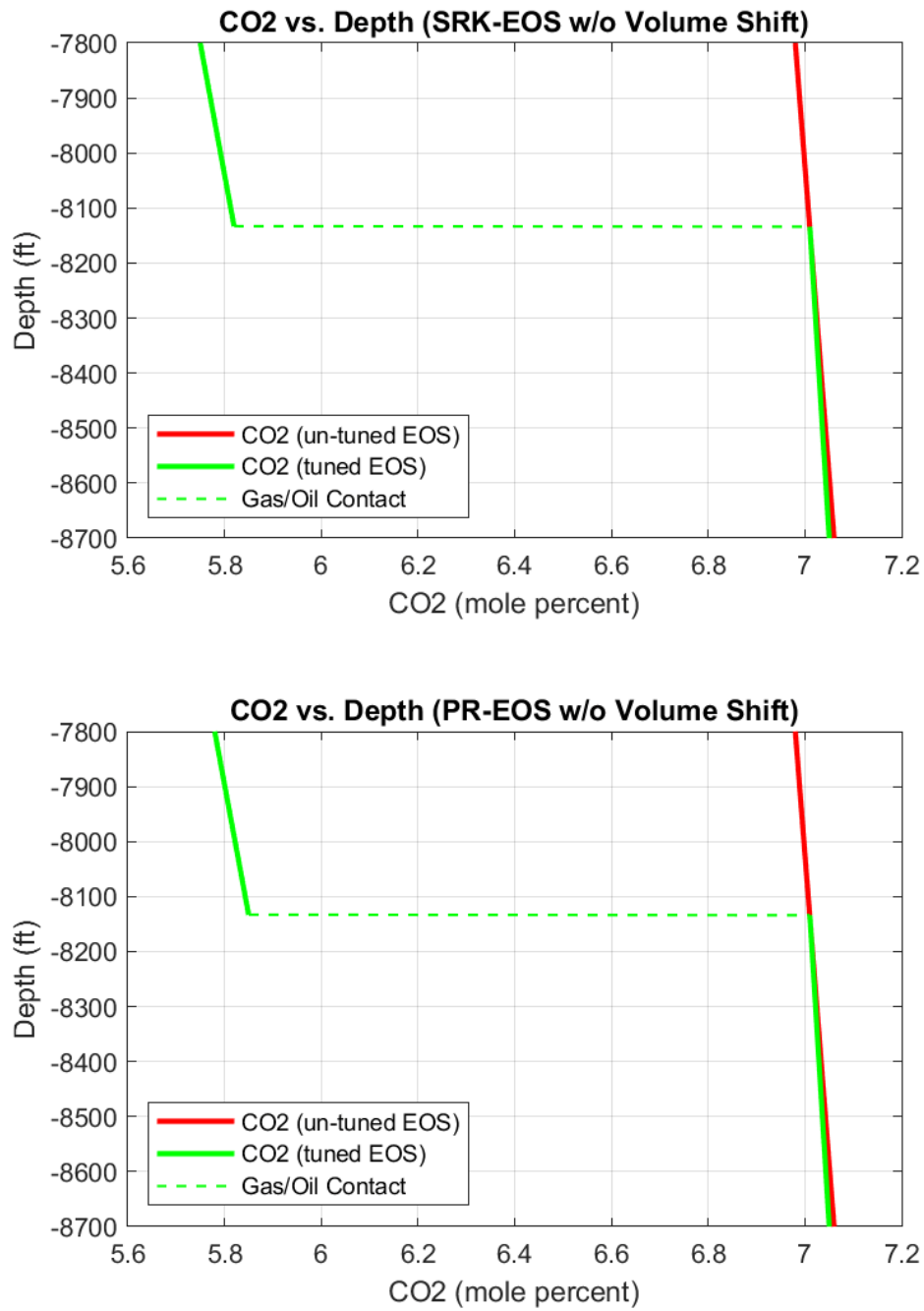


Figure A.70: CO₂ composition plots without volume shift using MATLAB®

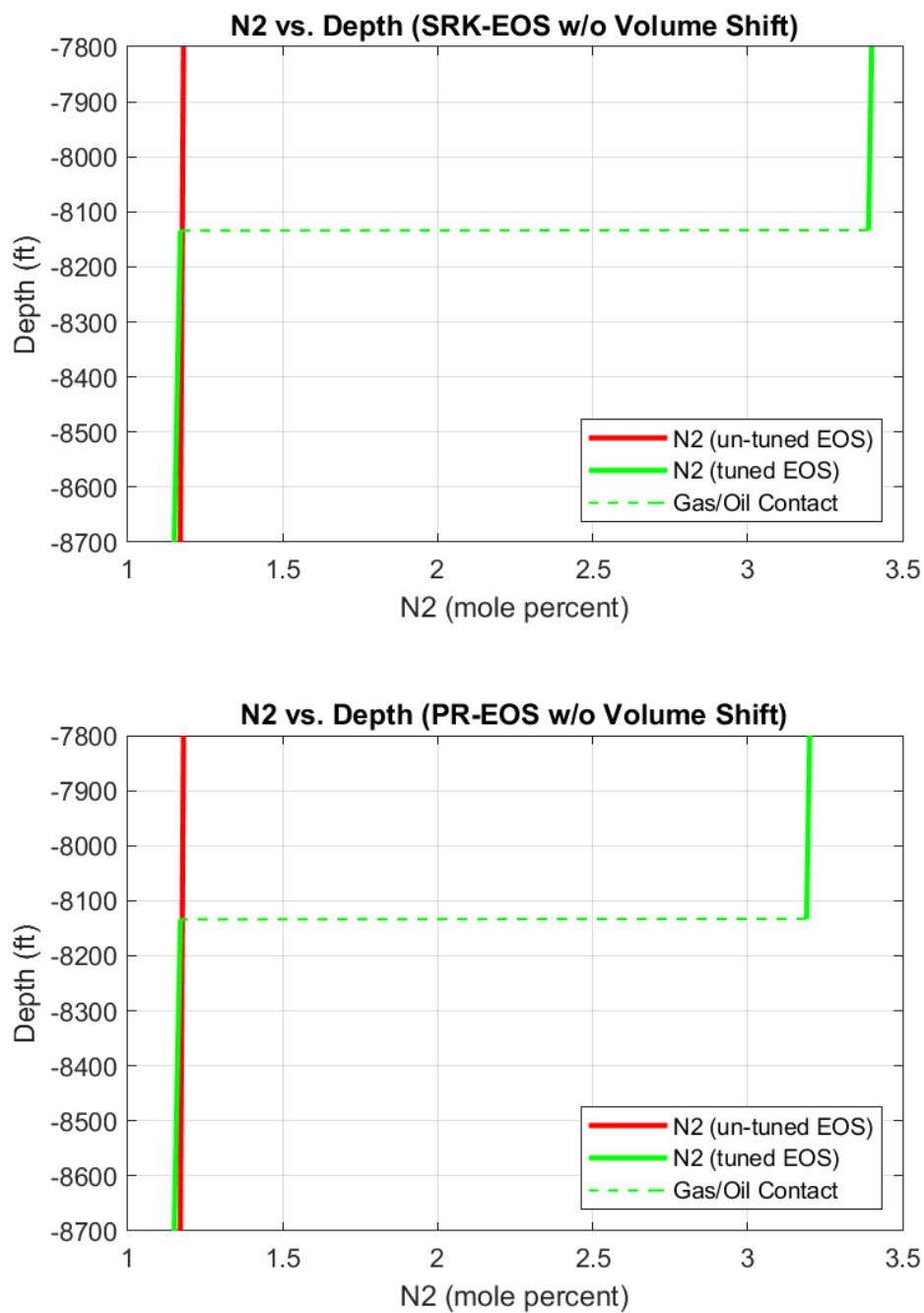


Figure A.71: N₂ composition plots without volume shift using MATLAB®

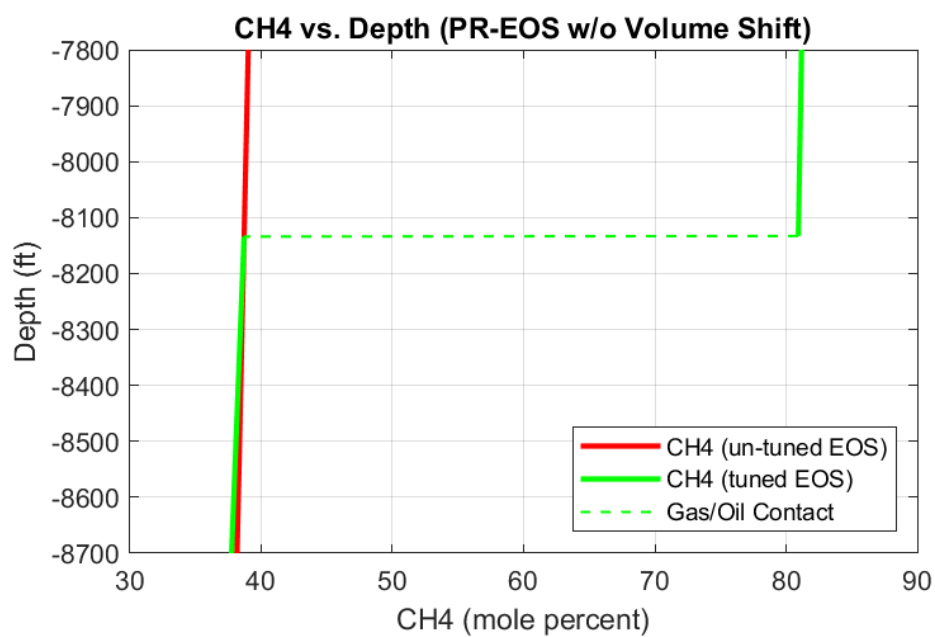
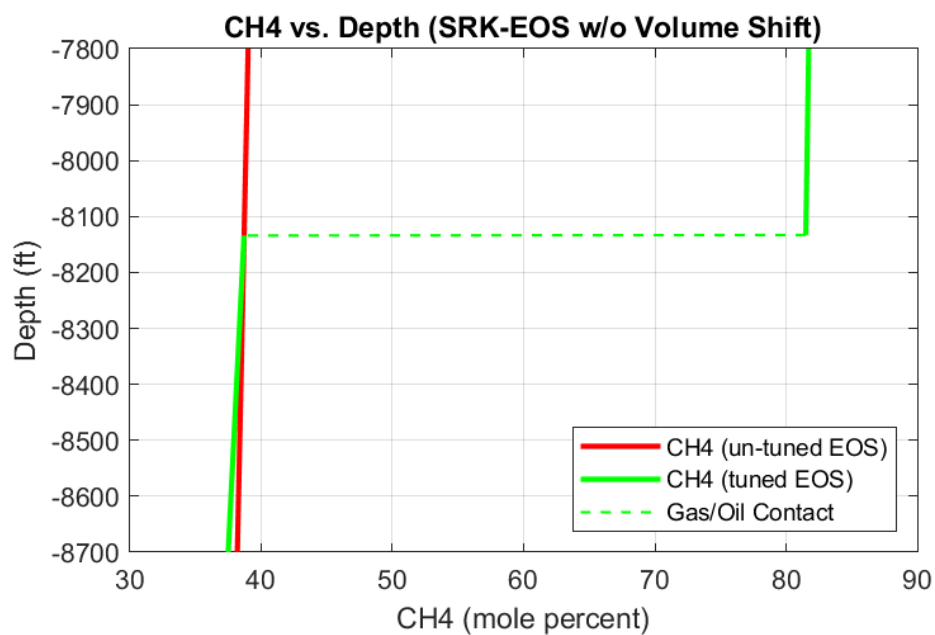


Figure A.72: CH₄ composition plots without volume shift using MATLAB®

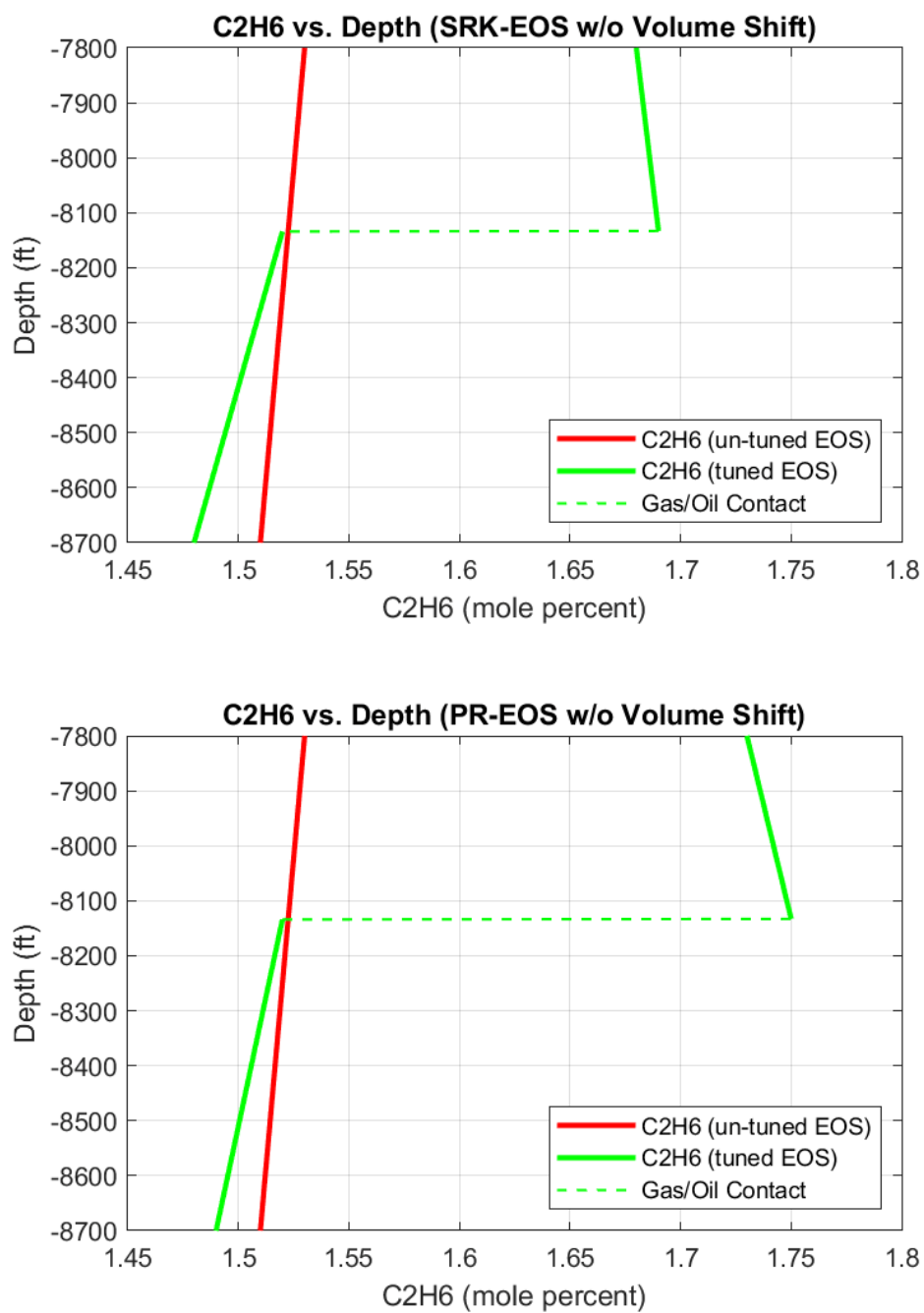


Figure A.73: C₂H₆ composition plots without volume shift using MATLAB®

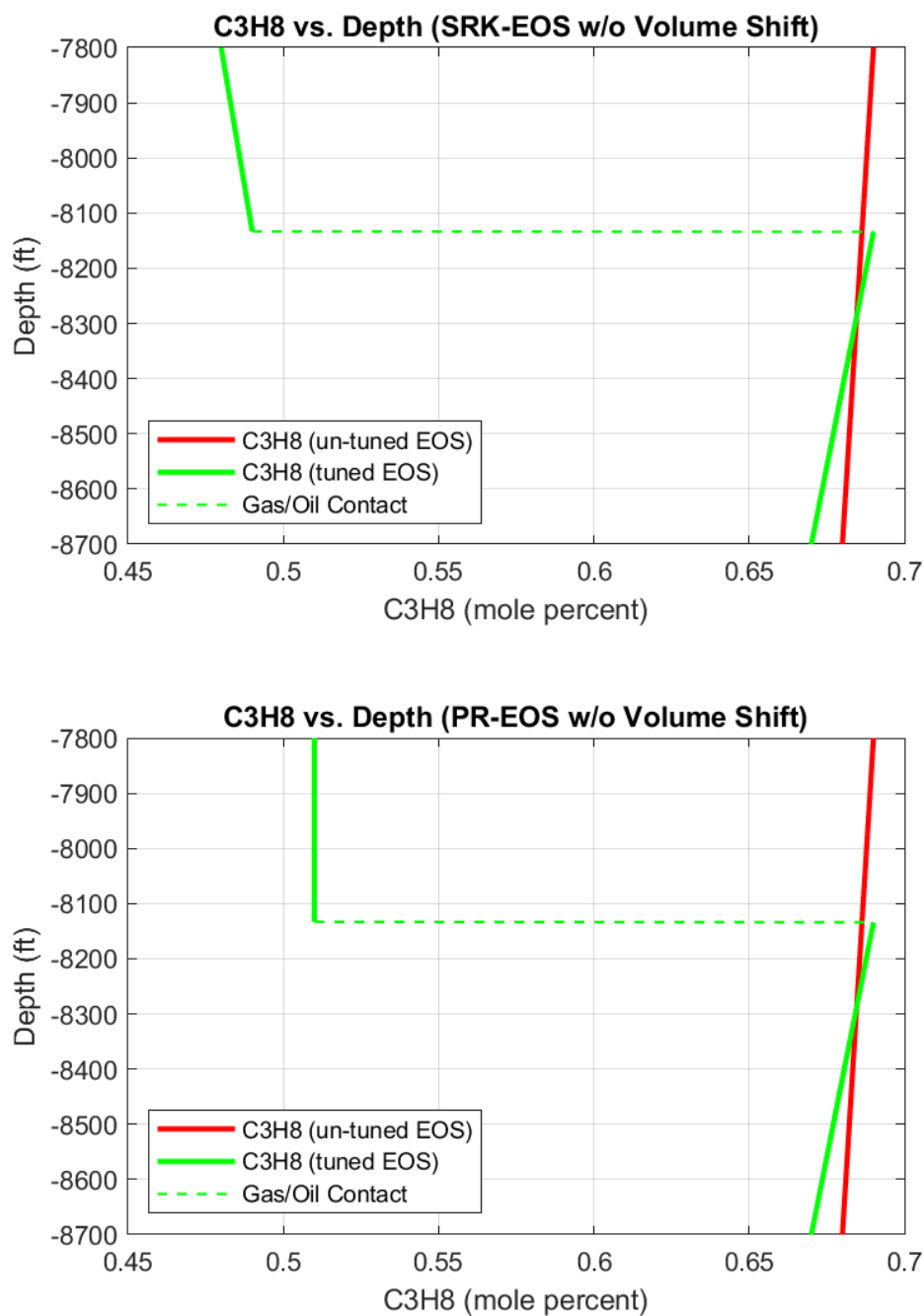


Figure A.74: C₃H₈ composition plots without volume shift using MATLAB®

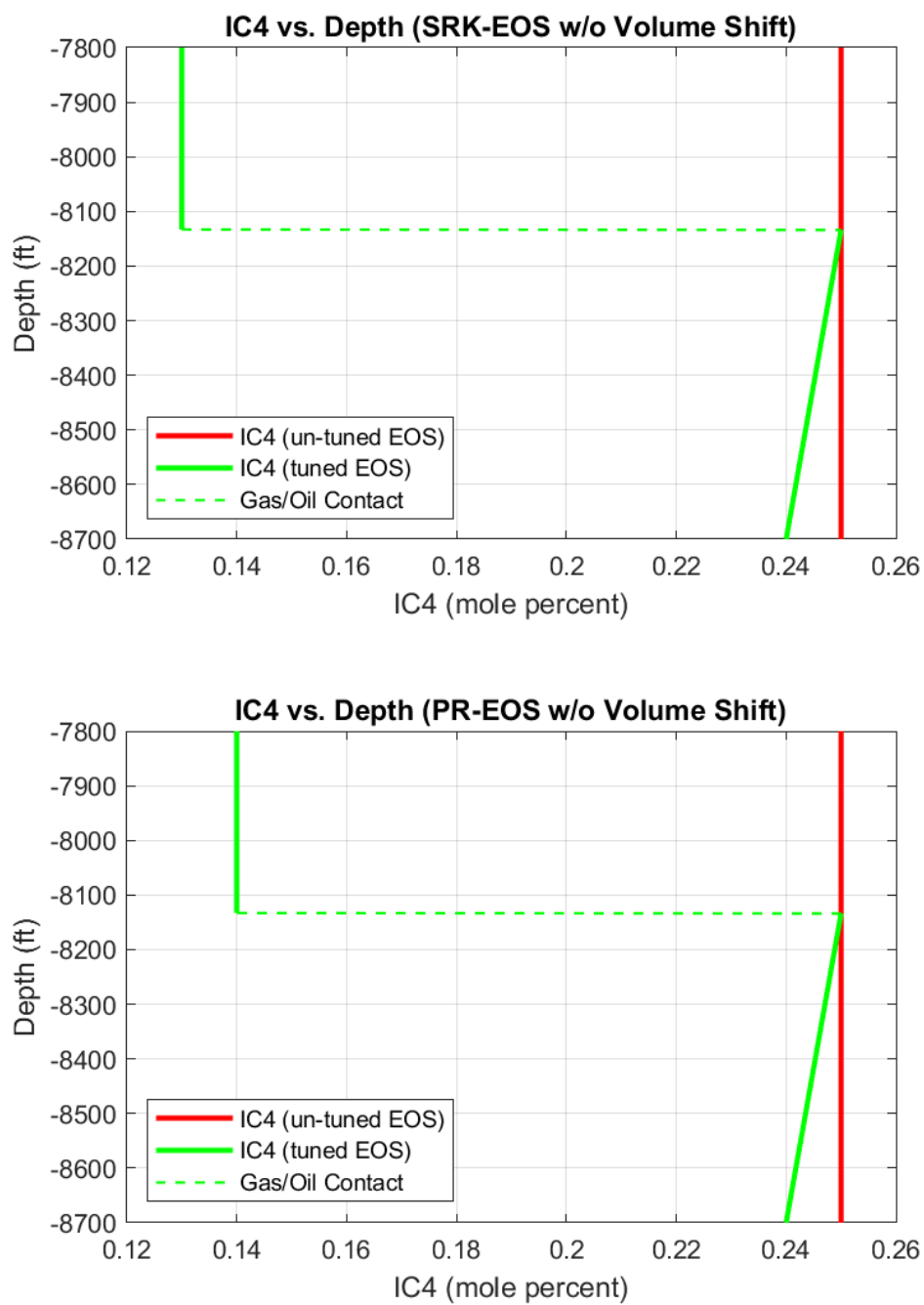


Figure A.75: IC4 composition plots without volume shift using MATLAB®

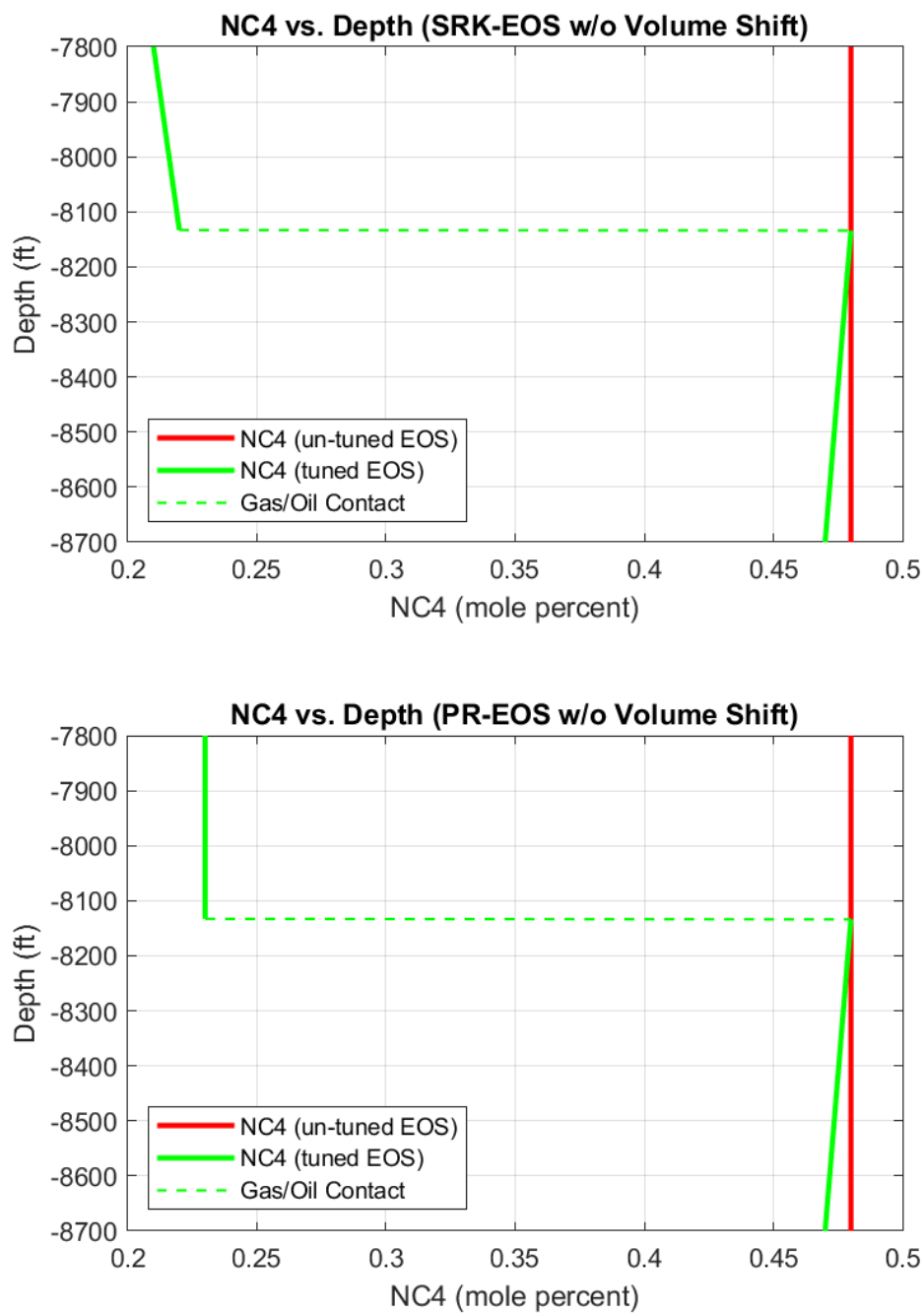


Figure A.76: NC4 composition plots without volume shift using MATLAB®

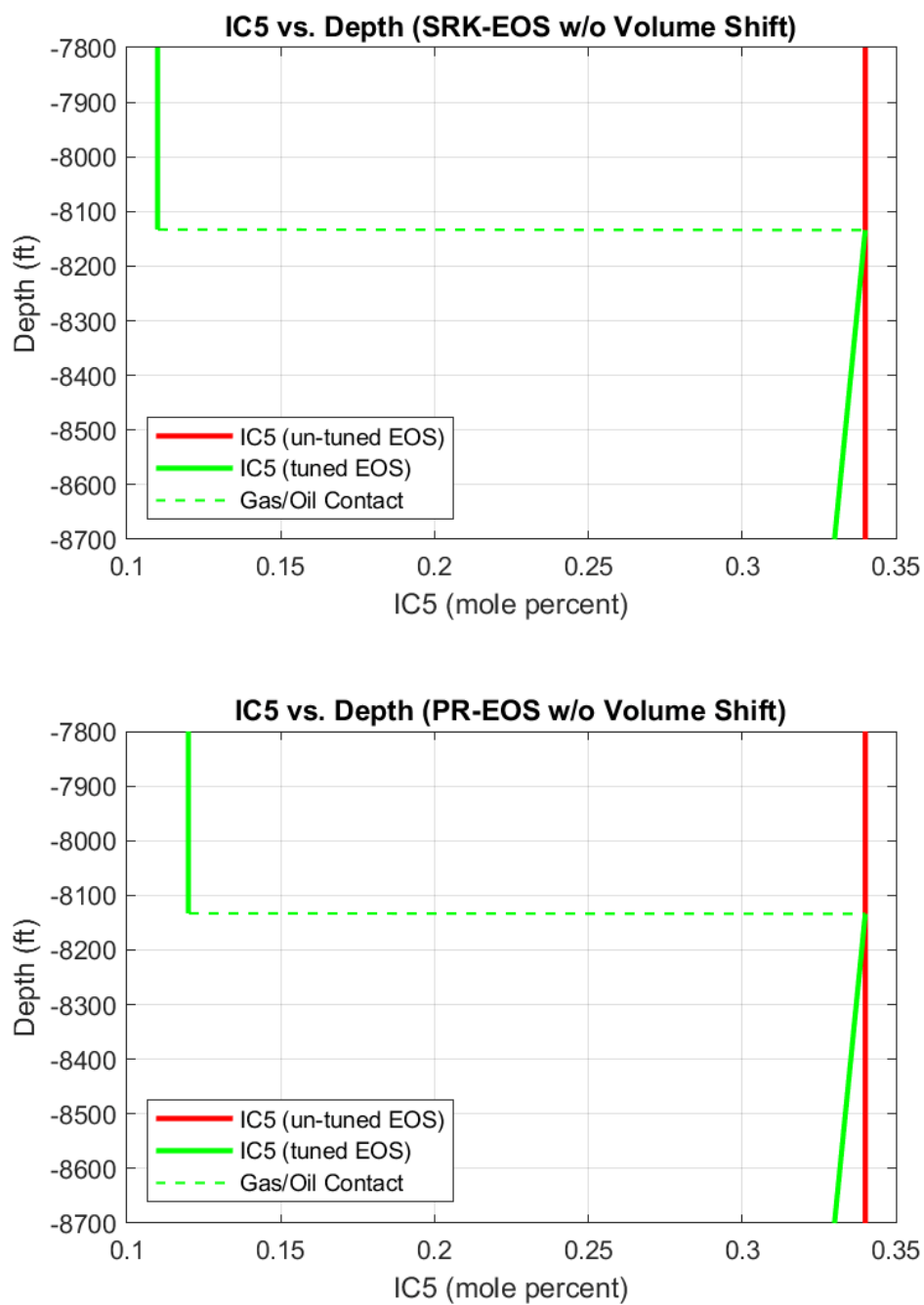


Figure A.77: IC₅ composition plots without volume shift using MATLAB®

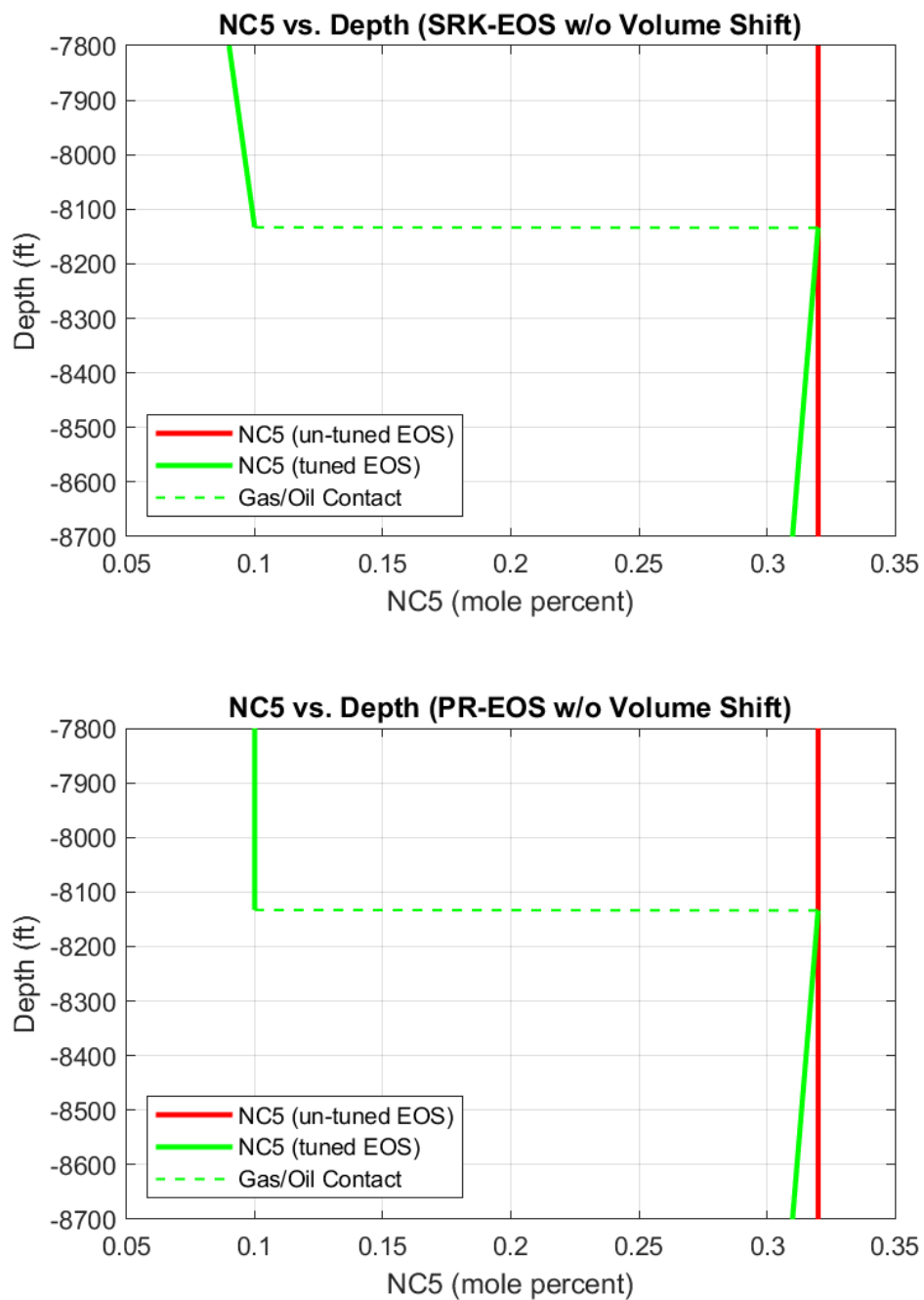


Figure A.78: NC5 composition plots without volume shift using MATLAB®

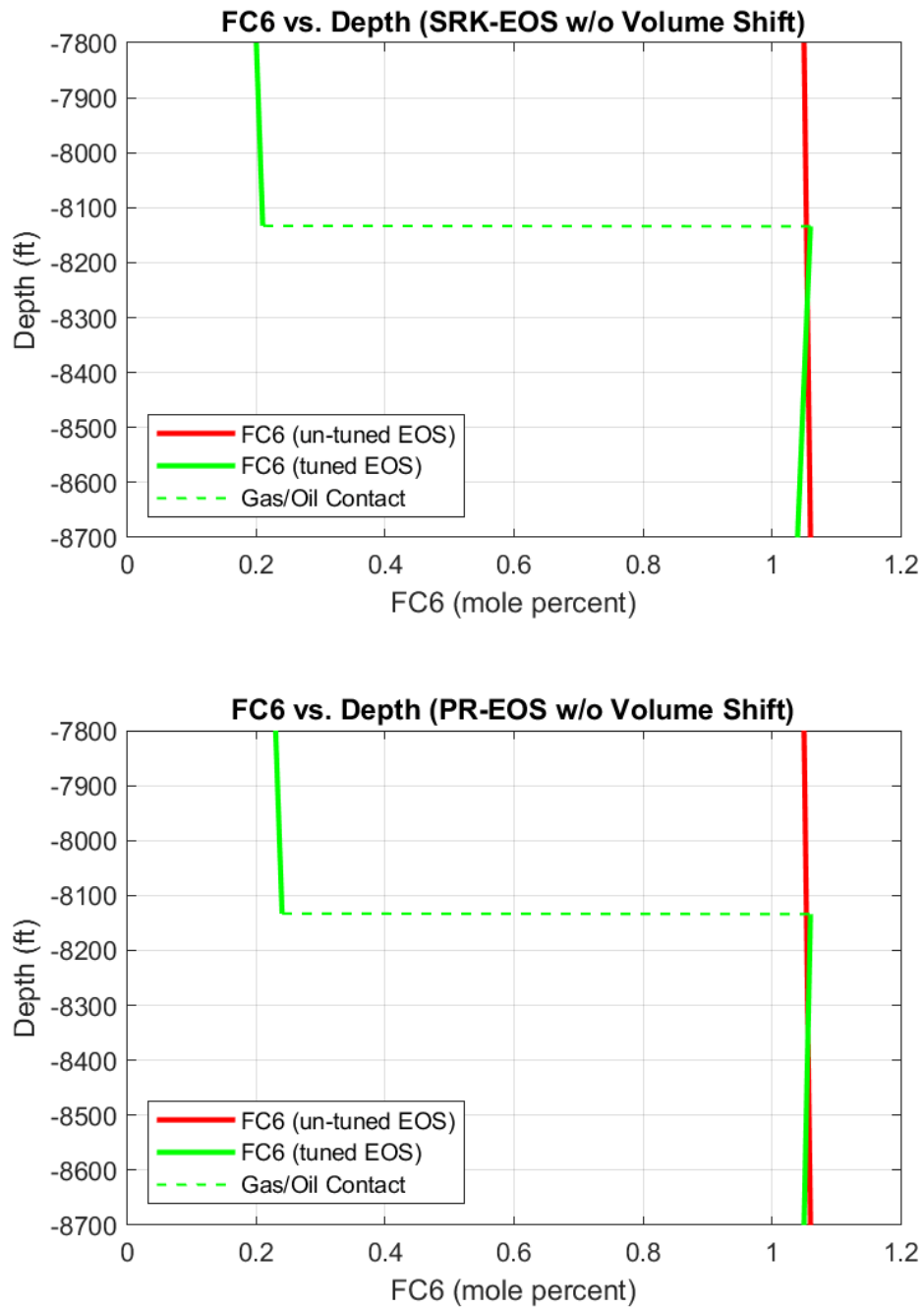


Figure A.79: FC6 composition plots without volume shift using MATLAB®

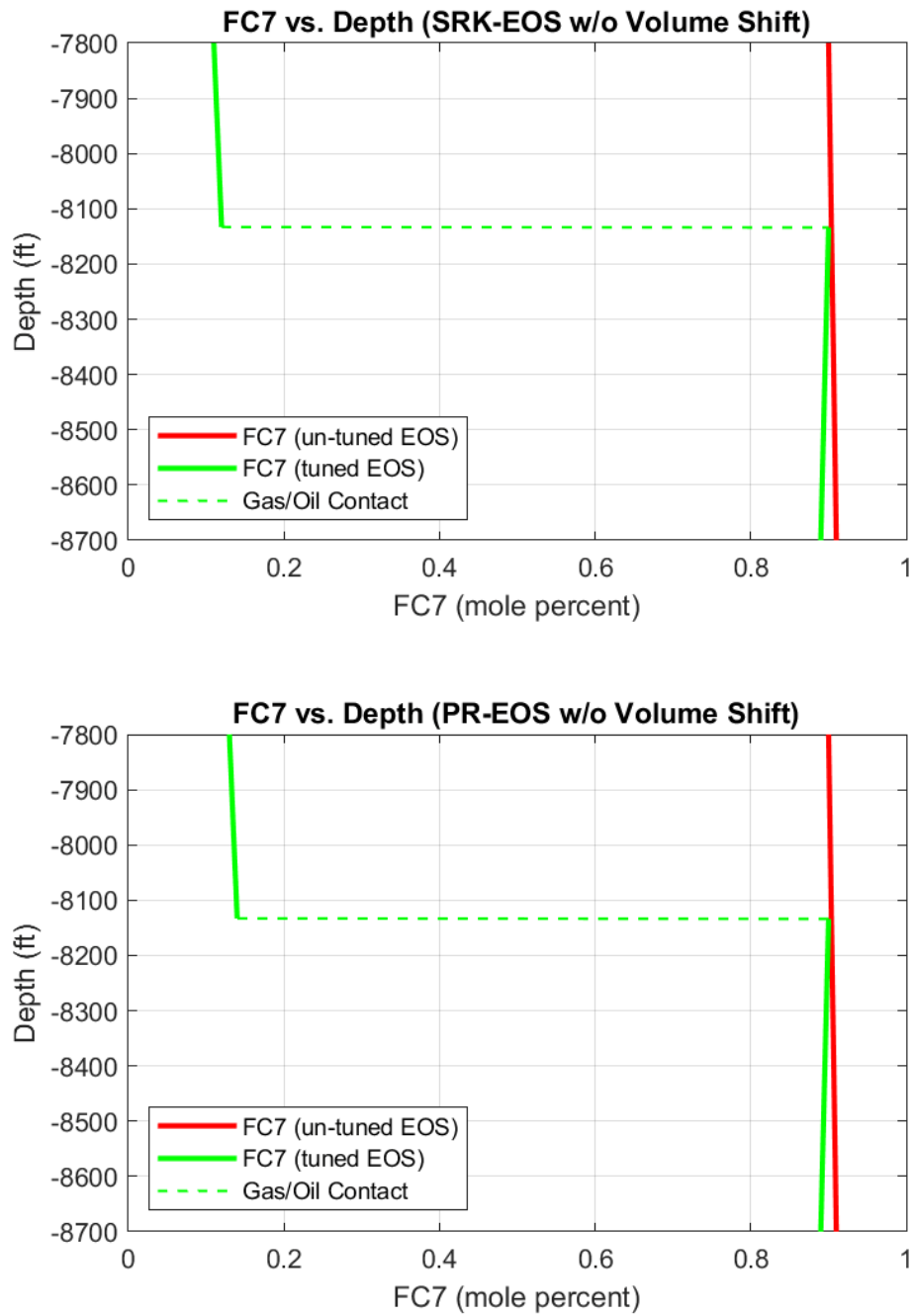


Figure A.8o: FC7 composition plots without volume shift using MATLAB®

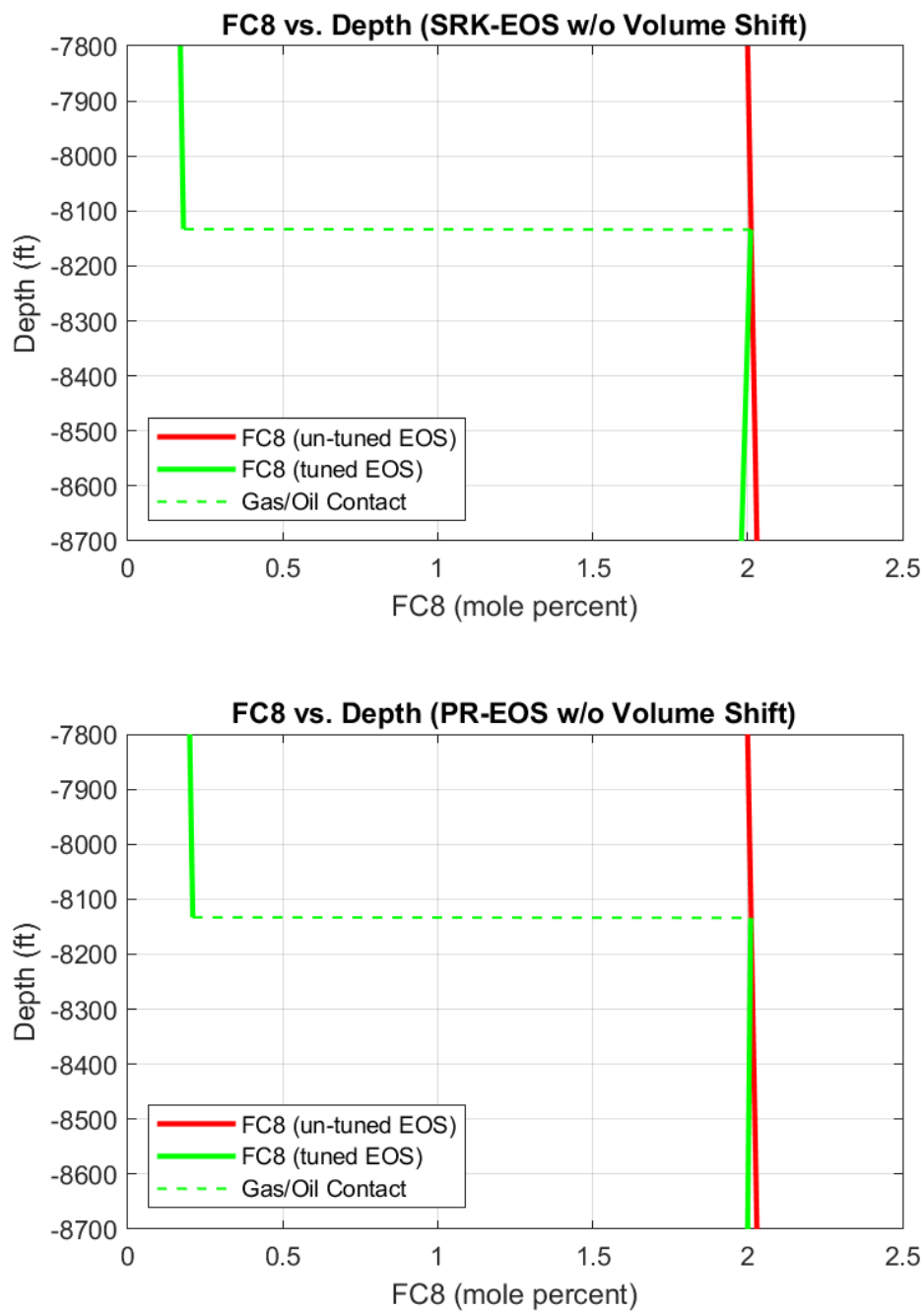


Figure A.81: FC8 composition plots without volume shift using MATLAB®

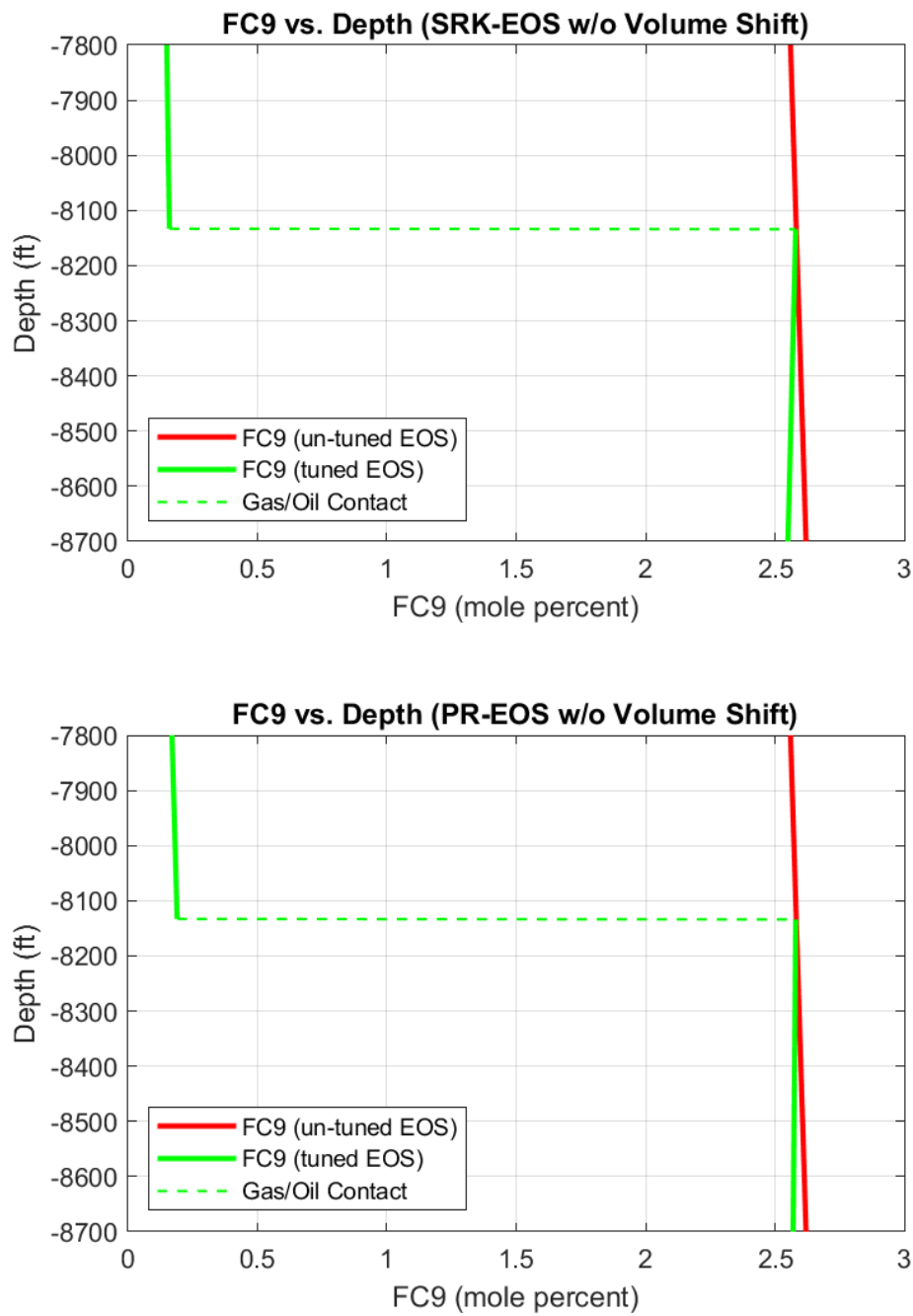


Figure A.82: FC9 composition plots without volume shift using MATLAB®

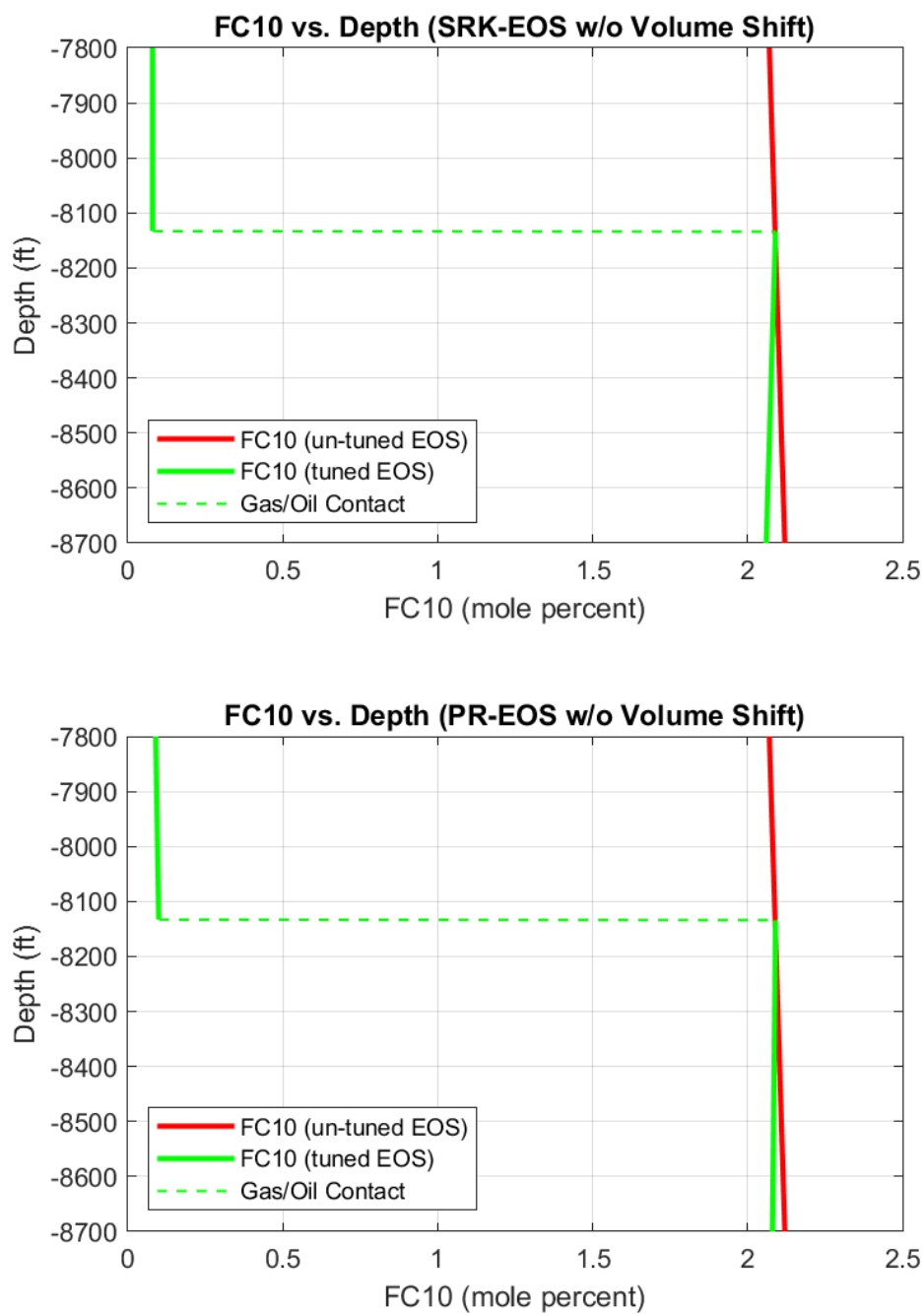


Figure A.83: FC10 composition plots without volume shift using MATLAB®

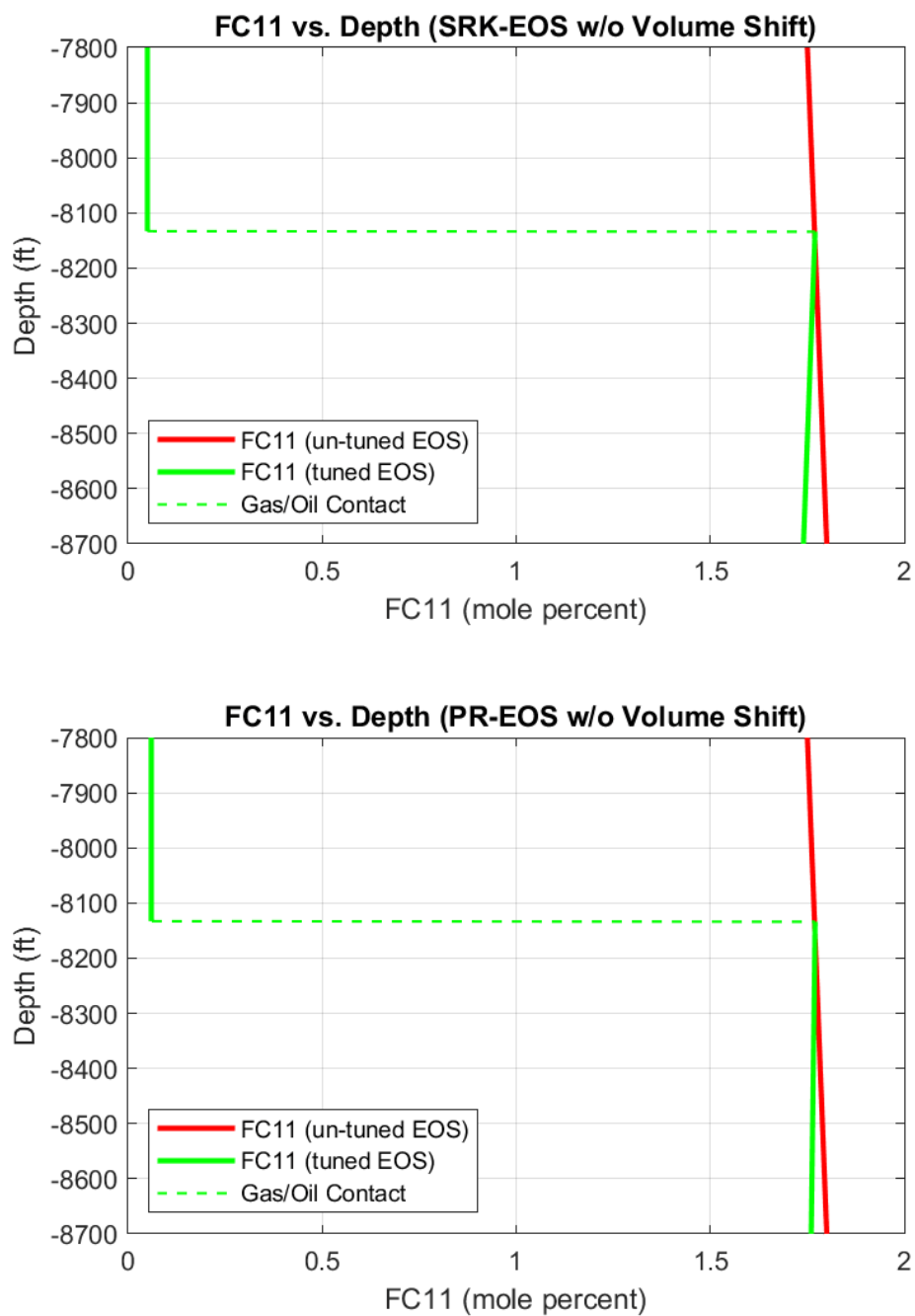


Figure A.84: FC11 composition plots without volume shift using MATLAB®

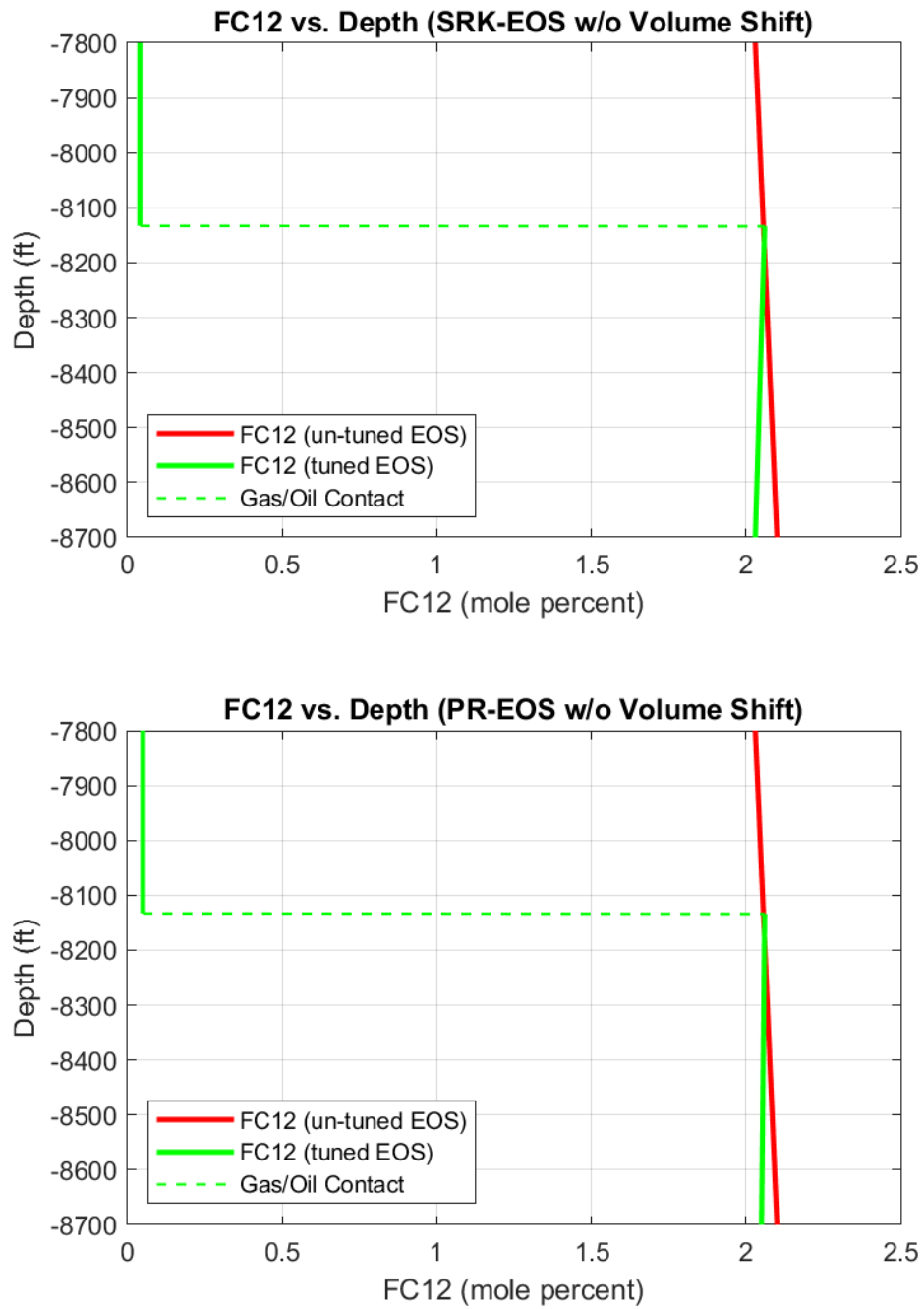


Figure A.85: FC12 composition plots without volume shift using MATLAB®

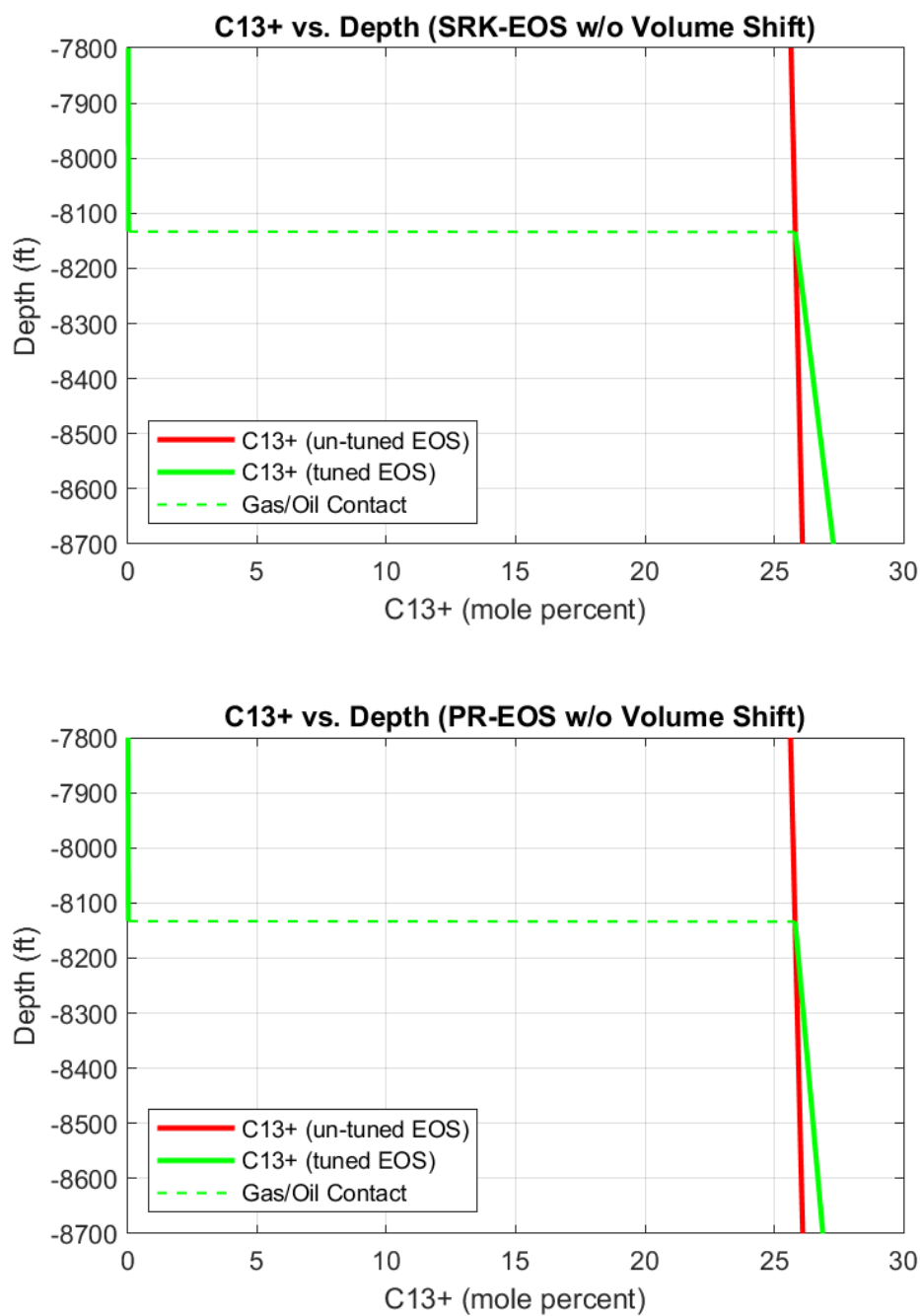


Figure A.86: C₁₃₊ composition plots without volume shift using MATLAB®

Appendix B

MATLAB® Open Source Code

- Reservoir fluid EOS model script

```
% This script uses a reservoir fluid EOS model (SRK or PR) to perform the
% following simulation procedures:
% ~Stability analysis
% ~Saturation pressure calculation
% ~Two-phase flash calculation
% ~Compositional gradient calculation
% ~Gas/oil contact location
clear all
clc
format compact
%% Set Reference Conditions
href_ft=8134 % Reference depth in feet
Tref_F=134.6 % Reference Temperature in degF
T_K=(Tref_F-32)/1.8+273.15; % Convert Temperature to Kelvin
Pref_psia=3826.1 % Reference Pressure in psia
P_Pa=Pref_psia*6.8948e+03; % Convert Pressure to Pa
P_MPa=P_Pa*1.0e-06; % Convert Pressure to MPa
%% Reservoir fluid initialization
% Set component ID numbers
component_id_or_Tc=(1:18);
% Load variables structure
load('greek_oilfield.mat')
% Display component names
names=greek_oilfield.names(component_id_or_Tc)
% Set given feed composition
zi_feed=greek_oilfield.feed_composition_zi(component_id_or_Tc)
% Rename composition for brevity
zi=zi_feed;
%% EOS fluid characterization
% Set the type of EOS used
EOS_type='SRK' % SRK or PR
% Cast component properties from the structure to variables
[Pc_MPa,Tc_K,w,Si,Mi]=critical_prop_selector_f...
(EOS_type,component_id_or_Tc,greek_oilfield);
% Compute the handles to ai, bi
[ai,bi]=a_aibi_cubic_f(EOS_type,component_id_or_Tc);
% Compute component "attraction" and "repulsion" parameters ai, bi
ai_c=ai(T_K);
bi_c=bi(T_K);
% Cast the binary interaction coefficients from the structure to variables
kij=IntCoeff_selector_f(EOS_type,greek_oilfield);
%% Stability analysis
% Compute Ki initial estimates
[Ki]=a_Wilsonmethod_initial_estimates__f(T_K,P_Pa,Tc_K,Pc_MPa,w);
% Perform stability tests
disp('Stability analysis results:')
% Vapor-like search
[S_v,yi_stab,Ki_v]=stability_test_vapor_f(Ki,zi,kij,ai_c,bi_c,P_Pa,T_K,EOS_type);
% Liquid-like search
[S_L,xi_stab,Ki_L]=stability_test_Liq_f(Ki,zi,kij,ai_c,bi_c,P_Pa,T_K,EOS_type);
% Check for stability
if S_v<=1&&S_L<=1 % stable solution
    disp(['Mixture is stable'])
elseif S_v>1||S_L>1
    disp(['Mixture is unstable']) % unstable solution
    % Use the unstable solution K-values to initialize the two-phase flash
    Ki=Ki_v.*Ki_L;
end
%% Saturation pressure calculation
disp('Saturation pressure calculation results:')
% Compute saturation pressure and saturation properties
[Psat_psia,yi_sat,Ki_sat,Z_L_sat,Z_v_sat,fi_sat_Pa,lnfi_sat_atm]=Psat_calc_f...
(P_Pa,T_K,Tc_K,Pc_MPa,w,zi,kij,ai_c,bi_c,EOS_type)
%% Two-phase flash calculation
% Perform two-phase split
[xi,yi,fv]=two_phase_split_f(Ki,zi);
% Compute EOS mixing rules am, bm
```



```
[am_L,bm_L,am_v,bm_v]=mixing_rules_f(kij,ai_c,xi,bi_c,yi);
% Compute liquid and vapor phase Z-factors and component fugacities using an EOS
[Z_L,Z_v,fi_L_Pa,fi_v_Pa]=SRK_PR_Z_fug_f...
    (kij,ai_c,am_L,xi,bi_c,bm_L,P_Pa,T_K,yi,am_v,bm_v,EOS_type);
disp('Two-phase flash results:')
% Compute equilibrium properties
[xi_eq,yi_eq,fv_eq,Ki_eq,Z_L_eq,Z_v_eq,fi_eq_Pa,lnfi_eq_atm]=Ki_SS_method_f...
    (Ki,fi_L_Pa,fi_v_Pa,zi,kij,ai_c,bi_c,P_Pa,T_K,EOS_type)
% Rename equilibrium fugacities for brevity
fi_Pa=fi_eq_Pa;
%% Volume shift (remove this section if not used)
% Compute modified (volume-corrected) fugacities
fi_mod_Pa=Vshift_fug_correction_f(EOS_type,greek_oilfield,bi_c,fi_Pa,P_Pa,T_K);
% Rename fugacities for the gradient calculation
fi_Pa=fi_mod_Pa;
%% Isothermal compositional gradient calculation
% Set reservoir boundaries
htop_ft=7800; % top depth
hbot_ft=8700; % bottom depth
disp('ISOTHERMAL COMPOSITIONAL GRADIENT RESULTS:')
% Compute gradient to top
disp('Reference depth to top depth:')
for h_ft=8070:-90:htop_ft
    % Display next depth in feet
    h_ft
    % Compute fi, zi, P, Psat at the next depth
    [fi_h_Pa,zi_h,P_h_psia,Psat_h_psia]=GCE_algorithm...
        (href_ft,h_ft,fi_Pa,Mi,T_K,zi,P_Pa,kij,ai_c,bi_c,EOS_type,greek_oilfield,Tc_K,Pc_MPa,w)
    % Stop if bottom depth is reached
    if href_ft==hbot_ft
        break
    end
    % Reset names for the next iteration
    href_ft=h_ft;
    fi_Pa=fi_h_Pa;
    zi=zi_h;
    P_Pa=P_h_psia*6.8948e+03;
end
% Reset to reference depth data for the next calculation
href_ft=8134;
fi_Pa=fi_mod_Pa;
zi=zi_feed;
P_Pa=Pref_psia*6.8948e+03;
% Compute gradient to bottom
disp('Reference depth to bottom depth:')
for h_ft=8160:90:hbot_ft
    % Display next depth in feet
    h_ft
    % Compute fi, zi, P, Psat at the next depth
    [fi_h_Pa,zi_h,P_h_psia,Psat_h_psia]=GCE_algorithm...
        (href_ft,h_ft,fi_Pa,Mi,T_K,zi,P_Pa,kij,ai_c,bi_c,EOS_type,greek_oilfield,Tc_K,Pc_MPa,w)
    % Stop if bottom depth is reached
    if href_ft==hbot_ft
        break
    end
    % Reset names for the next iteration
    href_ft=h_ft;
    fi_Pa=fi_h_Pa;
    zi=zi_h;
    P_Pa=P_h_psia*6.8948e+03;
end
%% GOC location
% Reset to reference depth data
href_ft=8134;
fi_Pa=fi_mod_Pa;
zi=zi_feed;
P_Pa=Pref_psia*6.8948e+03;
disp('Gas/Oil Contact:')
% Compute GOC depth (remove this section if the mixture is single-phase)
[hGOC_ft,zi_GOC,P_GOC_psia,Psat_GOC_psia]=GOC_calc...
    (htop_ft,hbot_ft,href_ft,fi_Pa,Mi,T_K,zi,P_Pa,kij,ai_c,bi_c,EOS_type,greek_oilfield,Tc_K,Pc_MPa,w)
format loose
```

- EOS a_i , b_i function

```
function varargout=New_a_aibi_cubic_f(EOS_type,component_id_or_Tc,Pc,w)
%{
This function accepts as inputs the following:
EOS_type, is a string of the Cubic equation to be used. It can be
'SRK', 'SRK-GD', 'SRK-GD-B1' or 'PR'. If the EOS_type is not defined, the default is
'SRK'.
component_id_or_Tc: is a double variable..
```



```

        if there are no other input arguments, then component_id_or_Tc is a [nx1]
        vector, containing the id-number of each component.
        When Pc, and w are also input arguments, then component_id_or_Tc is a [nx1]
        vector, containing the critical temperature (in Kelvin) of each component
    Pc, is the [nx1] vector of critical pressures (in bar)
    w, is the [nx1] vector of acentric coefficients
    The number of output variables varies according to the calling command:
        1st output variable is ai
        2nd output variable is bi
        3rd output variable is the gradient of ai(T) with respect to T
        4th output variable is the gradient of bi(T) with respect to T
        5th output variable is the vector of the diagonal of the hessian matrix
          of ai(T) with respect to T
        6th output variable is the vector of the diagonal of the hessian matrix
          of bi(T) with respect to T
    })
    if nargin<2;
        varargout=cell(nargout,1);
        disp('Insufficient number of input arguments')
        return
    end
    % Check the EOS_type input argument
    if not (ischar(EOS_type)) || not (any(ismember(EOS_type,{'SRK','SRK-GD','SRK-GD-B1','PR'})));
        % In any other case use SRK EOS as default
        disp('The input argument was not in correct format. SRK was used')
        EOS_type='SRK';
    end
    % Check the component_id_or_Tc input argument
    if not (isvector(component_id_or_Tc));
        % Terminate the routine and display error message
        disp('the input is not valid')
        disp('Input should be in (, EOS_type[string], component_id[nx1] or Tc (Kelvin), Pc (bar), w')
        varargout=cell(nargout,1);
        return
    end
    % Convert component_id_or_Tc to column vector format
    if size(component_id_or_Tc,2)>1; component_id_or_Tc=component_id_or_Tc';end
    % formulate a help variable
    n=length(component_id_or_Tc);
    if nargin==2;
        % if only component_id is input
        % ===== load data structures =====
        %{
        The following lines will load the {SRT_properties_columns/struct},
        and {ideal_gas_component_coefficients/struct} into the workspace of
        the function
        SRT_properties_columns(struct_vectors.[number],.{names}.[Tc],.[Pc],.[w],
        ,...,kij struct[.names,.kij]);
        NOTE:Direct assignment from the function to the workspace of the calling
        routine is not allowed
        %}
        S = load('greek_oilfield.mat');
        greek_oilfield = S.greek_oilfield;
        clear ('S');
        % ===== Check input =====
        % Set a logic value for components selection that exist in the respective
        % database {Solute_properties_columns/struct} of the aqua phase
        [logic,comp_index]=ismember(component_id_or_Tc,greek_oilfield.number);
        % Check if the input argument has valid entries in the
        % SRT_properties_columns structure. Otherwise stop the function.
        if any(not(logic));
            disp('Invalid input. The input component_id should have valid entries in')
            disp('the SRT_parameters_Ballardthesis structure')
            varargout=cell(nargout,1);
            return
        end
        % ===== Cast the necessary data to the respective variables ===
        Tc=greek_oilfield.Tc_K(comp_index);
        Pc=greek_oilfield.Pc_MPa(comp_index);
        Pc = Pc*1e6 ; % convert to Pascal
        w=greek_oilfield.acentric_factor_w(comp_index);
        if ismember(EOS_type,{'SRK-GD-B1'});
            names=greek_oilfield.names(comp_index);
            S2=greek_oilfield.S2(comp_index);
        end
        % extract the names of the components from the database structure
        names=greek_oilfield.names(comp_index);
    elseif nargin<4 || any([length(Pc)~=n,length(w)~=n]);
        % Terminate the routine and display error message
        disp('the input is not valid')
        disp('Input should be in (, EOS_type[string], component_id[nx1] or Tc (Kelvin), Pc (bar), w')
        varargout=cell(nargout,1);
        return
    else
        % Convert component_id_or_Tc to Tc
        Tc=component_id_or_Tc;
        % Convert Pc to column vector format
        if size(Pc,2)>1; Pc=Pc';end

```



```

    % convert Pc from bar to Pascal
    Pc = Pc*1e5 ;
    % Convert w to column vector format
    if size(w,2)>1; w=w';end
end
% ===== Constants and coefficients =====
% gas constant [=] J/(mol K): Pa*m3/(mol*K)
R = 8.314472;
% Set an auxiliary variable
sqrt_Tc=sqrt(Tc);
% ===== Formulate ai bi =====
% Switch according to EOS_type string argument
flag_type = EOS_type;
if ismember(EOS_type,{'SRK-GD-B1'});
    % Typical SRK-EOS(1972)
    % SRK Typical Parameters
    Omega_a = 0.42747;
    Omega_b = 0.08664;
    Zc = 0.333333;
    % coefficients for the generic cubic EOS
    d1=1; d2=0;
    % formulate the constant S1 (as it is referenced in Ballard thesis pg
    % 42
    S1 = 0.48508+1.55171*w-0.15613*(w.^2);
    % If there are water / methanol /ethanol among the components, use the
    % special S1 as they are stated in Ballard thesis pg 350 Table E.11
    logic_Water=ismember(names,{'Water'});
    logic_Methanol=ismember(names,{'Methanol'});
    logic_Ethanol=ismember(names,{'Ethanol'});
    if any(logic_Water);
        S1(logic_Water)=1.2440;
    end
    if any(logic_Methanol);
        S1(logic_Methanol)=1.8283;
    end
    if any(logic_Ethanol);
        S1(logic_Ethanol)=1.6787;
    end
    ac = Omega_a * ((R*Tc).^2)./Pc;
    % Initialize the ai,bi routine, ai=f(T), bi=f(T)
    ai = @(T) ac.*(1+S1.*(1-sqrt(T)./sqrt_Tc)+S2.*(sqrt_Tc./sqrt(T)-1)).^2);
    divai = @(T) -ac.*(1+S1.*(1-sqrt(T)./sqrt_Tc))+S2.*(sqrt_Tc./sqrt(T)-1).*...
        (S1./(sqrt(T)*sqrt_Tc)+S2.*sqrt_Tc./sqrt(T)./T);
    div2ai = @(T) ac.*((S1./sqrt(T)*sqrt_Tc)+S2.*sqrt_Tc./sqrt(T)./T).^2+...
        (1+S1.*(1-sqrt(T)./sqrt_Tc)+S2.*(sqrt_Tc./sqrt(T)-1)).*...
        (S1./(sqrt(T)*sqrt_Tc)+3*S2.*sqrt_Tc./sqrt(T)./T)./(2.*T));
else
    if ismember(EOS_type,{'SRK','SRK-GD'});
        % Typical SRK-EOS(1972)
        % SRK Typical Parameters
        Omega_a = 0.427480234;
        Omega_b = 0.08664035;
        Zc = 0.333333;
        m_coefficient = [0.480 , 1.574 , -0.176]';
        % coefficients for the generic cubic EOS
        d1=1; d2=0;
    end
    if strcmp(EOS_type,'PR');
        % Typical PR-EOS (1976)
        % PR Typical Parameters
        Omega_a = 0.457235528921;
        Omega_b = 0.0777960739039;
        Zc = 0.307401;
        m_coefficient = [0.37464, 1.54226, -0.26992]';
        % coefficients for the generic cubic EOS
        d1=1+sqrt(2); d2=1-sqrt(2);
    end
    % formulate the constants
    m = [ones(n,1) , w , w.^2] * m_coefficient ;
    ac = Omega_a * ((R*Tc).^2)./Pc;
    % Initialize the ai,bi routine, ai=f(T,V), bi=f(T,V)
    ai = @(T) ac.*(1+m.*(1-sqrt(T./Tc))).^2);
    divai = @(T) -ac.*(1+m.*(1-sqrt(T)./sqrt_Tc)).*m./sqrt(T)./sqrt_Tc./Tc;
    div2ai = @(T) ac.*(1/2.*m.^2/T./Tc +1/2*(1+m.*(1-sqrt(T)./sqrt_Tc)).*m./(T*sqrt(T)*sqrt_Tc));
end
% Formulate the repulsive constants
bi = @(T) Omega_b * R * (Tc./Pc);
divbi= @(T) zeros(n,2);
div2bi= @(T) zeros(n,2);
% ===== Formulate output =====
switch nargout
case 0
    disp('No output arguments')
    varargout={};
case 1
    varargout={ai};
case 2
    varargout={ai,bi};
end

```



```

case 3
    varargout={ai,bi,divai};
case 4
    varargout={ai,bi,divai,divbi};
case 5
    varargout={ai,bi,divai,divbi,div2ai};
case 6
    varargout={ai,bi,divai,divbi,div2ai,div2bi};
otherwise
    varargout=horzcat({ai,bi,divai,divbi,div2ai,div2bi},cell(1,nargout-6));
end
% end of function
end

```

- **Wilson method function**

```

function [Ki]=a_Wilsonmethod_initial_estimates_f(T_K,P_Pa,Tc_K,Pc_MPa,w)
% The function returns the handles of ki=f(T,P) initial estimates for the
% flash problem, based on the Wilson's equation.
% ki [nx1] are the partition coefficients between two phases.
% Ki = fugacity of i component in phase1/ fugacity of i component in
% phase2.
% Tc is the critical pressure of each component in Kelvin (vector nx1)
Tc=Tc_K;
% Pc is the critical pressure of each component in Pascal (vector nx1)
Pc=1.0e6*Pc_MPa ; % convert to Pascal
%{
The function will calculate the Wilson Ki=yi/xi=fug_coef(xi)/fug_coef(yi),
given the Temperature in Kelvin and Pressure in Pascal.
The final output will be an estimation of the fugacity coefficient ratio
between the liquid and vapor components that satisfies the Wilson's Kis
%}
% Calculate the coefficients with respect to Wilson correlation
Log_Ki_Wilson=5.37.*(1+w).*(1-Tc./T_K)+log(Pc./P_Pa);
% Normalize the Kis with respect to the "average" Ki
Ki=exp(Log_Ki_Wilson);
% End of the primary function
end

```

- **Stability test function (vapor-like search)**

```

function [S_v,yi_stab,Ki_v]=stability_test_vapor_f(Ki,zi,kij,ai_c,bi_c,P_Pa,T_K,EOS_type)
%{
This function is based on the stability test algorithm provided by C. H.
Whitson and M. R. Brule in "Phase Behavior, SPE Monograph Vol. 20, Henry L.
Doherty Series", Chap. 4, Sec. 4.4, pp. 9-15.
The algorithm assumes the second phase to be vapor.
The input arguments are the following:
Ki, the Wilson method computed K-values, [nx1]
zi, the mixture feed composition [nx1]
kij, the binary interaction coefficients [nxn]
ai_c, bi_c, the component "attraction" and "repulsion" parameters [nx1]
P_Pa, the reference pressure in Pascal [1x1]
T_K, the reference temperature in Kelvin [1x1]
EOS_type, the type of EOS used (character array)
The output arguments are:
S_v, the sum of second phase mole numbers [nx1]
yi_stab, the stability test second phase composition [nx1]
Ki_v, the stability test K-values [nx1]
%}
% Mixture is liquid
xi=zi;
yi=deal(nan);
% Compute mixture fugacities
[am_L,bm_L,am_v,bm_v]=mixing_rules_f(kij,ai_c,xi,bi_c,yi);
[Z_L,Z_v,fi_L_Pa,fi_v_Pa]=SRK_PR_Z_fug_f...
(kij,ai_c,am_L,xi,bi_c,bm_L,P_Pa,T_K,yi,am_v,bm_v,EOS_type);
fi_z_Pa=fi_L_Pa;
% Begin iteration sequence (iterate until convergence is achieved)
for n=1:1000
    % Begin Successive-Substitution (four iterations)
    for m=1:4
        % Compute second phase mole numbers
        Yi_v=zi.*Ki; % after (4.65)
        % Sum the mole numbers
        S_v=sum(Yi_v); % after (4.66)
        % Compute second phase composition

```



```

        yi=Yi_v/S_v; % after (4.67)
        % Compute second phase component fugacities using an EOS
        [am_L,bm_L,am_v,bm_v]=mixing_rules_f(kij,ai_c,xi,bi_c,yi);
        [Z_L,Z_v,fi_L_Pa,fi_v_Pa]=SRK_PR_Z_fug_f...
            (kij,ai_c,am_L,xi,bi_c,bm_L,P_Pa,T_K,yi,am_v,bm_v,EOS_type);
        % Compute fugacity ratio corrections
        ri=(fi_z_Pa./fi_v_Pa)/S_v; % after (4.68)
        % Update K-values using SS
        Ki_new=Ki.*ri; % after (4.70)
        % Rename K-values for the next iteration
        Ki=Ki_new;
    end
    % Rename fugacity ratio corrections for the next iteration
    ri_old=ri;
    % Begin GDEM acceleration (one iteration)
    % Compute second phase mole numbers
    Yi_v=zi.*Ki;
    % Sum the mole numbers
    S_v=sum(Yi_v);
    % Compute second phase composition
    yi=Yi_v/S_v;
    % Compute second phase component fugacities using an EOS
    [am_L,bm_L,am_v,bm_v]=mixing_rules_f(kij,ai_c,xi,bi_c,yi);
    [Z_L,Z_v,fi_L_Pa,fi_v_Pa]=SRK_PR_Z_fug_f...
        (kij,ai_c,am_L,xi,bi_c,bm_L,P_Pa,T_K,yi,am_v,bm_v,EOS_type);
    % Compute fugacity ratio corrections
    ri=(fi_z_Pa./fi_v_Pa)/S_v;
    % Compute  $\lambda$  after Eq. (4.72)
    b01=sum(log(ri).*log(ri_old));
    b11=sum(log(ri_old).^2);
    lamda=abs(b11/(b11-b01));
    % Update K-values using GDEM
    Ki_new=Ki.*(ri.^lamda); % after (4.72)
    % Check for convergence
    if sum((ri-1).^2)<1.0e-12 % after Eq.(4.69)
        break
    end
    % Check for convergence at a trivial solution
    if sum((log(Ki_new)).^2)<1.0e-04 % after Eq.(4.71)
        break
    end
    % Rename K-values for the next iteration
    Ki=Ki_new;
end
% Update output variable names
yi_stab=yi;
Ki_v=Ki_new;
end

```

- **Stability test function (liquid-like search)**

```

function [S_L,xi_stab,Ki_L]=stability_test_Liq_f(Ki,zi,kij,ai_c,bi_c,P_Pa,T_K,EOS_type)
%{
    This function is based on the stability test algorithm provided by C. H.
    Whitson and M. R. Brule in "Phase Behavior, SPE Monograph Vol. 20, Henry L.
    Doherty Series", Chap. 4, Sec. 4.4, pp. 9-15.
    The algorithm assumes the second phase to be liquid.
    The input arguments are the following:
    Ki, the Wilson method computed K-values, [nx1]
    zi, the mixture feed composition [nx1]
    kij, the binary interaction coefficients [nxn]
    ai_c, bi_c, the component "attraction" and "repulsion" parameters [nx1]
    P_Pa, the reference pressure in Pascal [1x1]
    T_K, the reference temperature in Kelvin [1x1]
    EOS_type, the type of EOS used (character array)
    The output arguments are:
    S_L, the sum of second phase mole numbers [nx1]
    xi_stab, the stability test second phase composition [nx1]
    Ki_L, the stability test K-values [nx1]
%}
% Mixture is vapor
yi=zi;
xi=deal(nan);
% Compute mixture fugacities
[am_L,bm_L,am_v,bm_v]=mixing_rules_f(kij,ai_c,xi,bi_c,yi);
[Z_L,Z_v,fi_L_Pa,fi_v_Pa]=SRK_PR_Z_fug_f...
    (kij,ai_c,am_L,xi,bi_c,bm_L,P_Pa,T_K,yi,am_v,bm_v,EOS_type);
fi_z_Pa=fi_v_Pa;
% Begin iteration sequence (iterate until convergence is achieved)
for n=1:1000
    % Begin Successive-Substitution (four iterations)
    for m=1:4

```



```

    % Compute second phase mole numbers
    Yi_L=zi./Ki; % after (4.65)
    % Sum the mole numbers
    S_L=sum(Yi_L); % after (4.66)
    % Compute second phase composition
    xi=Yi_L/S_L; % after (4.67)
    % Compute second phase component fugacities using an EOS
    [am_L,bm_L,am_v,bm_v]=mixing_rules_f(kij,ai_c,xi,bi_c,yi);
    [Z_L,Z_v,fi_L_Pa,fi_v_Pa]=SRK_PR_Z_fug_f...
        (kij,ai_c,am_L,xi,bi_c,bm_L,P_Pa,T_K,yi,am_v,bm_v,EOS_type);
    % Compute fugacity ratio corrections
    ri=(fi_L_Pa./fi_v_Pa)*S_L; % after (4.68)
    % Update K-values using SS
    Ki_new=Ki.*ri; % after (4.70)
    % Rename K-values for the next iteration
    Ki=Ki_new;
end
% Rename fugacity ratio corrections for the next iteration
ri_old=ri;
% Begin GDEM acceleration (one iteration)
% Compute second phase mole numbers
Yi_L=zi./Ki;
% Sum the mole numbers
S_L=sum(Yi_L);
% Compute second phase composition
xi=Yi_L/S_L;
% Compute second phase component fugacities using an EOS
[am_L,bm_L,am_v,bm_v]=mixing_rules_f(kij,ai_c,xi,bi_c,yi);
[Z_L,Z_v,fi_L_Pa,fi_v_Pa]=SRK_PR_Z_fug_f...
    (kij,ai_c,am_L,xi,bi_c,bm_L,P_Pa,T_K,yi,am_v,bm_v,EOS_type);
% Compute fugacity ratio corrections
ri=(fi_L_Pa./fi_v_Pa)*S_L;
% Compute  $\lambda$  after Eq. (4.72)
b0l=sum(log(ri).*(log(ri_old)));
b1l=sum(log(ri_old).^2);
lamda=abs(b1l/(b1l-b0l));
% Update K-values using GDEM
Ki_new=Ki.*(ri.^lamda); % after (4.72)
% Check for convergence
if sum((ri-1).^2)<1.0e-12 % after Eq.(4.69)
    break
end
% Check for convergence at a trivial solution
if sum((log(Ki_new)).^2)<1.0e-04 % after Eq.(4.71)
    break
end
% Rename K-values for the next iteration
Ki=Ki_new;
end
% Update output variable names
xi_stab=xi;
Ki_L=Ki_new;
end

```

- Saturation pressure calculation function

```

function [Psat_psia,yi_sat,Ki_sat,Z_L_sat,Z_v_sat,fi_sat_Pa,lnfi_sat_atm]=Psat_calc_f...
    (P_Pa,T_K,Tc_K,Pc_MPa,w,zi,kij,ai_c,bi_c,EOS_type)
%{
This function is based on the saturation pressure calculation algorithm
provided by C. H. Whitson and M. R. Brule in "Phase Behavior, SPE Monograph
Vol. 20, Henry L. Doherty Series", Chap. 4, Sec. 4.5, pp. 16-17.
The input arguments are the following:
P_Pa, the reference pressure in Pascal [1x1]
T_K, the reference temperature in Kelvin [1x1]
Pc_Pa, the component critical pressure in Pascal [nx1]
Tc_K, the component critical temperature in Kelvin [nx1]
w, the component acentric factor [nx1]
zi, the dominant phase (liquid) composition [nx1]
kij, the binary interaction coefficients [nxn]
ai_c, bi_c, the component "attraction" and "repulsion" parameters [nx1]
EOS_type, the type of EOS used (character array)
The output arguments are:
Psat_psia, the saturation pressure in psia [1x1]
yi_sat, the incipient phase (vapor) composition [nx1]
Ki_sat, the bubble-point component K-values [nx1]
Z_L_sat, the dominant phase (liquid) Z-factor [1x1]
Z_v_sat, the incipient phase (vapor) Z-factor [1x1]
fi_sat_Pa, the bubble-point component fugacities in Pa [nx1]
lnfi_sat_atm, the bubble-point logarithmic fugacities in atm [nx1]
%}
% Initial guess for saturation pressure

```


Appendix B: MATLAB® Open Source Code

```
Psat_Pa=P_Pa-500*6.8948e+03;
% Rename saturation pressure for brevity
P_Pa=Psat_Pa;
% Perform stability test at the current saturation pressure estimate
% Compute initial K-values
[Ki]=a_Wilsonmethod_initial_estimates_f(T_K,P_Pa,Tc_K,Pc_MPa,w);
% Vapor-like search
[S_v,yi_stab,Ki_v]=stability_test_vapor_f(Ki,zi,kij,ai_c,bi_c,P_Pa,T_K,EOS_type);
% Compute incipient phase mole numbers
Yi=zi.*Ki_v; % after Eq. (4.80.a)
% Dominant phase is liquid
xi=zi;
% Begin iteration sequence (iterate until convergence is achieved)
for n=1:1000
    % Begin Successive-Substitution (four iterations)
    for m=1:4
        % Compute incipient phase composition yi
        yi=Yi/sum(Yi); % after Eq. (4.81)
        % Compute dominant and incipient phase mixing rules
        [am_L,bm_L,am_v,bm_v]=mixing_rules_f(kij,ai_c,xi,bi_c,yi);
        % Compute dominant and incipient phase Z-factors and component fugacities
        [Z_L,Z_v,fi_L_Pa,fi_v_Pa]=SRK_PR_Z_fug_f...
            (kij,ai_c,am_L,xi,bi_c,bm_L,P_Pa,T_K,yi,am_v,bm_v,EOS_type);
        % Compute fugacity ratio corrections
        ri=(fi_L_Pa./fi_v_Pa)/sum(Yi); % after Eq. (4.82)
        % Update mole numbers using SS
        Yi_new=Yi.*ri; % after Eq. (4.83) with  $\lambda=1$ 
        % Compute Q function
        Q=1-sum(Yi); % after Eq. (4.78)
        % Compute fugacity gradients
        gradfi_L=gradient(fi_L_Pa,P_Pa); % liquid phase
        gradfi_v=gradient(fi_v_Pa,P_Pa); % vapor phase
        % Compute Q function gradient
        gradQ=sum(Yi.*ri.*(gradfi_v./fi_v_Pa+gradfi_L./fi_L_Pa)); % after Eq. (4.86)
        % Update saturation pressure estimate using the Newton-Raphson method
        P_new=P_Pa+Q/gradQ; % after Eq. (4.85)
        % Rename mole numbers and saturation pressure estimates for the next iteration
        Yi=Yi_new;
        P_Pa=P_new;
    end
    % Rename fugacity ratio corrections for GDEM
    ri_old=ri;
    % Begin GDEM acceleration (one iteration)
    % Compute incipient phase composition yi
    yi=Yi/sum(Yi);
    % Compute dominant and incipient phase mixing rules
    [am_L,bm_L,am_v,bm_v]=mixing_rules_f(kij,ai_c,xi,bi_c,yi);
    % Compute dominant and incipient phase Z-factors and component fugacities
    [Z_L,Z_v,fi_L_Pa,fi_v_Pa]=SRK_PR_Z_fug_f...
        (kij,ai_c,am_L,xi,bi_c,bm_L,P_Pa,T_K,yi,am_v,bm_v,EOS_type);
    % Compute fugacity ratio corrections
    ri=(fi_L_Pa./fi_v_Pa)/sum(Yi);
    % Compute  $\lambda$  after Eq. (4.84)
    b01=sum(log(ri).*log(ri_old));
    b11=sum(log(ri_old).^2);
    lamda=abs(b11/(b11-b01));
    % Update mole numbers using GDEM
    Yi_new=Yi.*(ri.^lamda); % after Eq. (4.83)
    % Compute Q function
    Q=1-sum(Yi);
    % Compute fugacity gradients
    gradfi_L=gradient(fi_L_Pa,P_Pa); % liquid phase
    gradfi_v=gradient(fi_v_Pa,P_Pa); % vapor phase
    % Compute Q function gradient
    gradQ=sum(Yi.*ri.*(gradfi_v./fi_v_Pa+gradfi_L./fi_L_Pa));
    % Update saturation pressure estimate using the Newton-Raphson method
    P_new=P_Pa+Q/gradQ;
    % Check for convergence using the criteria after Eq.(4.87)
    if abs(1-sum(Yi_new))<1.0e-13 || (sum(log(ri)./log(Yi_new./zi)))^2<1.0e-08
        break
    end
    % Check for convergence at a trivial solution
    if sum((log(Yi_new./zi)).^2)<1.0e-04 % after Eq. (4.88)
        break
    end
    % Rename mole numbers and saturation pressure estimates for the next iteration
    Yi=Yi_new;
    P_Pa=P_new;
end
% Perform stability test at the final saturation pressure estimate
P_Pa=P_new;
[Ki]=a_Wilsonmethod_initial_estimates_f(T_K,P_Pa,Tc_K,Pc_MPa,w);
[S_v,yi_stab,Ki_v]=stability_test_vapor_f(Ki,zi,kij,ai_c,bi_c,P_Pa,T_K,EOS_type);
% Update output variable names
Psat_psia=P_Pa/6.8948e+03; % Convert saturation pressure to psia
yi_sat=yi;
Ki_sat=Ki_v;
Z_L_sat=Z_L;
```



```
Z_v_sat=Z_v;
fi_sat_Pa=fi_v_Pa;
lnfi_sat_atm=log(fi_sat_Pa)-log(101325); % Convert logarithmic fugacities to atm
end
```

- Dew-point pressure calculation function

```
function [Pdew_psia,xi_dew,Ki_dew,Z_L_dew,Z_v_dew,fi_dew_Pa,lnfi_dew_atm]=Pdew_calc_f...
(P_Pa,T_K,Tc_K,Pc_MPa,w,zi,kij,ai_c,bi_c,EOS_type)

%{
This function is based on the saturation pressure calculation algorithm
provided by C. H. Whitson and M. R. Brule in "Phase Behavior, SPE Monograph
Vol. 20, Henry L. Doherty Series", Chap. 4, Sec. 4.5, pp. 16-17.
The input arguments are the following:
P_Pa, the reference pressure in Pascal [1x1]
T_K, the reference temperature in Kelvin [1x1]
Pc_Pa, the component critical pressure in Pascal [nx1]
Tc_K, the component critical temperature in Kelvin [nx1]
w, the component acentric factor [nx1]
zi, the dominant phase (vapor) composition [nx1]
kij, the binary interaction coefficients [nxn]
ai_c, bi_c, the component "attraction" and "repulsion" parameters [nx1]
EOS_type, the type of EOS used (character array)
The output arguments are:
Psat_psia, the saturation pressure in psia [1x1]
xi_dew, the incipient phase (liquid) composition [nx1]
Ki_dew, the dew-point component K-values [nx1]
Z_L_dew, the dominant phase (liquid) Z-factor [1x1]
Z_v_dew, the incipient phase (vapor) Z-factor [1x1]
fi_dew_Pa, the dew-point component fugacities in Pa [nx1]
lnfi_dew_atm, the dew-point logarithmic fugacities in atm [nx1]
%}

% Initial guess for dew-point pressure
Pdew_Pa=P_Pa-500*6.8948e+03;
% Rename dew-point pressure for brevity
P_Pa=Pdew_Pa;
% Perform stability test at the current dew-point pressure
[Ki]=a_Wilsonmethod_initial_estimates_f(T_K,P_Pa,Tc_K,Pc_MPa,w);
% Liquid-like search
[S_L,xi_stab,Ki_L]=stability_test_Liq_f(Ki,zi,kij,ai_c,bi_c,P_Pa,T_K,EOS_type);
% Compute incipient phase mole numbers
Yi=zi./Ki_L; % after Eq. (4.80.b)
% Dominant phase is vapor
yi=zi;
% Begin iteration sequence (iterate until convergence is achieved)
for n=1:1000
    % Begin Successive-Substitution (four iterations)
    for m=1:4
        % Compute incipient phase composition xi
        xi=Yi/sum(Yi); % after Eq. (4.81)
        % Compute dominant and incipient phase mixing rules
        [am_L,bm_L,am_v,bm_v]=mixing_rules_f(kij,ai_c,xi,bi_c,yi);
        % Compute dominant and incipient phase Z-factors and component fugacities
        [Z_L,Z_v,fi_L_Pa,fi_v_Pa]=SRK_PR_Z_fug_f...
        (kij,ai_c,am_L,xi,bi_c,bm_L,P_Pa,T_K,yi,am_v,bm_v,EOS_type);
        % Compute fugacity ratio corrections
        ri=(fi_v_Pa./fi_L_Pa)/sum(Yi); % after Eq. (4.82)
        % Update mole numbers using SS
        Yi_new=Yi.*ri; % after Eq. (4.83) with λ=1
        % Compute Q function
        Q=1-sum(Yi); % after Eq. (4.78)
        % Compute fugacity gradients
        gradfi_L=gradient(fi_L_Pa,P_Pa); % liquid phase
        gradfi_v=gradient(fi_v_Pa,P_Pa); % vapor phase
        % Compute Q function gradient
        gradQ=sum(Yi.*ri.*(gradfi_v./fi_v_Pa+gradfi_L./fi_L_Pa)); % after Eq. (4.86)
        % Update dew-point pressure estimate using the Newton-Raphson method
        P_new=P_Pa+Q/gradQ; % after Eq. (4.85)
        % Rename mole numbers and dew-point pressure estimates for the next iteration
        Yi=Yi_new;
        P_Pa=P_new;
    end
    % Rename fugacity ratio corrections for GDEM
    ri_old=ri;
    % Begin GDEM acceleration (one iteration)
    % Compute incipient phase composition xi
    xi=Yi/sum(Yi);
    % Compute dominant and incipient phase mixing rules
    [am_L,bm_L,am_v,bm_v]=mixing_rules_f(kij,ai_c,xi,bi_c,yi);
    % Compute dominant and incipient phase Z-factors and component fugacities
    [Z_L,Z_v,fi_L_Pa,fi_v_Pa]=SRK_PR_Z_fug_f...
    (kij,ai_c,am_L,xi,bi_c,bm_L,P_Pa,T_K,yi,am_v,bm_v,EOS_type);
```



```

% Compute fugacity ratio corrections
ri=(fi_v_Pa./fi_L_Pa)/sum(Yi);
% Compute  $\lambda$  after Eq. (4.84)
b01=sum(log(ri).*log(ri_old));
b11=sum(log(ri_old).^2);
lamda=abs(b11/(b11-b01));
% Update mole numbers using GDEM
Yi_new=Yi.*(ri.^lamda); % after Eq. (4.83)
% Compute Q function
Q=1-sum(Yi);
% Compute fugacity gradients
gradfi_L=gradient(fi_L_Pa,P_Pa); % liquid phase
gradfi_v=gradient(fi_v_Pa,P_Pa); % vapor phase
% Compute Q function gradient
gradQ=sum(Yi.*ri.*(gradfi_v./fi_v_Pa+gradfi_L./fi_L_Pa));
% Update dew-point pressure estimate using the Newton-Raphson method
P_new=P_Pa+Q/gradQ;
% Check for convergence using the criteria after Eq.(4.87)
if abs(1-sum(Yi_new)/zi)<1.0e-13|| (sum(log(ri)./log(Yi_new./zi)))^2<1.0e-08
    break
end
% Check for convergence at a trivial solution
if sum((log(Yi_new./zi)).^2)<1.0e-04 % after Eq. (4.88)
    break
end
% Rename mole numbers and dew-point pressure estimates for the next iteration
Yi=Yi_new;
P_Pa=P_new;
end
% Update output variable names
Pdew_psia=P_new/6.8948e+03; % Convert dew-point pressure to psia
xi_dew=yi;
Ki_dew=Ki_L;
Z_L_dew=Z_L;
Z_v_dew=Z_v;
fi_dew_Pa=fi_L_Pa;
lnfi_dew_atm=log(fi_dew_Pa)-log(101325); % Convert logarithmic fugacities to atm
end

```

- Two-phase split function

```

function [xi,yi,fv]=two_phase_split_f(Ki,zi)
% The function uses a modified 2-pole method to calculate the vapor phase
% fraction in a 2-phase problem. If the convergence fails it uses the
% matlab standard root finding function
%{
The following method is based on the 2-pole method described in the article
" A general framework of model functions for rapid and robust solution of
Rachford-Rice type of equations" Gaganis, Marinakis ,Varotsis.
Fluid Phase Equilibria 322-323 (2012) 9-18
Input: Ki vector [nx1] of the equilibrium coefficients K=yi/xi for each component
Input: zi vector [nx1] of feed composition
Output
fv: (2x1 vector) [molar fraction of the yi's phase, molar fraction of the xi's
                  phase with respect to feed]
xi: vector [nx1] composition of the "liquid" phase
yi: vector [nx1] composition of the "vapor" phase

The function was last update on 25/11/2018
%}
%% Check input
if nargin<2|| length(Ki)~= length(zi) || any(Ki<=0) || any(zi<=0)
    [xi,yi,fv]=deal(nan);
    return
end
% set constants and limits
convergenceRRlimit=eps;
% Set Criticality index
criticality=false; %%ok<*NASGU>
%% Set limits for Ki's
%Ki close to 1 limit
Ki_closeTo1 = abs(Ki-1)<=eps;
% if any component has Ki values close to 1 do not use them for computing RR function
% since they don't affect the sum (Ki-1)*zi=0;
% They will be added at the end at equal concentrations xi=zi;
if any(Ki_closeTo1)
    % Cast the original values into a permanent variable
    zi_initial=zi;
    % reformulate Ki and zi
    Ki(Ki_closeTo1)=[];
    zi(Ki_closeTo1)=[];
    Ki_closeTo1_logic=true;

```



```

else
    Ki_closeTo1_logic=false;
end
%% Check for dominant phase
% if the mixture is dominant gas reverse the reference phase
if (zi'*Ki)/(zi'*(1./Ki))>1e6
    Ki=1./Ki;
    Ki_reverse_logic=true;
else
    Ki_reverse_logic=false;
end
% Find the minimum and maximum Ki values to set the limits for phase
% fraction
[~,Ki_max_index]=max(Ki);
[~,Ki_min_index]=min(Ki);
% formulate bi s
bi=1./(1-Ki);
b_min=bi(Ki_max_index);
b_max=bi(Ki_min_index);
% Check for criticality
if (b_max-b_min)>10
    b_max=min([1.1,b_max]);
    b_min=max([-0.1,b_min]);
    a_criticality=(b_max-b_min)/(bi(Ki_min_index)-bi(Ki_max_index));
    b_criticality=b_min-a_criticality*bi(Ki_max_index);
    % Transformation of poles to [b_min,b_max] space
    bi=a_criticality*bi+b_criticality;
    criticality=true;
else
    criticality=false;
end
%% formulate the subfunctions
%1. The Rachford Rice function = sum( (ki-1)*zi/(1+fv*(ki-1)) )
function RR=hf(fv)
    RR=zi'*(1./(fv-bi));
end
% 2. The Rachford Rice without max bi value sum( (ki-1)*zi/(1+fv*(ki-1)) )
function RR2=h2f(fv)
    zi_int=zi;
    zi_int(Ki_min_index)=[];
    bi_int=bi;
    bi_int(Ki_min_index)=[];
    RR2=zi_int'*(1./(fv-bi_int));
end
% 3. The Rachford Rice without min bi value sum( (ki-1)*zi/(1+fv*(ki-1)) )
function RR2=h3f(fv)
    zi_int=zi;
    zi_int(Ki_max_index)=[];
    bi_int=bi;
    bi_int(Ki_max_index)=[];
    RR2=zi_int'*(1./(fv-bi_int));
end
%% Convergence routine selection
%{
    The selected convergence routines are the 2-poles except the case where
    the root is close to the b_min and b_max limit and there is a "knee" in
    the RR function (see chapter 4."Treating knees" in the reference
    paper). In this case the successive substitution method will be used
    instead of the proposed one in the paper.
    SS method is based on the fact that h1 is very fast decaying function
    with respect to h2+ so the next step can be calculated from the
    following equation: h1(b_new)=h2+(b_old) or
        b_new =b_min-zi(bi=b_min)/h2+(b_old)
    The respective applies for the b_max limit
%}
Two_pole_logic=true;
% Check for the possibility of a "knee"
if h3f(b_min)<-0.2 % "knee" on the left side
    % set the initial solution estimates
    Two_pole_logic=false;
    zmin=zi(Ki_max_index);
    h_old=h3f(b_min*0.999);
    b_old=b_min*0.999;
    for i=1:100
        b_new=b_min-zmin/h_old;
        % check for instability and if so proceed to 2 pole solution
        if b_new<=b_min || b_new>=b_max
            Two_pole_logic=true;
            break
        end
        %Check for convergence
        h_new=hf(b_new);
        if abs(h_new)<convergenceRRlimit ||...
            (abs(h_new)<1e-5&& ...
            (abs(b_new- b_old)/min([1,mean([abs(b_new),abs(b_old)])])<2*eps)
            break
        end
        % Update the values

```



```

        h_old=h3f(b_new);
        b_old=b_new;
    end
    if i==100
        Two_pole_logic=true;
    end
elseif h2f(b_max)>0.2 % "knee" on the right side
    % set the initial solution estimates
    Two_pole_logic=false;
    zmax=zi(Ki_min_index);
    h_old=h2f(b_max*0.999);
    b_old=b_max*0.999;
    for i=1:100
        b_new=b_max-zmax/h_old;
        % check for instability and if so proceed to 2 pole solution
        if b_new<=b_min || b_new>=b_max
            break
        end
        %Check for convergence
        h_new=hf(b_new);
        if abs(h_new)<convergenceRRlimit ||...
            (abs(h_new)<1e-5&& ...
            (abs(b_new- b_old)/min([1,mean([abs(b_new),abs(b_old)])])<2*eps)
            break
        end
        % Update the values
        h_old=h2f(b_new);
        b_old=b_new;
    end
    if i==100
        Two_pole_logic=true;
    end
end
if Two_pole_logic
    % Convergence using the routine of 2-poles. See eq. 13 on the reference paper.
    %  $h(b) \sim t(b) = w_1/(b-b_{leftLim}) + w_2/(b-b_{rightLim})$ 
    % set the initial solution estimates
    b1=(b_max-b_min)/3+b_min;
    b2=2*(b_max-b_min)/3+b_min;
    h1=hf(b1);
    h2=hf(b2);
    for i=1:100
        bisection_logic=false;
        % if the 2-pole matrix is close to singular use the bisection method
        if cond ([1/(b1-b_min),1/(b1-b_max);1/(b2-b_min),1/(b2-b_max)])>1e15
            bisection_logic=true;
        else
            % solve the system for [w1,w2] using the b1 and b2 solution estimates
            W=[1/(b1-b_min),1/(b1-b_max);1/(b2-b_min),1/(b2-b_max)]\ [h1;h2];
            % new estimation
            b_new=W*[b_max;b_min]/sum(W);
            % In case of negative values for W the solution is outside the feasible
            % area so proceed to corrections with bisection
            % In case where b_new is equal to either b1 or b2 the routine will
            % not converge or run into singularity, so proceed to corrections with
            % bisection
            if any(W<=0) || any(abs([b1,b2]-b_new)<eps)
                bisection_logic=true;
            end
        end
        % Use the bisection logic in case it is required
        if bisection_logic
            if h2>0 % the root lies between b2 and bmax
                b_new=(b2+b_max)/2;
            elseif h1*h2<0 % the root lies between b1 and b2
                b_new=(b1+b2)/2;
            else % the root lies between bmin and b1
                b_new=(b1+b_min)/2;
            end
        end
        % Set the convergence
        h_new=hf(b_new);
        if abs(h_new)<convergenceRRlimit || abs(b2-b1)/min([1,mean([abs(b1),abs(b2)])])<2*eps
            break
        end
    else
        % update the 2 poles
        if b_new>b2
            h1=h2;
            b1=b2;
            h2=h_new;
            b2=b_new;
        elseif b_new<b1
            h2=h1;
            b2=b1;
            h1=h_new;
            b1=b_new;
        elseif h1*h2<0
            if h1*h_new<0

```



```

                h2=h_new;
                b2=b_new;
            else
                h1=h_new;
                b1=b_new;
            end
        else
            if abs(h1)>abs(h2)
                h1=h_new;
                b1=b_new;
            else
                h2=h_new;
                b2=b_new;
            end
        end
    end
end
end
% Use a safeguard minimization function
if i==100
    b_new_fzer=fzero(@hf,b_new);
    if all([b_new_fzer>b_min, b_new_fzer<b_max, abs(h_new)>abs(hf(b_new_fzer))])
        b_new=b_new_fzer;
    end
end
%% Formulate output
% Function root transformation in case where criticality was applied
if criticality
    b_new=(b_new-b_criticality)/a_criticality;
end
fv=b_new;
[xi,yi]=deal(zeros(length(Ki_closeTol),1));
if Ki_reverse_logic
    % The reference phase is gas (dominant phase)
    yi(not(Ki_closeTol),1)=zi./(1+fv*(Ki-1));
    xi(not(Ki_closeTol),1)=Ki.*yi(not(Ki_closeTol),1);
    fv=[1-fv;fv];
else
    % The reference phase is liquid (dominant phase)
    xi(not(Ki_closeTol),1)=zi./(1+fv*(Ki-1));
    yi(not(Ki_closeTol),1)=Ki.*xi(not(Ki_closeTol),1);
    fv=[fv;1-fv];
end
if Ki_closeTol_logic
    % Recast the Ki=1 values to the original form
    xi(Ki_closeTol,1)=zi_initial(Ki_closeTol,1);
    yi=xi;
end
% To be modified in the future
fv=fv(1); % if the calling function has fv as scalar
end

```

- EOS mixing rules function

```

function [am_L,bm_L,am_v,bm_v]=mixing_rules_f(kij,ai_c,xi,bi_c,yi)
%{
This function is based on the cubic EOS mixing rules provided by Abbas
Firoozabadi in his book "Thermodynamics of Hydrocarbon Reservoirs", after
Eq.(3.29)-(3.31), Chap.3, pp.143
The input arguments are the following:
kij, the binary interaction coefficients [nxn]
ai_c, bi_c, the component "attraction" and "repulsion" parameters [nx1]
xi, yi, the liquid and vapor phase compositions [nx1]
The output arguments are:
am_L, am_v, the liquid and vapor phase quadratic mixing rules [1x1]
bm_L, bm_v, the liquid and vapor phase linear mixing rules [1x1]
%}
% Compute auxiliary matrix aij [nxn]
aij=(1-kij).*sqrt(ai_c*ai_c'); % after Eq.(3.30)
%% LIQUID PHASE
% Check if liquid phase exists
if isnan(xi)
    [am_L,bm_L]=deal(nan);
else
    % Compute auxiliary matrix xij [nxn]
    xij=xi*xi';
    % Compute mixing rules for the liquid phase
    am_L=sum(sum(xij.*aij)); % after Eq.(3.29)
    bm_L=sum(xi.*bi_c); % after Eq.(3.31)
end
%% VAPOR PHASE
% Check if vapor phase exists

```



```

if isnan(yi)
    [am_v,bm_v]=deal(nan);
else
    % Compute auxiliary matrix yij [nxn]
    yij=yi*yi';
    % Compute mixing rules for the vapor phase
    am_v=sum(sum(yij.*aij));
    bm_v=sum(yi.*bi_c);
end
end

```

- EOS Z-factor & fugacity function

```

function [Z_L,Z_v,fi_L_Pa,fi_v_Pa]=SRK_PR_Z_fug_f...
    (kij,ai_c,am_L,xi,bi_c,bm_L,P_Pa,T_K,yi,am_v,bm_v,EOS_type)
%{
This function is based on the Z-factor and fugacity coefficient expressions
for mixture components provided by the SRK and PR EOS's.
The SRK-EOS is presented by G. Soave in his paper "Equilibrium constants
from a modified Redlich-Kwong equation of state", Chemical Engineering
Science, Vol.27, No.6, pp.1197-1203, (1972).
https://doi.org/10.1016/0009-2509(72)80096-4
The PR-EOS is presented by D.-Y. Peng and D. B. Robinson in their paper "A
New Two-Constant Equation of State", Ind. Eng. Chem. Fundam., Vol.15, No.1,
pp.59-64, (1976). https://doi.org/10.1021/i160057a011
The input arguments are the following:
kij, the binary interaction coefficients [nxn]
ai_c, bi_c, the component "attraction" and "repulsion" parameters [nx1]
xi, yi, the liquid and vapor phase compositions [nx1]
am_L, am_v, the liquid and vapor phase quadratic mixing rules [1x1]
bm_L, bm_v, the liquid and vapor phase linear mixing rules [1x1]
P_Pa, the reference pressure in Pascal [1x1]
T_K, the reference temperature in Kelvin [1x1]
EOS_type, the type of EOS used (character array)
The output arguments are:
Z_L, Z_v, the liquid and vapor phase Z-factors [1x1]
fi_L_Pa, fi_v_Pa, the liquid and vapor phase component fugacities [nx1]
%}
% Set the universal gas constant in Pa*m^3/(mol*K)
R=8.314472;
% Compute auxiliary matrix aij [nxn]
aij=(1-kij).*sqrt(ai_c*ai_c'); % after Eq. (22), pp.60 (Peng & Robinson)
%% LIQUID PHASE
% Check if liquid phase exists
if isnan(xi)
    [AAi_L,BBi_L,Am_L,Bm_L]=deal(nan);
else
    % Compute auxiliary vectors AAi, BBi [nx1]
    AAi_L=(2/am_L)*sum(xi.*aij)';
    BBi_L=bi_c/bm_L;
    % Compute mixture dimensionless parameters Am, Bm [1x1]
    Am_L=(am_L*P_Pa)/(R*T_K)^2; % after Eq.(6), pp.60 (Peng & Robinson)
    Bm_L=(bm_L*P_Pa)/(R*T_K); % after Eq.(7), pp.60 (Peng & Robinson)
end
%% VAPOR PHASE
% Check if vapor phase exists
if isnan(yi)
    [AAi_v,BBi_v,Am_v,Bm_v]=deal(nan);
else
    % Compute auxiliary vectors AAi, BBi [nx1]
    AAi_v=(2/am_v)*sum(yi.*aij)';
    BBi_v=bi_c/bm_v;
    % Compute mixture dimensionless parameters Am, Bm [1x1]
    Am_v=(am_v*P_Pa)/(R*T_K)^2;
    Bm_v=(bm_v*P_Pa)/(R*T_K);
end
%% SRK-EOS case
if ismember(EOS_type,{'SRK'})
    %% LIQUID PHASE
    % Check if liquid phase exists
    if isnan(xi)
        [Z_L,fi_L_Pa]=deal(nan);
    else
        % Compute polynomial coefficients after Eq.(4), pp.1197 (Soave)
        x3=1;
        x2=-1;
        x1=Am_L-Bm_L-Bm_L^2;
        x0=-Am_L*Bm_L;
        % Compute Z factor
        Z_L=roots([x3 x2 x1 x0]);
        % Eliminate negative/zero values & imaginary roots
        Z_L(Z_L<=0 | imag(Z_L)~=0)=[];
    end
end

```



```

        % Choose the largest root for liquids
        Z_L=max(Z_L);
        % Compute lnphi=ln(f/P) after Eq.(21), pp.1200 (Soave)
        lnphi_L=BBi_L*(Z_L-1)-log(Z_L-Bm_L)-(Am_L/Bm_L)*(AAi_L-BBi_L)*...
            log(1+Bm_L/Z_L);
        % Eliminate infinite values & imaginary roots
        lnphi_L(lnphi_L==Inf|imag(lnphi_L)~=0|Z_L<Bm_L)=[];
        % Compute fugacity from Eq.(21), pp.1200 (Soave)
        fi_L_Pa=exp(lnphi_L).*xi*P_Pa;
    end
    %% VAPOR PHASE
    % Check if vapor phase exists
    if isnan(yi)
        [Z_v,fi_v_Pa]=deal(nan);
    else
        % Compute polynomial coefficients
        y3=1;
        y2=-1;
        y1=Am_v-Bm_v-Bm_v^2;
        y0=-Am_v*Bm_v;
        % Compute Z factor
        Z_v=roots([y3 y2 y1 y0]);
        % Eliminate negative/zero values & imaginary roots
        Z_v(Z_v<=0|imag(Z_v)~=0)=[];
        % Choose the smallest root for gases
        Z_v=min(Z_v);
        % Compute ln(f/P)=lnphi
        lnphi_v=BBi_v*(Z_v-1)-log(Z_v-Bm_v)-(Am_v/Bm_v)*(AAi_v-BBi_v)*...
            log(1+Bm_v/Z_v);
        % Eliminate infinite values & imaginary roots
        lnphi_v(lnphi_v==Inf|imag(lnphi_v)~=0|Z_v<Bm_v)=[];
        % Compute fugacity
        fi_v_Pa=exp(lnphi_v).*yi*P_Pa;
    end
    %% PR-EOS case
elseif ismember(EOS_type,{'PR'})
    %% LIQUID PHASE
    % Check if liquid phase exists
    if isnan(xi)
        [Z_L,fi_L_Pa]=deal(nan);
    else
        % Compute polynomial coefficients after Eq.(5), pp.60 (Peng & Robinson)
        x3=1;
        x2=-(1-Bm_L);
        x1=Am_L-3*Bm_L^2-2*Bm_L;
        x0=-(Am_L*Bm_L-Bm_L^2-Bm_L^3);
        % Compute Z factor
        Z_L=roots([x3 x2 x1 x0]);
        % Eliminate negative/zero values & imaginary roots
        Z_L(Z_L<=0|imag(Z_L)~=0)=[];
        % Choose the largest root for liquids
        Z_L=max(Z_L);
        % Compute lnphi=ln(f/P) after Eq.(19), pp.60 (Peng & Robinson)
        lnphi_L=BBi_L*(Z_L-1)-log(Z_L-Bm_L)-(Am_L/(2*sqrt(2)*Bm_L))*...
            (AAi_L-BBi_L)*log((Z_L+(sqrt(2)+1)*Bm_L)/(Z_L-(sqrt(2)-1)*Bm_L));
        % Eliminate infinite values & imaginary roots
        lnphi_L(lnphi_L==Inf|imag(lnphi_L)~=0|Z_L<Bm_L)=[];
        % Compute fugacity from Eq.(19), pp.60 (Peng & Robinson)
        fi_L_Pa=exp(lnphi_L).*xi*P_Pa;
    end
    %% VAPOR PHASE
    % Check if vapor phase exists
    if isnan(yi)
        [Z_v,fi_v_Pa]=deal(nan);
    else
        % Compute polynomial coefficients
        y3=1;
        y2=-(1-Bm_v);
        y1=Am_v-3*Bm_v^2-2*Bm_v;
        y0=-(Am_v*Bm_v-Bm_v^2-Bm_v^3);
        % Compute Z factor
        Z_v=roots([y3 y2 y1 y0]);
        % Eliminate negative/zero values & imaginary roots
        Z_v(Z_v<=0|imag(Z_v)~=0)=[];
        % Choose the smallest root for gases
        Z_v=min(Z_v);
        % Compute ln(f/P)=lnphi
        lnphi_v=BBi_v*(Z_v-1)-log(Z_v-Bm_v)-(Am_v/(2*sqrt(2)*Bm_v))*...
            (AAi_v-BBi_v)*log((Z_v+(sqrt(2)+1)*Bm_v)/(Z_v-(sqrt(2)-1)*Bm_v));
        % Eliminate infinite values & imaginary roots
        lnphi_v(lnphi_v==Inf|imag(lnphi_v)~=0|Z_v<Bm_v)=[];
        % Compute fugacity
        fi_v_Pa=exp(lnphi_v).*yi*P_Pa;
    end
end
end
end

```


- Two-phase flash SS method function

```
function [xi_eq,yi_eq,fv_eq,Ki_eq,Z_L_eq,Z_v_eq,fi_eq_Pa,lnfi_eq_atm]=Ki_SS_method_f...
(Ki,fi_L_Pa,fi_v_Pa,zi,kij,ai_c,bi_c,P_Pa,T_K,EOS_type)
%{
This function is based on the Successive-Substitution method for the update
of K-values provided by C. H. Whitson and M. R. Brule in "Phase Behavior,
SPE Monograph Vol. 20, Henry L. Doherty Series", Chap. 4, Sec. 4.3, pp. 6-9.
The input arguments are the following:
Ki, the previously computed K-values [nx1]
fi_L_Pa, fi_v_Pa, the previously computed phase component fugacities [nx1]
zi, the mixture feed composition [nx1]
kij, the binary interaction coefficients [nxn]
ai_c, bi_c, the component "attraction" and "repulsion" parameters [nx1]
P_Pa, the reference pressure in Pascal [1x1]
T_K, the reference temperature in Kelvin [1x1]
EOS_type, the type of EOS used (character array)
=====VAPOR/LIQUID EQUILIBRIUM CONDITION=====
The output arguments are:
xi_eq, yi_eq the VLE liquid and vapor phase compositions [nx1]
fv_eq, the VLE vapor phase fraction [1x1]
Ki_eq, the VLE component K-values [nx1]
Z_L_eq, Z_v_eq, the VLE liquid and vapor phase Z-factors [1x1]
fi_eq_Pa, the VLE component fugacities in Pa [nx1]
lnfi_eq_atm, the VLE logarithmic fugacities in atm [nx1]
%}
% Set the recommended convergence tolerance
epsilon=1.0e-13;
% Check the equal-fugacity constraint for convergence
if sum((fi_L_Pa./fi_v_Pa-1).^2)>=epsilon % after Eq. (4.30)
    % Rename K-values and component fugacities for SS
    Ki_old=Ki;
    fi_L_old=fi_L_Pa;
    fi_v_old=fi_v_Pa;
    % Begin iteration sequence (iterate until convergence is reached)
    for n=1:1000
        % Update K-values with SS
        Ki=Ki_old.*fi_L_old./fi_v_old; % after Eq. (4.48)
        % Update liquid composition (xi), vapor composition (yi) and vapor phase fraction (fv)
        [xi,yi,fv]=two_phase_split_f(Ki,zi);
        % Update EOS mixing rules am, bm
        [am_L,bm_L,am_v,bm_v]=mixing_rules_f(kij,ai_c,xi,bi_c,yi);
        % Update phase Z-factors Z_L, Z_v and component fugacities fi_L, fi_v
        [Z_L,Z_v,fi_L_Pa,fi_v_Pa]=SRK_PR_Z_fug_f...
            (kij,ai_c,am_L,xi,bi_c,bm_L,P_Pa,T_K,yi,am_v,bm_v,EOS_type);
        % Check the equal-fugacity constraint for convergence
        if sum((fi_L_Pa./fi_v_Pa-1).^2)<epsilon
            break
        end
        % Check for convergence at a trivial solution
        if sum((log(Ki)).^2)<1.0e-04 % after Eq. (4.51)
            break
        end
        % Reset names for the next iteration
        Ki_old=Ki;
        fi_L_old=fi_L_Pa;
        fi_v_old=fi_v_Pa;
    end
    % Equilibrium fugacities of both phases are equal (fi_L_Pa=fi_v_Pa)
    fi_Pa=fi_L_Pa;
    % Case vapor phase does not exist
    if fv<0
        Ki=deal(nan);
        yi=deal(nan);
        % Liquid phase composition equals feed composition
        xi=zi;
        % Compute EOS mixing rules am, bm
        [am_L,bm_L,am_v,bm_v]=mixing_rules_f(kij,ai_c,xi,bi_c,yi);
        % Compute liquid phase Z-factor Z_L and component fugacities fi_L
        [Z_L,Z_v,fi_L_Pa,fi_v_Pa]=SRK_PR_Z_fug_f...
            (kij,ai_c,am_L,xi,bi_c,bm_L,P_Pa,T_K,yi,am_v,bm_v,EOS_type);
        fi_Pa=fi_L_Pa;
    % Case liquid phase does not exist
    elseif fv>1
        Ki=deal(nan);
        xi=deal(nan);
        % Vapor phase composition equals feed composition
        yi=zi;
        % Compute EOS mixing rules am, bm
        [am_L,bm_L,am_v,bm_v]=mixing_rules_f(kij,ai_c,xi,bi_c,yi);
        % Compute vapor phase Z-factor Z_v and component fugacities fi_v
        [Z_L,Z_v,fi_L_Pa,fi_v_Pa]=SRK_PR_Z_fug_f...
            (kij,ai_c,am_L,xi,bi_c,bm_L,P_Pa,T_K,yi,am_v,bm_v,EOS_type);
        fi_Pa=fi_v_Pa;
    end
end
```



```
end
% Update output variable names
xi_eq=xi;
yi_eq=yi;
fv_eq=fv;
Ki_eq=Ki;
Z_L_eq=Z_L;
Z_v_eq=Z_v;
fi_eq_Pa=fi_Pa;
lnfi_eq_atm=log(fi_eq_Pa)-log(101325); % Convert logarithmic fugacities to atm
end
```

- Volume shift function

```
function fi_mod_Pa=Vshift_fug_correction_f(EOS_type,greek_oilfield,bi_c,fi_Pa,P_Pa,T_K)
%{
This function is based on the fugacity correction expressions provided by
C. H. Whitson and M. R. Brule in "Phase Behavior, SPE Monograph Vol. 20,
Henry L. Doherty Series", Chap. 4, Sec. 4.2.6, pp. 5-6.
The input arguments are the following:
EOS_type, the type of EOS used (character array)
greek_oilfield, the structure array used
bi_c, the component "repulsion" parameter (co-volume) [nx1]
fi_Pa, the component fugacities in Pa [nx1]
P_Pa, the reference pressure in Pa [1x1]
T_K, the reference temperature in Kelvin [1x1]
The output argument is:
fi_mod_Pa, the modified (volume-corrected) component fugacities in Pa [nx1]
%}
% Set the universal gas constant in Pa*m^3/(mol*K)
R=8.314472;
% SRK-EOS case
if ismember(EOS_type,{'SRK'})
    % Cast the volume shift parameters of the SRK-EOS
    Si=greek_oilfield.Vol_Shift.SRK;
% PR-EOS case
elseif ismember(EOS_type,{'PR'})
    % Cast the volume shift parameters of the PR-EOS
    Si=greek_oilfield.Vol_Shift.PR;
end
% Compute volume correction terms c after Eq. (4.28)
ci=Si.*bi_c;
% Compute modified component fugacities after Eq. (4.26)
fi_mod_Pa=fi_Pa.*exp(-ci*P_Pa/(R*T_K));
end
```

- Isothermal GCE function

```
function [fi_h_Pa,zi_h,P_h_psia,Psat_h_psia]=GCE_algorithm_f...
(href_ft,h_ft,fi_Pa,Mi,T_K,zi,P_Pa,kij,ai_c,bi_c,EOS_type,greek_oilfield,Tc_K,Pc_MPa,w)
%{
This function is based on the isothermal gravity/chemical equilibrium (GCE)
solution algorithm provided by C. H. Whitson and P. Belery in their paper
"Compositional Gradients in Petroleum Reservoirs" presented at the
University of Tulsa Centennial Petroleum Engineering Symposium, Tulsa,
Oklahoma, August 1994. https://doi.org/10.2118/28000-MS
This function optionally incorporates volume shift for the fugacity expressions
The input arguments are the following:
href_ft, the reference depth in feet [1x1]
h_ft, the next arbitrary depth in feet [1x1]
fi_Pa, the component fugacities in Pa [nx1]
Mi, the component molar masses in kg/mol [nx1]
T_K, the reference temperature in Kelvin [1x1]
zi, the mixture feed composition (mole fraction) [nx1]
P_Pa, the reference pressure in Pascal [1x1]
kij, the binary interaction coefficients [nxn]
ai_c, bi_c, the component "attraction" and "repulsion" parameters [nx1]
EOS_type, the type of EOS used [character array]
greek_oilfield, the structure array used
Tc_K, the component critical temperature in K [nx1]
Pc_MPa, the component critical pressure in MPa [nx1]
w, the component acentric factor [nx1]
The output arguments are:
fi_h_Pa, the component fugacities in Pa at the next depth [nx1]
zi_h, the mixture composition at the next depth (mole fraction) [nx1]
P_h_psia, the pressure in psia at the next depth [1x1]
Psat_psia, the saturation pressure in psia at the next depth [1x1]
%}
```



```

%}
%% GCE algorithm initialization
% Set the acceleration of gravity in m/s^2
g=9.81;
% Set the universal gas constant in Pa*m^3/(mol*K)
R=8.314472;
% Convert reference depth to m
href_m=href_ft*0.3048;
% Convert given depth to m
h_m=h_ft*0.3048;
% Compute gravity-corrected fugacities (this is only made once)
fi_ref_corr=fi_Pa.*exp(Mi*g*(h_m-href_m)/(R*T_K)); % after Eq. (8)
%% Single-phase fluid case
% Initial estimates of composition and pressure are values at href_ft
xi=zi;
yi=deal(nan);
P_Pa;
% Begin iteration sequence (iterate until convergence is achieved)
for n=1:1000
    % Begin Successive-Substitution (four iterations)
    for m=1:4
        % Compute fugacities of the composition estimates using an EOS
        [am_L,bm_L,am_v,bm_v]=mixing_rules_f(kij,ai_c,xi,bi_c,yi);
        [Z_L,Z_v,fi_L_Pa,fi_v_Pa]=SRK_PR_Z_fug_f...
            (kij,ai_c,am_L,xi,bi_c,bm_L,P_Pa,T_K,yi,am_v,bm_v,EOS_type);
        % Mixture fugacities are liquid phase fugacities
        fi_Pa=fi_L_Pa;
        % Apply volume shift (remove this step if not used)
        fi_mod_Pa=Vshift_fug_correction_f(EOS_type,greek_oilfield,bi_c,fi_Pa,P_Pa,T_K);
        % Rename fugacities for brevity
        fi_Pa=fi_mod_Pa;
        % Compute mole numbers
        Yi=xi.*(fi_ref_corr./fi_Pa); % after Eq. (7)
        % Compute fugacity ratio corrections
        ri=(fi_ref_corr./fi_Pa)/sum(Yi); % after Eq. (9)
        % Update mole numbers using SS
        Yi_new=Yi.*ri; % after Eq. (10) with λ=1
        % Update composition estimates
        xi_new=Yi_new/sum(Yi_new); % after Eq. (12)
        % Compute Q function
        Q=1-sum(Yi); % after Eq. (6)
        % Compute fugacity gradient
        gradfi=gradient(fi_Pa,P_Pa);
        % Compute Q function gradient
        gradQ=sum(Yi.*ri.*gradfi./fi_Pa); % after Eq. (14)
        % Update pressure estimate using the Newton-Raphson method
        P_new=P_Pa+Q/gradQ; % after Eq. (13)
        % Rename composition and pressure estimates for the next iteration
        xi=xi_new;
        P_Pa=P_new;
    end
    % Rename fugacity ratio corrections for GDEM
    ri_old=ri;
    % Begin GDEM acceleration (one iteration)
    % Compute fugacities of the composition estimates using an EOS
    [am_L,bm_L,am_v,bm_v]=mixing_rules_f(kij,ai_c,xi,bi_c,yi);
    [Z_L,Z_v,fi_L_Pa,fi_v_Pa]=SRK_PR_Z_fug_f...
        (kij,ai_c,am_L,xi,bi_c,bm_L,P_Pa,T_K,yi,am_v,bm_v,EOS_type);
    % Mixture fugacities are liquid phase fugacities
    fi_Pa=fi_L_Pa;
    % Apply volume shift (remove this step if not used)
    fi_mod_Pa=Vshift_fug_correction_f(EOS_type,greek_oilfield,bi_c,fi_Pa,P_Pa,T_K);
    % Rename fugacities for brevity
    fi_Pa=fi_mod_Pa;
    % Compute mole numbers
    Yi=xi.*(fi_ref_corr./fi_Pa);
    % Compute fugacity ratio corrections
    ri=(fi_ref_corr./fi_Pa)/sum(Yi);
    % Compute λ after Eq. (11)
    b01=sum(log(ri).*log(ri_old));
    b11=sum(log(ri_old).^2);
    lamda=abs(b11/(b11-b01));
    % Update mole numbers using GDEM
    Yi_new=Yi.*(ri.^lamda); % after Eq. (10)
    % Update composition estimates
    xi_new=Yi_new/sum(Yi_new);
    % Compute Q function
    Q=1-sum(Yi);
    % Compute fugacity gradient
    gradfi=gradient(fi_Pa,P_Pa);
    % Compute Q function gradient
    gradQ=sum(Yi.*ri.*gradfi./fi_Pa);
    % Update pressure estimate using the Newton-Raphson method
    P_new=P_Pa+Q/gradQ;
    % Check for convergence using the criteria after Eq. (15)
    if abs(1-sum(Yi_new))<1.0e-13 || (sum(log(ri)./log(Yi_new./xi_new)))^2<1.0e-08
        break
    end
end

```



```

        % Rename composition and pressure estimates for the next iteration
        xi=xi_new;
        P_Pa=P_new;
    end
    % Update output variable names
    fi_h_Pa=fi_Pa;
    zi_h=xi_new;
    P_h_Pa=P_new;
    P_h_psia=P_h_Pa/6.8948e+03; % Convert pressure to psia
    %% Perform stability test to determine if solution is valid
    [Ki]=a_Wilsonmethod_initial_estimates_f(T_K,P_Pa,Tc_K,Pc_MPa,w);
    % Rename pressure estimate for stability test
    P_Pa=P_h_Pa;
    % Vapor-like search
    [S_v,yi_stab,Ki_v]=stability_test_vapor_f(Ki,zi,kij,ai_c,bi_c,P_Pa,T_K,EOS_type);
    %% Unstable solution case
    if S_v>1
        % Reinitialize gradient calculation with vapor phase composition
        xi=deal(nan);
        yi=yi_stab;
        % Begin iteration sequence (iterate until convergence is achieved)
        for n=1:1000
            % Begin Successive-Substitution (four iterations)
            for m=1:4
                % Compute fugacities of the composition estimates using an EOS
                [am_L,bm_L,am_v,bm_v]=mixing_rules_f(kij,ai_c,xi,bi_c,yi);
                [Z_L,Z_v,fi_L_Pa,fi_v_Pa]=SRK_PR_Z_fug_f...
                    (kij,ai_c,am_L,xi,bi_c,bm_L,P_Pa,T_K,yi,am_v,bm_v,EOS_type);
                % Mixture fugacities are vapor phase fugacities
                fi_Pa=fi_v_Pa;
                % Apply volume shift (remove this step if not used)
                fi_mod_Pa=Vshift_fug_correction_f(EOS_type,greek_oilfield,bi_c,fi_Pa,P_Pa,T_K);
                % Rename fugacities for brevity
                fi_Pa=fi_mod_Pa;
                % Compute mole numbers
                Yi=yi.*(fi_ref_corr./fi_Pa);
                % Compute fugacity ratio corrections
                ri=(fi_ref_corr./fi_Pa)/sum(Yi);
                % Update mole numbers using SS
                Yi_new=Yi.*ri;
                % Update composition estimates
                yi_new=Yi_new/sum(Yi_new);
                % Compute Q function
                Q=1-sum(Yi);
                % Compute fugacity gradient
                gradfi=gradient(fi_Pa,P_Pa);
                % Compute Q function gradient
                gradQ=sum(Yi.*ri.*gradfi./fi_Pa);
                % Update pressure estimate using the Newton-Raphson method
                P_new=P_Pa+Q/gradQ;
                % Rename composition and pressure estimates for the next iteration
                yi=yi_new;
                P_Pa=P_new;
            end
            % Rename fugacity ratio corrections for GDEM
            ri_old=ri;
            % Begin GDEM acceleration (one iteration)
            % Compute fugacities of the composition estimates using an EOS
            [am_L,bm_L,am_v,bm_v]=mixing_rules_f(kij,ai_c,xi,bi_c,yi);
            [Z_L,Z_v,fi_v_Pa,fi_v_Pa]=SRK_PR_Z_fug_f...
                (kij,ai_c,am_L,xi,bi_c,bm_L,P_Pa,T_K,yi,am_v,bm_v,EOS_type);
            % Mixture fugacities are vapor phase fugacities
            fi_Pa=fi_v_Pa;
            % Apply volume shift (remove this step if not used)
            fi_mod_Pa=Vshift_fug_correction_f(EOS_type,greek_oilfield,bi_c,fi_Pa,P_Pa,T_K);
            % Rename fugacities for brevity
            fi_Pa=fi_mod_Pa;
            % Compute mole numbers
            Yi=yi.*(fi_ref_corr./fi_Pa);
            % Compute fugacity ratio corrections
            ri=(fi_ref_corr./fi_Pa)/sum(Yi);
            % Compute  $\lambda$  after Eq. (11)
            b01=sum(log(ri)).*log(ri_old));
            b11=sum(log(ri_old).^2);
            lamda=abs(b11/(b11-b01));
            % Update mole numbers using GDEM
            Yi_new=Yi.*(ri.^lamda);
            % Update composition estimates
            yi_new=Yi_new/sum(Yi_new);
            % Compute Q function
            Q=1-sum(Yi);
            % Compute fugacity gradient
            gradfi=gradient(fi_Pa,P_Pa);
            % Compute Q function gradient
            gradQ=sum(Yi.*ri.*gradfi./fi_Pa);
            % Update pressure estimate using the Newton-Raphson method
            P_new=P_Pa+Q/gradQ;
            % Check for convergence using the criteria after Eq. (15)

```



```

        if abs(1-sum(Yi_new))<1.0e-13 || (sum(log(ri)./log(Yi_new./xi_new)))^2<1.0e-08
            break
        end
        % Rename composition and pressure estimates for the next iteration
        yi=yi_new;
        P_Pa=P_new;
    end
    % Update output variable names
    fi_h_Pa=fi_Pa;
    zi_h=yi_new;
    P_h_Pa=P_new;
    P_h_psia=P_h_Pa/6.8948e+03; % Convert pressure to psia
end
%% Saturation pressure calculation
% Rename pressure and composition estimates for the calculation
P_Pa=P_h_Pa;
zi=zi_h;
% Compute saturation pressure
[Psat_psia,yi_sat,Ki_sat,Z_L_sat,Z_v_sat,fi_sat_Pa,lnfi_sat_atm]=Psat_calc_f...
    (P_Pa,T_K,Tc_K,Pc_MPa,w,zi,kij,ai_c,bi_c,EOS_type);
% Compute dew-point pressure
[Pdew_psia,xi_dew,Ki_dew,Z_L_dew,Z_v_dew,fi_dew_Pa,lnfi_dew_atm]=Pdew_calc_f...
    (P_Pa,T_K,Tc_K,Pc_MPa,w,zi,kij,ai_c,bi_c,EOS_type);
% For the vapor phase composition, saturation pressure equals dew-point pressure
% (Remove the following condition if the mixture is single-phase)
if Pdew_psia>Psat_psia
    Psat_psia=Pdew_psia;
end
% Update saturation pressure name
Psat_h_psia=Psat_psia;
end

```

- GOC location function

```

function [hGOC_ft,zi_GOC,P_GOC_psia,Psat_GOC_psia]=GOC_calc_f...
    (htop_ft,hbot_ft,href_ft,fi_Pa,Mi,T_K,zi,P_Pa,kij,ai_c,bi_c,EOS_type,Tc_K,Pc_MPa,w)
%{
    This function locates the Gas/Oil Contact depth using an interval halving
    algorithm based on reservoir pressure provided that the user knows the
    pressure at the GOC (i.e. saturation pressure at reference conditions).
    The input arguments are the following:
    htop_ft, the top depth of the reservoir in feet [1x1]
    hbot_ft, the bottom depth of the reservoir in feet [1x1]
    href_ft, the reference depth in feet [1x1]
    fi_Pa, the component fugacities in Pa [nx1]
    Mi, the component molar masses in kg/mol [nx1]
    T_K, the reference temperature in Kelvin [1x1]
    zi, the mixture feed composition (mole fraction) [nx1]
    P_Pa, the reference pressure in Pascal [1x1]
    kij, the binary interaction coefficients [nxn]
    ai_c, bi_c, the component "attraction" and "repulsion" parameters [nx1]
    EOS_type, the type of EOS used [character array]
    Tc_K, the component critical temperature in K [nx1]
    Pc_MPa, the component critical pressure in MPa [nx1]
    w, the component acentric factor [nx1]
    The output arguments are:
    hGOC_ft, the GOC depth in feet [1x1]
    zi_GOC, the GOC mixture composition (mole fraction) [nx1]
    P_GOC_psia, the GOC pressure in psia [nx1]
    Psat_GOC_psia, the GOC saturation pressure in psia [nx1]
%}
% Set the GOC pressure (experimental saturation pressure)
P_GOC_psia=3826.1;
% Set convergence tolerance
dh_ft=0.1;
for n=1:100
    % GOC depth estimate
    hGOC_ft=0.5*(htop_ft+hbot_ft);
    % Rename hGOC for GCE
    h_ft=hGOC_ft;
    % Compute fi, zi, P, Psat at the depth estimate
    [fi_h_Pa,zi_h,P_h_psia,Psat_h_psia]=GCE_algorithm_f...
        (href_ft,h_ft,fi_Pa,Mi,T_K,zi,P_Pa,kij,ai_c,bi_c,EOS_type,Tc_K,Pc_MPa,w);
    % Check for convergence
    if n>1.5*log((htop_ft-hbot_ft)/dh_ft)
        break
    end
    % Update GOC depth search boundaries
    if P_h_psia>P_GOC_psia
        hbot_ft=hGOC_ft;
    elseif P_h_psia<P_GOC_psia
        htop_ft=hGOC_ft;
    end
end

```



```
end
% Reset names for the next iteration
href_ft=h_ft;
fi_Pa=fi_h_Pa;
zi=zi_h;
P_Pa=P_h_psia*6.8948e+03;
end
% Update output variable names
zi_GOC=zi_h;
P_GOC_psia=P_h_psia;
Psat_GOC_psia=Psat_h_psia;
end
```